The Co-ordination Chemistry of Some Metal Ions with Saturated, Quadridentate, Macrocyclic Ligands.

by

Norman Herron

A thesis submitted in partial fulfilment of the requirements for the degree of Doctor of Philosophy from the University of Warwick, Department of Chemistry and Molecular Sciences.

September. 1978.

CONTENTS.

LIST OF TABLES.

Acknowledgement

I would like to thank all members of the department of Chemistry and Molecular Sciences for their help and encouragement. In particular, my thanks go to my supervisor, Dr. P. Moore for his undying enthusiasm, optimism and friendship throughout the course of this work. I would also like to thank Dr. N.W. Alcock, for his patient guidance through darkest crystallography, and Dr. O.W. Howarth for helpful discussions during the work.

Finally I would like to thank my wife, not only for her efforts in assisting with the typing of this thesis, but also for tolerating the author during its preparation.

A postgraduate studentship from the Science Research Council is gratefully acknowledged.

Parts of the work reported in this thesis have been published or accepted for publication in the scientific literature with the following references:

N. Herron, O.W. Howarth and P. Moore, Inorg. Chim. Acta, 1976, 20, L43.

N.W. Alcock, N. Herron and P. Moore, J.C.S. Chem. Commun., 1976, 886.

N.W. Alcock, N. Herron and P. Moore, J.C.S. Dalton, 1978, 394.

N.W. Alcock, N. Herron and P. Moore, J.C.S. Dalton, in press.

N. Herron and P. Moore, J.C.S. Dalton, in press.

TO MARGARET.

Abstract

The co-ordination chemistry of macrocyclic ligands, to the heavier, environmentally hazardous, metal ions (Hg(II), Cd(II), Pb(II)) and to lighter transition metal ions (Ni(II), Co(III), Rh(III), Zn(II)) as models, has been studied. The macrocycles of major interest are the simple 14-membered saturated quadridentate rings (figure) with donor sets X = S, NH or NMe. A comparison of the structural and kinetic properties of their complexes with the metal ions above has been principally performed by ^{13}C, ^{1}H and ^{15}N n.m.r. spectroscopy and X-ray single crystal diffraction.

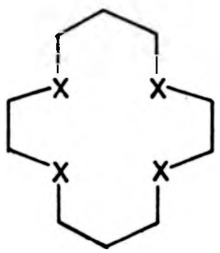

When X = S, the complex with nickel(II) displays a dynamic equilibriu between two trans-isomers, trans-I and trans-III, in nitromethane solutio Complexes with mercury(II) adopt either a bridging bidentate conformation when co-ordinating counteranions are present, or a trans-I quadridentate square-pyramidal geometry when they are not. No complexes of Cd(II) or Pb(II) were isolated.

When X = NH, the nickel(II) complex is square-planar but readily solvates in donor solvents to give solid octahedral complexes. Cd(II) forms a complex which is a mixture of trans-III and folded trans-I isomers in solution, while the Hg(II) complex is postulated as being square-pyramidal in solution. The crystal structure of the complex with Pb(II) shows a distorted cis-octahedral geometry, in agreement with the ^{13}C n.m.r., having co-ordinated nitrate ions. The lone pair of the lead ion is found to be stereochemically inactive. ^{1}J metal-^{15}N coupling constants for all three of the heavy metal complexes have been obtained and for Pb(II) have very different values for axial and equatorial nitrogens, consistent with the observed axial distortion in the crystal. Dynamic phenomena are observed in both the ^{13}C and ^{15}N n.m.r. spectra of the Cd(II) and Pb(II) complexes.

When X = NMe, the Zn(II) complexes are found to adopt square-pyramidal co-ordination in the crystalline state while in solution, folding to a trigonal-bipyramid may occur. Such behaviour is also postulated for the complexes with Cd(II) and Hg(II) but Pb(II) is found to form a thermodynamically unstable complex and macrocycle exchange may be observed in the ^{13}C n.m.r. spectra. Two isomers of the complex with

nickel(II) are extensively investigated and the acetonitrile exchange kinetics of each isomer have been measured and related to their structures. The trans-I isomer is postulated to form a trigonal-bipyramidal complex with acetonitrile and solvent exchange proceeds through an associative mechanism. The trans-III isomer displays normal octahedral exchange kinetics via a dissociative mechanism.

SYMBOLS.

n.m.r.	nuclear magnetic resonance.
e.s.r.	electron spin resonance
I.R.	infra-red
UV	ultra violet
λ	wavelength
ϵ	extinction coefficient
υ	frequency of absorption maximum
δ	chemical shift
ppm	parts per million
f.i.d.	free induction decay (n.m.r.)
r.f.	radio frequency
NOE	nuclear Overhauser enhancement

ABBREVIATED CHEMICALS.

B.A.L.	British Anti-Lewisite, 2,3-dimercaptopropanol.
C.D.T.A.	N,N,N',N'-tetraacetate-1,2-cyclohexanediamine.
E.D.T.A.	N,N,N',N'-tetraacetate-1,2-diaminoethane.
DMSO	dimethyl sulphoxide
DMF	N,N -dimethyl formamide.
en	1,2-ethylenediamine.
Me_2en	N,N'-dimethyl-1,2-ethylenediamine.
Me_6tren	N-hexamethyl-tren (below)
THF	tetrahydrofuran
TMS	tetramethylsilane
2,3,2-tet	1,4,8,11-tetraazaundecane
3,2,3-tet	1,5,8,12-tetraazadodecane
tren	2,2',2"-triaminotriethylamine
trien	1,4,7,10-tetraazadecane

MACROCYCLIC LIGANDS DISCUSSED IN THIS THESIS.

X = S, [12]aneS$_4$
X = N, [12]aneN$_4$

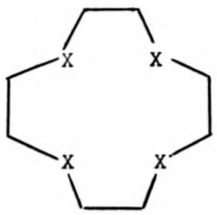

X = S, [13]aneS$_4$
X = N, [13]aneN$_4$

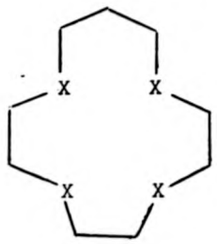

X = S, [14]aneS$_4$
X = N, [14]aneN$_4$

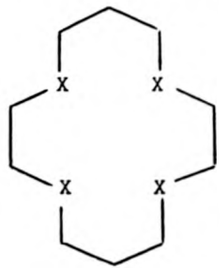

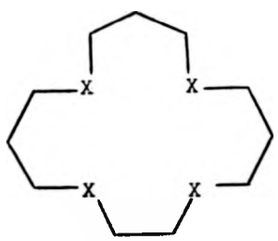

X = S, [15]aneS$_4$
X = N, [15]aneN$_4$

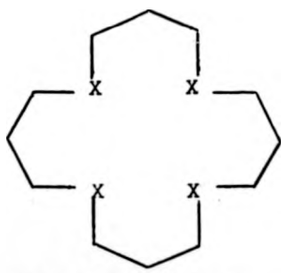

X = S, [16]aneS$_4$
X = N, [16]aneN$_4$

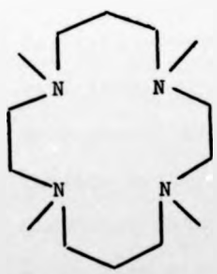

NMe$_4$-[14]aneN$_4$

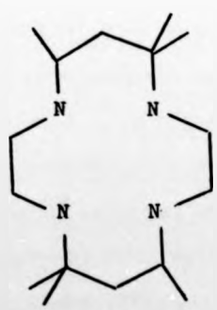

Me$_6$-[14]aneN$_4$

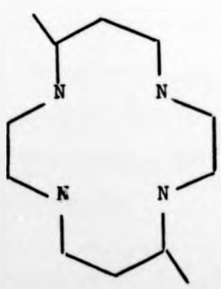

5,12-Me$_2$-[14]aneN$_4$

CHAPTER 1

INTRODUCTORY CHAPTER

INTRODUCTION

The work in this thesis primarily concerns an investigation into the co-ordinative properties of macrocyclic ligands to heavy metal ions and the later transition metal ions, with a view to elucidating the structural factors involved in complexation. This work has been carried out with the long-term ideal of improving current chemotherapeutic techniques, which involve the use of compounds such as B.A.L.[1] and E.D.T.A.[2] for the treatment of heavy metal (e.g. Pb^{2+}, Cd^{2+}, Hg^{2+}, $MeHg^{+}$) poisoning, by gaining a greater understanding of the inorganic chemistry involved.

There are four major areas to be considered in the treatment of heavy metal poisoning, and of relevance to chemotherapeutic drug design:

(1) Any drug used must obviously be capable of reaching the site to which the offending metal is bound, while not being metabolised into some non-potent breakdown product en route.

(2) Once at the required site, the drug must successfully compete with this *in vivo* binding site for the metal ion, and in so doing form a stable complex which may be eventually excreted.

(3) The drug should itself be non-toxic and this includes the very important point of specificity. This means that the drug should specifically seek out and complex with only the foreign toxic metals in the system, whilst leaving the essential micro-nutrient and bulk metals, such as Calcium Zinc, Iron and Copper, alone. This is a major problem with both B.A.L. and E.D.T.A.[2,3] which remove not only the heavy metals but also certain essential metals to such an extent that they must be re-injected after a course of therapy

using these drugs[3].

(4) The final 'drug-metal' complex must be successfully excreted without further damage to the body organs, preferably *via* the gut so avoiding possible secondary kidney damage[4,5].

It is clear that functions (1) and (4) are primarily the province of biochemistry and biology, where the location of *in vivo* binding sites and the identification of excretion pathways are still being elucidated[5]. It is not my concern here, therefore, to consider such processes in any depth, being content to be merely aware of such factors in relation to the main theme of this work which involves functions (2) and (3). From the standpoint of an inorganic chemist functions (2) and (3) above are an interesting challenge in the area of co-ordination chemistry, since some understanding of the properties of model complexes may well be directly relevant to the *in vivo* problem, and may therefore assist in the 'tailoring' of new drugs for its treatment.

With an awareness of the exacting limitations on drug design imposed above, it is natural to begin with a consideration of the fundamental properties of the heavy metals which are the cause of the problem, Pb^{2+}, Cd^{2+}, Hg^{2+}. All are d^{10} metal ions and so strictly speaking are not members of the d-block transition series, although despite this their properties may be regarded as a simple extension of this series (especially Cd^{2+}, Hg^{2+}). They are all large, diffuse ions [ionic radii are 1.21Å $(Pb^{2+})^6$, 0.97Å $(Cd^{2+})^6$, 1.04Å $(Hg^{2+})^7$] with correspondingly high polarisability. As such they have all of the classic requirements for class 'b' or 'soft' character described by Pearson[8], with a corresponding affinity for 'soft' donor ligands

such as RS^-, R_2S, $[CN]^-$, (although Pb^{2+} is a little anomalous)[9], and all form kinetically labile complexes with donor ligands (exchange rate constant $> 10^8$)[10], even though the complexes may be thermodynamically very stable[11].

It is clear that any molecule designed to specifically sequester such metals must take advantage of or modify these properties so as to produce stable excretable complexes. With regard to (3) above we can see that exploitation of the 'soft' character of these metals and of their large ionic radii would be an advantage in producing a ligand capable of selectively removing these metals whilst leaving the 'harder', smaller trace-metal ions behind. This may be done in two ways, a) by selecting a ligand which contains class 'b' type donor atoms and b) by arranging these donor atoms in such a way that their spatial arrangement favours co-ordination to a large rather than to a small metal ion. Consideration b) leads to the selection of a multidentate chelate as a likely candidate for investigation, and this view is reinforced by consideration of (2) above. In order to produce a stable complex with these metal ions, the ligand must be capable of competing with the *in vivo* binding sites which can have stability constants $\geq 10^{18}$ (e.g. for $MeHg^+$ binding to a thiol-containing enzyme, papain)[12], so it is necessary to create several metal to ligand bonds making use of the chelate effect[13] to enhance stability. If one also considers (1) and (4) above it is clearly desirable that both the ligand and its complexes should be non-metabolisable.

We would conclude therefore that what is required is a stable multidentate chelate of the correct size and containing carefully selected donor atoms. One attractive interpretation of such a

specification is to use a large ring (macrocyclic) molecule incorporating several selected donor sites, and in so doing judiciously choose an overall ring size compatible with the metals under study. Such an idea will be pursued in this thesis, where it is felt that a detailed exploration of the co-ordination chemistry of heavy metals with such macrocycles may be of relevance to chemotherapeutic drug design. The possibility, offered by macrocycles, of tailoring a ring to specifically complex with a given metal suggest this to be a promising area of research.

With these considerations in mind it seems desirable to review the current state of the literature, and select the salient features of the chemistry of macrocycles and their metal complexes.

SECTION 1 MACROCYCLES (General)

Naturally-occurring macrocyclic ligand-metal complexes, especially those complexes of the porphyrin, corrin and phthalocyanine ring systems[14,15,16], have been studied for many years. More recently however complexes containing synthetic macrocycles have received a great deal of attention[16] and this increased interest is attributable to two related factors. Firstly, advances on the organic synthetic front have produced synthetic procedures capable of yielding reasonable quantities of these ligands which in turn has meant that the preparation and characterisation of their co-ordination complexes have become easier. Secondly, and perhaps more significantly, macrocycles have engendered increasing interest by virtue of the wide range of unusual properties such ligands impart to their complexes with metal ions. The structural, thermodynamic, kinetic, spectroscopic and redox parameters of such complexes have all been studied

and in many cases the cyclic nature of the ligand is found to greatly modify the chemistry of the metal ion involved. It is as well, therefore, to outline the basic properties of such ligands,and several closely related properties are described below.

SECTION 1.1 CAVITY SIZE RELATED TO CATION RADIUS

A marked correlation exists between the stability constants (K) and cation size (ionic radius[6]) for a given ligand cavity diameter, and it is generally true that for a given macrocycle there will exist an optimum cationic radius for formation of a stable complex. This correlation has been extensively explored for the polyether type of macrocycle[17,18,19](Section 2.1) and results are illustrated in Fig. 1.1.1[17]. Four points are immediately apparent from this figure:

a) Both mono- and divalent cations have a maximum stability for a given cation size.

b) The change in log K with cationic radius is smaller with monovalent cations.

c) Marked selectivity exists for certain ions, e.g. Ca^{2+} and Pb^{2+} have K values differing by five orders of magnitude.

d) For cations of about the same radius such as K^+ (1.33Å) and Ba^{2+} (1.35Å), K increases by ca. 10^2 for the doubly charged ion.

The simplest interpretation of the lower stability with cations larger than the optimum is that such cations are too large to fit into the ligand cavity, and this conclusion is borne out by X-ray data[20,21]. On the other hand, as the cation becomes too small, the hydration energy becomes predominant and so again reduces the stability of the macrocycle complex. Thermodynamic data[17], showing the dependence of log K on $\Delta H^\bullet$ and $\Delta S^\bullet$, illustrates that in going from K^+ to Rb^+ to Cs^+

Figure 1.1.1.

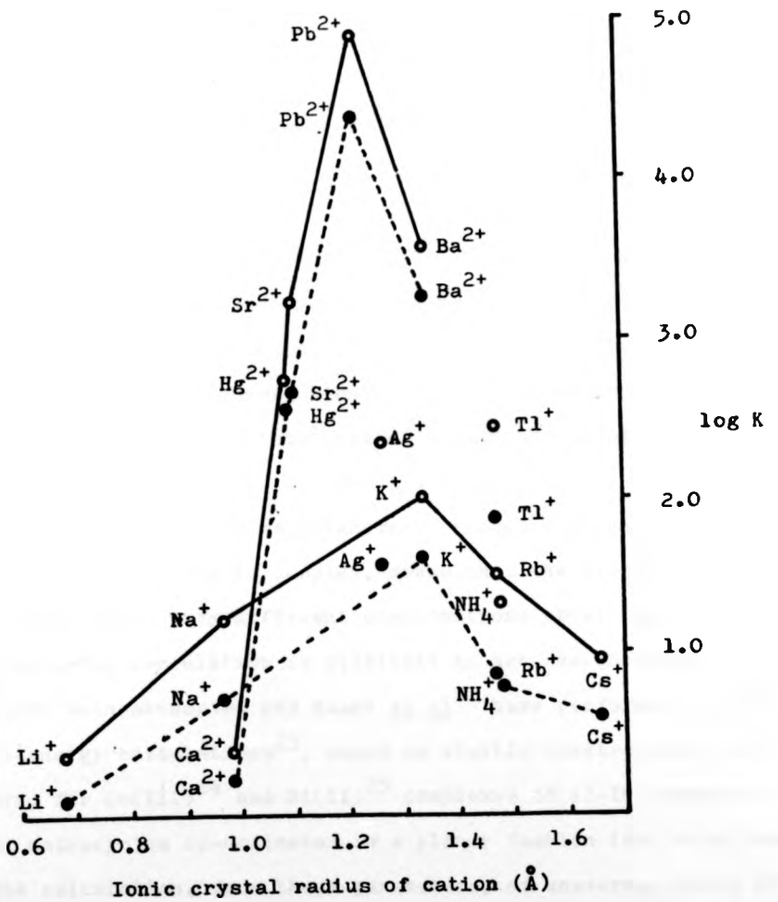

Stability constants (log K) for the formation of 1:1 complexes with dicyclohexyl-18-crown-6 (Fig. 2.1.1. b). Isomer A = o, and isomer B = •, T = 25°C. Isomers are meso and dl-racemic although which is A and which B is unknown. (From ref. 17)

the $\Delta H^{\bullet}$ term is predominantly responsible for the observed trend in stability. However, the increase in log K in going from K^{+} to Ba^{2+} is determined by both $\Delta H^{\bullet}$ and $\Delta S^{\bullet}$ showing entropy and so presumably electrostatic contributions to cation solvation to be important factors in determining stability.

Although similar correlations between cavity size and cationic radius have not been as extensive for other classes of macrocycle, the saturated amine ligands (Section 2.2.) have been under increasing investigation especially in relation to the so called macrocyclic effect (Section 1.3.). With this type of ligand the situation is a little more complex since the strong directionality (ie. preference for regular geometries such as octahedral or square-planar) of the metal ions that they tend to complex, means that the different ring sizes may well adopt very different conformations about the metal and thus a meaningful correlation is difficult to achieve. However, such studies have been attempted and Busch *et al*[22] have performed a number of strain-energy calculations[23], based on visible spectroscopic Dq parameters, for Co(III)[24] and Ni(II)[25] complexes of 12-16 membered tetra-aza macrocycles co-ordinated in a planar fashion (see also Section 1.4.). The calculation, from these parameters, of anaverage ideal metal to nitrogen bond length for each macrocycle results in the values shown in Table 1.1.1.[22]. As most transition metal-nitrogen linkages fall in the range 1.8-2.4Å[22] it is clear that a correlation of such bond lengths with the idealised values given in Table 1.1.1. will allow a prediction of the macrocycle which best fits a given metal in a planar fashion.

As an example, the copper-nitrogen bond distance in typical

Table 1.1.1.

Ideal metal-nitrogen bond lengths and deviations from planarity of tetra-amine macrocycles. (Calculated from strain-energy calculations for square-planar co-ordination of the ligand)[22].

Ligand	Ideal M-N length/ Å	Deviation from ideal N_4 plane./ Å
[12]aneN$_4$	1.83	±0.41
[13]aneN$_4$	1.92	±0.12
[14]aneN$_4$	2.07	0.00
[15]aneN$_4$	2.22	±0.14
[16]aneN$_4$	2.38	0.00

Figure 1.1.2.

Enthalpies of formation for cyclic polyamine ligands[27].

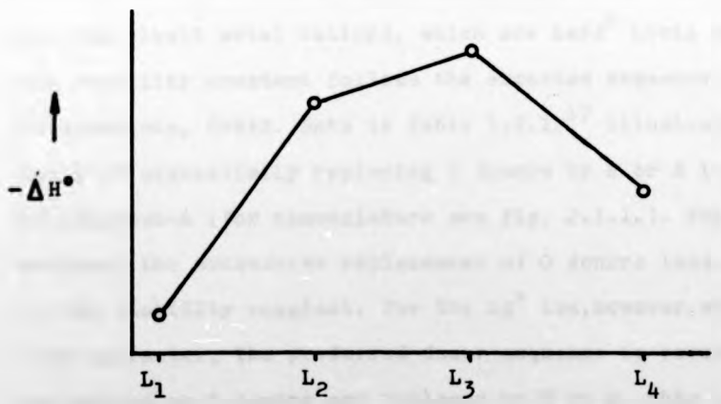

L_1-L_4 = [12], [13], [14], [15]aneN$_4$. (Ring sizes above)

tetragonal polyamine complexes ranges from 2.03 to 2.10Å[26] and we would therefore predict, based on Table 1.1.1., that the Cu^{2+} ion would be of an ideal size for the ligand [14]aneN$_4$. A microcalorimetric study of the enthalpies of formation of copper(II) complexes with tetra -aza ligands [12],[13],[14], and [15]aneN$_4$[27] has indicated just this predicted behaviour, with [14]aneN$_4$ forming a complex with the largest $-\Delta H^{\bullet}$ value (Fig 1.1.2.). Similar studies with Zn^{2+} [27,28] and Hg^{2+} [29,30] have, however, failed to produce such clear-cut results and this may well be due to the problem mentioned above, that with these larger metals which have no strong preference for planar co-ordination of the macrocycle totally different ligand geometries may exist for the different cavity sizes. It becomes increasingly clear that factors other than cavity/cation size become more important as one progresses from the simple 'crown' ether-alkali to more rigid macrocycle-transition metal complexes, and such factors are discussed below.

SECTION 1.2 DONOR ATOM TYPE AND NUMBER

The stability of macrocyclic complexes is found to markedly depend on the nature of the donor atoms situated in the binding site. For the alkali metal cations, which are hard[8] Lewis acids, the value of the stability constant follows the expected sequence for electrostatic interactions, O>N>S. Data in Table 1.2.1.[17] illustrates the effect on log K of sequentially replacing O donors by N or S in the 1,10 positions of 18-crown-6 (for nomenclature see Fig. 2.1.1.). For the K^+ ion in methanol the successive replacement of O donors leads to a 10^5 decrease in the stability constant. For the Ag^+ ion,however,which has significant soft character, the preferred donor sequence is reversed, the stability increasing as O donors are replaced by N or S. This is attributable to to the increased covalent character of the metal-donor bond for such

Table 1.2.1.

Stability constants (log. K) for the formation of 1:1 complexes with the ligands $A(CH_2CH_2OCH_2CH_2OCH_2CH_2)_2B$ (see figure 2.1.1. for similar ligands.)

A	B	K^+ in H_2O	Ag^+ in MeCH
O	O	6.10	1.60
NH	O	3.90	3.30
NH	NH	2.04	7.80
S	S	1.15	4.34

soft cations with soft donors. It follows, therefore, that the macrocycles containing soft donor atoms will necessarily tend to form complexes with more regular geometries (octahedral, tetrahedral, square planar etc.) by virtue of this covalency.The overall mode of macrocycle co-ordination in suchcases is therefore likely to be severly restricted since, for the first row transition metals at least, six-co-ordination tends to be the maximum and therefore inclusion of more than six soft donor sites within a single macrocycle, even if co-ordination of such were sterically possible, seems unlikely to increase the stability of the complex, and by virtue of the considerations in Section 1.1. will probably lessen it.

SECTION 1.3 THE MACROCYCLIC EFFECT

As outlined above, macrocyclic ligands produce marked changes in the properties of their metal complexes when compared to those of the equivalent linear ligands. The origin of the high thermodynamic stability,as reflected in the stability constants of macrocyclic complexes[30,31] (which can be several orders of magnitude greater than the corresponding linear ligand complexes), has been the subject of much investigation and controversy.

In 1969[32] it was found that the stability constant for the copper (II) complex of Me_6-[14]aneN_4, log K = 28, was much higher than that found for the similar non-cyclic ligand 2,3,2-tet, log K = 23.9, Table 1.3.1. This large increase in stability cannot be attributed solely to the usual chelate effect[33], in terms of changes in translational entropy, and so was termed the 'macrocyclic effect'. (It is to be noted that the stability of the cyclic complex is greatly increased despite the more restricted geometry forced upon the metal-

nitrogen bonds by the macrocycle.)

The macrocyclic effect is a Gibbs energy term, referring to the metathetical reaction 1.3.1, and the enhanced stability of the

$$\underset{\text{non-cyclic}}{[ML]^{n+}} + \underset{\text{cyclic}}{L'} \longrightarrow \underset{\text{cyclic}}{[ML']^{n+}} + \underset{\text{non-cyclic}}{L} \qquad (1.3.1.)$$

macrocyclic complex[30] may have its basis in both enthalpy and entropy terms. Several attempts have been made to separate the effect into contributions from each term and one of the first was conducted on the copper(II) Me_6-[14]aneN_4 complex mentioned above. Because of the extreme inertness[34] of the complex, making conventional calorimetry impossible, it was not feasible to directly rationalize the contributions of $\Delta H^\bullet$ and $\Delta S^\bullet$ from the Gibbs-Helmholtz equation. However an approximate value of $\Delta H^\bullet$ can be obtained from spectroscopic correlations of the position of the visible absorption maxima for copper(II) polyamines[35,36], and for this complex such a process gives a $\Delta H^\bullet$ of about -126kJ mol^{-1} which is considerably higher than for corresponding linear tetra-amine complexes (Table 1.3.1.).

The value of $\Delta S^\bullet$ for the same complex, obtained from the Gibbs-Helmholtz equation using the value of $\Delta G^\bullet$[32] and $\Delta H^\bullet$ above, is about 113 J mol^{-1} K^{-1} which again is appreciably higher than is observed for linear tetra-amines (Table 1.3.1.). From these values it would appear that the macrocyclic effect is due in equal parts to both entropy and enthalpy effects but, since this early analysis, considerable controversy has arisen.

Using the temperature dependence of equilibrium data for the

Table 1.3.1.

Comparison of thermodynamic parameters for the formation of 1:1 complexes in aqueous media.

Complex	Log K	$\Delta H^{\bullet}$ kJ mol^{-1}	$\Delta S^{\bullet}$ J K^{-1} mol^{-1}	Ref.
$Ni(2,3,2\text{-tet})^{2+}$	15.3	-70.6	58.0	37
$Ni([14]aneN_4)^{2+}$	22.2	-130.0	-8.4	37
$Ni(5,12\text{-}Me_2\text{-}[14]aneN_4)^{2+}$	21.9	-117.0	33.6	37
$Cu(2,3,2\text{-tet})^{2+}$	23.9	-116.0	24.4	38
$Cu(Me_6\text{-}[14]aneN_4)^{2+}$	28.0	-126.0	113.0	32
$Cu([12]aneN_4)^{2+}$	24.8	-77.0	216.0	39
$Cu([12]aneN_4)^{2+}$	24.8	-95.3	152.0	27
$Cu([13]aneN_4)^{2+}$	29.1	-122.7	141.0	42
$Cu([14]aneN_4)^{2+}$	27.2	-127.7	95.0	30
$Cu([15]aneN_4)^{2+}$	24.4	-111.3	95.0	27

system Ni(II)-[14]aneN$_4$, Hinz and Margerum[37] obtained a value of log K = 22.2 with $\Delta H^\bullet$ = -130 kJ mol^{-1} and $\Delta S^\bullet$ = -8.4 J mol^{-1} K^{-1}. In this case a comparison with values for typical linear tetra-amine nickel(II) complexes (Table 1.3.1.) shows that the enhanced stability is due almost entirely to the enthalpic contribution.

Kodama and Kimura[39], however, reached the opposite conclusion for copper(II) co-ordinating with [12]aneN$_4$ that the entropy term was solely responsible (Table 1.3.1.). The method employed by both sets of workers for determining $\Delta H^\bullet$, from the temperature dependence of equilibrium data, is at best only approximate since small errors in the equilibrium constants may result in very large errors in $\Delta H^\bullet$ and ideally, more direct methods of determining enthalpies are desirable. Calorimetric determination of $\Delta H^\bullet$ is one such method but has previously appeared impossible for metal-macrocycle complexes since both formation and destruction (with H^+ or $[CN]^-$) of such complexes are extremely slow, too slow for conventional calorimeters.

Very recently however the experimental difficulties have been overcome using microcalorimetric techniques[40,41] at high pH, and more accurate estimates of the enthalpic contribution to the macrocyclic effect have been achieved. Results (Table 1.3.1.) from this work[27] on copper(II) complexes with [12], and [15]aneN$_4$ seem to vindicate the original hypothesis that both enthalpic and entropic terms make significant contributions to the overall macrocyclic effect, but with the added condition that a favourable enthalpy term is critically dependent on matching the size of the metal ion to that of the aperture in the macrocyclic ligand as discussed in Section 1.1. above.

Conclusions drawn from such findings are tentative but the

favourable nature of both $\Delta H^\bullet$ and $\Delta S^\bullet$ for metal-macrocycle complexes, leading to the macrocyclic effect, may be summarised as follows:

a) A favourable $\Delta H^\bullet$ is an indication that an arrangement in which the chelate rings are fused in a cyclic fashionis favoured only when no severe mismatch between metal ion size and hole size occurs in the complex.

b) A favourable $\Delta H^\bullet$ is also said to reflect the increased relative strength of the co-ordinate bonds in macrocycle complexes resulting from the increased ligand-field strength of the donors when constrained in a ring.

c) A favourable $\Delta S^\bullet$ is interpreted as follows. When a linear ligand co-ordinates to a metal ion it goes from a state in which it has many possible configurations (degrees of freedom) to one in which its configuration is fixed, with a concommitant loss of entropy. However, with a macrocycle, where the donor atoms are already more severely constrained by the cyclic nature of the ligand, much less entropy is lost on co-ordination and so macrocycles would always be expected to show a favourable entropy term for complex formation.

d) Both $\Delta H^\bullet$ and $\Delta S^\bullet$ are favourable if one considers ligand solvation effects. Work by Margerum[43] on a nickel(II) tetra-thiaether macrocycle complex has indicated only a slight macrocyclic effect (ratio of $K_{cyclic}/K_{linear} = 180 \pm 70$) in a non-aqueous solvent (nitromethane) where ligand solvation is likely to be less important. Although the treatment of this system was oversimplified in light of work reported later in this thesis (Chapter 2, Section 2.), the evidence that ligand solvation is more important for linear than for cyclic ligands in donor solvents leads again to the conclusion that both $\Delta H^\bullet$ and $\Delta S^\bullet$

favourable nature of both $\Delta H^{\bullet}$ and $\Delta S^{\bullet}$ for metal-macrocycle complexes, leading to the macrocyclic effect, may be summarised as follows:

a) A favourable $\Delta H^{\bullet}$ is an indication that an arrangement in which the chelate rings are fused in a cyclic fashionis favoured only when no severe mismatch between metal ion size and hole size occurs in the complex.

b) A favourable $\Delta H^{\bullet}$ is also said to reflect the increased relative strength of the co-ordinate bonds in macrocycle complexes resulting from the increased ligand-field strength of the donors when constrained in a ring.

c) A favourable $\Delta S^{\bullet}$ is interpreted as follows. When a linear ligand co-ordinates to a metal ion it goes from a state in which it has many possible configurations (degrees of freedom) to one in which its configuration is fixed, with a concommitant loss of entropy. However, with a macrocycle, where the donor atoms are already more severely constrained by the cyclic nature of the ligand, much less entropy is lost on co-ordination and so macrocycles would always be expected to show a favourable entropy term for complex formation.

d) Both $\Delta H^{\bullet}$ and $\Delta S^{\bullet}$ are favourable if one considers ligand solvation effects. Work by Margerum[43] on a nickel(II) tetra-thiaether macrocycle complex has indicated only a slight macrocyclic effect (ratio of $K_{cyclic}/K_{linear} = 180 \pm 70$) in a non-aqueous solvent (nitromethane) where ligand solvation is likely to be less important. Although the treatment of this system was oversimplified in light of work reported later in this thesis (Chapter 2, Section 2.), the evidence that ligand solvation is more important for linear than for cyclic ligands in donor solvents leads again to the conclusion that both $\Delta H^{\bullet}$ and $\Delta S^{\bullet}$

contributions, this time from solvation phenomena, are important to the overall effect.

SECTION 1.4 SPECTROCHEMICAL EFFECTS

Extensive papers by Busch et al[22,44,45] have recently appeared in which the contributions of macrocyclic ring-size effects to the spectrochemical properties of transition-metal ions are explored. Results for both Co(III)[22,44] and Ni(II)[45,46] indicate a pronounced variation of the quantity Dq^{xy}, the in-plane ligand-field splitting parameter, with various tetra-aza macrocyclic ring sizes (Table 1.4.1.) The quantity Dq^{xy} can be derived from Gaussian analysis, and subsequent data reduction, of the electronic spectra of the complexes[24,25]. $10Dq^{xy}$ corresponds to the orbital splitting (in the strong ligand-field model[47]) between the d_{xy} orbital, which is usually non-bonding, and the $d_{x^2-y^2}$ orbital which is strongly σ-antibonding. In the simplest cases, Dq^{xy} varies directly with the extent of σ-bonding in the macrocycle plane and therefore gives a measure of the efficacy of the macrocycle as a ligand.

Selected results from this work[44,45] are illustrated in Table 1.4.1. and it is clear that Dq^{xy} is strongly dependent on ring-size, varying in the sequence $[13]aneN_4 > [14]aneN_4 > [15]aneN_4 > [16]aneN_4$ for both Co(III) and Ni(II). It is well known that the chelate[48] and macrocyclic[27] effects may have an enthalpy contribution, suggesting that bonding may change for the same donor atom depending on other geometric constraints within the molecule. This assumption is dramatised by the data cited in Table 1.4.1. where geometric constraints within a constant microsymmetry can change Dq^{xy} over a range of 33% of its low value (Ni(II)).

Table 1.4.1.

Ligand-field splitting parameters (Dq^{xy}) for trans-dichloro tetra-amine complexes of Co(III) and Ni(II).

Ligand	$Dq^{xy}/(cm^{-1})$		Ideal M-N/(Å)[c]
	Co(III)[a]	Ni(II)[b]	
[13]aneN$_4$	2750	--	1.92
[14]aneN$_4$	2562	1480	2.07
[15]aneN$_4$	2421	1242	2.22
[16]aneN$_4$	2341	1116	2.38
(en)$_2$	2530[d]	--	Unconstrained
(Me$_2$en)$_2$	--	1215[e]	Unconstrained

N.B. Typical values of M-N distances in unconstrained systems are, Co(III) 1.94-2.03Å[51] and Ni(II) high-spin 2.12Å[52]. There is, therefore, a clear correlation between optimum M-N distance and ligand-field splitting parameters such that [14]aneN$_4$ is best for Co(III) and [15]aneN$_4$ is best for Ni(II).

References:

a) 44 b) 45 c) 22 d) 49 e) 50

These results clearly demonstrate the large effect of ring-size on the ligand-field strengths of donor atoms in complexes with macrocyclic ligands. Although a good correlation between the normal metal-donor distance and the most favourable hole size (Table 1.1.1.) for a given macrocycle facilitates binding with normal ligand-field strengths, poor fits between ring and cation size lead to alterations in the metal-donor bond. This effect may be very large when the fit is poor and so the ligand-field strength may be greatly increased or decreased by an inadequate fit between metal and ring.

It is interesting to note that these results irrefutably demonstrate that mechanical constraint, of molecular origin, on the metal-donor bond can have a profound effect on the strength of that interaction. Such results may have important consequences in the understanding of natural systems, e.g. tertiary structure of proteins around metal binding sites, which may produce similar constraints in order to modify the characteristics of a co-ordinated metal ion.

SECTION 1.5 ELECTROCHEMICAL PROPERTIES

The ability of macrocycles to stabilize a range of oxidation states for a given metal ion has been clearly demonstrated by Olson and Vasilevskis[53,54]. In these studies they have prepared and isolated stable oxidation states of +1, +2 and +3 for both nickel[53] and copper[54] complexes of the saturated tetra-amine ligand Me_6-[14]aneN_4, and subsequent work by Busch[55], on Fe, and Endicott[56], on Fe Co Ni Cu and Zn, has proven the generality of these observations.

The redox properties of metal complexes with macrocyclic ligands

are closely related to their spectrochemical properties mentioned in the previous section, since both are primarily dependent on ring-size effects, and the unusual oxidation states of the metal ions in such complexes are stabilised by having constrained metal-donor distances. The redox potentials between oxidation states are similarly ring-size dependent and the simplest explanation of these properties is that the metal ion will tend to adjust its size (ionic radius), by oxidation or reduction, so as to compromise between fitting ideally into the ring[22] and producing acceptable redox potentials for the resulting complex. The recognition of this property of macrocyclic ligands has lead to an extensive study of the electrochemistry of their metal complexes, as it is likely to have a direct bearing on much of their reactivity (e.g. ligand substitution, metal alkylation etc.) where lower or higher oxidation states of the metal may function as reactive intermediates.

The correlation between ring-size and electrochemistry has been under increasing investigation; for example electrochemical studies[57] show that the Ni(II)/Ni(III) couple shifts towards greater stability for the trivalent state as the macrocycle ring-size decreases ($E_{\frac{1}{2}}$ = +1.3, +0.9, +0.69 volts for [16], [15] and [14]aneN$_4$ respectively). similarly the Ni(I)/Ni(II) couple progressively favours the monovalent ion as the ring-size increases ($E_{\frac{1}{2}}$ = -1.7, -1.57, -1.4 volts for [14], [15] and [16]aneN$_4$ respectively). These results are consistent with the expected changes in metal ion size with oxidation state.

Complexes of silver(I)[58] with the macrocycles [14]aneN$_4$, Me$_6$-[14]aneN$_4$ and NMe$_4$-[14]aneN$_4$, disproportionate to give the silver(II) complex of the macrocycle, and metallic silver. The fact

that the Ag(I)/Ag(II) couple lies well on the side of the divalent state is clear indication of the constricting effect of the 14-membered ring upon the large Ag^{+} ion. This results in spontaneous oxidation to produce the smaller Ag^{2+} ion, so as to allow stronger co-ordination of the ring by producing a better fit between metal and hole-size. Indeed, further oxidation to give Ag^{3+}, diamagnetic d^{8}, complexes of the macrocycle is possible (e.g. with conc. HNO_3 or $[NO][ClO_4]$) so demonstrating the same effect, although these complexes are strongly oxidising.

Low temperature electrochemical oxidation of a mercury(II) complex of [14]aneN$_4$ produces a short lived species which has been identified, by e.s.r. and electronic spectroscopy, as mercury(III) ($t_{\frac{1}{2}}$ of Hg([14]aneN$_4$)$^{3+}$ = 5 sec at 195K)[59]. This unique example of Hg(III) again illustrates the strong driving force towards producing a good fit between metal and ring, the large Hg(II) d^{10} ion being oxidised to the smaller Hg(III) d^{9} ion in order to become accommodated within the macrocycle.

Such studies have not been restricted to tetra-amine ligands and an investigation of the redox properties of copper thiaether complexes (e.g. [14],[15],[16]aneS$_4$), with special regard to the blue copper proteins, has been carried out to determine the Cu(I)/Cu(II) couple in relation to ring-size[60]. Again, this type of study is important in the understanding of biological processes since it illustrates how the constraints applied by a macrocycle can influence the oxidation state of a metal. This behaviour is mimicked <u>in vivo</u> by the binding sites of metallo-proteins and enzymes whose functions are highly dependent on redox properties.

The ability of macrocycles to produce and stabilise unusual oxidation states has been put to synthetic use by Chan and Poon[61] who have prepared complexes containing Mn(III), Fe(III) and Ni(III) with the macrocycle [14]aneN$_4$ all of which are air-stable solid trans-diacido complexes.

SECTION 2. SYNTHETIC MACROCYCLES.

Having now outlined the general properties of metal complexes with macrocyclic ligands, it is possible to review, against this background, the various classes of synthetic macrocycles which are available. Synthetic macrocycles may be divided into four broad classes according to donor atom type.

SECTION 2.1 POLYETHERS.

Included in this section are the cyclic polyether 'crown' and 'cryptate' type ligands (Figures 2.1.1 and 2.1.2 respectively) incorporating mainly hard, class A, oxygen donor atoms with a nomenclature illustrated in the figures. These ligands are very important in the area of non-transition, mainly alkali-metal chemistry, especially in relation to their similarity with certain naturally occuring antibiotics such as valinomycin and the actins[62]. The ion-transport and phase-transfer properties of such synthetic macrocycles has correspondingly received a great deal of attention since the first publication, by Pedersen in 1967[63], of synthetic procedures to 50 cyclic polyethers. Pedersen exploited the unexpected side reaction below (Scheme 2.1.1.) to produce polyethers such as A with the number of ring and donor atoms ranging from 9 (3 oxygen) to 30 (10 oxygen).

Figure 2.1.1.

Representative Crown ethers and their nomenclature.

a) 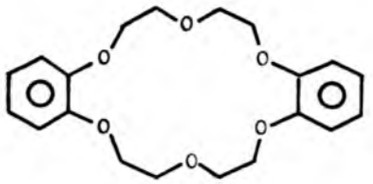

Dibenzo-18-crown-6

Dibenzo describes the non-ethyleneoxy content; 18, the total number of atoms in the crown ring and 6, the number of heteroatoms in the ring.

b) 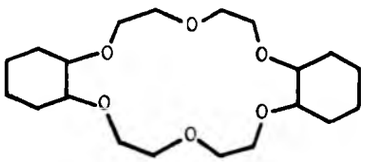

Dicyclohexyl-18-crown-6.

c) 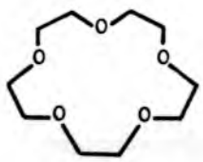

15-crown-5.

d) 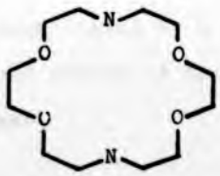

1,10-diaza-18-crown-6.

Figure 2.1.2.

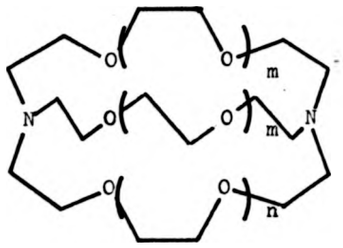

(1.1.1.) m:n: 0.
(2.1.1.) m: 0; n: 1.
(2.2.1.) m: 1; n: 0.
(2.2.2.) m:n: 1.
etc.

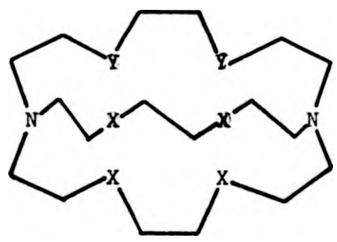

(2o.2o.2s.) X: O; Y: S.
(2o.2os.2s.) 3X: O; X,2Y: S.
(2o.2o.2n.) X: O; Y: NCH_3.
(2.2.C_8) X: O; Y: CH_2.

Representative cryptates and their nomenclature.

Systematic naming of bicyclic amines is long and complex and J.M. Lehn designates each ligand by a symbol given in brackets[70]. These give the number and nature of the heteroatoms and other structural variations of the bridges.

Scheme 2.1.1.

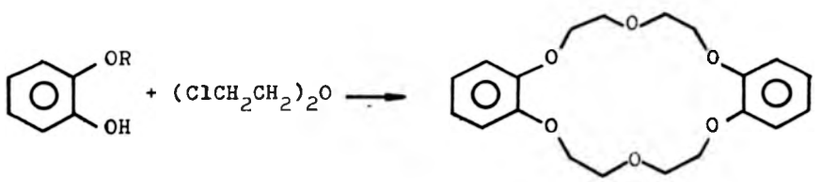

Dibenzo-18-crown-6. A

The discovery that these compounds, insoluble in hydroxylic solvents, could be solubilized by the addition of alkali metal ions lead to the realisation that thesemacrocycles were acting as complexing agents for such cations and, as such, closely mimicked the properties of known antibiotic molecules (e.g. from fungal sources) capable of transporting Na^+,K^+ in vivo. X-ray crystal studies on naturally occuring antibiotics[64] and synthetic macrocycles[20,21,65] of this type confirm the basic similarity of both in their mode of co-ordination to alkali metal cations. The similarity between the crystal structure, with the metal ion situated at the centre of inwardly orientated oxygen donors surrounded by a puckered alkane ring, and a royal crown lead to the coining of the term 'crown' ethers to describe this class of synthetic macrocycles and the resulting nomenclature is illustrated in figure 2.1.1. The 'crown' ether field has flourished in recent years with the identification of three types of metal:ligand ratios in their complexes with cations[63,66]. The 1:1 (doughnut), 1:2 (sandwich) and 2:3 (club sandwich) complexes have all been isolated and the whole area has been extensively reviewed[67].

Movement away from the two-dimensional circular cavities of the 'crowns' and towards the three-dimensional macropolycyclic cryptates[68]

(Figure 2.1.2.) has taken place in recent years. These rigid cage, usually bicyclic, ligands contain both amine and oxygen donor atoms and their nomenclature is illustrated in fig. 2.1.2. These ligands form inclusion complexes in which the substrate cation is contained inside the, essentially spherical, cavity (or crypt) and this leads to their ability to define co-ordination sites of finite diameter giving much more specific metal complexation than the crown ethers[69]. Cations of diameter larger than the optimum may be excluded from the cage while smaller cations 'rattle' around inside the cavity forming only weak complexes. Again, the area has very recently been reviewed by Lehn[70] and this range of ligands is being extended by replacing hard oxygen donors by nitrogen and thiaether atoms, so producing ligands (e.g. sepulchrates) capable of trapping transition metal ions such as Co(III)[71]. The co-ordination properties of these latter ligands should prove to be increasingly important in coming years, especially in relation to their selective complexation of toxic heavy metal cations[70,72,73].

The stuctural co-ordination chemistry of the polyether type of macrocycle in general has recently been under investigation by a variety of techniques including ^{13}C n.m.r.[74] and I.R. spectroscopy[75]. The x-ray structure of a strontium complex with an N_2O_4 Schiffs-base macrocycle containing a furanyl residue (Figure 2.1.3. below) displays nona-co-ordination of the cation with the macrocycle co-ordinated roughly in a plane with one water and two thiocyanate molecules completing the co-ordination above and below the plane[76]. This macrocycle is interesting as it is one of the few examples of a

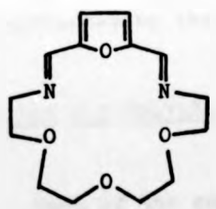

Figure 2.1.3.

predominantly polyether ligand prepared by a 'template' synthesis. Here the strontium atom organises the reactant molecules prior to their cyclisation whilst still co-ordinated, and this type of synthetic procedure is becoming increasingly important, especially for the polyaza type of macrocycle (Section 2.2.).

Complexes of dibenzo- and dicyclohexyl-18-crown-6 (a and b figure 2.1.1.) with copper(II) have been prepared and their electronic spectra studied in order to elucidate the structure and possible biological relevance of the binding site (*cf.* blue copper proteins)[77]. This area of complexes other than with the alkali metals or alkaline earths has been broadened[78] and extrapolated to the lanthanides[79] and actinides[80] such that the whole field of polyether co-ordination chemistry is now expanding very rapidly.

Crown ethers have found application in organic synthesis[81] where their ability to surround a cation, thereby conferring lipophilicity and hence solubility in organic media upon that cation, mean that the associated anion may also be carried into solution at the same time. This process renders previously organic insoluble bases, such as KOH, soluble in aprotic media allowing previously impossible synthetic procedures to take place by means of this phase-transfer catalysis[82]. Overall, the polyether area is yet rich in unmined chemistry and this is reflected by the great activity in the field[67].

SECTION 2.2 POLYAZA MACROCYCLES.

Much of the general chemistry of this class of macrocycles, especially the saturated quadridentate members, has been used to illustrate the properties of macrocycles in Section 1 and this section

will therefore be confined to synthetic procedures for, and unusual reactivity of , such rings.

Two distinct synthetic methods have been applied to the preparation of polyaza macrocycles a) standard organic synthesis and b) metal ion 'template' reactions.

a) The organic synthetic procedures leading to macrocycles are typified by multistep reaction schemes leading to a linear precursor of the ring followed by a ring-closure step carried out at high dilution in order to avoid polymerisation side reactions. This final step is usually very low yielding making the whole synthesis not only tedious but frustrating (yields typically <10% overall) and so, much investigatio into improving the yields of the ring closure step has taken place.

One of the most deliberate syntheses of simple, saturated polyaza macrocycles involves the condensation of tosylated reactants in DMF at 100°C[83]. Scheme 2.2.1.

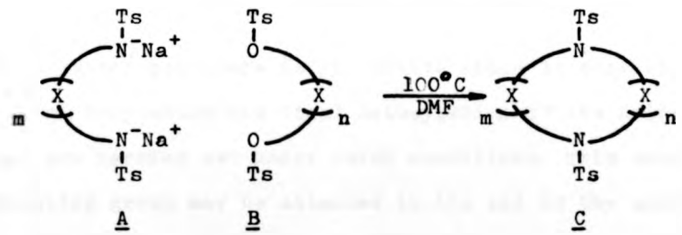

A B C

Ts = p-toluene sulphonyl. X = O or N-Ts m=n = 1→3

Scheme 2.2.1.

The reaction takes advantage of the increased acidity of primary sulphonamide groups to make the nucleophilic sodium salt A. This readily

displaces the OTs leaving group from B and, if carried out in aprotic media (DMF, HMPA, DMSO) , cyclisation in 80% yield occurs to produce the tosylated macrocycle C. Removal of the tosyl groups in conc. H_2SO_4 gives the protonated amine, and this method has found general application[84].

More recently, a ring-closure procedure utilising the formation of amide linkages, with subsequent reduction to give simple saturated amine macrocycles, has been reported[85,86], Scheme 2.2.2.

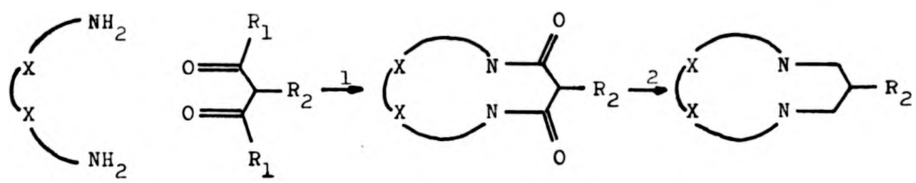

X = NH or O R_1 = Cl or OEt R_2 = any substituent group

1 = reflux. 2 = B_2H_6/THF Reflux 24 hrs.

Scheme 2.2.2.

This latter procedure is attractive since it does not require the initial tosylation and final detosylation of the amine groups, both of which are carried out under harsh conditions. This means that a co-ordinating group may be attached to the end of the substituent R_2, so producing interesting quinquedentate macrocycles with a dangling arm. Such macrocycles are likely to be of importance in the chelation therapy of methylmercury(II) and the field is only just developing, no metal complexes having been reported as yet. Very recently however, unsaturated tetra-aza rings with a dangling arm attached to one of the amine nitrogen have been reported; these complex with Ni, Cu, and Zn, and interesting

structural phenomena have been observed[87].

b) The second, and increasingly more common[88], method of synthesis involves the use of template methods. Here, one of the macrocycle precursors is co-ordinated to a central metal atom which holds this reactant in a fixed geometry, favourable for eventual ring formation. The ringclosing step is carried out whilst the reactants are still co-ordinated- the juxtaposition of the reacting groups being held by the metal so as to facilitate macrocycle formation and disfavour polymerisation.

The most commonly used method of ring-closure in template syntheses is Schiffs-base condensation of a diketone with the co-ordinated primary amine ends of a linear multidentate ligand. The reaction is well illustrated in the synthesis of $[14]aneN_4$[89] shown in Scheme 2.2.3. where the diketone glyoxal condenses to produce the di-imine **A**.

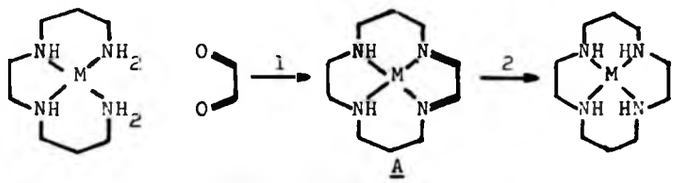

A

M = Ni. 1) H_2O, cool to 5°C, 4hrs. 2) BH_4^-, 5°C.

Scheme 2.2.3.

Subsequent reduction with $[BH_4]^-$ gives good yields of the nickel complex of the saturated ligand. It is clear that this type of synthesis is more elegant than conventional organic methods since high-dilution is not necessary in order to obtain reasonable yields in the final ring-closure. The method does, however, have one drawback in that to obtain

the free macrocycle one must remove the metal ion template. In this instance Ni^{2+} can easily be removed by treatment of the complex with excess $[CN]^-$, but in some cases any attempt to remove the metal results in ring opening of the macrocycle, especially where unreduced imine linkages still remain (see below).

One of the most elegant examples of the template effect is provided by the syntheses of Curtis *et al.*[90] who have used simple diamines and acetone to produce multi-substituted macrocycles of many sizes by simply allowing the metal complexes of the amines to stand in acetone for long periods. A typical synthesis of this type is illustrated in Scheme 2.2.4. and the whole area has been reviewed[90].

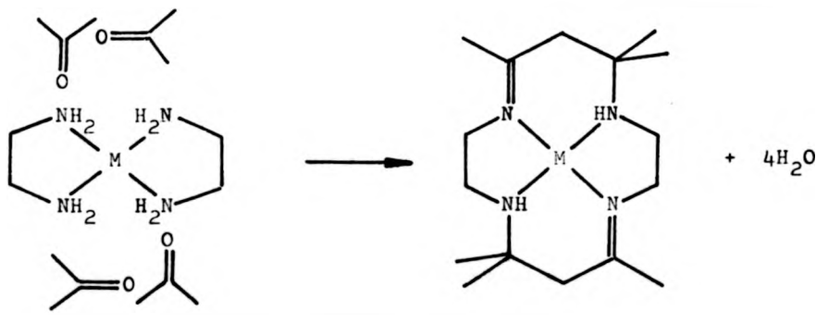

Scheme 2.2.4.

Many examples of macrocycles containing 2,6-pyridine residues are now available[88,91], and almost all are prepared by template Schiffs-base condensations of 2,6-diacetyl-pyridine with a co-ordinated linear amine. Scheme 2.2.5. (overleaf).

It is often the case with such macrocycles that removal of the central metal template ion leads to eventual decomposition of the imine linkages, with associated ring-opening in hydroxylic solvents via

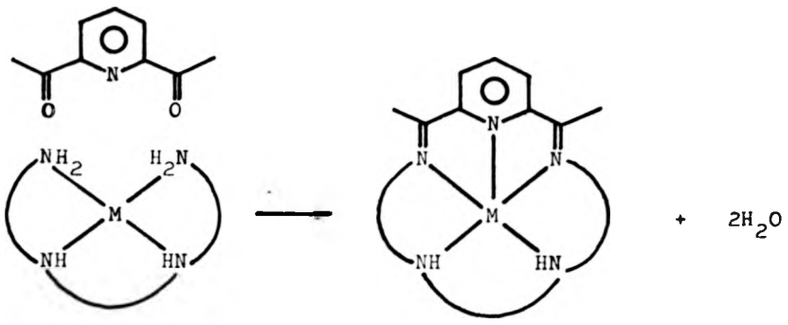

Scheme 2.2.5.

solvent attack at the imine carbons[92]. This makes isolation of the free macrocycle and investigation of metal complexes with non-template metals very difficult. Macrocycle syntheses in general have been extensively reviewed[16].

Many metals have found use in template reactions, although Ni(II) and Cu(II), because of their strong tendency for planar co-ordination, have been the most common[90]. Other transition metals have become increasingly popular especially for the polyaza macrocycles[93], and more recently non-transition metals such as Mg(II)[94] and Pb(II)[95] have found applications in the template synthesis of polyaza/polyether macrocycles, following scheme 2.2.5. above.

Although the structural chemistry of these polyaza macrocycles, as studied by X-ray techniques, has shown many unusual co-ordination geometries[96,97], the reactivity of such complexes is, perhaps, even more interesting. For example, Busch et al. have recently reported an extraordinary reaction between the iron(II) complexes of 15 and 16 membered tetra-aza unsaturated macrocycles and the two co-ordinated acetonitrile molecules which complete the co-ordination sphere

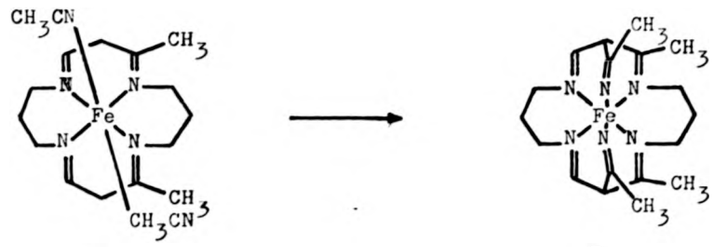

A B

Scheme 2.2.6.

of the metal Scheme 2.2.6.[98,99]

The formation of the novel sexadentate ligand in B, by the electrophilic attack of the co-ordinated nitrile upon the γ carbon of the macrocycle, is remarkable in view of the chemical properties of nitriles. This mode of electrophilic activation of co-ordinated nitriles is under considerable investigation[98]. Other examples of the reactivity of co-ordinated macrocycles are rare, although one report of electrophilic substitution at a 14-membered tetra-aza macrocycle complexed to Ni(II) has appeared. The ring unsaturation is very similar to that shown in A scheme 2.2.6. above, and again, electrophilic attack at the γ position, this time by diazonium ions, occurs.[100]

Recently, interest has begun to focus on the organo-metallic chemistry of poly-aza macrocyclic complexes, and several such complexes have been studied. Treatment of the nickel(II) complex of a saturated tetra-aza ring with dimethyl magnesium results in the formation of a 5-co-ordinate 'square-pyramidal' complex containing a nickel-methyl bond. This rare example of a high-spin nickel(II) alkyl complex is stable under N_2 and in nucleophilic solvents, but decomposes slowly in water, evolving methane[101]. Endicott has studied the photochemical kinetics of cobalt-alkyl bond cleavage in a series of complexes containin 14-membered tetra-aza macrocycles, and correlated the kinetic data to

produce a coherent orbital energy level scheme accommodating the weak Co-CH_3 bond and most of the spectroscopic properties[102]. This latter study has obvious relevance to methyl-cobalamin and vitamin B_{12} chemistry where the geometric environment of the metal is similar. A metal-metal bond has been inferred from the X-ray structure of a tetra-aza macrocycle simultaneously complexed, in a bidentate manner, to two rhodium dicarbonyl groups and it is possible that such a geometry involving 'vacant' co-ordination sites at two, close, fixed rhodium atoms may have very interesting catalytic properties[103].

Conventional kinetics for both the macrocycle and associated monodentate ligands, which total the co-ordination sphere of the central metal ion have been studied for many years. For example, cis-Trans isomerisation of a quadridentate macrocycle on Co(III)[104] and the aquations and anations of unidentate ligands in cis[105] and trans[106,107] formsof the same molecule have all been studied with mechanistic interpretation of the results in terms of structure (see Chapter 3, section 2 for a more detailed discussion.)

Polyaza macrocycles have been used in two studies of direct relevance to the theme of this thesis, where the complexing properties with heavy metal ions have been explored. Stetter and Frank[108] made potentiometric evaluations of the stability constants for the 1:1 complexes of the ligand L_a, shown below, with dipositive metal ions including those of Zn, Pb, Cd. This potentially octadentate macrocycle

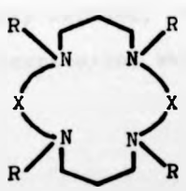

L_a: R= CH_2COOH, X= $(CH_2)_2$

L_b: R= CO- 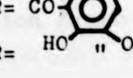 , X= "

L_c: R= HO " OH, X= $(CH_2)_3$

was found to form less stable complexes with these metals than did E.D.T.A. making it less attractive as a chemotherapeutic chelate. Studies with the ligands, L_b, L_c above, indicate however that they may act as specific sequestring agents for the actinides[109]. Utilising the biomimetric design principle, 2,3-dihydroxybenzoyl groups were attached to the macrocyclic amine nitrogen atoms in order to copy known biological binding sites e.g. enterobactin. The resulting ligand, L_c, complexes with Pu(IV) with a formation constant $>10^{52}$ suggesting that this class of ligand will be of increasing importance for chelation therapy purposes. For this reason it is felt that structural and kinetic characterisations of complexes formed with macrocyclic ligands are important background parameters to be established.

SECTION 2.3 POLYTHIAETHER MACROCYCLES.

The sulphur containing macrocycles have been little explored when compared to the enormous amount of work with poly-ether and aza ligands reported in the previous two sections. This is due,in part, to the more difficult syntheses involved in making members of this class but also because the chemistry of their complexes is not as rich.

Polythiaether macrocycles are almost exclusively synthesised by means of tedious multi-step procedures culminating in a last-step, low yielding, high-dilution ring closure. The low sulphur-active metal ion co-ordination renders template effects of little consequence. The competition between cyclisation and linear polymerisation is thus statistically defined, entropy constraints of cyclisation favoring linear polymerisation whereas high-dilution favours cyclisation kinetically.

Such syntheses typically involve the preparation of a linear multidentate chelate with terminal thiol groups[110], followed by ring closure by mercaptide displacement of a halide function. Such a synthesis is illustrated in Scheme 2.3.1. below for [14]aneS$_4$[111].

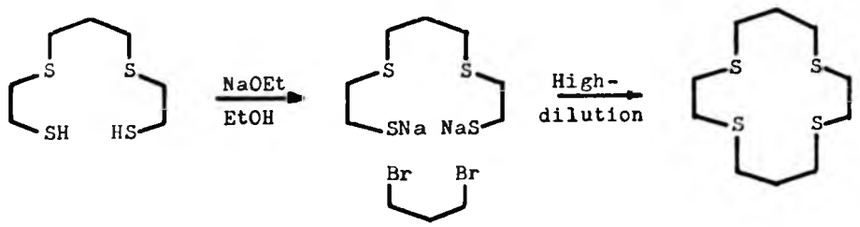

Scheme 2.3.1.

Identical synthetic methods have lead to a large variety of ring sizes containing differing numbers of thiaether[112,113], ether[114] and amine[115] donors. Relatively few macrocycles, containing exclusively sulphur donors, having unsaturation in the ring, similar to the pyridine containing macrocycles (Section 2.2.), have been synthesised. This is mainly because the introduction of unsaturation tends to lower the co-ordinative ability of the thiaether since the lone pairs on the sulphur atom become involved in π-bonding within the macrocycle framework, and hence do not donate so readily to a metal ion. One such ligand based on a 2,5-thiophene linkage has been synthesised and the resultingquadridentate ring co-ordinates to copper(II)[116]. Again, a similar synthetic procedure to that in scheme 2.3.1. is used and a catalogue of similar synthetic procedures for thiaether macrocycles has been produced[16].

The co-ordination chemistry of thiaether donors in general has been

the subject of several reviews[117,118,119] and, as expected, proves this type of donor to be best for the class b or soft metals. A common feature of the structural chemistry of such macrocycle complexes is the wide range of ligand geometries the macrocycle may adopt, for example the ligand [14]aneS$_4$ (Scheme 2.3.1.) can be mono-[120], bi-[121], tri-[122], or quadridentate[123] depending on the central metal and the presence of other co-ordinating anions. This facet of the chemistry is investigated in detail in Chapter 2 and is quite unlike that displayed by the polyaza macrocycles of the preceeding section 2.2.

The polythiaethers have found application as solvent extraction reagents for mercury(II) and silver(I) where initial complexation in aqueous media is followed by phase transfer to nitrobenzene[124]. Such behaviour closely mimics that of the polyether macrocycles with alkali cations as discussed in section 2.1., and the structural basis for this process and other chemical properties are explored in more detail in Chapter 2.

SECTION 2.4. POLYPHOSPHORUS MACROCYCLES.

Although chelating ligands containing phosphorus have long been known[117,125] it is only recently that synthetic macrocycles containing phosphorus donors have been prepared and their co-ordination chemistry is still very much in its infancy.

The introduction of more than one phosphorus atom into macrocyclic ligands is of potential interest in view of the known ability of phosphorus to stabilise low oxidation states. This property, in combination with the special properties of macrocyclic ligands (Section 1.5),

makes the attempt to synthesise polyphosphorus macrocycles an attractive one. Nelson et al.[126] have investigated the ability of several metal ions to promote the template synthesis of N_3P_2 pentadentate macrocycles Scheme 2.4.1.

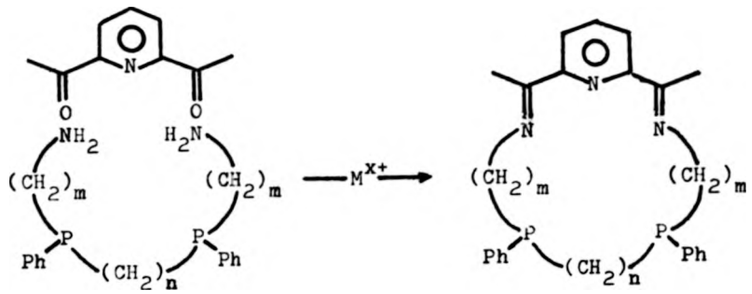

M^{x+} = Cd^{2+}, m=3 n=2 or m=n=3

M^{x+} = Ag^{+} , m=3 n=2 or m=n=3

Scheme 2.4.1.

Only silver(I) and cadmium(II) act as suitable template cations and both appear to form 5-co-ordinate complexes of unknown structure, although analogy with a similar N_3S_2 macrocycle indicates pentagonal planar co-ordination to be likely.

The synthesis of a tetra-phosphine macrocycle, the first containing only phosphorus donors, appeared in 1977 and is outlined in Scheme 2.4.2. below (ref. 127). The template reaction on nickel(II) produced the nickel complex of the macrocycle in 35-40% yield, and isolation of the free macrocycle (mac) by treatment with excess $[CN]^-$ yielded an air sensitive oil with physical properties consistent with the cyclic product. The nickel complexes $Ni(mac)X_2$, where X = Cl^-, $[SCN]^-$ are

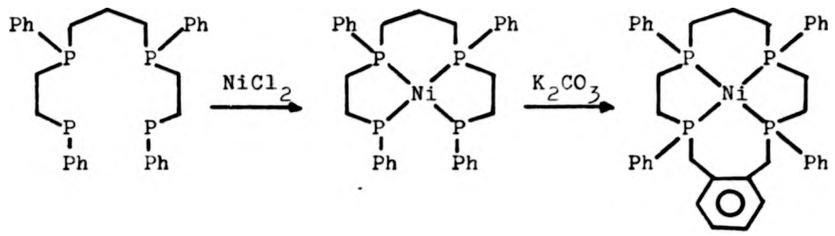

Scheme 2.4.2.

diamagnetic, 2:1 electrolytes in water suggesting the complexes are square-planar without axial ligation. Indeed, it has thus far proved to be impossible to induce any monodentate ligands to form tetragonal complexes, implying that the axial sites are relatively inaccessible for steric or electronic reasons.

At the same time that this first polyphosphine macrocycle was being reported, Kyba et al. reported the synthesis of several other phosphine containing rings[128]. Unlike the reaction in Scheme 2.4.2. which used nickel(II) as a template ion, Kyba made use of the high-dilution technique to induce ring closure as in Scheme 2.4.3.

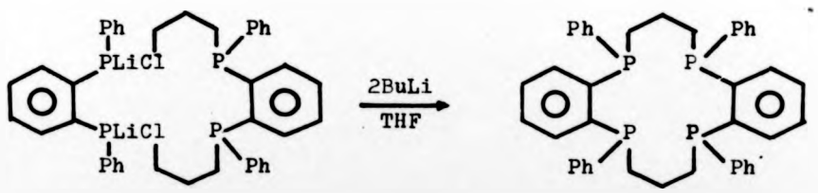

Scheme 2.4.3.

This procedure appears to have general application for production of a range of donor atoms and ring sizes for these air-sensitive macro-

cycles. Preliminary experiments indicate that these latter macrocycles will complex with molybdenum or chromium carbonyls and nickel salts to form 1:1 complexes. The results of these, and other[129], investigations will be of great interest in relation to the use of macrocycle-transition metal complexes as catalysts in organic reactions.

CHAPTER 2

SOME CO-ORDINATION CHEMISTRY OF 1,4,8,11-TETRA -THIACYCLOTETRADECANE, [14]ANE-S_4

SECTION 1. INTRODUCTION.

The co-ordination chemistry of thiaether donors has been reviewed by Livingstone[119] and M^{c}Auliffe[117] and attention is being paid increasingly to such compounds for several reasons: a) the interaction of metal ions with several sulphur centres is important biologically, e.g. in the enzyme nitrogenase[130], in the blue copper proteins (below); b) heavy donor atom chelates tend to encourage a wide-range of co-ordination geometries, often with unusual low-spin metal ions[132]; c) metal catalysed S-dealkylation reactions continue to intrigue inorganic chemists[131].

Although the metal complexes of open-chain thiaether chelates have been briefly investigated[133], the great majority of the work in this area has centred on the macrocyclic tetrathiaether class of ligand. Most of the chemistry of such macrocycles will be discussed in the following sections, but one early (and continuing) interest concerned their copper(II) complexes. A great deal of effort had been expended in the search for low molecular weight models for the blue copper proteins, such as plastocyanin, ceruloplasmin etc.[134], and it was only recently that copper(II) complexes of [12], [13], [14], [15] and [16]aneS_4 were synthesised and shown to be the first to not only mimic the spectral characteristics of these proteins, but also to exhibit similar redox potentials[60,135]. These results established two previously disputed points:

a) that simple thiaether sulphur atoms bonded to copper(II) are capable of producing spectra which mimic those of the relatively complex copper proteins, and

b) that distortion from tetragonal symmetry is not a requirement for producing these spectral similarities.

These findings have helped reawaken a more general interest in thiaether macrocycles and the structural co-ordination chemistry of these ligands with many other metals has now been studied. most of these studies have tended to concentrate on [14]aneS$_4$, as this ring-size has been established to be about optimum for the first row transition metal ions[136]. It was this ligand that was chosen as a starting point for the present work and the reasons for such a choice may be summarised as follows:

1) The considerations listed in the introduction to Chapter 1, as well as indicating a macrocycle to be a suitable specific ligand for the heavy metals, also suggested that the use of soft donor atoms such as thiaethers would enhance the selective properties of such ligands towards the soft metal ions of interest.

2) Since the metal ions of primary interest in this work are d^{10} ions with correspondingly no visible spectroscopy, n.m.r. spectroscopy was chosen as the best, routine technique for monitoring the solution structural chemistry of any heavy metal complexes prepared. Previous workers[137] have proven the power of ^{13}C n.m.r. as a tool for the inorganic chemist, where the spectral simplicity compared to that of equivalent ^{1}H spectra makes structural assignment and interpretation much easier. With this in mind, ^{13}C n.m.r. spectroscopy is clearly a good choice for the present investigation, and it is desirable, therefor that the particular macrocycle chosen for the work should be sufficientl symmetrical to make the ^{13}C n.m.r. spectra of its complexes not only simple, but also readily interpretable in terms of structure. As will become increasingly clear throughout this thesis, 14-membered saturated quadridentate ring systems fit this latter criterion perfectly and many structural types may be identified from the spectra of such rings.

3) The synthesis of this particular macrocycle, [14]aneS$_4$, and the

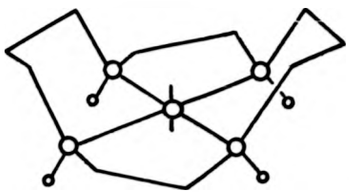

Trans-I

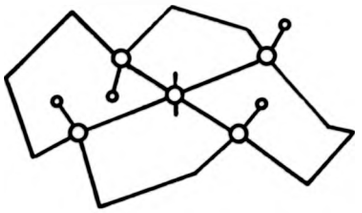

Trans-II

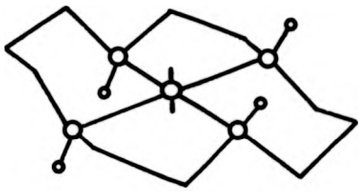

Trans-III

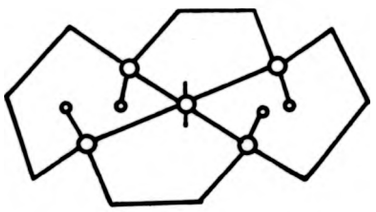

Trans-IV

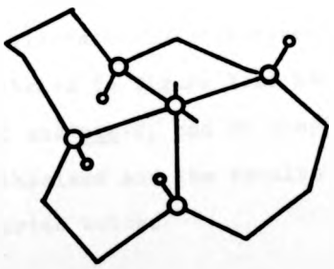

Cis-V

Figure 1.1.

Five idealised structures of strain-free octahedral complexes of quadridentate 14-membered saturated macrocycles.

structures of several metal complexes are well established in the literature and it was hoped that the ^{13}C n.m.r. characterisation of both the free ligand and its known complexes would provide a platform for predicting the structures of any novel heavy metal complexes prepared in the course of this work.

The conformations of 14-membered quadridentate macrocycles in octahedral complexes have been analysed by Bosnich *et al.*[138] who have predicted five possible strain-free structures as illustrated in Figure 1.1. It is clear that *trans* structures I to IV differ in their relative configurations at the co-ordinated sulphur atoms and so may be interconverted by appropriate sulphur configurational inversions. The fifth structure, *cis*-V, is related to the *trans* structures not only by sulphur inversions but also by metal-sulphur bond migration between adjacent octahedral sites. It was decided to synthesise as many of these structural types as were known and to record and interpret their ^{13}C n.m.r. spectra in order to provide a framework for the structural characterisation of the heavy metal complexes of direct interest to the present work. A literature search revealed that only two of the five possible geometries in figure 1.1. had been previously established , *trans*-III and *cis*-V, and so complexes with these ligand conformations were synthesised and the results of the ^{13}C n.m.r. investigations are reported below.

SECTION 2. COMPLEX WITH NICKEL(II).

The first ever metal complex of [14]aneS$_4$ was also the first of nickel(II) to be low-spin with four thiaether donors. The complex [Ni([14]aneS$_4$)](BF$_4$)$_2$ may be prepared by mixing hexakis-(acetic acid) nickel(II) fluoroborate with the macrocycle in dry nitromethane[111,139].

The complex forms immediately and crystallises from nitromethane/ether as a bright orange-red solid. This rather unusual synthetic procedure, utilising the hexakis-(acetic acid)nickel(II) ion in non-co-ordinating nitromethane, is necessitated by the low stability of the complex in the presence of donor solvents (H_2O, ethanol, DMSO) which react with the complex to give free macrocycle and solvated nickel(II) ion. Magnetism, conductivity and electronic spectroscopy of the complex all indicate it to contain diamagnetic square-planar nickel(II) with non-co-ordinated fluoroborate counterions[139]. The assignment of the precise structure from the four possible trans geometries shown in figure 1.1. was attempted by comparing the ^1H n.m.r. spectrum with that of the nickel(II) complex of the analogous tetra-aza macrocycle [14]aneN$_4$, whose structure had already been crystallographically assigned as trans-III. A similar geometry was therefore assigned to the $[Ni([14]aneS_4)]^{2+}$ cation.

This interpretation of the solution structure was apparently confirmed by an X-ray crystal structure[123], which showed the nickel ion sitting in a perfect square plane, the six-membered chelate rings adopting the 'up and down' chair conformations of the predicted trans-III geometry (fig. 1.1.). A subsequent crystal structure of the complex $[Cu([14]aneS_4)](ClO_4)_2$ also showed the exact same ligand conformation, trans-III, this time with tetragonally co-ordinated perchlorate anions[140]. These results therefore tended to confirm the findings with [14]aneN$_4$ that the trans-III geometry seems to be the most thermodynamically stable trans form of these ligands. With this background of apparently well established structural chemistry, the diamagnetic $[Ni([14]aneS_4)](BF_4)_2$ complex seemed an ideal trans-III reference compound for the present ^{13}C n.m.r. work.

The variable temperature ^1H-decoupled ^{13}C n.m.r. investigation

Figure 2.1.

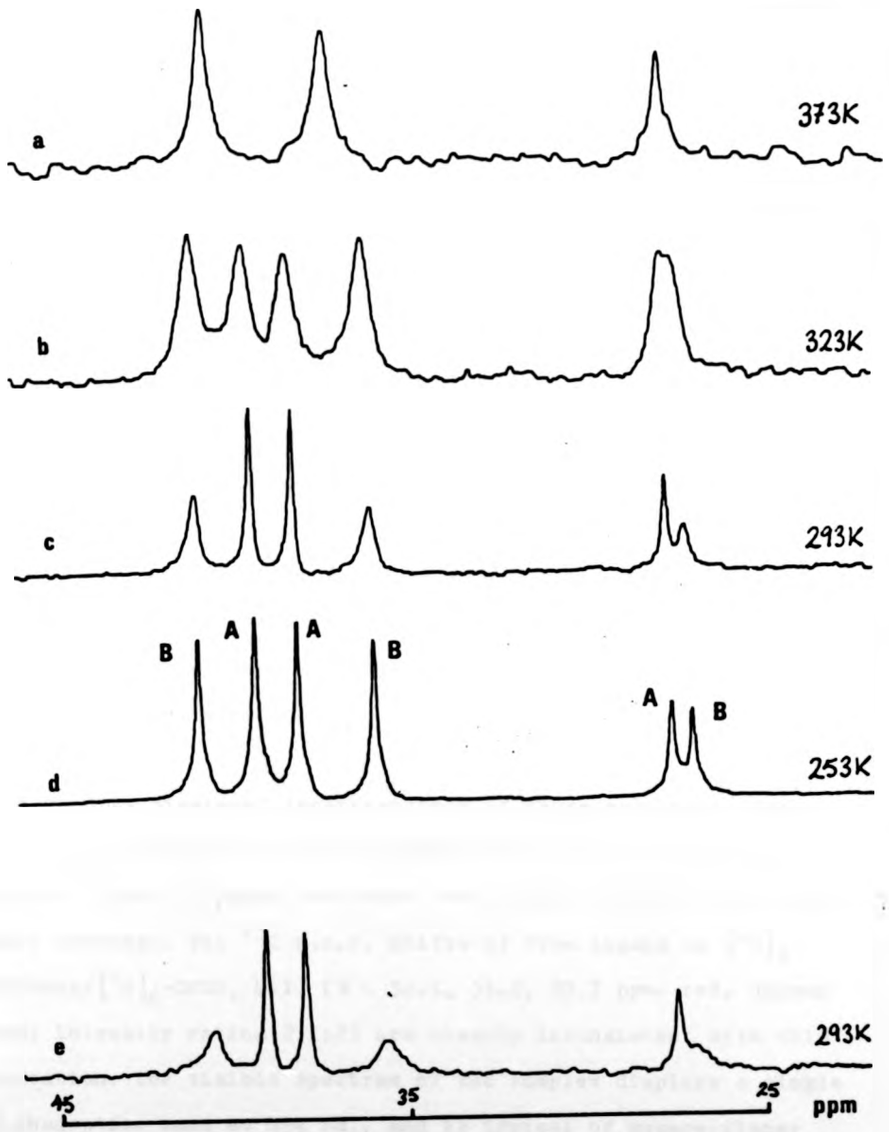

V.T. ^{13}C n.m.r. spectra of $[Ni([14]aneS_4)](BF_4)_2$ at 0.202 mol dm^{-3} $[^2H]_3$-nitromethane.

of this complex in $[^2H]_3$-nitromethane is shown in Figure 2.1. The predicted spectrum for the centrosymmetric trans-III geometry (fig. 2.2.) would display only three resonances with relative peak intensities 1:2:2 (neglecting T_1 or Overhauser effects) corresponding to:

a) the central methylene carbons of the six-membered chelate rings (2 carbons),

b) the methylene carbons next to sulphur in the six-membered chelate rings (4 carbons),

c) the methylene carbons next to sulphur in the five-membered chelate rings (4 carbons).

However, the low temperature (253K) spectrum reveals the presence of two sets of three resonances, A and B (A: δ = 26.9, 37.6, 38.6 ppm; B: δ = 26.3, 35.4, 40.3 ppm. ref. dioxan 67.3 ppm.), each set having the expected intensity ratio of 1:2:2. The relative populations of the two species are 50±5% A and 50±5% B at 283K. As the temperature is raised the two sets of resonances broaden and then merge, until at 373K (boiling nitromethane) a single set of three resonances appears in the 1:2:2 intensity ratio.

One readily dismissed interpretation of these results is that three of the resonances in the low temperature spectra are due to uncomplexed ligand [14]aneS$_4$ and that the dynamic process being observed is ligand exchange. The ^{13}C n.m.r. shifts of free ligand in $[^2H]_3$-nitromethane/$[^2H]_6$-DMSO, 4:1, (δ = 32.1, 31.2, 30.7 ppm. ref. dioxan 67.3 ppm; intensity ratios 2:1:2) are clearly inconsistent with this interpretation. The visible spectrum of the complex displays a single strong absorption band at 494 nm., and is typical of square-planar nickel(II) complexes[141], the extinction coefficient (ϵ_{494} = 271 dm^3 mol^{-1} cm^{-1}) is almost identical to that reported by Busch[111]

Figure 2.2.

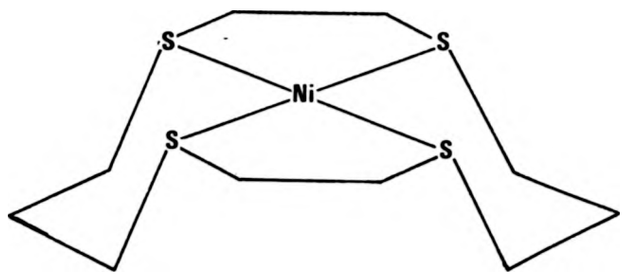

trans-I

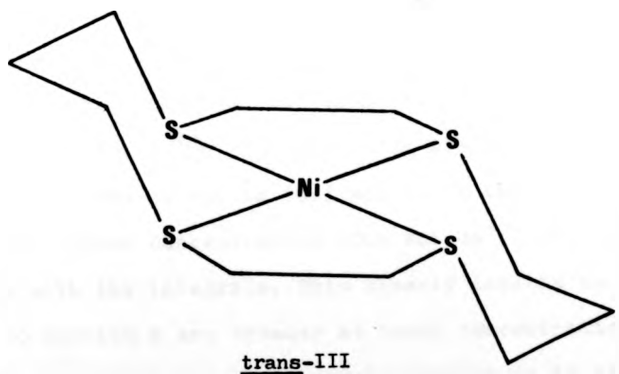

trans-III

The two postulated geometries for the species present in nitromethane solutions of $[Ni([14]aneS_4)](BF_4)_2$.

(ϵ_{494} = 263 dm^3 mol^{-1} cm^{-1}) also indicating that no impurity (free ligand or other) is present to any significant extent. These observations show that, whatever the structures of the two species present in the ^{13}C n.m.r. spectra at low temperatures, they both contain nickel(II) in a square-planar environment which is electronically very similar.

The n.m.r. spectra show no concentration dependence, spectra at 0.1, 0.2, 0.4, and 0.58 mol dm^{-3} showing the same relative populations of A and B and an identical dynamic profile. This indicates that oligomerisation to give, say, dimers is not responsible for one of the species in the ^{13}C n.m.r. spectra. Such a phenomenon is known for other sulphur chelated square-planar nickel(II) species in non-co-ordinating solvents.[142]

One clue to the assignment of structures for A and B comes from this variable concentration study. It was noted that whereas the ratio of A:B based on integrals is close to 1:1 at all concentrations, the ratio of the heights of the ^{13}C resonances for A:B varies with concentration. At low concentration (0.1 mol dm^{-3}) this ratio is almost 2:1 whereas at the higher concentration (0.4 mol dm^{-3}) the ratio is 1:1 in agreement with the integrals. This clearly implies that the resonances due to species B are broader at lower concentrations. One simple explanation of this apparently complex behaviour is that residual water (D_2O or H_2O) in the nitromethane solvent (which is hygroscopic) is co-ordinating <u>preferentially</u> to species B. This would be expected to produce a small amount of a high-spin (paramagnetic) complex which, in equilibrium with the bulk square-planar diamagnetic complex B, would slightly broaden the ^{13}C resonances of this species. If this is the case, then increasing the concentration of B relative

to the approximately constant aquo complex of B will lessen the averaged broadening of the ^{13}C n.m.r. resonances due to this species. Therefore such a situation will mimic the observed system where resonances due to species B sharpen as the concentration of B rises.

If this interpretation were correct, then one would predict that addition of small amounts of water (larger quantities cause complex dissociation) would specifically broaden resonances due to species B. This prediction is borne out in spectrum (e) of figure 2.1. which shows the effect on spectrum (c) of adding one equivalent of water (based on concentration of species B).

To summarise therefore, the experimental data above indicates:

a) the presence of two square-planar diamagnetic nickel(II) species with very similar nickel ion environments,
b) these two species are in dynamic equilibrium,
c) one of the species is preferentially solvated by donor solvents such as H_2O.

The most attractive interpretation of these results is based on a dynamic equilibrium between two of the four possible trans structures shown in figure 1.1. Only structures I, III and IV would give a three line ^{13}C n.m.r. spectrum, and simple strain-energy considerations indicate that the two structures with chair conformations of the six-membered chelate rings will be most favoured. These geometries, trans-I and trans-III shown in figure 2.2., are seen to have quite different accessibility for further ligation by donor molecules (e.g. H_2O). The trans-I geometry has one very open, accessible face on the same side of the macrocycle plane as the four lone pairs of the sulphur atoms,

the opposite side of this plane being blocked by the folded alkyl backbone of the six-membered rings. The trans-III geometry, on the other hand, has two equally accessible faces but both are more sterically hindered, by the alkyl backbone, than the corresponding face of the trans-I structure. It would, therefore, be reasonable to expect the trans-I structure to preferentially solvate. This interpretation is fully consistent with the structures of nickel complexes of NMe_4-[14]aneN_4 discussed in Chapter 4. It is , therefore, consistent with the observed results to assign a trans-I geometry to species B, and a trans-III geometry to species A as in figure 2.2.

This assignment requires the interpretation of the dynamic process which exchanges structures A and B to be configurational inversion of two co-ordinated sulphur atoms of either six-membered chelate ring. A complete lineshape analysis[143] of both pairs of exchanging resonances in the low field region of the ^{13}C n.m.r. spectrum in the temperature range 301-320K gives the kinetic data in Table 2.1. (Least-square fit of calculated exchange rate constants to the Arrhenius equation).

Table 2.1.

Kinetic Data for Exchange Phenomenon Observed in the ^{13}C n.m.r. Spectra of $[Ni([14]aneS_4)](BF_4)_2$, figure 2.1.

Resonances Fitted (ref. 143)	No. of temps.	$\Delta H^{\ddagger}_{298}$/kJ mol^{-1}	$\Delta S^{\ddagger}_{298}$/J K^{-1}mol^{-1}	k_{298}/s^{-}
low-field pair.	3	73(4)	22(13)	14.1
high-field pair.	3	63(5)	-10(15)	20.0
combination.	6	70(6)	14(19)	16.4

Although this data is very crude it indicates a small entropy of activation, which is reasonable for the predicted simple intramolecular rearrangement. The approximate value of $\Delta G^{\ddagger}_{298}$ = 70±10 kJ mol^{-1} can be favourably compared with the free energies of activation in the range 56-68 kJ mol^{-1} found for inversion at a single sulphur atom (platinum(II) complexes[144,145]). Although the present interpretation requires two linked sulphur atom inversions, the fact that the proposed mechanism is nucleophilic attack of the sulphur lone pair at the metal[144] means that where nickel(II) is the metal ion involved it is not unreasonable to expect a $\Delta G^{\ddagger}_{298}$ value similar to that for the single inversion in the more substitutionally inert platinum(II) complexes. Two, linked, sulphur atom inversions in one six-membered ring is also reasonable if one remembers the pronounced tendency of such chelate rings to adopt the chair conformation, ie. the second inversion will have a strong thermodynamic driving force in order to achieve this favoured conformation

The elucidation of this scheme for the $[Ni[14]aneS_4]^{2+}$ system again illustrates the power of ^{13}C n.m.r. as a solution structural tool, since the presence of the equilibrium between trans geometries I and III was not detected by any of the other techniques (^{1}H n.m.r., electronic spectroscopy, X-ray analysis) previously applied to the system. Indeed results such as those obtained here suggest that ^{13}C n.m.r. spectra should be routinely recorded if at all possible. The identification of two species in this system also has serious implications for several kinetic studies on the macrocyclic effect which have treated the metal-$[14]aneS_4$ complexes as a simple one species system[43,136].

The observed equilibrium between the two geometries trans-I and III is most probably a consequence of the ionic radius of the nickel(II)

ion. If this ion is slightly too large to precisely fit inside the macrocycle (this seems a reasonable assumption, see section 3) then the thermodynamically most stable geometry of the ligand trans-III, which requires the nickel ion to sit perfectly within the macrocycle, may well become destabilised with respect to the trans-I geometry. This geometry readily allows the nickel ion to move to a position slightly above the plane just as has been observed in the analogous complexes of nickel(II) with NMe_4-[14]aneN$_4$ in a trans-I arrangement (Chapter 4). This reasoning is strongly supported by the crystal structure of [Hg([14]aneS$_4$)(OH_2)](ClO_4)$_2$ reported below (figure 4.3.2.) where the large mercury(II) ion will not fit inside the macrocycle and so forces a trans-I geometry upon the ligand, thereby allowing its movement out of the ligand plane.

The identification of significant amounts of the trans-I structure in this system also goes some way towards explaining the previously puzzling behaviour of the complex [Ni([14]aneS$_4$)]I_2 which conductivity studies have shown to be a mixture of four, five, and six-co-ordinate species[111]. This behaviour is readily interpreted by assuming trans-I (five-co-ordinate) and trans-III (six-co-ordinate or square-planar) ligand geometries to be in equilibrium in solution exactly as proposed above.

Apart from being the first reported instance of the trans-I geometry for complexes of [14]aneS$_4$, this system is also the first where sulphur inversion kinetics on nickel(II) ion have been observed. From a more immediately practical viewpoint the ^{13}C n.m.r. spectra obtained for this system have allowed spectra of both trans-I and trans-III geometries to be successfully characterised.

SECTION 3. COMPLEXES OF COBALT(III) AND RHODIUM(III).

Apart from the trans-III geometry discussed above (Section 2.), the only other quadridentate geometry of [14]aneS$_4$ previously observed is folded cis-V (figure 1.1.). This geometry has been reported only for cis-octahedral complexes of cobalt(III) and rhodium(III) and work by Travis and Busch on these complexes[146] has indicated that the 14-membered ring of [14]aneS$_4$ is marginal in size for encompassing the first-row transition metals. Nickel(II) (0.69Å) and copper(II) (0.72Å) have been shown (above) to have trans configurations of the macrocycle whereas cobalt(III) (0.63Å), although smaller, forms folded cis complexes with all anions except I^- (this gives a trans complex, presumably because of the steric requirements of the large iodide ions). Rhodium(III) (0.68Å) also gives predominantly cis complexes except under extreme preparitive conditions[147] when trans geometries may be produced. (Ionic radii[6] in parenthesis). It is interesting to note that without the restrictions imposed by the cyclic structure of [14]aneS$_4$, only trans geometries are obtained for rhodium(III) thiaether complexes e.g. trans- $Rh(DTH)_2X_2^+$ where DTH is 2,5-dithiahexane[148].

It is clearly desirable to characterise the cis-V geometry by ^{13}C n.m.r. since all of the heavy metals of direct interest to this thesis have large ionic radii which would be expected to produce folding of the macrocycle to a cis-V conformation. It was therefore decided to synthesise several cis cobalt(III) and rhodium(III) complexes and to catalogue their ^{13}C n.m.r. spectra.

Consideration of the [14]aneS$_4$ ligand in a cis-V octahedral complex (figure 1.1.) reveals that the macrocycle is folded about the two

diagonally placed sulphur atoms which occupy the axial octahedral sites. This is illustrated by the dotted line in figure 3.1. and the presence of a C_2-axis, perpendicular to this fold, passing through the central metal atom means that there are five pairs of equivalent carbon atoms in this geometry. This leads to the prediction of five equal intensity resonances in the ^{13}C n.m.r. spectrum of cis-V octahedral complexes.

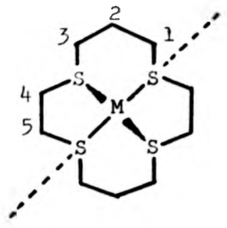

Figure 3.1.

Four cis-octahedral complexes of the type cis-$[M([14]aneS_4)X_2]^{n+}$ were prepared as described in the experimental Section 6, following the procedure of Busch[146]. The diaquo complex was prepared from the chloride dimer by refluxing with silver nitrate in water and is a previously unreported species. The ^{13}C n.m.r. spectra of all four complexes in D_2O gave the predicted five line spectrum although limited solubility meant that certain complexes had to be kept hot in solution for long periods leading to partial aquation during long accumulations. This resulted in the appearance of minor species in the spectra of such complexes as well as the five major resonances expected. The ^1H-decoupled ^{13}C n.m.r. data is given in Table 3.1. below.

All four spectra are basically unremarkable, the resonance due to the central methylenes of the six-membered chelate rings being considerably to high-field of the remaining four resonances as would be predicted on simple electronegativity grounds (carbon atoms next to donor atoms are more deshielded than those next to other carbons only[149]). Within the remaining group of four resonances, however, it is clear that one is considerably more deshieded than the other three which

Table 3.1.

^{13}C n.m.r. Data for cis-$[M([14]aneS_4)X_2]^{n+}$ Species in D_2O.

M	X	n	Shift ppm. (ref dioxan δ = 67.26ppm.)					Comments
Co	Cl	1	39.36	31.60	30.95	29.49	22.97	333K
Rh	Cl	1	39.83	31.63	31.10	30.93	24.89	303K
Rh	I	1	41.25	33.16	32.19	31.11	23.99	Minor species present for both at 333K
Rh	H_2O	3	40.23	33.00	32.30	30.25	25.18	

Rh	Cl	1	142.8Hz	150Hz	150Hz	150Hz	129.4Hz*

*Coupling constants. $^1J_{^{13}C-^1H}$

Table 3.1.

^{13}C n.m.r. Data for cis-$[M([14]aneS_4)X_2]^{n+}$ Species in D_2O.

M	X	n	Shift ppm. (ref dioxan δ = 67.26ppm.)					Comments
Co	Cl	1	39.36	31.60	30.95	29.49	22.97	333K
Rh	Cl	1	39.83	31.63	31.10	30.93	24.89	303K
Rh	I	1	41.25	33.16	32.19	31.11	23.99	Minor species present for both at 333K
Rh	H_2O	3	40.23	33.00	32.30	30.25	25.18	
Rh	Cl	1	142.8Hz	150Hz	150Hz	150Hz	129.4Hz*	

*Coupling constants. $^1J_{^{13}C-^1H}$

are very similar. This is a little unexpected since each of the four resonances is due to a pair of carbon atoms next to a sulphur atom, two of them being in five-membered chelate rings and two in six-membered rings. Why only one of these pairs of carbons shifts to low-field is puzzling, and in an attempt to assign them a fully ^{1}H-coupled ^{13}C spectrum of the cis-dichloro rhodium complex was run in D_2O. This revealed $^{1}J_{^{13}C-^{1}H}$ coupling constants as shown in Table 3.1. and, although the proximity of the three middle resonances meant that only an average ^{1}J value could be assigned (ca. 150Hz) to them, the interesting low-field resonance displayed a $^{1}J_{^{13}C-^{1}H}$ value of 142.8Hz. Both shift and coupling constant data indicate that this latter resonance belongs to the carbons in the six-membered chelate ring (comparison with data for cycloalkane models indicates six-membered rings are usually to low-field with lower ^{1}J values than the five-membered rings[149]). If this assignment is correct then consideration of molecular models shows that the pair of carbons next to the axial sulphur atoms in the six-membered chelate rings lie in a position almost eclipsed by the X group of cis-$[M([14]aneS_4)X_2]^{n+}$. This non-bonded interaction may have two effects:

a) the physical bulk of ligand X may cause steric crowding of the methylene group which will shift it upfield[149],

b) the electronegativity of the X moiety may effectively deshield the carbon nucleus of electron density, so shifting its resonance to lower-field.

Unfortunately the present data does not allow a distinction between these effects and so assignment of the low-field resonance must remain as 'one of the pairs of carbons next to sulphur within the six-membered rings'.

Having now characterised the ^{13}C n.m.r. spectra of three possible

geometries for [14]aneS$_4$ in octahedral complexes (trans-I, trans-III, section 2 and cis-V) it was possible to begin a systematic study of this macrocycle's complexes with heavy metal ions.

SECTION 4. COMPLEXES WITH HEAVY METAL IONS, Pb(II), Cd(II), Hg(II) AND Ag(I).

All of the complexes discussed so far have been with metals of ionic radius <0.75Å and all such complexes contain endo-quadridentate ligand (ie. all four sulphur atoms co-ordinated to the same metal ion, figure 4.a). The reasoning behind why certain metal ions produce folding to a cis-V geometry was discussed above simply in terms of their ionic radii but this parameter is clearly only one contributor to the overall structure. For example, although the rhodium(III) cation imposes a folded cis geometry upon the ligand[146], the even larger rhodium(I) ion forms only trans complexes with planar co-ordination of the macrocycle[147]. A clue to other factors affecting the structure is provided by complexes containing the macrocycle in an exo-conformation (figure 4.b) where the macrocycle bridges between two metal ions. In the molecule $(NbCl_5)_2$[14]aneS$_4$, the macrocycle adopts a bis-mono-dentate exo-conformation bridging two $NbCl_5$ units[120,150]. In this case it seems that availability of co-ordination sites on the central metal is more important than cation size, since the vacant octahedral site of the $NbCl_5$ units is occupied by a single sulphur atom of the macrocycle. A similar interpretation is probably true for the only other reported exo-conformation of [14]aneS$_4$ that seen in the [Cu([14]aneS$_4$)](ClO$_4$) complex[122]. In this, the very strong preference of Cu(I) for tetrahedral co-ordination forces the ligand to become tridentate to one copper atom whilst bridging monodentate to another so producing an infinite polymeric structure.

Figure 4.

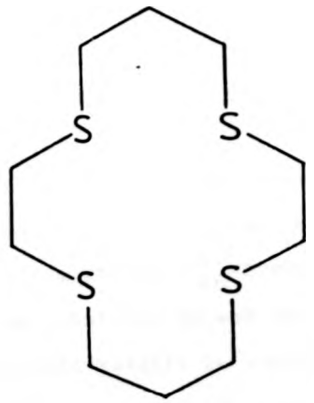

endo-conformation (a)

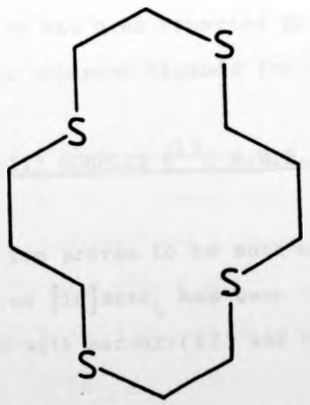

exo-conformation (b)

Diagrammatic representation of the endo- and exo- conformations of [14]aneS$_4$

In order to evaluate the contributions to complex stability and to structure with heavy metal ions, syntheses of complexes with Pb(II), Cd(II), Hg(II) and Ag(I) were attempted and results are summarised below.

SECTION 4.1. LEAD(II) AND CADMIUM(II).

The attempted preparation of complexes with lead(II)acetate and cadmium(II)nitrate was carried out by mixing the metal salt 1:1 with [14]aneS$_4$ in [^{2}H]$_3$-nitromethane/[^{2}H]$_6$-DMSO, 1:1. The ^{13}C n.m.r. spectra of the resulting clear solutions showed the same three resonances in both cases and these could readily be assigned to the resonances of free ligand in this solvent medium (δ = 32.14, 31.17, 30.68ppm; ref. dioxan 67.26ppm; intensity ratio 2:1:2). This indicates that neither lead(II) nor cadmium(II) forms stable complexes with this ligand, suggesting thiaether donors are not the best donor atoms for such metals. This conclusion has been reported previously[9] and the harder amine donors are often superior ligands for these metal ions.

SECTION 4.2. MERCURY(II) COMPLEX (^{13}C N.M.R.)

The mercury(II) ion proves to be much more interesting and the majority of the work on [14]aneS$_4$ has been carried out with this ion. No previous complexes with mercury(II) nad been reported beforethe start of this work.

As an exploratory investigation of the system, it was decided that the use of non-co-ordinating anions and solvent were most likely to produce complexation by the ligand since there would then be no competition for binding such as that described above for the exo-

complexes of niobium and copper. Therefore hexakis-(dimethyl sulphoxide) mercury(II) perchlorate (a better characterised complex than the hexa-aquo compound) was mixed with one equivalent of [14]aneS$_4$ in [^{2}H]$_3$-nitromethane. The ^{13}C n.m.r. spectrum of this solution contained three resonances due to the ligand which were all considerably shifted from those of the free ligand in the same solvent, indicating complex formation had occurred (Table 4.2.1.).

The presence of only three resonances in the spectrum was, however, a little suprising since this superficially indicated trans co-ordination of the ligand, whereas the large size of the mercury(II) ion (1.04Å[7]) had suggested folding to give a cis-geometry might occur. Upon careful consideration, there are three possible interpretations of the observed spectrum:

i) [14]aneS$_4$ is co-ordinated in a trans-I type geometry (Figure 1.1. with the large mercury(II) ion sitting out of the plane of the four sulphur atoms (trans-III geometry is unlikely for the large mercury(II) ion).

ii) [14]aneS$_4$ is co-ordinated in a cis-V type geometry (Figure 1.1.) but is in fast exchange between mercury ions, so producing an averaged three line spectrum instead of the five-line spectrum expected for cis co-ordination.

iii) The ligand has folded to adopt a symmetric bridging exo-conformation (Figure 4.b.).

Of course all three explanations may have the [14]aneS$_4$ in fast exchange between equivalent sites (and free ligand) but only interpretation (ii) requires this.

A ratio study of the system, involving metal:ligand ratios of

2:1, 1:1, 1:2, proved that fact ligand exchange was indeed occurring since in all three cases only three lines were present with shifts as shown below (Table 4.2.1.).

Table 4.2.1.

^{13}C n.m.r. data for ratio study of the mercury(II)-[14]aneS$_4$ system.

metal:ligand* ratio	^{13}C n.m.r. shifts δ/ppm.(ref. dioxan 67.26ppm.) at 303K in nitromethane.	Intensity ratio.
2:1	36.23, 33.23, 26.37	2:2:1
1:1	36.21, 33.18, 26.26	2:2:1
1:2	33.75, 32.99, 29.13	2:2:1
free ligand	31.14, 32.64, 31.37	2:2:1

* metal supplied as $(DMSO)_6$ salt.

This data clearly indicates that the complex is a 1:1 adduct of metal to [14]aneS$_4$ with a very high stability constant but a dissociation rate constant too high to allow the observation of free and bound ligand in the ^{13}C n.m.r. spectrum. Cooling of the solution containing a 1:2 metal:ligand ratio produced pronounced broadening of all three resonances but no splitting could be detected before the solution froze at 235K. A lower limit for the dissociation rate constant of *ca.* 100 s^{-1} at 235K may be deduced on the basis of the shift separation of free and bound resonances from Table 4.2.1.

The data doesnot, however, allow a distinction between the three possible structures above, although it modifies interpretation (iii) in that any bridge must now be doubled in order to maintain a 1:1 metal

to ligand ratio.

In order to help elucidate the structure of this compound, and to investigate the effect of co-ordinating anions as discussed above, the complexes of mercury(II) chloride and iodide with [14]aneS$_4$ were prepared (Section 6). Unfortunately these complexes were extremely insoluble in almost all solvents except DMSO (in which they dissociated) and so ^{13}C n.m.r. characterisation was impossible.

SECTION 4.3. MERCURY(II), X-RAY CRYSTAL STRUCTURES.

It was felt that a characterisation of the structures of the mercury complexes with [14]aneS$_4$ was sufficiently important to warrant an X-ray determination of the crystal structures of both the perchlorate and chloride complexes. This would not only allow a comparison of the effects of co-ordinating anions upon the structure, but also permit a comparison with the ^{13}C n.m.r. results for the perchlorate.

The complexes were prepared as described in section 6 and Hg, C, and H analyses indicated them to be [Hg([14]aneS$_4$)(OH$_2$)](ClO$_4$)$_2$, I, and (Cl$_2$Hg)$_2$[14]aneS$_4$, II, showing 1:1 and 2:1 metal to ligand ratios respectively. The former confirms the conclusions from the ^{13}C n.m.r. work of the previous section. The structure solutions are described in section 6, while crystal data are summarised in Table 6.3. and atomic co-ordinates, bond lengths and angles are given in Tables 6.4, 6.5. and 6.6. respectively.

The molecular structure of (Cl$_2$Hg)$_2$[14]aneS$_4$, II, figure 4.3.1. may be described in terms of the macrocyclic ligand being simultaneously bidentate to two distinct HgCl$_2$ moieties and therefore bridging in a

Figure 4.3.1.

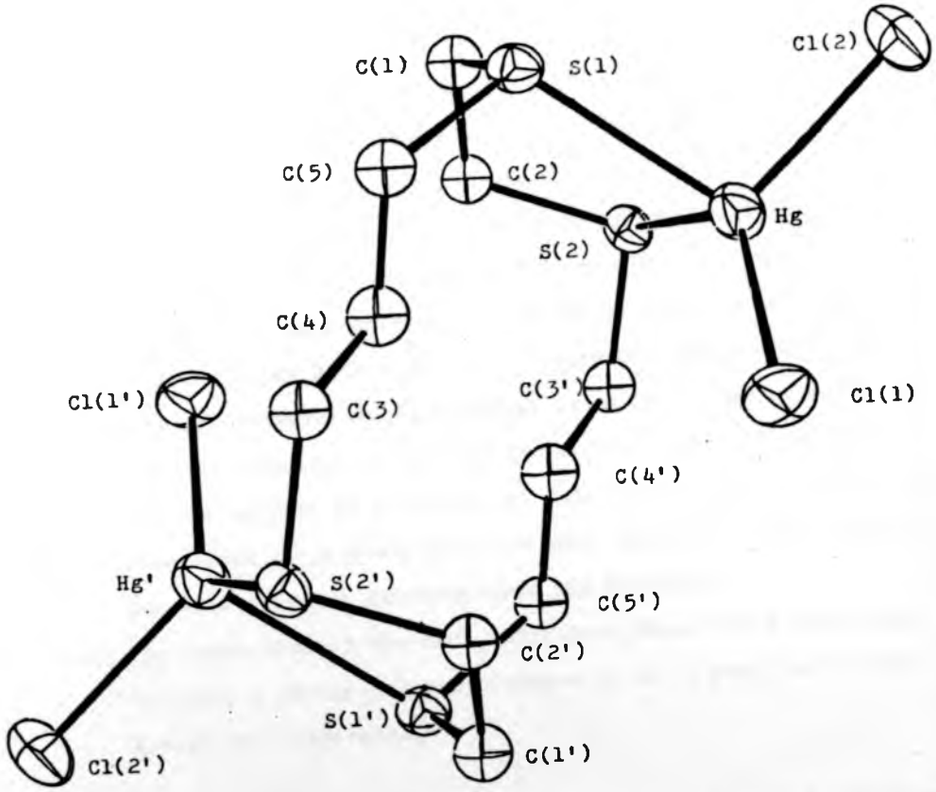

Molecular structure of $(Cl_2Hg)_2$[14]ane S_4.

symmetrical exo-dentate manner between them. The co-ordinated chloride ions therefore impose a distorted tetrahedral geometry upon the metal ion. This geometry is relatively commo n for mercury(II)[151] although the conformation adopted by the ligand is, as yet, unique. This conformation displays several interesting features including the preferential formation of five-membered chelate rings as opposed to the more flexible six-membered rings. Thus, while constraining the S(1)-Hg-S(2) angle to 83° and imposing considerable strain as shown by the lengthening of the S(2)-Hg bond relative to S(1)-Hg (difference 0.12Å), this allows the ligand to adopt a more extended conformation enabling a greater separation of the bulky $HgCl_2$ groups. It therefore seems likely that the structure of the molecule is a result of at least two effects:

(i) a greater bond strength from mercury(II) to chloride ion than to sulphur in a thiaether. This prevents all four sulphur atoms from co-ordinating to the same metal ion, and therefore forces tetrahedral geometry upon the mercury;

(ii) the large size of the $HgCl_2$ moieties. These force the ligand to adopt a strung-out conformation so as to keep these bulky groups well separated.

It is clear that the co-ordinating anions have a marked effect on the conformation that the ligand adopts, and this is emphasised by consideration of the structure of $[Hg([14]aneS_4)(OH_2)](ClO_4)_2$, I, (figure 4.3.2.). In this case, the four sulphur atoms occupy co-ordinatio sites on the same mercury atom and impose a tetragonal pyramidal environment upon it. The sulphur atoms S(1), S(2), S(3), S(4) occupy the base of the pyramid and lie approximately in a plane (±0.15Å). The Hg-O(11) vector (2.35(4)Å) is nearly perpendicular to this plane at an angle of 82°, while the mercury atom is 0.48Å above the plane.

Figure 4.3.2.

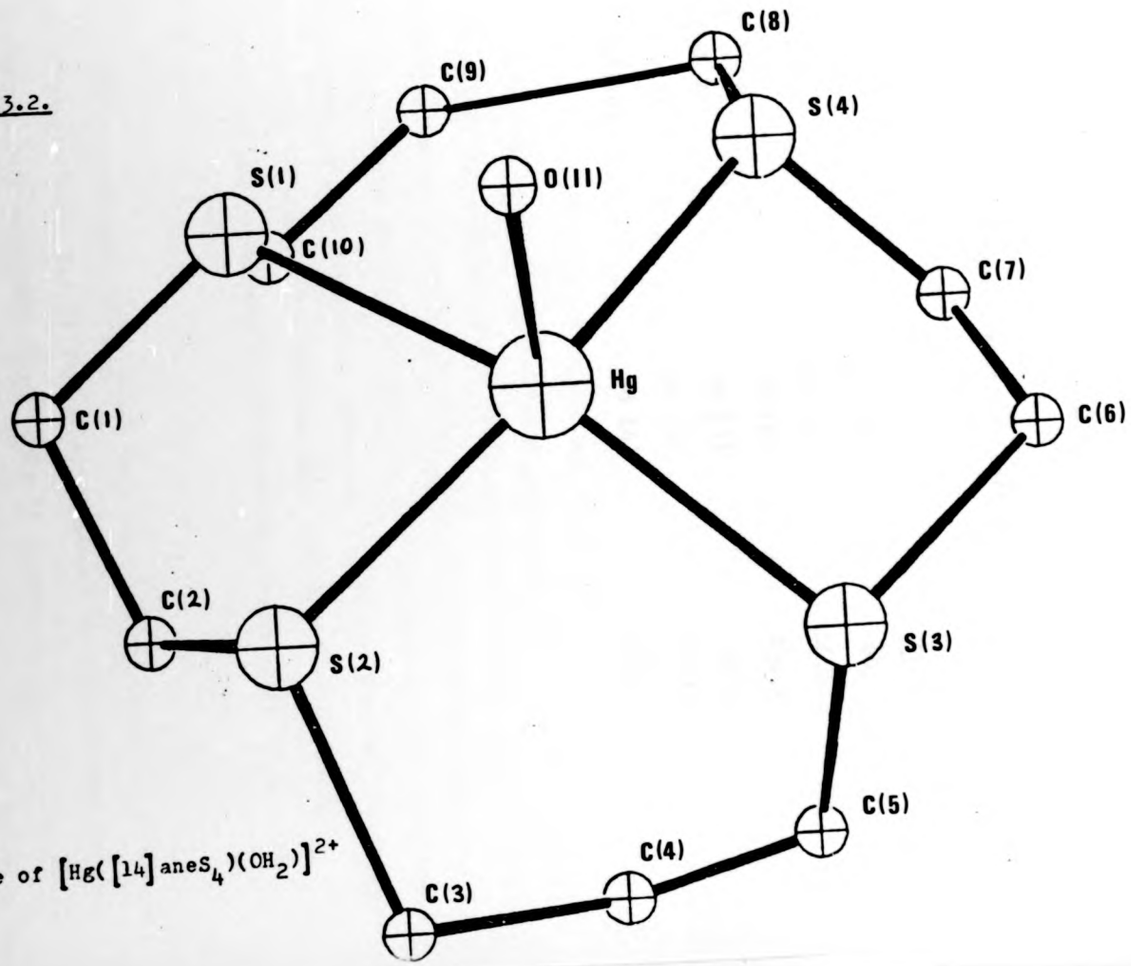

Molecular structure of $[Hg([14]aneS_4)(OH_2)]^{2+}$

Table 4.3.1.

Dihedral angles in degrees with standard deviations in parentheses.

About Bond	I	II
C(1)-C(2)	64 .(6)	60(1)
C(3)-C(4)	80(10)	160(1)
C(4)-C(5)	47(14)	151(2)
C(6)-C(7)	95 (3)	60(1)
C(8)-C(9)	50 (2)	160(1)
C(9)-C(10)	88 (4)	151(2)

Table 4.3.1.

Dihedral angles in degrees with standard deviations in parentheses.

About Bond	I	II
C(1)-C(2)	64 (6)	60(1)
C(3)-C(4)	80(10)	160(1)
C(4)-C(5)	47(14)	151(2)
C(6)-C(7)	95 (3)	60(1)
C(8)-C(9)	50 (2)	160(1)
C(9)-C(10)	88 (4)	151(2)

The ligand itself is apparently sufficiently flexible to adopt either configuration without substantial strain. This is shown by the dihedral angles within the macrocycle (Table 4.3.1.). The values for C(1)-C(2) and C(6)-C(7) correspond to those required for chelation with a twisted five-membered chelate ring, (ideally 60^{o}), though the large value for C(6)-C(7) in I is slightly unexpected. The remaining values are close to the ideal 180^{o} in the extended chain of II, and to the 60^{o} values expected for a six-membered chelate ring in I, although there are some minor deviations. In I these may be due to the size of Hg, preventing the two S-C bonds from being parallel, while in II they are possibly due to compression caused by packing forces.

Thus, when no competing anion is present it seems that [14]aneS$_4$ can become quadridentate although its constrained'hole-size'prevents the large mercury(II) ion from sitting completely inside the ring. In this case, therefore, metal-ion size is another factor contributing to the conformation adopted by the [14]aneS$_4$. The fact that the mercury(II) ion is forced out of the basal plane probably dictates the remainder of the co-ordination geometry in that the ion then has one open face which is occupied by a solvent water molecule. The vacant site in the trans position to this water molecule is then obstructed by the carbon backbone of the macrocycle which prevents co-ordination of a sixth ligand.

The crystal-packing diagrams show that the molecules in structure II (figure 4.3.3.) lie in chains with Cl...Cl as the dominant contacts between molecules in the chain. Between chains, H...H contacts are the major packing forces. In structure I (figure 4.3.4.) the isolated cations are surrounded by perchlorate anions, and the crystal forces must be mainly the electrostatic interactions between these.

Figure 4.3.3.

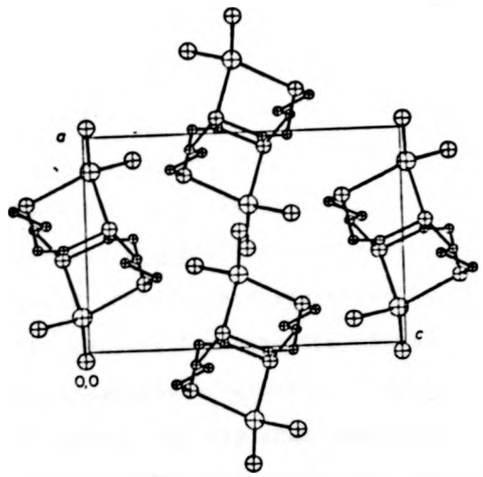

Crystal packing diagram for structure II viewed along the b axis.

Figure 4.3.4.

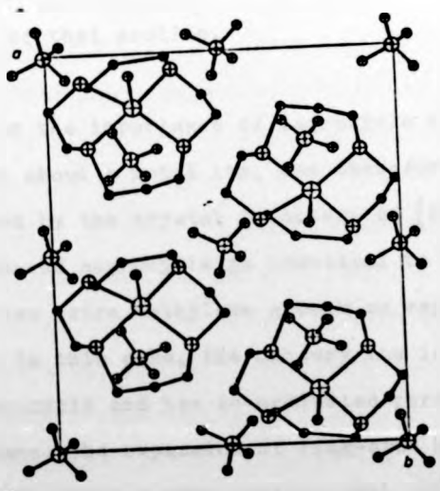

Crystal packing diagram for structure I viewed along the c axis.

It is interesting to note that the ligand conformation in I is the first found for [14]aneS$_4$ in which all four sulphur atoms have their lone pairs of electrons on the same side of the plane defined by the sulphur atoms, the trans-I geometry (figure 1.1.). This is in contrast to Ni(II)[123] and Cu(II)[140] crystal structures, which have [14]aneS$_4$ in the common centrosymmetric trans-III geometry (figure 1.1.). This can be rationalised since the trans-III geometry with Hg(II) would require either short Hg...C contacts and overcrowding of the macrocycle or else a movement of the mercury ion into the plane of the four sulphur atoms which is disfavoured on grounds of metal ion size. The trans-I geometry is, of course, exactly that postulated in section 2 for [Ni([14]aneS$_4$)]$^{2+}$ based on ^{13}C n.m.r. work, and interestingly the species postulated there, as being responsible for the observed broadening of one set of resonances, has a directly analogous structure to the [Hg([14]aneS$_4$)(OH$_2$)]$^{2+}$ ion determined here. The structure is also consistent with one of the three interpretations of the ^{13}C n.m.r. results outlined in the previous section (interpretation (i)) and vindicates the findings of that section.

Further evidence for the importance of macrocycle hole-size in determining the geometry about a metal ion, and therefore its own conformation, is provided by the crystal structure of [Hg([16]aneS$_4$)](ClO$_4$)$_2$ [152]. The 16-membered macrocycle is identical to [14]aneS$_4$ except that the ring contains two extra methylene groups so expanding the ring hole-size considerably. In this case, the mercury ion is found to sit in the plane of the macrocycle and has co-ordinated perchlorate groups above and below this plane. The expansion of ring-size has therefore allowed the mercury ion to adopt a more conventional octahedral co-ordination geometry.

Complexes of [16]aneS$_4$ with copper(II) have been postulated to have directly analogous structures to those found in the present study[153] It is thought that in the presence of co-ordinating ligands such as chloride ion, a bridged binuclear complex $(CuCl_2)_2$[16]aneS$_4$ is produced with a structure almost identical to II. If $[ClO_4]^-$ or $[BF_4]^-$ are the counter anions, they do not co-ordinate and a square-planar copper(II) complex is formed. It is clear that the factors important in determining the conformation of a macrocycle, namely metal ion size and the presence of co-ordinating anions, are identical for copper(II) complexes of [16]aneS$_4$ as for complexes of mercury(II) with [14]aneS$_4$.

Whilst the work on mercury(II) complexes of [14]aneS$_4$ was in progress two brief papers on the extraction of microamounts of mercury(II) using this macrocycle were reported[124,154]. It was found that [14]aneS$_4$ would succesfully extract mercury(II) ions from chloride or perchlorate media into nitrobenzene solution and that both 1:1 and 1:2 metal to ligand ratios could be prepared, depending on the counterion. It was postulated that the 1:1 species were octahedral[154], which is incorrect since the crystal structure of I shows penta-co-ordination of the mercury(II) ion, and the assignment of structures based simply on C,H analyses and ambiguous I.R. data is,at best,tentative. This work did, however, show the perchlorate complex to have a stability constant (log K = 11.11) much greater than that of the chloride complex (log K = 2.92), consistent with the observed structures described above. Related work on the silver(I) perchlorate-[14]aneS$_4$ system[154] proposed that complexes were formed with metal to ligand ratios of 1:1, 2:1 and 1:2 although the 1:2 complexes could not be isolated. The 1:1 complex was prepared in order to compare the ^{13}C n.m.r. of this complex with the corresponding mercury (II) complex discussed above.

SECTION 4.4. COMPLEX WITH SILVER(I).

The white complex $[Ag([14]aneS_4)](ClO_4)$ is only slightly soluble in almost all common solvents but ^{13}C n.m.r. spectra could be obtained on the $[^2H]_6$-DMSO solutions at 333K. The spectrum displayed only three resonances (δ = 31.61, 31.49, 28.58ppm, ref. dioxan 67.26ppm; intensity ratio 2:2:1) all of which show a shift from free ligand and so indicate complex formation as expected. The behaviour of the silver(I)-$[14]aneS_4$ system, as discussed above, closely mimics that of the mercury(II) system and it would seem logical therefore to assign a trans-I geometry to this silver(I) complex by analogy with the 1:1 mercury complex.

If this is the case it suggests that the structure of the 1:2 metal to ligand complexes proposed in the solvent extraction work may very well involve co-ordination of two $[14]aneS_4$ ligands in trans-I geometries, with the silver(I) ion sitting out of the sulphur atom plane of both ligands and sandwiched between them in effective eight co-ordination. This interesting structure is a direct analogue of the 2:1 'sandwich' complexes with the crown ether type macrocycles discussed in Chapter 1 and if confirmed would be the first instance of such a structure with a transition element. The fact that silver(I) can adopt this type of structure whereas mercury(II) shows no tendency to do so is a reflection of the increased size of the silver(I) ion (1.26Å[96] *cf.* 1.04Å[97]) which allows greater space for co-ordination of a second ligand.

SECTION 5. CONCLUSIONS.

The ^{13}C n.m.r. results for cobalt(III) and rhodium(III) complexes

(section 3.) and especially the results with nickel(II) (section 2.) have proven the effectiveness of this technique for monitoring the structures of such rigidly endo-quadridentate (figure 4.a.) complexes. However, when one moves to more labile metals such as those of prime interest in this thesis, the identification of structure simply from n.m.r. data becomes much more difficult. If the macrocycle is found to be in rapid exchange such as with mercury(II) then one must resort to more classical structural techniques such as X-ray crystallography for the unique assignment of structure. Although automated diffractometer have removed one major problem with this latter technique, that of time involved in structure solution, there remains the problem of having to relate a crystalline phase structure to a solution phase structure which may be subtly different (e.g. the $[Ni([14]aneS_4)]^{2+}$ ion, section 2; also see Chapter 4.).

Nontheless the work described in this chapter has several relevant points to make regarding the chemotherapeutic use of macrocycles in general, and tetrathiaether rings in particular:

1) The versatility of structure displayed by the tetrathiaether macrocycles, and especially their ability to adopt exo-conformations (figure 4.b.) bridging between metals, means that the hoped for specificity of these macrocycles is being lost since such rings are not capable making use of their hole-size parameter to afford selection between metals of differing ionic radii. What is required, therefore, is a more rigidly endo-quadridentate type of ligand which will make use of this important selection parameter.
2) The non-complexation of both cadmium(II) and lead(II) and the general low stability of the thiaether-metal complexes (log K =

11.11 for $[Hg([14]aneS_4)]^{2+}$ *cf.* log K = 18 for typical *in vivo* binding[12]) indicates that, although thiol donors are strong ligands for the heavy metal ions, thiaethers do not have the required co-ordinative ability to compete for these metals *in vivo* or to produce stable excretable complexes. This is well illustrated by the structure of $(Cl_2Hg)_2[14]aneS_4$ (figure 4.3.1.) where the thiaether donors fail to compete effectively with the co-ordinated chloride ions.

3) The noted lability of the complexes of $[14]aneS_4$ with heavy metals (e.g. mercury(II) and silver(I)) is seen to make interpretation of the ^{13}C n.m.r. spectra in terms of structure extremely difficult (section 4.2.). If one is not to resort to classical X-ray crystal structure determinations with their inherent drawbacks (above), then kinetically inert complexes are required for ^{13}C n.m.r. work.

4) One positive aspect of this work is that the *trans*-I geometry (figure 1.1.) has been shown to be present in two instances and such a geometry is desirable, especially for methylmercury(II). This ion has a strong tendency towards linear co-ordination such that quadridentate macrocycles which allow co-ordination of a sixth ligand below the plane (in a position *trans* to the alkyl group) are unlikely to remove the metal from a thiol containing binding site since the S^--donor can still co-ordinate. The *trans*-I geometry, however, effectively blocks this site and is therefore likely to be a better geometry for sequestring methylmercury(II) *in vivo*. (*cf.* crystal structure of $[Hg([14]aneS_4)(OH_2)](ClO_4)_2$, figure 4.3.2.)

Conclusions drawn from these points indicate that further work shoul proceed, not with thiaether macrocycles, but with macrocycles which are:

a) rigidly endo-quadridentate.

b) capable of forming complexes with lead(II), cadmium(II) and mercury(II) which have very high thermodynamic stability constants.

c) kinetically inert, making ^{13}C n.m.r. a more useful and routine structural probe.

d) easily synthesised; by template methods perhaps.

e) capable of adopting trans-I geometries if need be.

All of these requirements almost insist that the next class of macrocycle for investigation should contain amine donors and the macrocycles [14]aneN$_4$, which fulfills all five criteria, and NMe$_4$-[14]aneN$_4$, which is especially suitable in terms of criterion (e), will form the subject matter of the following two chapters.

SECTION 6. EXPERIMENTAL.

Individual experimental techniques are discussed in detail in Chapter 6.

INSTRUMENTATION

Routine ^1H n.m.r. spectra were recorded using a Perkin Elmer R12 spectrometer. ^1H, ^{13}C and all variable temperature n.m.r. spectra were recorded with a Bruker WH90 pulse fourier transform spectrometer equipped with a standard Bruker temperature control unit. Temperatures were held constant $\pm 0.5^{\circ}C$ and, for kinetic data, measured externally using a calibrated Comark thermocouple. Complete line-shape analyses, of dynamic processes in ^{13}C n.m.r. spectra, were carried out on a Burroughs B6700 computer using the program of Moore[143], with 1,4-dioxane

as a shift and natural line-width reference. Rate data was fitted to the Eyring equation using the least-squares program ACTPAR on the Burroughs computer. All chemical shifts are quoted in ppm. in the delta δ scale (TMS = Oppm; 1,4-dioxane = 67.26ppm).

Infra-red spectra were recorded using a Perkin Elmer 457 instrument on liquid-film or nujol mulled samples. Electronic spectra were recorded with a Unicam SP800 or Cary 14 spectrophotometers. Mass spectra were recorded with a V.G. Micromass 12 spectrometer. Elemental analyses were carried out by C.H.N. Ltd. or Butterworth Microanalytical Consultancy (BMAC) Ltd. as stated in text. Metal analyses were carried out with a Varian AA6 atomic absorption spectrophotometer.

CHEMICALS AND SOLVENTS

All solvents and chemicals purchased were reagent grade and used without purification unless otherwise stated. Deuterated solvents (99.9% $[^2H]$) were used as supplied; spectrograde or A.R. solvents were used where possible for visible spectroscopy. Nujol for I.R. mulls was dried over sodium wire.

SYNTHESIS OF $[14]aneS_4$.

The macrocycle $[14]aneS_4$ was synthesised by the procedure of Travis and Busch[146] using the reaction scheme illustrated in figure 6.1. overleaf (yields based on each step).

Characterisation of compounds in the synthetic pathway:-

a) 1,11-dioxa-4,8-dithiaundecane, A: ^{13}C n.m.r. ($[^2H]$-chloroform,

Figure 6.1.

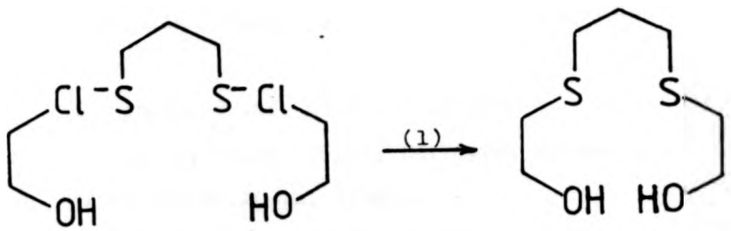

A yield = 76%

1) EtOH, reflux for 4hrs.

2) a- thiourea, conc. HCl, 12hrs reflux
   b- KOH, H_2O reflux for 3hrs.

3) a- metallic Na
   b- 1,3-dibromopropane added dropwise to a $2dm^3$ ethanolic solution over 56hrs.

(2)

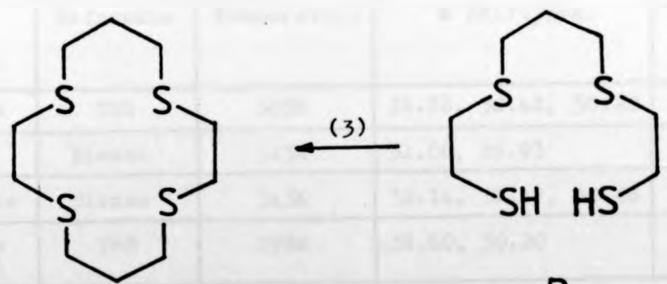

Sublimed yield = 26%

B yield = 64%

Schematic illustration of the synthesis of [14]aneS$_4$ [146].

Overall yield = 13%

ref. TMS δ = Oppm, 303K):-

observed δ = 60.78, 34.73, 30.67, 29.39ppm.

reported[155] δ = 61.12, 34.95, 30.83, 29.63ppm. intensity ratio 2:2:2:1.

b) 1.4.8.11-tetrathiaundecane, B: ^{13}C n.m.r. (i) ([^{2}H]-chloroform, ref. TMS δ = Oppm, 303K):-

observed δ = 35.88, 30.42, 29.25, 24.63ppm.

reported[155] δ = 36.02, 30.48, 29.44, 24.78ppm. intensity ratio 2:2:1:2.

(ii) (D_2O, ref. dioxan 67.26ppm, 313K):-

observed δ = 35.75, 28.58, 27.61, 23.45ppm.

Infra-red (liquid-film): υ(SH) = 2542; υ(CSC) = 705cm^{-1}.

c) [14]aneS$_4$: M.Pt. = 119°C, reported[146] = 119-120°C. ^{13}C n.m.r. data are tabulated below in Table 6.1.

Table 6.1.

^{13}C n.m.r. data for [14]aneS$_4$

Solvent deuterated	Reference	Temperature	δ Shift/ppm.	Intensity ratio
chloroform	TMS	303K	31.78, 30.42, 30.22	2:2:1
DMSO	Dioxan	313K	31.06, 29.93	3:2
nitromethane	Dioxan	343K	32.14, 31.17, 30.68	2:1:2
chloroform (ref 155)	TMS	298K	31.60, 30.20	2:3

It is clear that, contrary to previous reports[155], all three resonances expected for [14]aneS$_4$ are observed in the ^{13}C n.m.r. spectrum in chloroform.

Infra-red (nujol mull): υ(CSC) = 683cm^{-1}. Mass spectrum: 268 (M^+), 240, 208.

An X-ray crystal structure of [14]aneS$_4$[156] shows two crystallographically unique molecules in the unit cell both having an exo-conformation (figure 4.b.) similar to that found in (NbCl$_5$)$_2$[14]aneS$_4$ and consistent with this ligand's proven ability to act as a bridge between metal ions.

[Ni[14]aneS$_4$](BF$_4$)$_2$

The nickel(II) complex was prepared following published methods[111]. 1 gram of Ni(BF$_4$)$_2$.6H$_2$O was dissolved in 5Ccm^3 of nitromethane and 2 gra of acetic anhydride were added. The green solution was filtered and 0.8 grams of [14]aneS$_4$ were stirred in. The solution immediately turned deep red and evaporation down to 10cm^3 followed by addition of ether and cooling to 0^{o}C precipitated bright red crystals of the desired complex. Recrystallisation from nitromethane yielded 0.8 grams (65%). The crystals were dried in a vacuum dessicator and stored over P_2O_5. Solutions for ^{13}C n.m.r. were made up in a dry nitrogen atmosphere with [^{2}H]$_3$-nitromethane dried over 3A molecular sieves.

^{13}C n.m.r. data are reported in text. Visible spectroscopic spectra (Cary 14) in dry nitromethane show no thermochroism and have λ_{max} = 494nm (ϵ = 271 dm^3 mol^{-1} cm^{-1}); reported[111] λ_{max} = 494nm (ϵ = 263 dm^3 mol^{-1} cm^{-1}). Infra-red (nujol mull): υ(Ni-S) = 432cm^{-1}. (*cf.* Nickel(II) *bis*-dithiolate ion υ(Ni-S) = 333-435cm^{-1} [157])

Rhodium(III) complexes

The complex *cis*-[Rh([14]aneS$_4$)Cl$_2$]Cl was prepared following the method of Travis and Busch[146]. 1 gram of rhodium(III) chloride was

dissolved in 1.5cm^3 of water and added dropwise to 30cm^3 of a boiling ethanolic solution containing excess [14]aneS$_4$. A voluminous khaki coloured precipitate formed immediately whilst the solution turned yellow. The precipitated dimer cis-[Rh([14]aneS$_4$)Cl]$_2$Cl$_4$[146] was filtered and saved whilst the filtrate was evaporated to 5mls and upon addition of ether bright yellow crystals separated out. Recrystallisation from ethanol/ether and washing with acetone and ether yielded 0.73 grams (40%, based on Rh(III)).

The cis-diiodo complex was prepared as the iodide salt by exactly the same procedure except lithium iodide (large excess) was added to the solutions before mixing[146]. The iodide salt was converted to the nitrate, by treatment with one equivalent of silver nitrate, in order to increase solubility for ^{13}C n.m.r. The red-brown crystals were recrystallised from ethanol to give an overall yield of 26%.

The khaki coloured dimer from the cis-dichloro preparation was treated with a large excess of silver nitrate in water. The mixture (the dimer is insoluble) was refluxed for 72 hours, after which time the aqueous solution was deep orange. Removal of the precipitated silver chloride and evaporation of the clear solution gave bright orange crystal of, presumably, the cis-diaquo complex.

^{13}C n.m.r. data for the above three complexes in D_2O are reported in text and visible spectroscopic data are reported below (Table 6.2.) An infra-red spectrum was recorded only for cis-[Rh([14]aneS$_4$)Cl$_2$]Cl (nujol mull) and showed: υ(cis-RhCl$_2$) = 304, 288cm^{-1}.

Table 6.2.

Electronic spectroscopic data for cis-[Rh([14]aneS$_4$)X$_2$]Y (SP800).

X	Y	Observed* λ_{max},/nm(ϵ/dm^3 mol^{-1}cm^{-1})	Reported[146]* λ_{max},/nm(ϵ/dm^3 mol^{-1}cm^{-1})	Comments
Cl	Cl	348(2,200), 318sh(1,900), 252(27,000).	350(2,700), 320sh(1,900), 252(26,950).	
I	NO_3	404(2,280), 320sh(6,522), 271sh(15,866),248(18,860).	405(2,460), 320(8,550), 245(22,550).	Impurity present
H_2O	NO_3	338(-----), 249(-----)	----------	Unknown conc.

*measured in H_2O.

cis-[Co([14]aneS$_4$)Cl$_2$]ClO$_4$

This complex was again prepared following published procedures[146]. 0.5 grams of anhydrous cobalt(II) chloride, 2 grams of lithium perchlorate and 1.5 grams (50% excess) of [14]aneS$_4$ were strirred together in 50cm^3 of dry nitromethane. Aerial oxidation, caused by stirring in an open flask overnight, resulted in a deep red solution which was filtered, evaporated down to 10cm^3 and precipitated with ether. The red-violet complex crystallised out and was filtered, washed with ether and recrystallised from nitromethane/ether. Yield 1.1 grams (52%).

^{13}C n.m.r. data for a D_2O solution is reported in text. Visible spectroscopy gave (SP800) : λ_{max}, nm (observed) = 533, 420, 342, 319, 252; (reported[146]) = 535, 420, 340. Observation of the peak at 533nm for a water solution held at 60°C showed a pronounced decay (half-life *ca.* 20 hours) of this absorption due to solvolysis (aquation) to the mono or diaquo complex. This confirmed observations of the ^{13}C n.m.r.

spectrum which indicated other species to be present in long, high temperature accumulations.

$[Hg([14]aneS_4)(OH_2)](ClO_4)_2$, (I)

This new complex was prepared by mixing solutions of hydrated mercury(II) perchlorate (excess) with $[14]aneS_4$ (0.134g) in aqueous methanol ($10cm^3$). (The hydrated mercury salt was used in preference to the hexakis-DMSO complex, which was used for the n.m.r. work, following a violent explosion in these laboratories involving this latter compound.) The white powder which precipitated immediately was filtered and washed with water and chloroform. Recrystallisation was accomplished by very slow evaporation of an extremely dilute solution (0.1g in $500cm^3$) of the powder in 80% aqueous methanol. Small, poorly formed fragments of crystalline material were obtained and found to be acceptable for crystallographic study.

Analysis (C.H.N.) Calculated for $[Hg([14]aneS_4)(OH_2)](ClO_4)_2$: Hg, 29.2; C, 17.5; H, 3.21%; Found: Hg, 28.2; C, 17.8; H, 3.14%. Infra-red (nujol mull): observed(reported[154]), υ(CSC) = 687(690), 668(66[illegible] $\upsilon(ClO_4)$ = 1140(1140), 1115(1115), 1075(1085), 622(625); $\upsilon(H_2O)$ = 3440, 1640cm^{-1}. ^{13}C n.m.r. data are reported in text.

The crystal data are summarised in Table 6.3. Systematic absences, $hk0$ for h = 2n+1, $0kl$ for $k+l$ = 2n+1, indicated an orthorhombic space group $Pn2_1a$ or $Pnma$. The crystal density was measured by flotation in a bromoform/chloroform mixture and indicated Z = 4 molecules per unit cell. The unit cell dimensions and their estimated standard deviations were obtained by a least-squares fit to 15 strong reflections with

Table 6.3.

Crystal Data for $(Cl_2Hg)_2$[14]aneS_4, II, and $[Hg([14]aneS_4)(OH_2)](ClO_4)_2$, I

	I	II
Colour	White.	White.
Habit	Needle	Irregular
Crystal System	Orthorhombic	Monoclinic
a/Å	16.583(2)	8.080(2)
b/Å	13.986(3)	11.389(2)
c/Å	8.932(2)	10.706(2)
β/°	90.0(1)	92.15(1)
V/Å^3	2075.2(5)	984.5(3)
T/°C	18(2)	18(2)
Space group	$\underline{Pn2_1a}$	$\underline{P2_1/n}$
Equivalent positions	$\underline{x}$, $\underline{y}$, $\underline{z}$; $-\underline{x}$, $\frac{1}{2}+\underline{y}$, $-\underline{z}$; $\frac{1}{2}-\underline{x}$, $\frac{1}{2}+\underline{y}$, $\frac{1}{2}+\underline{z}$; $\frac{1}{2}+\underline{x}$, $\underline{y}$, $\frac{1}{2}-\underline{z}$.	$\pm$ $\underline{x}$, $\underline{y}$, $\underline{z}$; $\frac{1}{2}+\underline{x}$, $\frac{1}{2}-\underline{y}$, $\frac{1}{2}+\underline{z}$.
μ/cm^{-1}	84.5	164.4
Relative Molecular Mass	685.6	810.9
ρ_{obs}/g cm^{-3}	2.24(5)	2.80(5)
ρ_{calc}/g cm^{-3}	2.195	2.736
$\underline{Z}$	4	2
N(3σ)	1695	1675

MoKα radiation (λ = 0.71069Å). A small crystal of dimensions 0.05x0.18x 0.13mm. bounded by planes (Miller indices) {100},{010},{001} was selected and centred on a Syntex $P2_1$ automated diffractometer. Intensity data in the range $3^\circ<2\theta<50^\circ$ were collected by the θ-2θ scan technique and three check reflections were monitored after every 100 reflections and showed no systematic variation. 1695 observed reflections were collected ($I>3.0\sigma(I)$) and corrected for absorption (see chapter 6) with transmission factors in the range 0.60-0.25. A weighting analysis on the corrected data indicated unit weights were satisfactory.

$(Cl_2Hg)_2[14]aneS_4$, (II)

Solutions of mercury(II) chloride (0.27g) and $[14]aneS_4$ (0.134g) were mixed in boiling nitromethane ($10cm^3$). The white precipitate was collected and washed with chloroform and water to leave a dry white powder. Recrystallisation by very slow evaporation of a dilute (0.1g in $50cm^3$) nitromethane solution yielded clear lath crystals for crystallography.

After many attempts at obtaining a successful CH analysis from BMAC Ltd. the correct analysis was received from CHN Ltd. (identical batches of crystals were sent to both companies). Analysis (CHN) Calculated for $(Cl_2Hg)_2[14]aneS_4$: Hg, 49.3; C, 14.9; H, 2.50%; Found : Hg, 48.8; C, 15.2; H, 2.55%. Infra-red (nujol mull): observed (reported[154]), υ(HgCl) = 343; υ(CSC) = 665(666),686(685) cm^{-1}. M.Pt. = 160±1°C.

Crystal data are summarised in Table 6.3. Systematic absences, 0k0 for $k = 2n+1$ and h0l for $h+l = 2n+1$, were observed indicating the

monoclinic space group $\underline{P2_1/n}$, (a non-standard setting of $\underline{P2_1/c}$). Unit cell parameters and crystal density were measured as described for (I) above and the latter indicated $\underline{Z}$ = 2 molecules per unit cell, each therefore lying on a special position of symmetry $\bar{1}$. A crystal of approximate dimensions 0.05x0.05x0.30mm. bounded by the Miller planes {011} and {100} was mounted and aligned on a Syntex $\underline{P2_1}$ four-circle diffractometer. Intensity data in the range $3^{\circ}<2\theta<55^{\circ}$ were collected by the θ-2θ scan technique and three check reflections were monitored throughout the data collection as for (I) above. 1675 observed ($I>3.0\sigma(I)$) reflections were measured and corrected for absorption giving transmission factors in the range 0.500-0.401. Unit weights were again found to be adequate.

Structure Solution for (I) and (II) above.

The structures were both solved using the heavy atom method involving a three dimensional Patterson synthesis to locate the position of the mercury atoms. The remaining atoms were located in subsequent electron density maps and all atoms were refined by minimising the function $\Sigma(|F_o| - |F_c|)^2$. For (II), final refinement with anisotropic temperature factors for Hg, Cl and S atoms gave $\underline{R}$ 0.030. For (I), initial refinement in the centric space group Pnma produced a chemically inconsistent structure which would not refine below $\underline{R}$ 0.20. Conversion into the non-centric group $\underline{Pn2_1a}$ (a non-standard setting of $\underline{Pna2_1}$) allowed refinement to give a reasonable overall view of the chemical structure with $\underline{R}$ 0.116. Refinement to a higher accuracy proved impossible; this is probably due to:

(i) an irregular crystal, leading to uncertain absorption correction

(ii) disorder of the carbon backbone of the [14]aneS$_4$ ligand as shown by the high temperature factors associated with certain of the

backbone atoms. (Although alternative positions of these carbons were tried, they provided no improvement).

(iii) disorder of the oxygen atoms of the two perchlorate groups.

It is clear that (I) (figure 4.3.2.) is an adequate description of the molecular structure of this complex but also that the bond lengths and angles are less reliable than for structure (II).

Scattering factors and anomalous dispersion corrections[158] were used, and all computing was carried out with the XRAY76 programs (see Chapter 6) on a Burroughs B6700 computer. Final co-ordinates and temperature factors are in Table 6.4. Bond lengths and angles are included in Tables 6.5. and 6.6. respectively.

$\underline{[Ag([14]aneS_4)]ClO_4}$

0.207g of A.R. silver perchlorate were mixed with 0.268g of $[14]aneS_4$ in dry nitromethane (25 cm^3). The complex immediately precipitated as a fine white powder, was filtered, washed with water, acetone and chloroform and air dried. The complex was insoluble in all common solvents except DMSO with which it gave a pale yellow solution which was light sensitive.

^{13}C n.m.r. data in $[^2H]_6$-DMSO are reported in text (section 4.4.). Analysis (CHN): calculated for $[Ag([14]aneS_4)]ClO_4$, C, 25.2; H, 4.21%; Found, C, 24.5; H, 4.07%. Infra-red (nujol mull) : observed(reported[154]). $\upsilon(ClO_4)$ = 1115(1115), 1075(1085), 627(625); υ(CSC) = 676(670),691(688)cm

Table 6.4.

Atomic co-ordinates ($x10^4$) with standard deviations in parentheses.

I, $[Hg([14]aneS_4)(OH_2)](ClO_4)_2$

Atom	X	Y	Z
Hg	1368 (1)	2500	2113 (3)
S(1)	699(23)	1027(30)	890(27)
S(2)	2356(31)	1169(34)	2530(39)
S(3)	2387(40)	3902(31)	2407(45)
S(4)	421(27)	3597(24)	333(34)
O(11)	568(25)	2391(44)	4282(45)
C(1)	1396(56)	70(68)	934(93)
C(2)	2311(44)	562(58)	915(83)
C(3)	3525(51)	1729(65)	2310(98)
C(4)	3422(38)	2791(47)	1276(72)
C(5)	3197(69)	3752(84)	1482(123)
C(6)	1615(40)	4886(49)	1147(75)
C(7)	1089(39)	4465(50)	10079(72)
C(8)	5098(80)	3428(104)	6316(131)
C(9)	5247(52)	2001(64)	6486(87)
C(10)	797(49)	1220(60)	8910(85)
Cl(1)	2673(10)	2382(20)	6676(17)
O(1)	2430(23)	3134(33)	7651(54)
O(2)	1977(17)	1888(30)	6143(43)
O(3)	3104(29)	2771(41)	5441(36)
O(4)	3178(28)	1733(32)	7470(61)
Cl(2)	-53(19)	4955(22)	5229(23)
O(5)	621(31)	4780(50)	4278(59)
O(6)	-612(31)	5564(33)	4481(62)
O(7)	-434(34)	4073(26)	5587(54)
O(8)	217(37)	5406(55)	6570(35)

II, $(Cl_2Hg)_2[14]aneS_4$

Hg	1618 (1)	191 (1)	1668 (1)
S(1)	3072 (2)	-1821 (2)	1541 (2)
S(2)	4307 (3)	748 (2)	3118 (2)
Cl(1)	1147 (3)	1567 (2)	-15 (2)
Cl(2)	-413 (3)	113 (2)	3270 (2)
C(1)	5188(10)	-1509 (7)	2132 (7)
C(2)	5237(11)	-711 (7)	3287 (8)
C(3)	5744(10)	1613 (7)	2216 (8)
C(4)	5908(11)	1228 (8)	865 (8)
C(5)	6635(10)	2237 (7)	87 (8)

For temperature factors for both I and II see appendix.

Table 6.5.

Bond lengths in Å with standard deviations in parentheses.

Bond	I	II
Hg-Cl(1)	---	2.407(3)
Hg-Cl(2)	---	2.419(3)
Hg-S(1)	2.58 (4)	2.580(2)
Hg-S(2)	2.51 (5)	2.699(2)
Hg-S(3)	2.60 (5)	---
Hg-S(4)	2.71 (4)	---
Hg-O(11)	2.35 (4)	---
S(1)-C(1)	1.77(10)	1.838(8)
S(1)-C(10)	1.80 (8)	---
S(2)-C(2)	1.68 (8)	1.827(9)
S(2)-C(3)	2.10(10)	1.827(9)
S(3)-C(5)	1.60(13)	---
S(3)-C(6)	2.19 (8)	---
S(4)-C(7)	1.66 (8)	---
S(4)-C(8)	1.58(12)	---
C(1)-C(2)	1.67(12)	1.53 (1)
C(3)-C(4)	1.76(11)	1.52 (1)
C(4)-C(5)	1.38(13)	1.55 (1)
C(5)-C(7)	1.42 (9)	---
C(8)-C(9)	2.00(17)	---
C(9)-C(10)	1.47(12)	---

Table 6.6.

Bond angles in degrees with standard deviations in parentheses.

Angle	I	II
Cl(1)- Hg -Cl(2)	---	117.54(9)
Cl(1)- Hg -S(1)	---	126.71(8)
Cl(1)- Hg -S(2)	---	112.19(8)
Cl(2)- Hg -S(1)	---	109.11(8)
Cl(2)- Hg -S(2)	---	98.88(7)
S(1) - Hg -S(2)	76(1)	83.15(6)
S(1) - Hg -S(3)	157(1)	---
S(1) - Hg -S(4)	87(1)	---
S(1) - Hg -O(11)	93(1)	---

Table 6.6. (continued)

Angle	I	II
S(2) - Hg -S(3)	97(1)	---
S(2) - Hg -S(4)	152(1)	---
S(2) - Hg -O(11)	101(2)	---
S(3) - Hg -S(4)	90(1)	---
S(3) - Hg -O(11)	109(2)	---
S(4) - Hg -O(11)	101(1)	---
C(1) -S(1)-C(10)	94(4)	103.2(4)
C(1) -S(1)-Hg	108(3)	103.3(3)
C(10)-S(1)-Hg	105(3)	110.9(3)
C(2) -S(2)-C(3)	98(4)	106.0(4)
C(2) -S(2)-Hg	103(3)	99.2(3)
C(3) -S(2)-Hg	108(3)	109.8(3)
C(5) -S(3)-C(6)	109(5)	---
C(5) -S(3)-Hg	112(5)	---
C(6) -S(3)-Hg	92(3)	---
C(7) -S(4)-C(8)	102(6)	---
C(7) -S(4)-Hg	96(3)	---
C(8) -S(4)-Hg	131(5)	---
S(1) -C(1)-C(2)	106(6)	112.6(6)
C(1) -C(2)-S(2)	104(5)	117.8(6)
S(2) -C(3)-C(4)	106(5)	115.2(6)
C(3) -C(4)-C(5)	140(7)	110.2(7)
C(4) -C(5)-S(3)	116(8)	112.6(6)
S(3) -C(6)-C(7)	116(5)	---
C(6) -C(7)-S(4)	128(5)	---
S(4) -C(8)-C(9)	100(7)	---
C(8) -C(9)-C(10)	143(7)	---
C(9) -C(10)-S(1)	107(6)	---

CHAPTER 3

SOME CO-ORDINATION CHEMISTRY OF 1,4,8,11-TETRAAZACYCLOTETRADECANE, [14]ANE N_4

SECTION 1. INTRODUCTION

The work of the previous chapter suggested that amine macrocycles would be superior to the corresponding thiaether ligands for the complexation of the heavy metal ions. Despite their lower specificity for soft metals, amines form much more stable complexes with all metal ions[30] and have the additional property that they tend to produce exclusively endo-conformations with all their donor atoms co-ordinated to the same metal ion. This latter property makes such macrocycles ideal for chemotherapeutic work since it means that the hole-size parameter can be used to effect separation between metal ions of different ionic radius, as was discussed in Chapter 1.

The 14-membered saturated tetra-aza rings are by far the commonest class of amine macocycle and this is closely related to their ease of synthesis. Since Curtis demonstrated the important metal-ion template effect[90] the synthesis of 14-membered ring systems with an enormous array of different methyl substituents on their alkyl backbones have been reported[16,90]. Almost all such syntheses are based on Schiffs-base condensations of a ketone or aldehyde with a co-ordinated amine (see Chapter 1, section 2.2.), and one of these condensations, of glyoxal with the amine 3,2,3-tet co-ordinated to nickel(II), gives, on reduction of the imine linkages, the simple unsubstituted macrocycle [14]aneN$_4$ (section 8.1.).

Complexes of [14]aneN$_4$ have been reported with a wide range of metal ions (Cr(III)[159,160], Mn(III)[61], Fe(II)[161], Fe(III)[61], Ru(III)[162], Co(II)[163], Co(III)[105,164], Rh(III)[165], Ni(II)[166], Ni(III)[61], Cu(II)[167], Ag(II)[58], Ag(III)[58], Zn(II)[28], Hg(II)[59].) and, without exception, are

found to contain an endo-quadridentate conformation of the macrocycle. The structures of many of these complexes will be discussed below in greater detail, but those that have been determined may be summarised as belonging to trans-(Cr,Mn,Fe,Ru,Co,Rh,Ni,Cu,Ag) or cis-V (Cr,Co,Rh) geometries. Of the four possible trans geometries only trans-III has been crystallographically established and it appears that, as with [14]aneS$_4$ in Chapter 2, this conformation of the ligand is thermodynamically the most stable when the metal ion is small enough to be encompassed by the ring. The identification of only trans-III and cis-V geometries for [14]aneN$_4$ complexes is,therefore, exactly the situation which prevailed for [14]aneS$_4$ prior to the work reported in Chapter 2. By analogy with that work, therefore, it may be predicted that, for metal ions of ionic radius slightly larger than the macrocycle cavity, an equilibrium between trans-III and trans-I structures may be present. The nitrogen configurational inversions which relate these two isomers must proceed either a) by metal-nitrogen bond cleavage or else b) by deprotonation of the amine, both followed by umbrella inversion. Both mechanisms necessitate bond breaking and, therefore, it may also be predicted that the dynamic process relating the trans-I and trans-III isomers will have a higher energy profile for [14]aneN$_4$ than for [14]aneS$_4$ complexes.

The thermodynamic and kinetic properties of tetra-aza macrocyclic complexes have also been the subject of considerable investigation[30,168-]. An assortment of polarographic,microcalorimetric and equilibrium data have been used to determine the stability constants of [14]aneN$_4$ with nickel(II) (logK = 22.7)[37], copper(II) (logK = 27.2)[170], zinc(II) (logK = 15.5)[27] and mercury(II) (logK = 23.0)[29]. All indicate very strong complexes are formed and it is especially significant that the complex

with mercury(II) has a stability constant greater than that found for many *in vivo* binding sites[12], exactly the behaviour required for a chelation therapy drug. The rate constants for complex formation with [14]aneN$_4$ have also been measured for copper(II) (k_{298} = 8x10^6 dm^3 mol^{-1} s^{-1})[171], zinc(II) (k_{298} = 7.5x10^4 dm^3 mol^{-1} s^{-1})[28] and nickel(II) (k_{298} = 14 dm^3 mol^{-1} s^{-1})[171] and coupled with the thermodynamic data, they indicate that all of the complexes are kinetically very inert, making them amenable to an n.m.r. determination of their solution structure.

All of the observations above suggest that [14]aneN$_4$ is likely to be a very interesting ligand in many respects and, since it is the exact nitrogen donor analogue of [14]aneS$_4$, the observations made in Chapter 2 on the tetrathiaether ring should be directly applicable to this ligand. The unsubstituted ring system means that the ^{13}C n.m.r. spectra are again relatively simple, and directly analogous to those obtained for [14]aneS$_4$ complexes in Chapter 2, while the kinetic inertness of the complexes means that ligand lability will not confuse the ^{13}C n.m.r spectra (*cf.* Chapter 2, section 4.2.).

With these considerations in mind,it seems a logical progression of the work reported in Chapter 2 to investigate the metal complexes of [14]aneN$_4$. Diamagnetic complexes of 'known' geometry were synthesised in order to record their ^{13}C n.m.r. spectra for reference purposes exactly as for [14]aneS$_4$. The complexes with heavy metal ions were then prepared and their ^{13}C n.m.r. spectra interpreted against the background of these reference structures. The advent of practical natural-abundance nitrogen-15 n.m.r. spectroscopy also meant that, if the heavy metalcomplexes could be made in sufficient quantities and were highly soluble, the ^{15}N n.m.r. spectra could be recorded. This would be

expected not only to confirm the ^{13}C n.m.r. results but also, in the case of Cd, Hg and Pb which have a percentage of isotopes with nuclear spin = $\frac{1}{2}$, to provide one-bond metal-nitrogen coupling constants with associated information on the actual bonding of the metal ion to the macrocyclic donors. The results of these investigations are reported below.

SECTION 2. COMPLEX WITH RHODIUM(III)

As was mentioned above, the cis-V geometry of [14]aneN$_4$ has been established only for the inert metal ions Cr(III)[159], Co(III)[164] and Rh(III)[165]. In all three cases it is most likely that this cis-geometry is produced more as a result of the chemical inertness of the metal ions than by their ionic radius. Margerum et al[173] have postulated that complex formation between the macrocycle and a metal ion goes via an initial cis arrangement of the ligand followed by rapid isomerisation involving nitrogen configurational inversions, to give the thermodynamically more stable trans-III geometry. If the metal ion involved is substitutionally inert however, the second isomerisation step may well be slow and the complex will remain with its initially formed cis-geometry. This hypothesis seems to be reasonable and is supported by the behaviour of cis-Co(III) complexes where it is found that they will slowly isomerise to give trans-III complexes[104], indeed trans-III complexes of cobalt(III) are quite common[45]. The mechanism of the cis to trans isomerisation is, however, a little confused; Tobe[104] originally postulated that nitrogen inversion was followed by rearrangement to the trans-geometry. Recently, however, the isolation of cobalt(III) complexes with a trans-configuration which appears to have a set of nitrogen configurations identical to the cis isomer[174,175] would suggest that nitrogen inversion occurs after rearrangement to the trans-geometry. It

appears that pH is critical to the mechanistic course of the r action, high pH favouring the Tobe mechanism (since deprotonation of the amines is easier under alkaline conditions) whereas low pH favours rearrangement followed by inversion.

Both cis and trans-isomers of all three metal ions are known and recently the cis-dihalo rhodium(III)complexes have been the subject of a photochemical study of halide aquation[176]. Crystallographic evidence[177] indicates that the cis-isomers do indeed have the cis-V geometry shown in Chapter 2, figure 1.1..

The complex $[Rh([14]aneN_4)Cl_2]Cl$ was prepared as a mixture of cis and trans-isomers and recrystallised to separate out pure cis-isomer (section 8.2.). By analogy with the ^{13}C n.m.r. spectra obtained for the cis-V complexes of rhodium-$[14]aneS_4$ in Chapter 2, a simple five equal-intensity resonance spectrum may be predicted. The fully ^{1}H-decoupled spectrum, in D_2O at 323K, showed these five resonances (δ = 23.68, 46.95, 48.93, 50.88, 55.10 ppm, ref. dioxan 67.26ppm) and interestingly also indicated the same downfield shift of one of the four downfield resonances (carbons adjacent to nitrogen) as was observed for $[14]aneS_4$ complexes in Chapter 2. The effect is clearly not as marked with the tetra-aza macrocycle but is probably also the result of non-bonded interactions between the co-ordinated chloride ion and one of the carbon atoms next to nitrogen in a six-membered chelate ring (for discussion see Chapter 2, section 3).

This spectrum therefore served as a reference for the cis-V geometry and the only other geometry definitely established, trans-III, was characterised using the nickel(II) complex as a standard. This work is

now reported below.

SECTION 3. COMPLEXES WITH NICKEL(II)

Trans-geometries have been established for all of the metal ions whose complexes with [14]aneN$_4$ have been structurally investigated (see above). Even with the largest ions, silver(II) (r = 0.89Å)[6])[178] and cobalt (II) (r = 0.72Å)[6])[163], the 14-membered ring is found to completely encompass the metal ion in a perfect trans-III geometry, and all crystal structures of [14]aneN$_4$ complexes to date having trans-configurations show trans-III geometries[166,167,179]. One of the most recently prepared complexes of [14]aneN$_4$ is that with ruthenium(III), the trans-dichloro complex being prepared by refluxing the pentachloroaquoruthenium(III) cation with [14]aneN$_4$ for three days[162]. Structural and mechanistic studies of the acid and base hydrolysis of this complex have been performed[180,181] and results indicate that the macrocycle exerts a nephelauxetic effect on the central metal ion, thereby increasing the reactivity relative to uncyclised analogues. Similar behaviour is well characterised for trans-cobalt(III) complexes[182,183].

The first complex of [14]aneN$_4$ to have its structure determined crystallographically was the trans-III dichloronickel(II) complex and it was found that all the trans-dihalo complexes dissolved in water or methanol to give a solution visible spectrum consistent only with a square-planar environment for nickel(II)[166]. Conductivity measurements showed the complexes to be fully dissociated 2:1 electrolytes and it was generally assumed thereafter that aqueous solutions contained only square-planar diamagnetic $[Ni([14]aneN_4)]^{2+}$ cations and that the ligand-field strength of [14]aneN$_4$ was too great to allow axial co-ordination

of solvent[46].

Since the template synthesis of [14]aneN$_4$ (section 8.3.) yields this particular cation as its perchlorate salt[89], this complex was chosen as a reference compound for the trans-III geometry. Dissolution of the perchlorate complex in dried [^{2}H]$_3$-nitromethane gives a bright orange solution whose ^{1}H n.m.r. spectrum is similar to that reported[111], although all peaks in the present spectrum are much better resolved than that reported previcusly (see section 8.3.). The ^{13}C n.m.r. spectrum of the same solution shows only three sharp resonances corresponding to the expected trans-III geometry (δ = 50.88, 48.99, 26.63ppm ref. dioxan at 67.26ppm; intensity ratio 2:2:1).

When the complex is dissolved in D_2O however, it is immediately apparent that the solution is not diamagnetic as had previously been assumed. ^{1}H n.m.r. spectra of aqueous solutions show six broad resonances corresponding to the six different types of alkyl protons in figure 3.1. The lack of coupling information and the magnitude of the shifts (0-50ppm) clearly indicate the presence of significant quantities of a paramagnetic nickel(II) species formed by axial solvation of the square-planar complex, water interacting with the square-planar species to produce paramagnetic shifting and broadening of all resonances. The temperature dependence of the resonance shifts is shown in figure 3.2. and clearly does not follow the Curie-law behaviour ($\delta \propto \frac{1}{T}$) expected for pure contact shifting as produced by a magnetically isotropic, A or E ground-state paramagnetic ion such as nickel(II)[184]. This latter anomaly is easily explained if a temperature dependent equilibrium between the high-spin aquo-complex and the low-spin square-planar complex exists. This would imply that the percentage of paramagnetic

Figure 3.1.

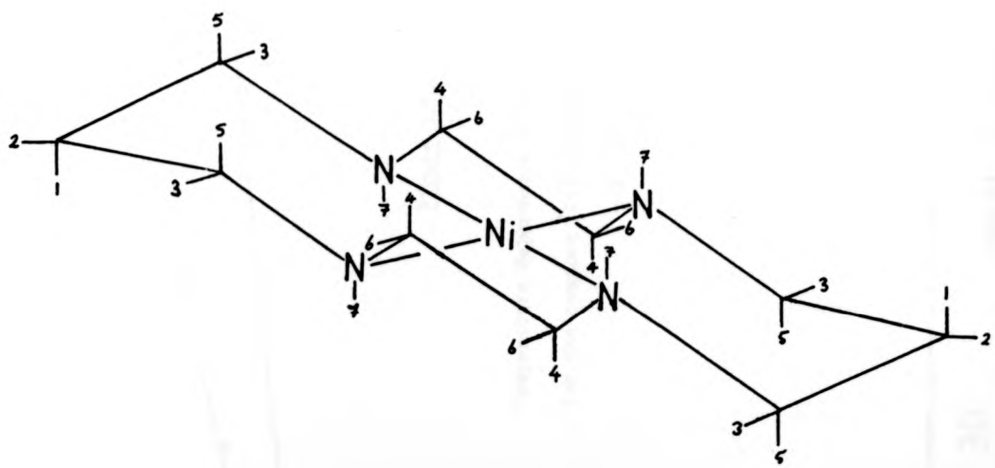

Illustration of the seven distinct types of proton in the cation $[Ni([14]aneN_4]^{2+}$.

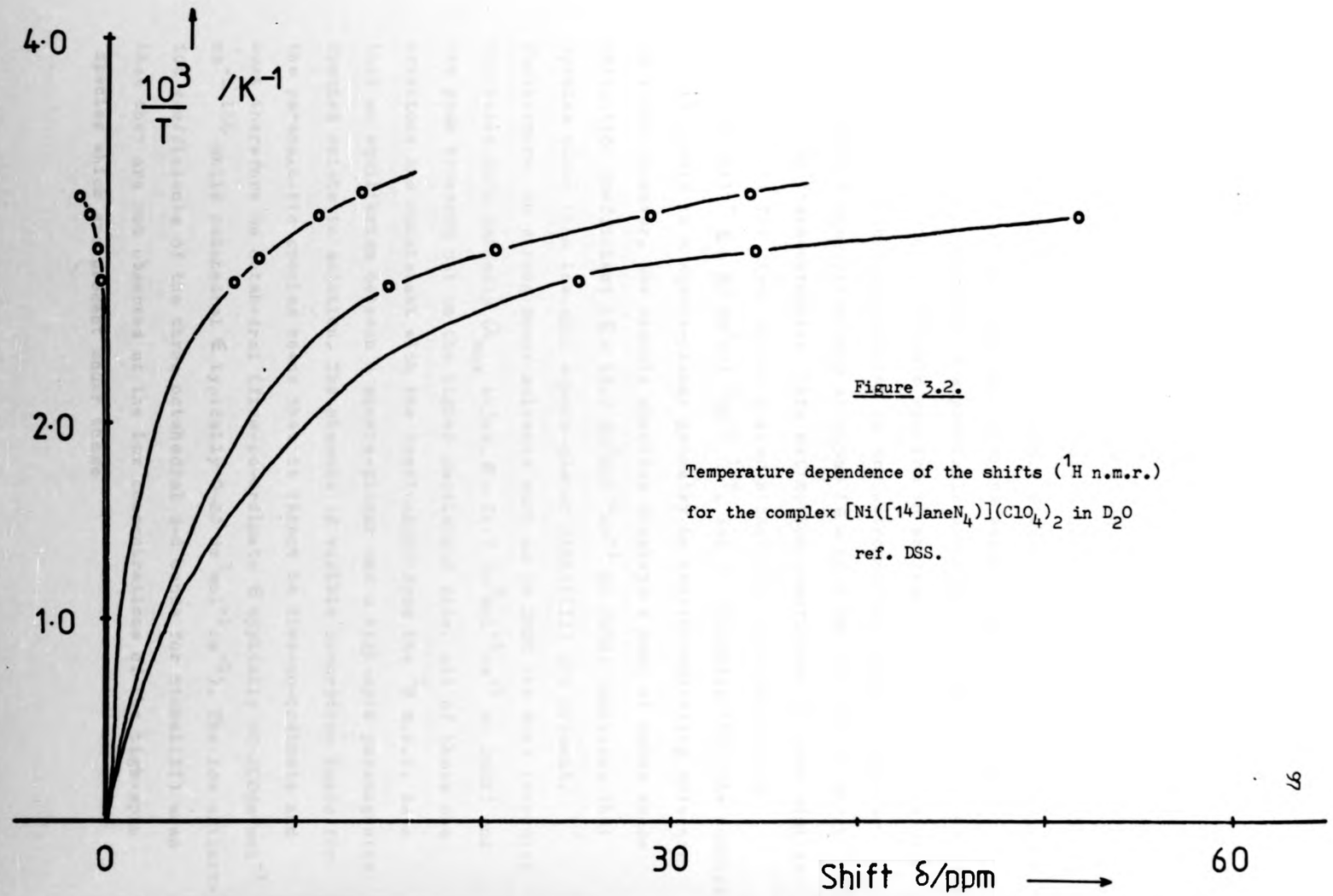

Figure 3.2.

Temperature dependence of the shifts (^{1}H n.m.r.) for the complex [Ni([14]aneN$_4$)](ClO$_4$)$_2$ in D$_2$O ref. DSS.

species is varying with temperature and such behaviour would be expected to produce the observed curvature of the Curie-law plots.

This data clearly calls into question such work as that of Hinz and Margerum[34] on the formation reaction between Ni(II) and [14]aneN$_4$ in aqueous solution, where they openly discuss and effectively dismiss the possibility of any high-spin complex being present. Additional evidence for the presence of appreciable amounts of a high-spin nickel(II) species comes from the visible spectra in various solvents. The rigourously dried perchlorate complex in dry nitromethane gives a spectrum with a single absorption band at 445nm (ϵ = 65.6 dm^3 mol^{-1}cm^{-1}) which displays no thermochroicity. This extinction coefficient is very similar to that found for other square-planar nickel(II) tetra-amines e.g. Ni(2,3,2-tet)$^{2+}$ ϵ = 67 dm^{3}mol^{-1}cm^{-1} 185, and so indicates that the complex exists purely in a square-planar geometry in non-co-ordinating solvents. In water, however, the visible spectrum displays a band at 448nm whose extinction coefficient (ϵ = 48.2 dm^{3}mol^{-1}cm^{-1} at 298K) indicates that species other than low-spin square-planar nickel(II) are present. Furthermore, in strong donor solvents such as in DMSO the band intensity decreases more markedly (λ_{max} 443nm, ϵ = 24.7 dm^{3}mol^{-1}cm^{-1} at 298K) and the peak broadens out on the higher wavelength side. All of these observations are consistent with the conclusions from the ^{1}H n.m.r. data that an equilibrium between a square-planar and a high-spin paramagnetic species exists in solution. The absence of visible absorption bands for the paramagnetic species means that it cannot be five-co-ordinate and must therefore be octahedral (five-co-ordinate ϵ typically 20-200dm^{3}mol^{-1} cm^{-1} 186 while octahedral ϵ typically 0-20 dm^{3}mol^{-1}cm^{-1}). The low extinction coefficients of the three octahedral d-d bands for nickel(II) mean that they are not observed at the low concentrations of the high-spin species which are present under these

species is varying with temperature and such behaviour would be expected to produce the observed curvature of the Curie-law plots.

This data clearly calls into question such work as that of Hinz and Margerum[34] on the formation reaction between Ni(II) and [14]aneN$_4$ in aqueous solution, where they openly discuss and effectively dismiss the possibility of any high-spin complex being present. Additional evidence for the presence of appreciable amounts of a high-spin nickel(II) species comes from the visible spectra in various solvents. The rigourously dried perchlorate complex in dry nitromethane gives a spectrum with a single absorption band at 445nm (ϵ = 65.6 dm^3 mol^{-1}cm^{-1}) which displays no thermochroicity. This extinction coefficient is very similar to that found for other square-planar nickel(II) tetra-amines e.g. Ni(2,3,2-tet)$^{2+}$ ϵ = 67 dm^{3}mol^{-1}cm^{-1} [185], and so indicates that the complex exists purely in a square-planar geometry in non-co-ordinating solvents. In water, however, the visible spectrum displays a band at 448nm whose extinction coefficient (ϵ = 48.2 dm^{3}mol^{-1}cm^{-1} at 298K) indicates that species other than low-spin square-planar nickel(II) are present. Furthermore, in strong donor solvents such as in DMSO the band intensity decreases more markedly (λ_{max} 443nm, ϵ = 24.7 dm^{3}mol^{-1}cm^{-1} at 298K) and the peak broadens out on the higher wavelength side. All of these observations are consistent with the conclusions from the ^{1}H n.m.r. data that an equilibrium between a square-planar and a high-spin paramagnetic species exists in solution. The absence of visible absorption bands for the paramagnetic species means that it cannot be five-co-ordinate and must therefore be octahedral (five-co-ordinate ϵ typically 20-200dm^{3}mol^{-1} cm^{-1} [186] while octahedral ϵ typically 0-20 dm^{3}mol^{-1}cm^{-1}). The low extinction coefficients of the three octahedral d-d bands for nickel(II) mean that they are not observed at the low concentrations of the high-spin species which are present under these

conditions.

Addition of an inert electrolyte to the solutions of the complex would be expected to reduce the solvent activity and so decrease the amount of octahedral solvento species present[187]. Adding increments of dry $NaClO_4$ to the aqueous solution produced a steady increase in the absorption band due to the square-planar species (448nm) until no further increase was observed when ϵ = 67.5 dm^3 mol^{-1} cm^{-1}. This demonstates that 100% conversions to the square-planar species has taken place as expected and the maximum value of the extinction coefficient, 67.5 dm^3 mol^{-1} cm^{-1}, maybe regarded as that of the square-planar species and is in good agreement with that derived from the nitromethane solutions.

Variable temperature visible spectra also displayed an increase in the square-planar absorption band as the temperature was increased (figure 3.3.). This is precisely the behaviour predicted from the ^1H n.m.r. studies above which show that the percentage of the diamagnetic species increases as the temperature is raised. Measurement of the extinction coefficient, at I= 0.1 ($NaClO_4$), in the temperature range 280-344K allows the estimation of ΔH^o and ΔS^o for the dia-para magnetic equilibrium since the percentage of each may be estimated by a comparison of the observed extinction coefficient, ϵ_{obs}, with that of the pure square-planar complex (67.5 dm^3 mol^{-1} cm^{-1}). $K_{eq} = 67.5-\epsilon_{obs}/\epsilon_{obs}$ for the equilibrium 3.1.

$$[Ni([14]aneN_4)]^{2+} + 2H_2O \underset{}{\overset{K_{eq.}}{\rightleftharpoons}} [Ni([14]aneN_4)(OH_2)_2]^{2+} \text{----3.1.}$$

A plot of $\ln K_{eq}$ *vs* $1/T$ is shown in figure 3.4. and gives values of ΔH^o and ΔS^o in Table 3.1. This data does not however allow for any

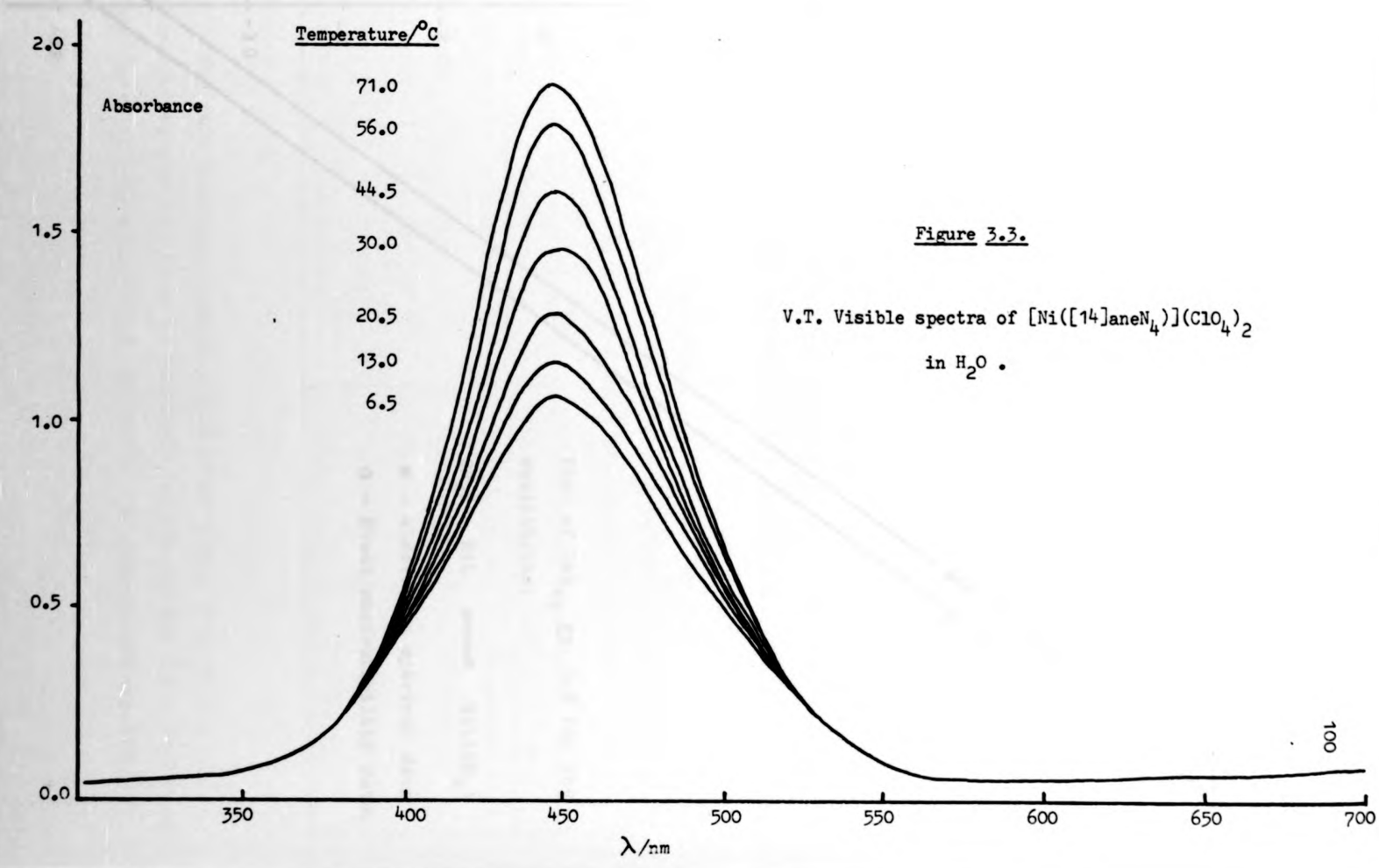

Figure 3.3.

V.T. Visible spectra of $[Ni([14]aneN_4)](ClO_4)_2$ in H_2O .

Figure 3.4.

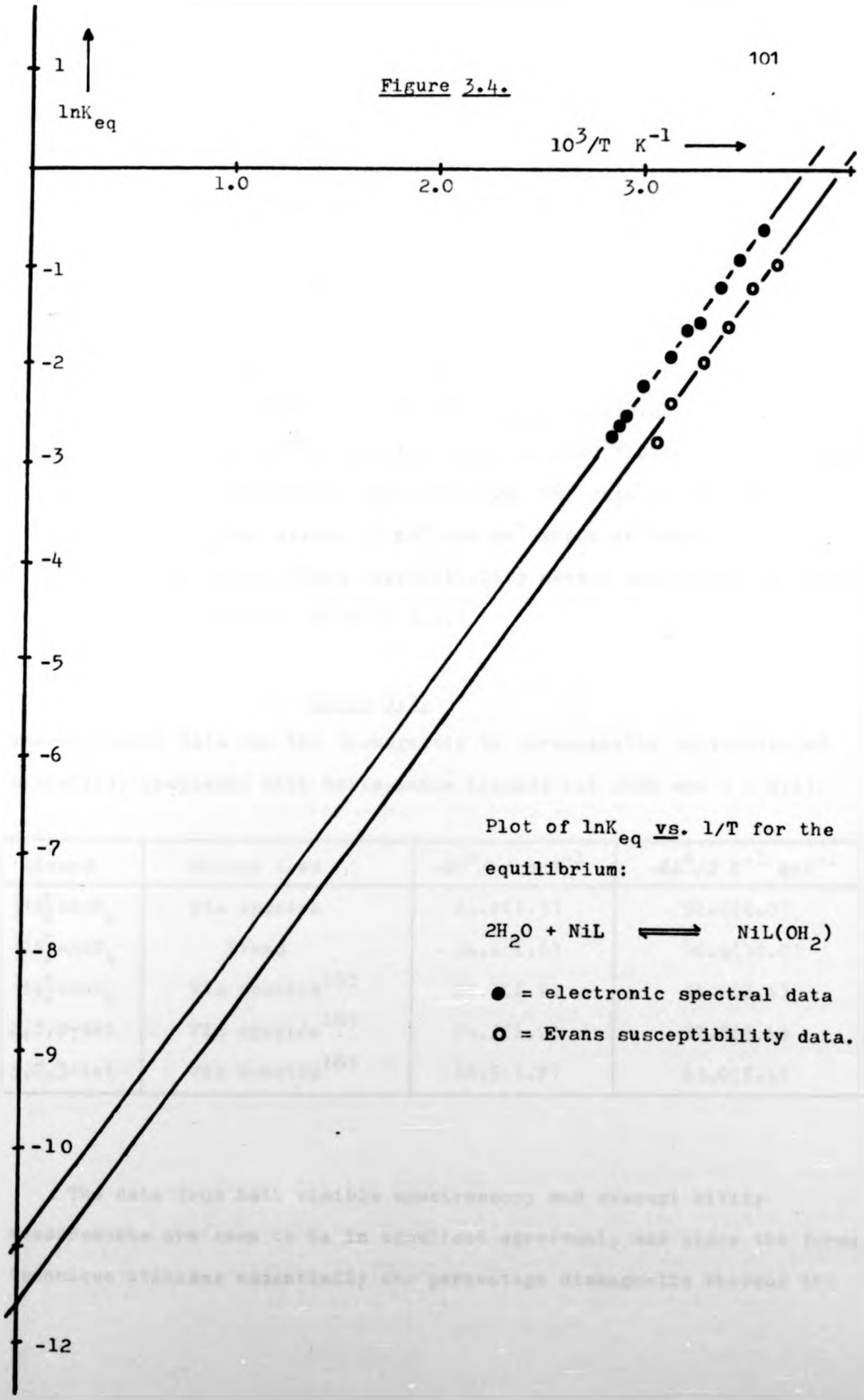

Plot of $\ln K_{eq}$ vs. 1/T for the equilibrium:

$2H_2O + NiL \rightleftharpoons NiL(OH_2)$

● = electronic spectral data

o = Evans susceptibility data.

possible overlap of the square-planar absorbance band with any of the bands due to the octahedral species and so small errors in K_{eq} may be present. As an additional check on the system the equilibrium data was also established using the percentages of paramagnetic species estimated from paramagnetic susceptibility measurements (using the Evans method i.e. from ^1H n.m.r. spectra) at I = 0.1 ($NaClO_4$). Assuming an effective magnetic moment of μ_{eff}= 3.1 β.M. for an octahedral nickel(II) complex (μ_{eff}= 3.09 and 3.06 β.M. for octahedral <u>trans</u>-dichloro and dibromo complexes respectively[166]) then the Evans method[188] allows the estimation of K_{eq} over the temperature range 270-320K. The data is plotted in figure 3.4. and gives values of ΔH^o and ΔS^o shown in Table 3.1. below. (For discussion of the Evans susceptibility method see Chapter 6, section 2; also see experimental section 8.3.)

<u>Table 3.1.</u>

Thermodynamic data for the diamagnetic to paramagnetic conversion of nickel(II) complexes with tetra-amine ligands (at 298K and I = 0.1).

Ligand	Method used	$-\Delta H^o$/kJ mol^{-1}	$-\Delta S^o$/J K^{-1} mol^{-1}
[14]aneN$_4$	Vis spectra	24.0(1.5)	91.2(8.0)
[14]aneN$_4$	Evans	24.1(1.8)	96.4(10.0)
[14]aneN$_4$	Vis spectra[185]	22.7(1.7)	84.0(8.4)
2,3,2-tet	Vis spectra[185]	14.3(1.7)	37.8(8.4)
3,2,3-tet	Vis spectra[185]	18.5(1.7)	63.0(8.4)

The data from both visible spectroscopy and suscept bility measurements are seen to be in excellent agreement, and since the former technique utilises essentially the percentage diamagnetic whereas the

latter uses only percentage paramagnetic data, these complementary results suggest that the assumptions inherent in each data set are valid (i.e. no interference from octahedral species in the visible spectra, and the octahedral species has an effective magnetic moment very close to 3.1 B.M.) Since the completion of this work, identical data has been published based on visible spectroscopy utilising exactly the procedure described above[185]. The thermodynamic data from this study are included in Table 3.1. on the previous page, together with equivalent data for the open-chain analogues of [14]aneN$_4$, 2,3,2-tet and 3,2,3-tet.

It is clear that both ΔH^o and ΔS^o decrease in the order 2,3,2-tet 3,2,3-tet [14]aneN$_4$ and this series has been explained in two ways[185]. The enthalpic trend is interpreted in terms of the size of the nickel(II) ion; with the flexible open-chain ligands 2,3,2 and 3,2,3-tet the conversion from high to low-spin nickel(II) with its associated reduction of the optimum M-N bond length (2.07Å to 1.91Å [189]) may easily be accommodated by a rearrangement of the donors. With [14]aneN$_4$, however, the cyclic nature of the ligand severly restricts any such rearrangement making the transition to the high-spin, larger ion less enthalpically favourable (the macrocycle favouring the smaller low-spin ion). The trend in entropy has been interpreted as reflecting the steric repulsions between the alkyl backbones of the ligands and the co-ordinated water molecules, [14]aneN$_4$ having the greatest preponderance of methylene groups has the greatest repulsions etc.

One observation from the parallel work mentioned above[185] was that very weak bands at 330nm and 650nm were present in the visible spectrum of the complex in water. These bands, observable in saturated solutions

in 4cm path length cells, readily ascribed to the $^3T_{1g}(P) \leftarrow {}^3A_{2g}$ and $^3T_{1g}(F) \leftarrow {}^3A_{2g}$ bands of an octahedral complex[185], and as such are direct proof of its existence. In order to eliminate the one other remaining possible interpretation of the system -that the octahedral species is in fact a dihydroxo complex formed in the presence of the basic amine macrocycle rather than a diaquo complex -a spectrophotometric pH titration of the system was performed. The titration is shown in figure 3.5. and displays excellent isosbestic points at 383 and 512nm, indicating the formationof the dihydroxo species is a simple one step reaction. The dihydroxy species has peaks at λ_{max}=350nm (ϵ = 18.1 dm^3 $mol^{-1}cm^{-1}$; $^3T_{1g}(P) \leftarrow {}^3A_{2g}$), λ_{max}=532nm (ϵ = 13.5 dm^3 $mol^{-1}cm^{-1}$; $^3T_{1g}(F) \leftarrow {}^3A_{2g}$) which are clearly different to those observed in neutral solution described above. This confirms that these latter bands are produced by the diaquo species.

An estimate of the formation constant of the dihydroxy species may be made from the pH titration[190] and displays the extraordinarily high value for reaction, $[Ni([14]aneN_4)]^{2+} \overset{K}{\rightleftharpoons} [Ni([14]aneN_4)(OH)_2]$ pK = 13.67$\pm$ 0.15 (analytical wavelength = 448nm, value is average of seven determinations at I= 1.1 (KNO_3) at 298.0$\pm$ 0.5K). The large value reflects the extreme reluctance of the $[Ni([14]aneN_4)]^{2+}$ cation to ligate on axis, probably as a result of the large in-plane ligand-field strength of the macrocycle[46].

A pale-blue complex may be precipitated from very strong alkaline solutions and this previously unreported species appears to be unstable in air, reverting to the orange $[Ni([14]aneN_4)]^{2+}$ cation in a few days. The diffuse reflectance spectrum of the solid is reported in Table 3.2. and the absorption bands do not correspond either to the diaquo or

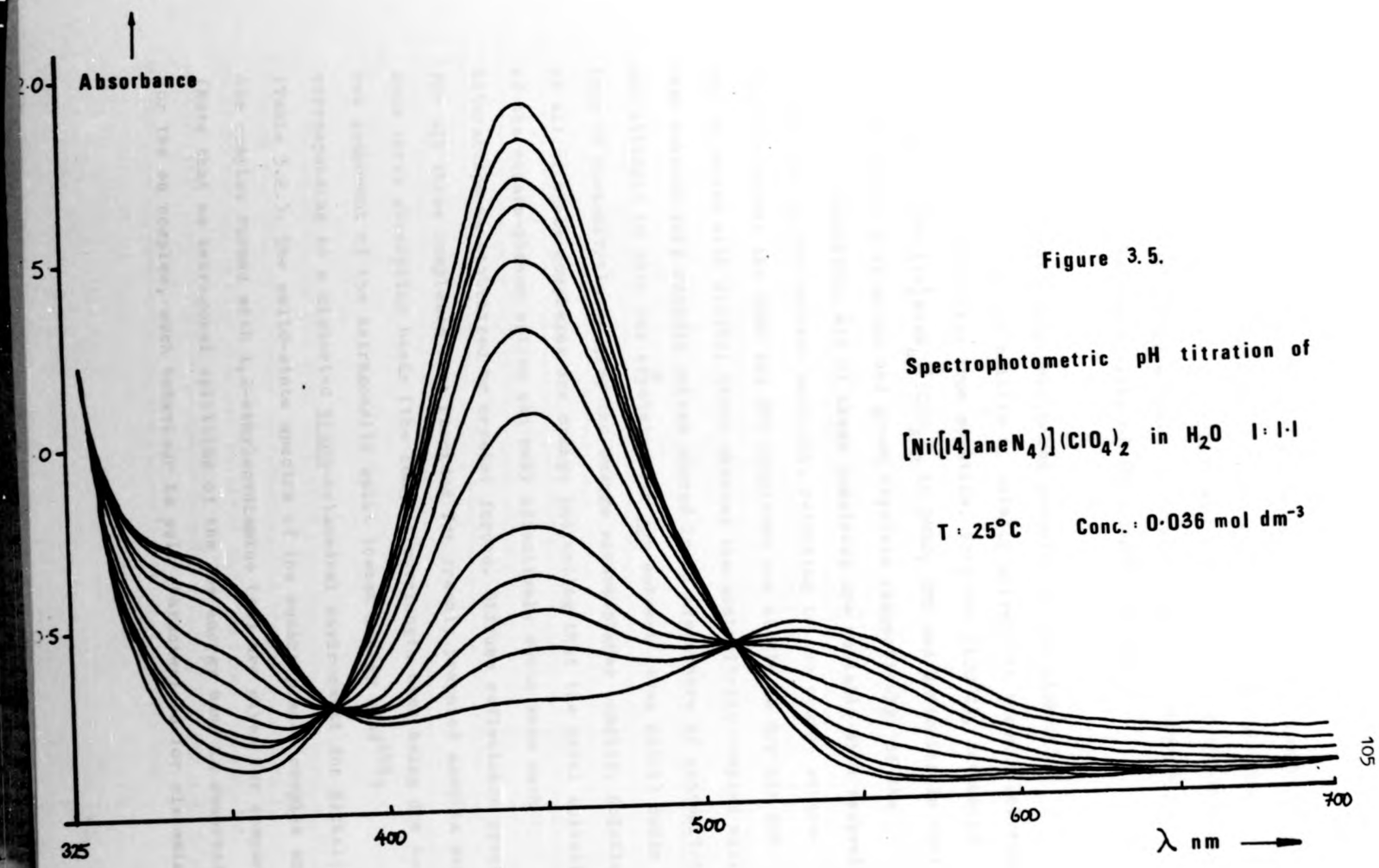

Figure 3.5.

Spectrophotometric pH titration of

$[Ni([14]aneN_4)](ClO_4)_2$ in H_2O I: 1·1

T: 25°C Conc.: 0·036 mol dm^{-3}

dihydroxy solution spectra. Speculation as to the composition of this species leads to the suggestion that deprotonation of one or more co-ordinated amines of the macrocycle may have occurred. Unfortunately no satisfactory CHN analysis could be obtained for this compound, probably due to the instability of the complex in air.

One other previously overlooked property of the nickel(II) macrocycle cation is its ability to axially solvate to produce solvento adducts which crystallise from solution. Very hot (100°C), saturated solutions of $[Ni([14]aneN_4)](ClO_4)_2$ in DMSO, DMF and acetonitrile cool to give mauve, grey-green and green crystals respectively, of the disolvento complexes. All of these complexes are unstable with respect to the loss of the solvent molecules returning to the orange square-planar complex; the DMSO and DMF complexes are stable in dry air and may be washed with diethyl ether whereas the acetonitrile complex will lose solvent very rapidly unless stored in an atmosphere of acetonitrile, and attempts to wash the crystals with <u>any</u> solvent (even nujol) cause loss of acetonitrile to give the orange square-planar complex. Solutions of all of these complexes are orange indicating that the axial solvation of the square-planar cation can only effectively occur when such interaction is stabilised by crystal forces. Diffuse reflectance spectra for all three complexes were recorded for freshly prepared samples and show three absorption bands (the longest wavelength band being due to one component of the tetragonally split lowest energy band[191]) corresponding to a distorted <u>trans</u>-octahedral environment for nickel(II) (Table 3.2.). The solid-state spectra of the square-planar complex and the complex formed with 1,2-ethylenediamine (en) are given for comparison. (Note that no tetragonal splitting of the low energy band is observed for the en complex, such behaviour is well characterised for six amine

dihydroxy solution spectra. Speculation as to the composition of this species leads to the suggestion that deprotonation of one or more co-ordinated amines of the macrocycle may have occurred. Unfortunately no satisfactory CHN analysis could be obtained for this compound, probably due to the instability of the complex in air.

One other previously overlooked property of the nickel(II) macrocycle cation is its ability to axially solvate to produce solvento adducts which crystallise from solution. Very hot (100°C), saturated solutions of $[Ni([14]aneN_4)](ClO_4)_2$ in DMSO, DMF and acetonitrile cool to give mauve, grey-green and green crystals respectively, of the disolvento complexes. All of these complexes are unstable with respect to the loss of the solvent molecules returning to the orange square-planar complex; the DMSO and DMF complexes are stable in dry air and may be washed with diethyl ether whereas the acetonitrile complex will lose solvent very rapidly unless stored in an atmosphere of acetonitrile, and attempts to wash the crystals with <u>any</u> solvent (even nujol) cause loss of acetonitrile to give the orange square-planar complex. Solutions of all of these complexes are orange indicating that the axial solvation of the square-planar cation can only effectively occur when such interaction is stabilised by crystal forces. Diffuse reflectance spectra for all three complexes were recorded for freshly prepared samples and show three absorption bands (the longest wavelength band being due to one component of the tetragonally split lowest energy band[191]) corresponding to a distorted <u>trans</u>-octahedral environment for nickel(II) (Table 3.2.). The solid-state spectra of the square-planar complex and the complex formed with 1,2-ethylenediamine (en) are given for comparison (Note that no tetragonal splitting of the low energy band is observed for the en complex, such behaviour is well characterised for six amine

donors on nickel(II)[191,192])

The three solvento compounds have absorption maxima which suffer a bathochromic shift as one proceeds from the weakest donor through to the strongest λ_{max} CH_3CN<DMF<DMSO. This series is the reverse of that expected based purely on donor strength[192] and it is significant that solvento complexes with water and with pyridine are not isolable, despite their comparable donor strengths to nickel(II). This data is probably a manifestation of the steric limitations to complex formation imposed by the macrocycle alkyl backbone.

Table 3.2.

Diffuse reflectance spectral data of some nickel(II)-[14]aneN$_4$ complexes.

Complex*	$^3T_{2g} \leftarrow {}^3A_{2g}$/nm	$^3T_{1g}(F) \leftarrow {}^3A_{2g}$/nm	$^3T_{1g}(P) \leftarrow {}^3A_{2g}$
$[Ni(L)](ClO_4)_2 + OH^-$	------	585(2)	370(2)
$[Ni(L)(DMSO)_2](ClO_4)_2$	650 (5)	520(2)	343(2)
$[Ni(L)(DMF)_2](ClO_4)_2$	630(10)	500(5)	335(2)
$[Ni(L)(CH_3CN)_2](ClO_4)_2$	620(10)	472(2)	322(2)
$[Ni(L)(en)](ClO_4)_2$	------	535(2)	345(2)
$[Ni(L)](ClO_4)_2$	453 ($^3A_{2g} \leftarrow {}^1A_{1g}$)		

*L = [14]aneN$_4$

The acetonitrile and DMSO complexes were subjected to differential scanning calorimetry in order to determine the number of co-ordinated solvents and the energy required to drive them from the complex. The acetonitrile complex showed a single endotherm at 82$\pm$ 1^{o}C and a sample weight loss corresponding to the removal of almost exactly two

equivalents of acetonitrile. The endotherm indicates an energy of 89± 5 kJ mol^{-1} (45 kJ per co-ordinated solvent) for the removal of acetonitrile from the complex at 82°C. Continued heating to higher temperatures gave further endotherms at 128± 2°C, and 339± 2°C and an exotherm at 296± 2°C. The resulting black powder indicated that these latter thermal phenomena were due to melting and charring of the sample. The DMSO complex showed more unusual thermal behaviour with a complex endotherm centred at 135± 2°C containing two components, a major peak at 126± 2°C followed by a smaller peak at 141± 2°C. This behaviour is typical of a process where the solvent molecules firstly dissociate from the nickel complex (126°C) and are then evaporated from the sample at a higher temperature (141°C, possibly decomposition to DMS). Because of this overlapping of endotherms, estimation of the energy required to drive off the solvents from the complex is difficult. The sample weight loss again corresponds almost exactly with the loss of two molecules of DMSO from the complex and so gives an energy of approximately 18± 10 kJ mol^{-1} (9kJ per co-ordinated solvent) for the removal of DMSO from the complex at 126°C. (Details of the experimental method and calculations are given in section 8.3.). This data is seen to confirm the conclusions from the reflectance spectra, above, that steric factors reverse the expected trend in solvento stabilities based on donicity[192], DMSO being less strongly co-ordinated than the weaker donor, acetonitrile.

The work outlined in this section shows the great depth of chemistry still unexplored for a relatively well characterised complex. The tacit assumption of many workers, that the cation $[Ni[14]aneN_4]^{2+}$ exists as purely diamagnetic in co-ordinating solvents has been shown to be false and again illustrates the necessity of obtaining n.m.r.

spectra whereever possible. One final experiment with this system involved the running of a ^{13}C n.m.r. spectrum of the complex in D_2O. The spectrumdisplayed the expected three broadened and paramagnetically shifted resonances, their behaviour being exactly the same as observed in the ^{1}H n.m.r. spectra. However, in addition to these resonances, three other very sharp resonances in the intensity ratio 2:2:1 at δ = 50.86, 49.01, 26.66ppm ref. dioxan 67.26ppm were present at low concentration. The shifts of these three resonances are identical to those observed for the purely diamagnetic complex in nitromethane (see above). The same three resonances were also present in a $[^{2}H]_6$-DMSO solution where, this time, the paramagnetically shifted resonances were well removed from this area of the spectrum. Close examination of the equivalent ^{1}H n.m.r. spectra also shows, quite clearly, the presence of a diamagnetic species which is not free macrocycle. Variable pH ^{13}C n.m.r. spectra show that the diamagnetic species is absent at low pH whilst it is favoured by high pH. Interpretation of these three resonances has not yet been possible, but may be due to a) a conformationa change in the ligand or else b) deprotonation of the co-ordinated amine groups either of which would then prevent axial solvation of the square-planar centrosymmetric complex. Neither interpretation seems wholly satisfactory to date.

The identification and characterisation of the cis-V and trans-III geometries (sections 2 and 3 respectively) are now used as the foundation for a systematic study of the heavy metal complexes of [14]aneN$_4$ below.

SECTION 4. COMPLEXES WITH CADMIUM(II)

Previous references to the cadmium complex of [14]aneN$_4$ are very confused. In 1976, Denning et al[59] very briefly reported the preparation

of the perchlorate salt from $Cd(OH)_2$ and perchloric acid in methanol. No work on the complex was reported and in 1977 when Kodama and Kimura[28] attempted to prepare the cadmium complexes of 12-15 membered rings during their polarographic studies on complex formation they categorically stated that no complex between cadmium(II) nitrate and [14]aneN$_4$ was formed.

Having eliminated the possibility of utilising the synthetic procedure of Denning *et al* as being potentially too dangerous (methanol and perchloric acid having already produced one violent explosion in these laboratories), it was found that, contrary to the observations above, simple 1:1 mixing of cadmium nitrate and [14]aneN$_4$ in methanol with subsequent evaporation of the solvent and washing with chloroform gave a white crystalline compound which analysed well for (Cd([14]aneN$_4$))$(NO_3)_2$. The complex was found to be extremely soluble in many solvents, water, methanol, DMSO and slightly soluble in nitromethane.

The ^{1}H-decoupled, variable temperature ^{13}C n.m.r. spectra of the complex in $D_2O/[^2H]_6$-DMSO 1:1 are shown in figure 4.1. Conductivity studies indicate that the complex is a 2:1 electrolyte in this solvent medium (data are summarised in Table 8.4. for *ca.* $2x10^{-3}$ mol dm^{-3} solutions) and that dissociation of the nitrate ions is complete in solution. The ^{13}C n.m.r. spectra are remarkably complex; at 253K (addition of 10% methanol is required to prevent freezing) the spectrum is seen to contain eight resonances which may readily be ascribed to two distinct species A and B (δ_A= 52.18, 47.51, 28.98ppm ratio 2:2:1; and δ_B= 50.20, 49.66, 49.05, 44.53, 25.54ppm equal intensities;ref. dioxan 67.26ppm.) of unequal populations. On elevation of the temperature the five-line species B undergoes a dynamic process which

Figure 4.1.

^{1}H-decoupled V.T. ^{13}C n.m.r. spectra of $[Cd([14]aneN_4)](NO_3)_2$ in D_2O/DMSO.

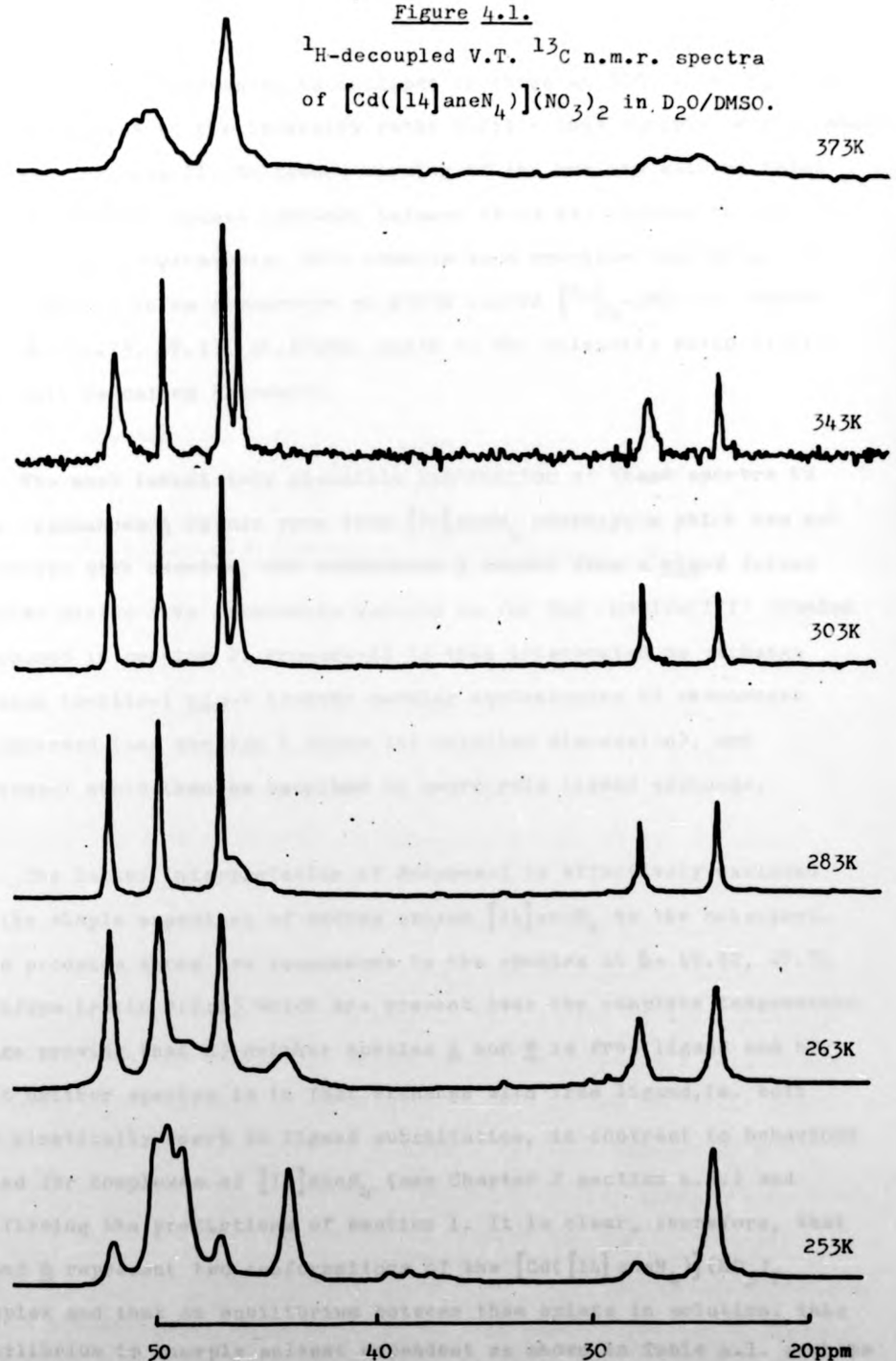

causes the five resonances to collapse to three at 303K with δ_B= 50.02, 46.83, 25.54ppm in the intensity ratio 2:2:1 - this dynamic process shall be termed Process-II. Continued warming of the now two sets of three lines eventually causes exchange between these two species to occur at very high temperatures. This results in a spectrum consisting of a single set of three resonances at >373K (extra $[^2H]_6$-DMSO was added) with δ= 51.13, 47.11, 26.28ppm. again in the intensity ratio 2:2:1 - this will be called Process-I.

The most immediately plausible explanation of these spectra is that resonances A result from free [14]aneN$_4$ macrocycle which has not complexed with cadmium, and resonances B result from a cis-V folded complex giving five resonances exactly as for the rhodium(III) complex discussed in section 2. Process-II is then interpreted as exchange between identical cis-V isomers causing equivalences of resonances as observed (see section 6 below for detailed discussion), and Process-I could then be ascribed to macrocycle ligand exchange.

The latter interpretation of Process-I is effectively excluded by the simple expedient of adding excess [14]aneN$_4$ to the solutions. This produces three new resonances in the spectra at δ= 49.82, 47.76, 26.42ppm (ratio 2:2:1) which are present over the complete temperature range proving that a) neither species A nor B is free ligand and b) that neither species is in fast exchange with free ligand,ie. both are kinetically inert to ligand substitution, in contrast to behaviour noted for complexes of [14]aneS$_4$ (see Chapter 2 section 4.2.) and confirming the predictions of section 1. It is clear, therefore, that A and B represent two conformations of the [Cd([14]aneN$_4$)](NO$_3$)$_2$ complex and that an equilibrium between them exists in solution. This equilibrium is sharply solvent dependent as shown in Table 4.1. perhaps

indicating some solvent involvement in the equilibrium.

Table 4.1.

Ratio of species A:B for $[Cd([14]aneN_4)]^{2+}$ based on integrals of the ^{13}C n.m.r. spectra in various solvents.

Solvent	Ratio A/B at 303K.
D_2O	1.43
$[^2H]_4$-methanol	2.63
$[^2H]_3$-nitromethane	1.57
$[^2H]_6$-DMSO	0.34

If one considers the spectra from 303 - 373K, their appearance and the dynamic process displayed are seen to be qualitatively very similar to those described for the complex $[Ni([14]aneS_4)](BF_4)_2$ in Chapter 2, section 2. There, the two species were assigned to have trans-I and trans-III geometries and interconversion of these was postulated as proceeding via double sulphur configurational inversions. It seems reasonable, therefore, to make a similar assignment in this instance implying that whereas the nickel(II) ion (r = 0.69Å[6]) is marginal in size for fitting within the ring of $[14]aneS_4$, the cadmium(II) ion (r = 0.97Å[6]) is sufficiently large to cause a similar equilibrium by being marginal in size for fitting within the larger cavity of $[14]aneN_4$. This latter hypothesis seems reasonable especially in view of the fact that even an ion as large as silver(II) (r = 0.89Å[6]) is still capable of being accommodated within the 14-membered ring in a perfect trans-III geometry[178] Process-I is, therefore, postulated to involve two configurational inversions of co-ordinated nitrogen atoms in either six-membered chelate ring. A complete line-shape analysis of this dynamic process[143] for all

three pairs of exchanging peaks gives activation parameters shown in Table 4.2. The activation energy is seen to be almost identical to that

Table 4.2.

Activation parameters (298K) for the dynamic processes in the ^{13}C n.m.r. spectra of $[Cd([14]aneN_4)](NO_3)_2$ in $D_2O/[^2H]_6$- DMSO (see text).

Process-II[a] δ/ppm of peaks	$\Delta H^{\ddagger}$/kJ mol^{-1}	$\Delta S^{\ddagger}$/J K^{-1} mol^{-1}	10^3 k_{298}/s^{-1}
28.98 25.54	75(12)	-18(30)	46
47.51 46.83*	112(20)*	85(44)*	0.2*
52.18 50.02	74 (4)	-23(11)	50
All data points	78(14)	-11(20)	49
Process-I[b]			
49.05 44.53	8.8(1.3)	-169(15)	2.85×10^5

a)Least-squares fit for four temperatures in the range 363-383K
b)Least-squares fit for four temperatures in the range 240-263K
*peaks too close for accurate fitting.

found for the $[Ni[14]aneS_4]^{2+}$system (70(10)kJ mol^{-1}) and likewise the entropy of activation is virtually zero as before. The data tends to confirm the similar interpretations for both systems and the energy of the inversion process is seen to be high as predicted in section 1 (remembering that cadmium(II) is a very labile metal ion compared to nickel(II)ion, and therefore would be expected to undergo much more rapid inversion kinetics for the same donor atom. Nitrogen inversions are therefore much more difficult than sulphur inversions.)

If the above interpretation of Process-II is correct, then Process-I

must be interpreted as folding of one of the trans species away from planarity. Two such foldings will result in the production of a five-line spectrum i) folding to a cis-V type geometry (cf. rhodium complex section 2) and ii) folding to a trigonal-bipyramidal type geometry previously determined for a copper(II) complex of rac-Me_6-[14]aneN$_4$[194]. Both processes will produce what are effectively axial and equatorial pairs of nitrogen atoms which will cause splittings of the carbon resonances next to these donors, exactly as observed.

Distinction between these two processes is difficult but several factors point to the second interpretation (folding to give a trigonal-bipyramidal geometry) as being more likely. These factors may be summarised as:

a) Folding to a cis-V type geometry requires at least two nitrogen configurational inversions for either trans isomer, whichis exactly the mechanism required for Process-II discussed above. The fact that the activation energy for Process-I (from a complete lineshape analysis Table 4.2.) is only 9kJ mol^{-1} compared with 78kJ mol^{-1} for Process-II indicates very different mechanisms.

b) The actual splitting pattern is quite different from all of the previous patterns obtained for 14-membered rings in cis-V geometries. Whereas the previous spectra all show one resonance to low-field of the others, the present spectrum shows three resonances to low-field.

c) The very low activation energy of the dynamic process coupled with the large negative entropy of activation imply some facile rearrangement process about the metal ion leading to increased solvation in the transition state. Both such phenomena may be reasonably accommodated by a simple bond-rotation process such as folding to a trigonal-bipyramid (details below)

If one accepts these pointers, then dynamic Process-I is interpreted as folding of one of the trans geometries to a trigonal-bipyramid. Consideration of the two trans geometries shows that trans-III cannot possibly fold away from planarity without inverting at least two nitrogen atom configurations[138]. A complex with the trans-I geometry, on the other hand, can easily fold back two of its nitrogen atoms on to the opposite side of the plane to the four amine protons[138]. Indeed this folding is seen to be favoured, from a consideration of molecular models, since it minimises any interaction between the amine protons and the fifth monodentate ligand whilst still allowing both six-membered chelate rings to adopt their favoured chair conformations.

It is clear, therefore, that, of the two trans species present, trans-I is the one which will readily fold to a trigonal-bipyramid and is therefore assigned as species B in the ^{13}C n.m.r. spectra; species A is therefore the trans-III conformer. The folding of a trans-I type conformation to give a trigonal-bipyramid has a precedent in the copper-(II) complex of a 14-membered ring mentioned above[194].

The whole system is best summarised by reference to figure 4.2. Beginning with Process-II (exchange process labelled k_2 in figure), it is seen that axial and equatorial nitrogen atoms of the trigonal-bipyramid may be interconverted by passage through a trans-I 'square-pyramidal' intermediate (solid and open circles represent pairs of equivalent nitrogen donors). This interconversion, when rapid, will produce the observed collapse of five resonances down to three. The activation parameters for the process may be interpreted as indicating that the bond rotation about the metal is a low-energy process, which is reasonable, while the large negative entropy indicates significantly

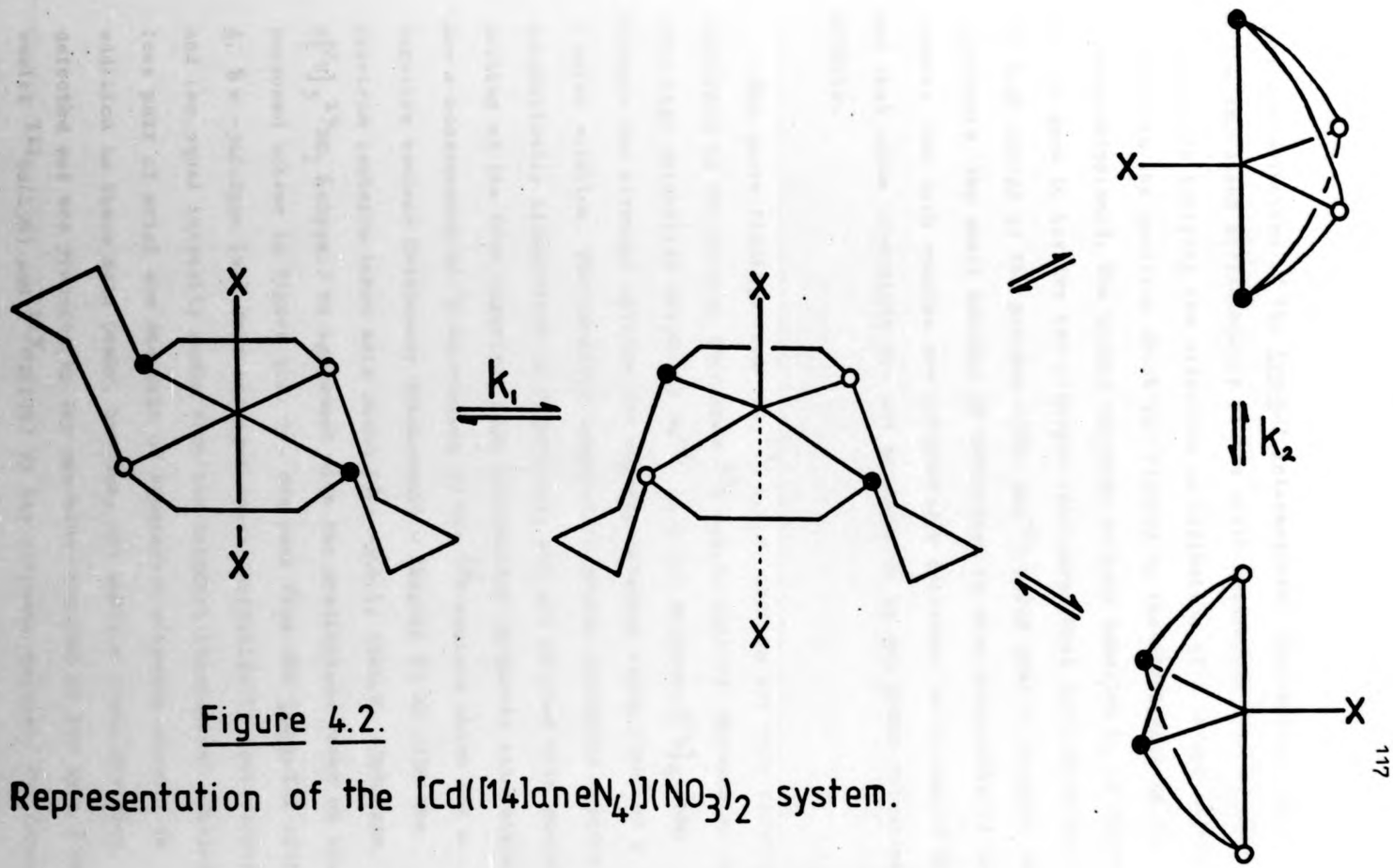

Figure 4.2.

Representation of the $[Cd([14]aneN_4)](NO_3)_2$ system.

increased solvation of the trans-I intermediate. This may well be due to the increased accessibility of the sixth octahedral site in the intermediate implying the effective co-ordination of a second solvent molecule in the position which was blocked by the macrocycle in the trigonal-bipyramid. The second exchange process labelled k_1 in figure 4.2. is seen to involve two nitrogen configurational inversions and the high energy of the process (78kJ mol^{-1}) would tend to support this hypothesis. The small entropy of activation is also reasonable if one assumes that both species are octahedrally solvated, as discussed above, and that amine inversions are not accompanied by any great solvation effects.

The above findings from the ^{13}C n.m.r. spectra are very clearly confirmed by the natural abundance ^{15}N n.m.r. spectra. Because of the very high solubility (>1.0 mol dm^{-3}) in a 1:1 methanol/$[^2H]_6$-DMSO mixture the nitrogen spectra are readily obtained using 15cm^3 of a 1 molar solution. The variable temperature proton decoupled spectra are schematically illustrated in figure 4.3. and are plotted with positive, instead of the true negative, peak intensities (negative intensities are a consequence of ^1H decoupling of the ^{15}N nucleus which has a negative nuclear Overhauser enhancement - Chapter 6) At 233K the spectrum contains three main peaks (δ = -344.1, -348.2, -349.0ppm, ref. $C[^2H]_3{}^{15}NO_2$ δ=0ppm.) in agreement with the predictions based on the proposed scheme in figure 4.2. ie. one peak from the trans-III species A, δ = -348.2ppm (all four nitrogen donors magnetically equivalent), and two equal intensity peaks from the trigonal-bipyramidal species B (one pair of axial and one pair of equatorial nitrogen atoms). In addition to these main peaks, however, six smaller peaks are also detected and are produced by the one-bond coupling to the spin ½ metal nuclei ^{111}Cd(13%) and ^{113}Cd(12%) by the nitrogen nucleus. The observati

Figure 4.3.

V.T. ^{15}N n.m.r. spectra of $[Cd([14]aneN_4)](NO_3)_2$ in DMSO/methanol.

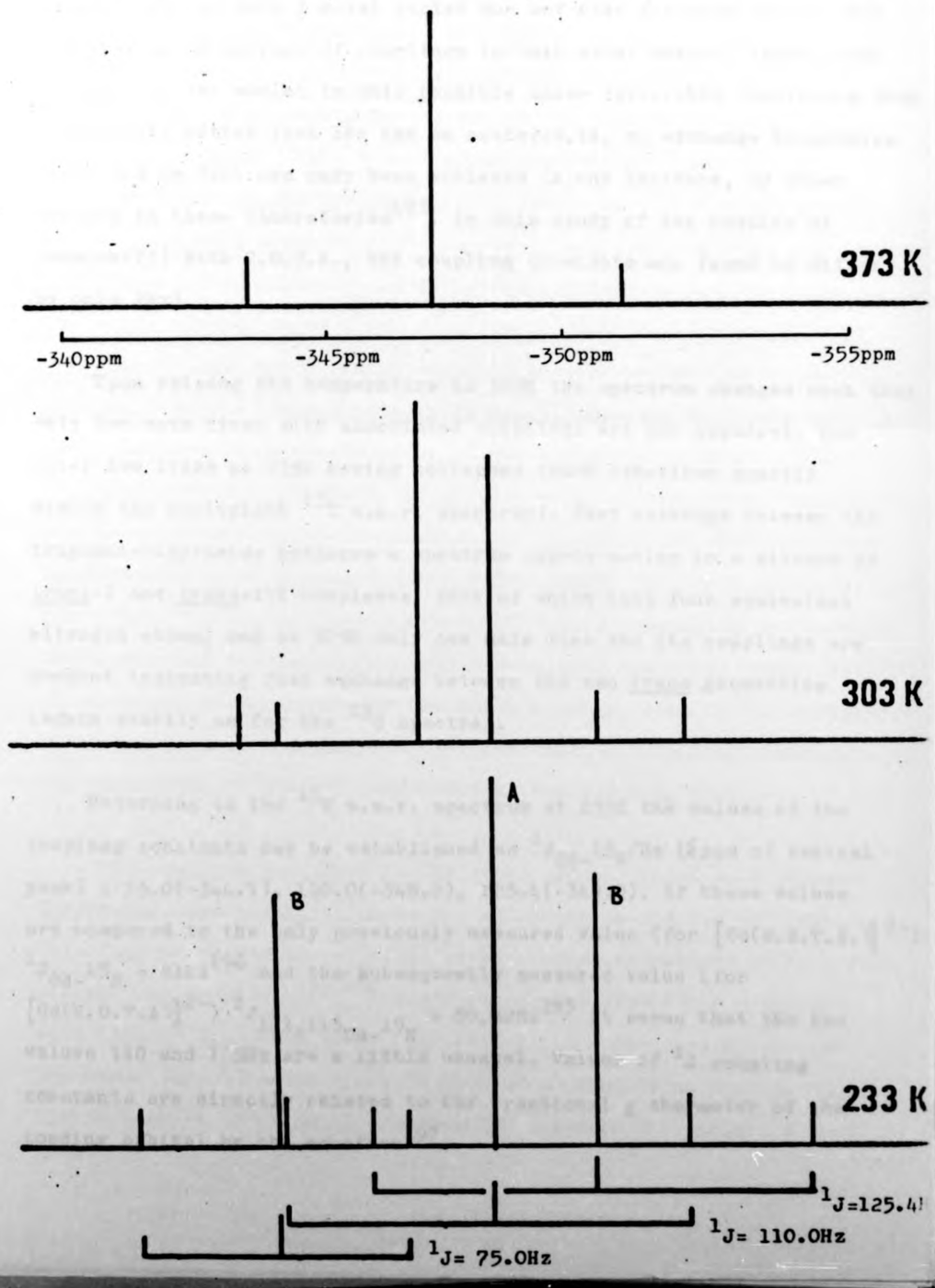

of only one pair of couplings to each main peak means that distinction between the two spin ½ metal nuclei has not been achieved and so each coupling is an average of couplings to both metal nuclei. (Resolution between the two nuclei is only possible under favourable conditions when line-widths better than 1Hz can be achieved, ie. no exchange broadening etc., and in fact has only been achieved in one instance, by other workers in these laboratories[195]. In this study of the complex of cadmium(II) with C.D.T.A., the coupling constants are found to differ by only 2Hz).

Upon raising the temperature to 303K the spectrum changes such that only two main lines with associated couplings are now apparent, the outer two lines at 233K having collapsed (such behaviour exactly mimics the equivalent ^{13}C n.m.r. spectrum). Fast exchange between the trigonal-bipyramids produces a spectrum approximating to a mixture of trans-I and trans-III complexes, both of which have four equivalent nitrogen atoms, and at 373K only one main line and its couplings are present indicating fast exchange between the two trans geometries (again exactly as for the ^{13}C spectra).

Returning to the ^{15}N n.m.r. spectrum at 233K the values of the coupling constants may be established as $^{1}J_{Cd-^{15}N}$/Hz (δppm of central peak) : 75.0(-344.1), 110.0(-348.2), 125.4(-349.0). If these values are compared to the only previously measured value (for $[Cd(E.D.T.A.)]^{2-}$) $^{1}J_{Cd-^{15}N}$ = 81Hz[196] and the subsequently measured value (for $[Cd(C.D.T.A)]^{2-}$) $^{1}J_{^{111,113}Cd-^{15}N}$ = 80,82Hz[195] it seems that the two values 110 and 125Hz are a little unusual. Values of ^{1}J coupling constants are directly related to the fractional s character of the bonding orbital by the equation[197]:

of only one pair of couplings to each main peak means that distinction between the two spin ½ metal nuclei has not been achieved and so each coupling is an average of couplings to both metal nuclei. (Resolution between the two nuclei is only possible under favourable conditions when line-widths better than 1Hz can be achieved,ie. no exchange broadening etc., and in fact has only been achieved in one instance, by other workers in these laboratories[195]. In this study of the complex of cadmium(II) with C.D.T.A., the coupling constants are found to differ by only 2Hz).

Upon raising the temperature to 303K the spectrum changes such that only two main lines with associated couplings are now apparent, the outer two lines at 233K having collapsed (such behaviour exactly mimics the equivalent ^{13}C n.m.r. spectrum). Fast exchange between the trigonal-bipyramids produces a spectrum approximating to a mixture of trans-I and trans-III complexes, both of which have four equivalent nitrogen atoms, and at 373K only one main line and its couplings are present indicating fast exchange between the two trans geometries (again exactly as for the ^{13}C spectra).

Returning to the ^{15}N n.m.r. spectrum at 233K the values of the coupling constants may be established as $^{1}J_{Cd-^{15}N}$/Hz (δppm of central peak) : 75.0(-344.1), 110.0(-348.2), 125.4(-349.0). If these values are compared to the only previously measured value (for $[Cd(E.D.T.A.)]^{2-}$) $^{1}J_{Cd-^{15}N}$ = 81Hz[196] and the subsequently measured value (for $[Cd(C.D.T.A)]^{2-}$) $^{1}J_{^{111},^{113}Cd-^{15}N}$ = 80,82Hz[195] it seems that the two values 110 and 125Hz are a little unusual. Values of ^{1}J coupling constants are directly related to the fractional s character of the bonding orbital by the equation[197]:

$$^{1}J_{Cd-^{15}N} = \alpha^2_{Cd}.\alpha^2_{N}.[\Psi_{Cd(5s)}(0)]^2[\Psi_{N(2s)}(0)^2](\Delta E)^{-1}$$

ΔE is the singlet-triplet excitation energy, the α's are the s character of the hybrids at each atom, and the $\Psi(0)$'s are the electron densities at the respective nuclei. The ^{1}J values are usually found to be independent of ΔE[198] and the coupling constant is then directly proportional to terms involving the s character of the bonding orbitals. It is clear that metal-nitrogen one-bond coupling constants are a direct reflection of the bonding scheme in the complex

The ^{1}J data may be satisfactorily interpreted within the scheme deduced from the ^{13}C n.m.r. results and illustrated in figure 4.2. If one considers first the ^{1}J value of the trans-III species = 110Hz, it is likely that co-ordination of the macrocycle to the large cadmium(II) ion in this rigidly planar fashion will constrict the metal-nitrogen bond lengths to be somewhat shorter than ideal. This well characterised phenomenon[45] would be expected to lead to a corresponding increase in the equatorial bond strengths whilst weakening the axial bonds. This constrictive strengthening of the metal-nitrogen bond in the macrocycle plane may well be the cause of the increased ^{1}J value as compared to the comparitively unrestricted E.D.T.A. and C.D.T.A. complexes.

The coupling constants to the other species which is trigonal-bipyramidal are quite different for axial and equatorial nitrogens. This fact is consistent with the known crystal structures of trigonal-bipyramidal complexes[199,200] where almost invariably the equatorial bond lengths are found to be significantly shorter (ca. 0.1Å) than the axial for d^{10} metal ions. If this distortion is present in this system then it is perfectly reasonable to assign the larger ^{1}J value

125.4Hz, to the equatorial donors and the 75Hz value is then associated with the axial donors. This would imply that axial and equatorial donors have very different s character which is in accord with the dsp^3 trigonal-bipyramidal hybridisation scheme which gives five non-equivalent hybrid orbitals. The assignment of the smaller ^1J value to the axial donors is also consistent with this hybridisation scheme since the axial hybrids are largely d_z2 and p_z in character whereas the equatorial are largely s, p_x and p_y.

The cadmium system is, therefore, seen to be extremely complex and yet a cogent interpretation of the species present has been possible using a combination of n.m.r. nuclei as structural probes. The analysis has produced several new results:

a) The existence of the complex has been confirmed (cf. ref. 28) and been shown to be non-labile with respect to dissociation (witnessed by no exchange between complex species and free ligand, and also by appearance of metal-nitrogen couplings over the full temperature range.)

b) The structure of species B provides the first indirect evidence of both a trans-I set of nitrogen configurations and folding of such a geometry to a trigonal-bipyramid for [14]aneN$_4$.

c) The ^{15}N n.m.r. spectrum at 233K has effectively tripled the amount of cadmium-nitrogen coupling data available in the literature and has allowed a direct comparison of the bonding to axial and equatorial donors in a trigonal-bipyramidal complex. These latter data may be of considerable theoretical interest.

These results indicate [14]aneN$_4$ to be a very suitable macrocycle for extensive investigation in relation to chelation therapy since

a very soluble, stable complex is formed with one of the toxic heavy metal ions of interest, cadmium(II). Investigation of the other heavy metal ion complexes is now reported.

SECTION 5. COMPLEX WITH MERCURY(II)

There are two previous references to the cation $(Hg[14]aneN_4)^{2+}$ in the literature and both imply that the mercury(II) ion ($r = 1.06\text{Å}$[87]) is too large to sit within the macrocycle cavity and that the complex must, therefore, have a folded geometry. Denning *et al*[59] have prepared and isolated the perchlorate and fluoroborate salts of the complex and subjected them to electrochemical oxidation in an attempt to produce the first ever mercury(III) species (see Chapter 1, section 1.4.). These workers propose that both the mercury(II) and(III) complexes have folded macrocycles based on size arguements and the value of g_{av} from the mercury(III) species e.s.r. spectrum. Kodama and Kimura have also studied the mercury(II) complex in an attempt to measure the complex formation rates by polarographic techniques[29]. These workers also argue that planar co-ordination is unlikely and that a folded geometry of the ring is probable. However, the stability data they obtain for 12-15 membered ring-sizes indicates that only the 14-membered ring displays a macrocyclic effect,implying its structure is somewhat different to the other, presumably folded *cis* , complexes studied. Kodama expresses this by saying "Some as yet unidentified properties attached to the $(Hg[14]aneN_4)^{2+}$ structure may be responsible for the anomalous thermodynamic data."

In order to structurally identify the mercury(II) complex the ^{13}C and ^{15}N n.m.r. spectra of the extremely soluble (>1.5 mol dm^{-3}) perchlora

salt were obtained in methanol/DMSO solvent. The complex is a 2:1 electrolyte in this medium indicating a totally ionised solution, (data are summarised in Table 8.4. for ca. 2×10^{-3} mol dm^{-3} solutions). Variable temperature proton decoupled ^{13}C n.m.r. spectra show only three resonances (δ = 53.47, 46.76, 29.37ppm, intensity ratio 2:2:1, ref. dioxan 67.26ppm) over the temperature range 233-373K with no significant broadening other than that due to viscosity effects. The presence of only three lines in this intensity ratio implies one of three interpretations:

i) a rigid trans geometry for the complex,

ii) a folding process as for cadmium(II) but which is proceeding very rapidly on the n.m.r. timescale and cannot be frozen out,

iii) the situation is exactly the same as for the $(Hg[14]aneS_4)^{2+}$ complex discussed in Chapter 2 where fast ligand exchange is occuring so producing an averaged three line spectrum.

Taking these interpretations in reverse order, (iii) necessitates a kinetically labile complex and this requirement is difficult to reconcile with the high stability constant ($\log K$ = 23.0)[29]. Prolonged accumulation of the ^{13}C n.m.r. spectrum at 300K shows minor couplings associated with each of the three main peaks. These couplings, to the spin ½ nucleus ^{199}Hg (16%), by their very presence, prove that the macrocycle is not in total fast exchange and that the ^{13}C spectrum is indeed the spectrum of the discreet complex. Values of the coupling constants are $^{2}J_{^{199}Hg-^{13}C}$/Hz (δppm. of central peak): 26.9 (53.47), 15.6 (46.76) and $^{3}J_{^{199}Hg-^{13}C}$/Hz (δppm.): 43.5 (29.37). The fact that the magnitude of the ^{3}J coupling is greater than the ^{2}J value is not unusual and is well characterised for many organomercury compounds[201]. The underlying theory of two and three bond coupling constants is not

well established other than for vicinal proton-proton coupling, and may qualitatively be said to include both an s orbital character term[201] and an angular term (e.g. the Karplus relationship for ^3J proton-proton couplings). Without knowledge of the sign of the observed coupling constants it is not possible to make any direct deductions from their values[202].

Interpretation (ii) above, whilst plausible, does require that the dynamic process causing the observation of only three resonances be very fast indeed on the n.m.r. timescale. Possible folding mechanisms are identical to those discussed for cadmium(II) complexes in section 4 (ie. to cis-V or to a trigonal-bipyramid). Folding to a cis-V geometry is immediately discounted since the energy of this process is very high (cf. lead(II) in section 6). If the dynamic process is therefore folding to a trigonal-bipyramid it is not clear why this process should be so much more rapid for mercury(II) than for cadmium(II) (above) where the dynamics could be frozen out at 253K. The fact that there is no broadening of any of the three resonances down to 233K suggests that there is no dynamic process involved and so would tend to discount this interpretation.

This leaves the seemingly unlikely explanation of the spectra as being due to a trans geometry with the macrocycle co-ordinated in a rigidly planar fashion. The arguements quoted above clearly imply that the mercury(II) ion is too large to sit in the macrocycle plane as would be required in a trans-III geometry and so the only plausible explanation of all the available data is that the macrocycle has adopted a trans-I geometry. With this macrocycle conformation the mercury(II) ion can then reside above the plane of the four donors

and so avoids having to fit into the ring. This postulated structure is identical to that found for the $[Hg[14]aneS_4.(OH_2)]^{2+}$ cation in Chapter 2 and leads to the prediction that the ion may be five-co-ordinate in a square-planar geometry just as for this latter ion. As a test of this prediction the complex $[Hg([14]aneN_4)Cl_2]$ was prepared and confirmed by ^{13}C n.m.r. to have a similar structure to the perchlorate in showing only three resonances δ= 52.67, 47.71, 29.31ppm, (2:2:1), ref. dioxan 67.26ppm in methanol/DMSO. This latter complex was found to be a 1:1 electrolyte in DMSO solution (data are summarised in Table 8.3. for ca. $2x10^{-3}$ mol dm^{-3} solutions) which clearly implies that one chloride ion remains co-ordinated in a five-co-ordinate complex.

The ^{15}N n.m.r. spectra of the perchlorate complex were recorded and they confirmed that no splitting or broadening due to a folding process could be detected to 253K. The single resonance at δ= -335.8ppm ref external $C[^2H]_3{}^{15}NO_2$ δ= Oppm. shows mercury couplings, as expected, with $^1J_{^{199}Hg-^{15}N}$ = 317.67Hz. (figure 5.1.) Since this is the first and only one bond mercury-nitrogen coupling constant ever observed it is difficult to make comparisons but if one does compare the reduced coupling constant[203] (which takes into account differing nuclei) of $^1K_{HgN} = 1.46 \times 10^{22}$ N A^2 m^{-3} with that of simple organo-mercury compound $^1K_{HgC} = 1.28 \times 10^{22}$ N A^2 m^{-3} (Me_2Hg)[201], the correlation is quite good indicating that this current value of the ^1J coupling constant may be regarded as fairly normal. This last point would also tend to support the postulated structure with the mercury sitting out of the plane of the ring and so not experiencing any great constrictive effect upon the coupling constant (cf. cadmium trans-III species in section 4).

The n.m.r. and conductivity data would therefore seem to imply a

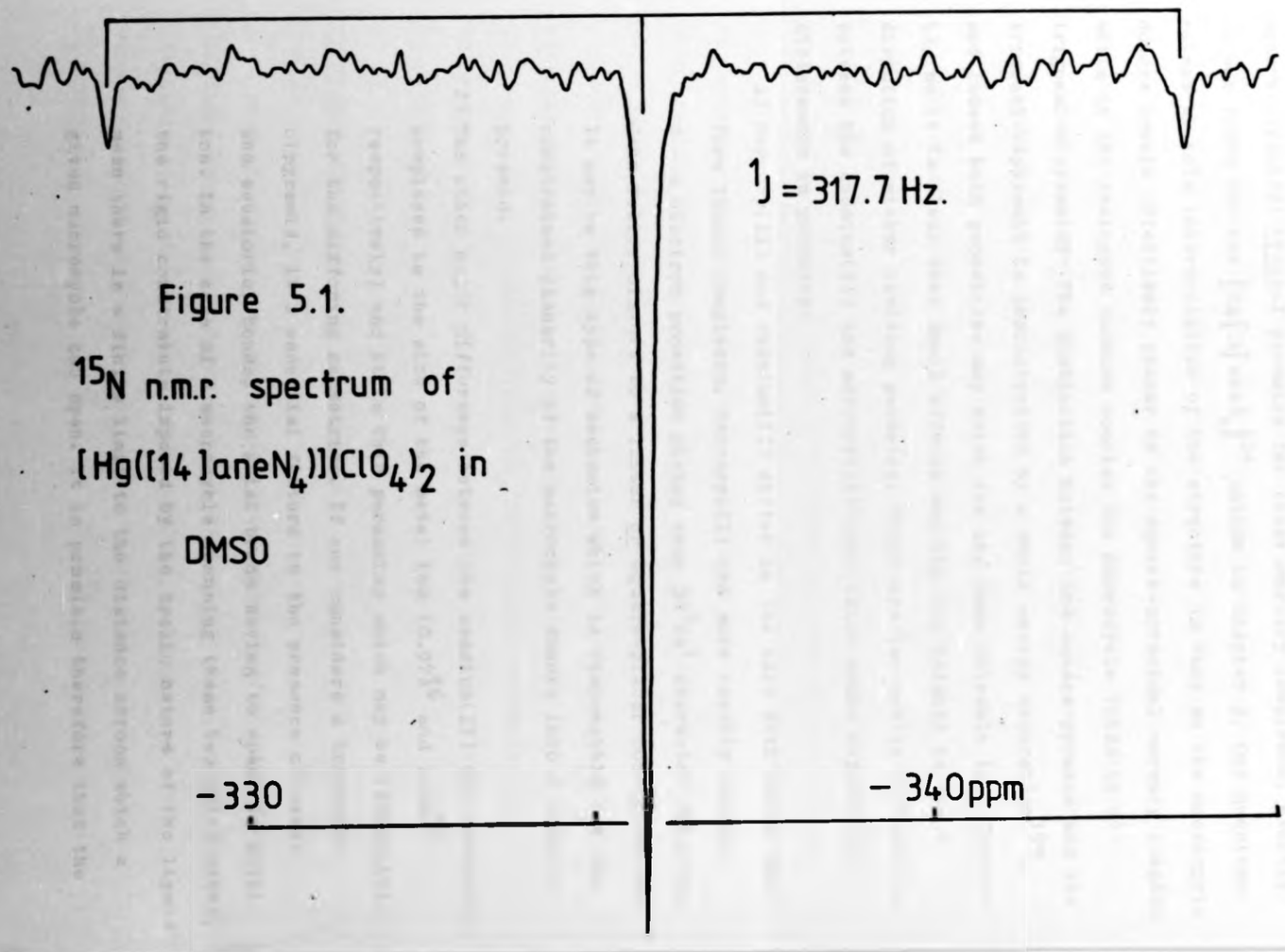

Figure 5.1.

^{15}N n.m.r. spectrum of

$[Hg([14]aneN_4)](ClO_4)_2$ in

DMSO

square-pyramidal trans-I geometry for these mercury complexes, exactly as was found for the $[Hg[14]aneS_4]^{2+}$ cation in Chapter 2. One question raised by this interpretation of the structure is "why do the macrocycle donors remain effectively planar in the square-pyramidal mercury complex while in the analogous cadmium complex the macrocycle folds to a trigonal-bipyramid?" The distinction between the square-pyramid and the trigonal-bipyramid is characterised by a small energy separation[199], and indeed both geometries may exist for the same molecule (see Chapter 4), so it is clear that small effects may tip the balance in the direction of either limiting geometry. There are two subtle differences between the cadmium(II) and mercury(II) ions which could explain the differences in geometry:

1) Mercury(II) and cadmium(II) differ in the ease with which they form linear complexes. Mercury(II) can more readily undergo d - s electron promotion giving some $5d^9 6s^1$ character which can Jahn-Teller distort to a linear or square-planar configuration. It may be this type of mechanism which is responsible for the constrained planarity of the macrocycle donors into a square-pyramid.

2) The other major difference between the cadmium(II) and mercury(II) complexes is the size of the metal ion (0.97Å[6] and 1.06Å[7] respectively) and it is this parameter which may be responsible for the differing geometries. If one considers a trigonal-bipyramid, it's essential feature is the presence of axial and equatorial bonds, the axial bonds having to span the metal ion. In the case of a macrocycle spanning these two axial sites, the rigid constraints imposed by the cyclic nature of the ligand mean there is a finite limit to the distance across which a given macrocycle can span. It is possible therefore that the

the cadmium(II) ion is just sufficiently small to allow the 14-membered ring to span these axial sites and so take up a folded geometry but that the larger mercury(II) ion prevents this. In the latter case, therefore, the macrocycle cannot physically fit around the mercury(II) ion in a regular trigonal-bipyramid and so the delicate structural balance may be tipped in favour of the less sterically constrained square-pyramid.

The mercury system is seen to again provide indirect evidence for a trans-I macrocycle geometry, this time in a rigid square-pyramidal complex and it is hoped that an X-ray crystal structure of the chloride complex may be completed in the near future in order to confirm the conclusions above. In addition to this structural data, which goes some way towards explaining other workers anomalous data[29], the system has also provided the first recorded $^{1}J_{^{199}Hg-^{15}N}$ coupling constant. This value may be of intrinsic theoretical interest, as well as providing a probe for the bonding in square-pyramidal complexes if it can be put into context with other values for known, more orthodox geometries. In connection with this latter point, work is proceeding towards the accumulation of $^{1}J_{HgN}$ values (e.g. for $Hg(C.D.T.A.)^{2-}$) in these laboratories.

SECTION 6. COMPLEXES WITH LEAD(II)

The current state of the literature for lead(II) complexes of [14]aneN$_4$ is much less confused than that for cadmium(II) and mercury(II) complexes above. Kodama and Kimura[28] simply report that no complex was formed during their polarographic studies and this they ascribe to a severe mismatch between the cation (r = 1.20Å[6]) and macrocycle size.

Contrary to this report, however, it is found from this work that a complex between $Pb(NO_3)_2$ and [14]aneN$_4$ is readily produced in dry DMSO. The use of dry DMSO as the preparative solvent was found to be essential since the complex does not appear to form in any other medium and if any water is present a white precipitate is immediately formed which is then insoluble in dry DMSO. This white precipitate is most likely a hydroxy complex and its presence is probably why previous workers failed to identify any complex in water[29].

The complex itself is extremely soluble in DMSO (>1 mol dm^{-3}), and conductivity measurements on a 2×10^{-3} mol dm^{-3} solution show it to be a 2:1 electrolyte, the nitrate ions being ionised in solution (data summarised in Table 8.4). The white crystalline compound resulting from precipitation of the DMSO solution with dry methanol analyses as $[Pb([14]aneN_4)](NO_3)_2$, proving that this complex is indeed the first of [14]aneN$_4$ with a non-transition metal. Consideration of the possible structure of this complex suggests that the lead(II) ion is too large to be accommodated within the plane of the macrocycle and so by analogy with the structures found for mercury(II) and cadmium (II) complexes some form of folding away from planarity or else the adoption of a trans-I geometry may be predicted.

The I.R. spectrum of the solid complex (nujol mull) shows bands which may be assigned to monodentate nitrate groups (see Section 8.6) implying these to be co-ordinated in the crystal. The variable temperature proton decoupled ^{13}C n.m.r. spectra in $[^2H]_6$-DMSO are shown in figure 6.1. The 303K spectrum shows five sharp equal intensity resonances at δ=50.93, 49.24, 48.01, 46.55, 26.11ppm, ref. dioxan 67.26ppm, while the peak at 49.24ppm also shows minor side bands due

Figure 6.1.

V.T. ^{13}C n.m.r. spectra of $[Pb([14]aneN_4)](NO_3)_2$ in $[^2H]_6$-DMSO.

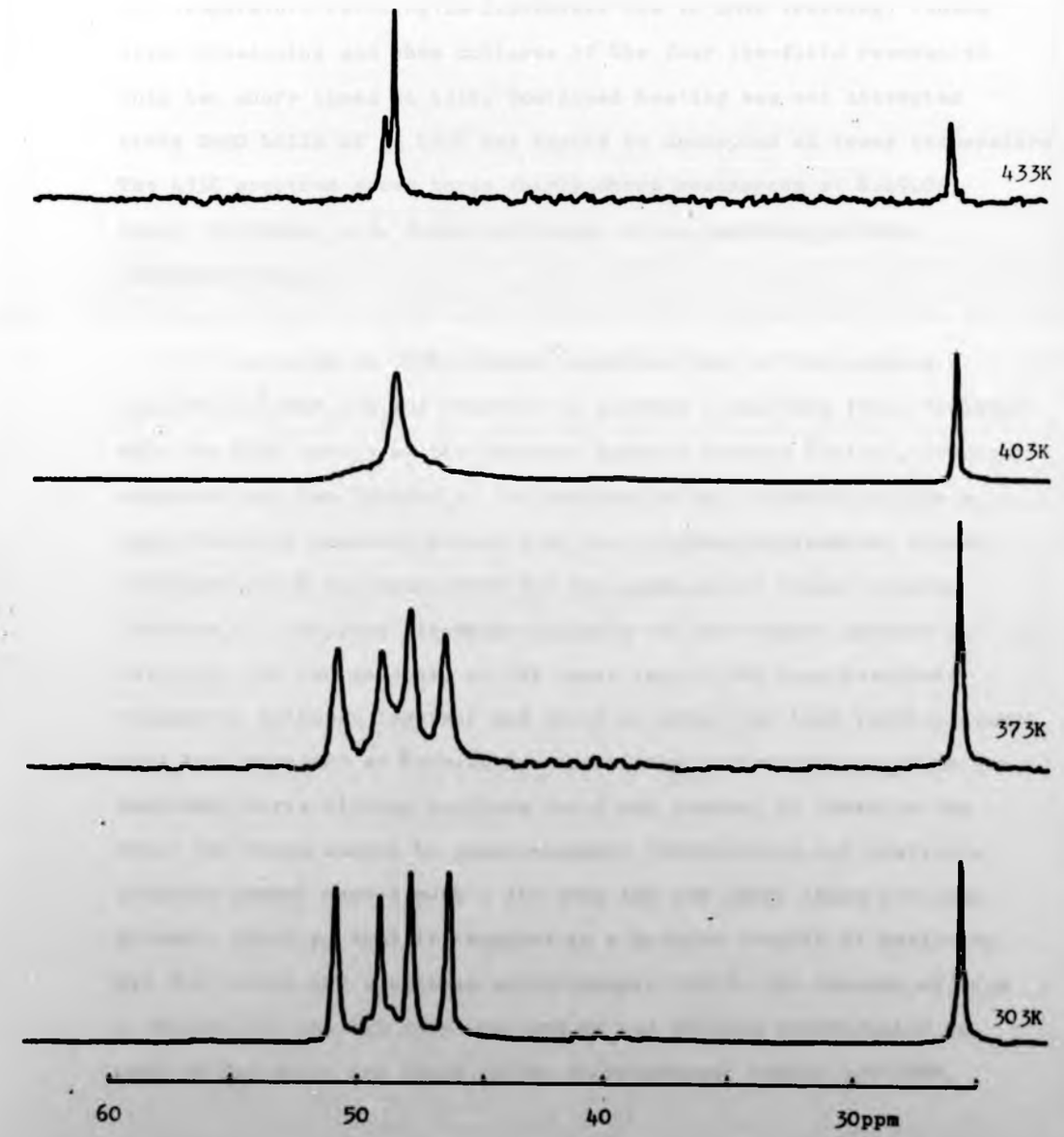

to coupling to the spin ½ nucleus ^{207}Pb (24%) $^{2}J_{^{207}Pb-^{13}C}$ = 21.3 Hz. The presence of five lines in the spectrum clearly implies a folded geometry for the macrocycle and the coupling on one of the peaks also proves that rapid macrocycle exchange is not occurring. Elevation of the temperature (cooling is impossible due to DMSO freezing) causes first broadening and then collapse of the four low-field resonances into two sharp lines at 433K. Continued heating was not attempted since DMSO boils at ca 450K and begins to decompose at lower temperatures. The 433K spectrum shows three fairly sharp resonances at δ=49.06, 48.69, 26.58ppm, ref. dioxan 67.26ppm, in an approximate 2:2:1 intensity ratio.

The spectrum at 303K closely resembles that of the complex cis-[Rh([14]aneN$_4$)Cl$_2$]Cl reported in section 2 and this fact, together with the high energy of the observed dynamic process (below), strongly suggests that the folding of the macrocycle has occurred to give a cis-octahedral geometry rather than the trigonal-bipyramidal stereochemistry which was postulated for the cadmium(II) folded complex (section 4). Complete lineshape analysis of the dynamic process is difficult for two reasons, a) the inner two of the four low-field resonances collapse together and would be ideal for line fitting except that the resonance at δ=49.24 has associated lead couplings which our available curve-fitting routines could not handle; b) likewise the outer two lines cannot be simultaneously fitted since our available programs cannot handle such a fit when the two inner lines are also present. Ideally, what is required is a program capable of analysing all four lines and couplings synchronously but in the absence of such a routine the spectra were analysed by (i) fitting individually to both of the outer two lines in the slow-exchange region 320-350K,

(ii) comparing the two values of the exchange rate with each other for consistency and (iii) simulating a complete spectrum using the derived value of the exchange rate parameter and comparing this simulation with the observed data. This process produced the rate data, of reasonable quality, shown in Table 6.1.

Table 6.1.

Activation parameters (298K) for the dynamic process in the ^{13}C n.m.r. spectra of $[Pb([14]aneN_4)](NO_3)_2$ in $[^2H]_6$-DMSO .

δppm of fitted peak	$\Delta H^{\ddagger}$/kJ mol^{-1}*	$\Delta S^{\ddagger}$/J K^{-1}mol^{-1}*	k_{298}/s^{-1}*
50.93	107(17)	95(50)	8.3×10^{-2}
46.55	113 (5)	111(13)	5.6×10^{-2}

*Least-squares analysis of rate data at four temperatures 320 - 350K.

If the activation parameters of the dynamic process are compared with those of the cadmium(II) system where folding to a trigonal-bipyramid has been deduced, the present process is seen to bear no relation to the latter in thermodynamic terms. This lends considerable weight to the interpretation of the structure in terms of a cis-V type 'octahedral' geometry, (the lone-pair remaining on the lead(II) ion being assumed to occupy an essentially spherically symmetrical orbital and therefore stereochemically inactive).

The dynamic process is therefore interpreted as being inter-conversion of two identical cis-octahedral geometries. This may proceed either by four, linked nitrogen inversions or (more likely) by passage of the lead(II) ion through the macrocycle ring and out the other side.

Figure 6.2.

Representation of the dynamic process evident in the ^{13}C n.m.r. spectra of $[Pb([14]aneN_4)](NO_3)_2$ in DMSO, (X =DMSO).

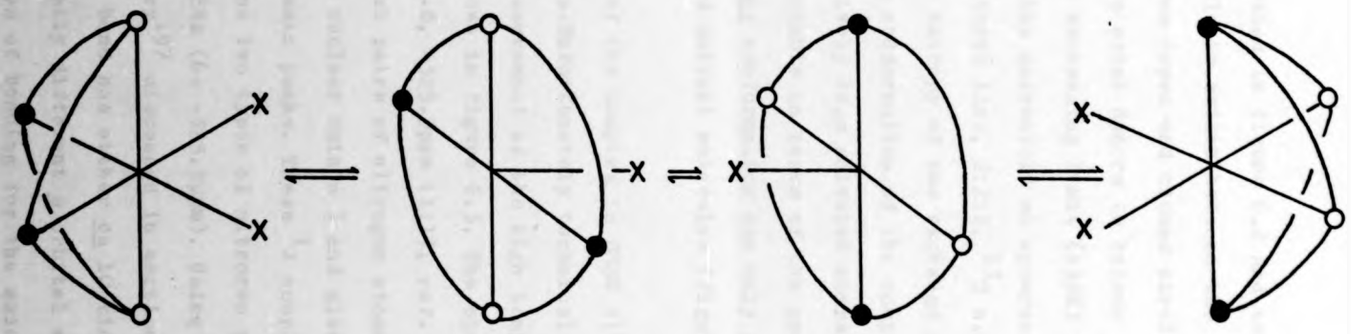

This latter process is illustrated in figure 6.2 and can be seen to allow the fold in the macrocycle to switch between the two pairs of diagonally placed nitrogen atoms (open and closed circles in figure). This switching allows what were axial donors to become equatorial and vice versa so that at the fast exchanging limit (433K) the averaging of these conformations will give the macrocycle an apparent square-planar geometry with a corresponding three line, 2:2:1, ^{13}C n.m.r. spectrum as observed. The high positive entropy of the exchange process would therefore imply that the trans conformation of the complex in the transition state must be relatively less solvated compared to the cis groundstate. This is very reasonable in terms of the proposed mechanism since rearrangement to the trans conformation can only proceed via the loss of one of the co-ordinated solvent molecules (figure 6.2).

The very high solubility of the complex in DMSO allowed the recording of ^{15}N n.m.r. spectra. Unfortunately technical difficulties have thus far prevented the measurement of the high temperature spectra but the spectrum at 300K is shown in figure 6.3. The spectrum shows the expected two main peaks δ=-318.8, -325.5ppm (1:1), ref. $C[^2H]_3{}^{15}NO_2$, δ=0ppm. for axial and equatorial pairs of nitrogen atoms for a cis complex. The ^{207}Pb isotope has nuclear spin = $\frac{1}{2}$ and gives rise to $^1J_{^{207}Pb-^{15}N}$ couplings to both main peaks. These ^1J coupling constants are remarkably different for the two types of nitrogen present, being 207.5Hz (δ= -318.8ppm) and 19.8Hz (δ= -325.5ppm). Using the theory of ^1J couplings of Pople and Santry[197] discussed in section 4, these values would indicate that one bond has either ca 10 times the s character of the other or a vastly different s orbital overlap integral[201], so implying very different modes of bonding for the axial and equatorial

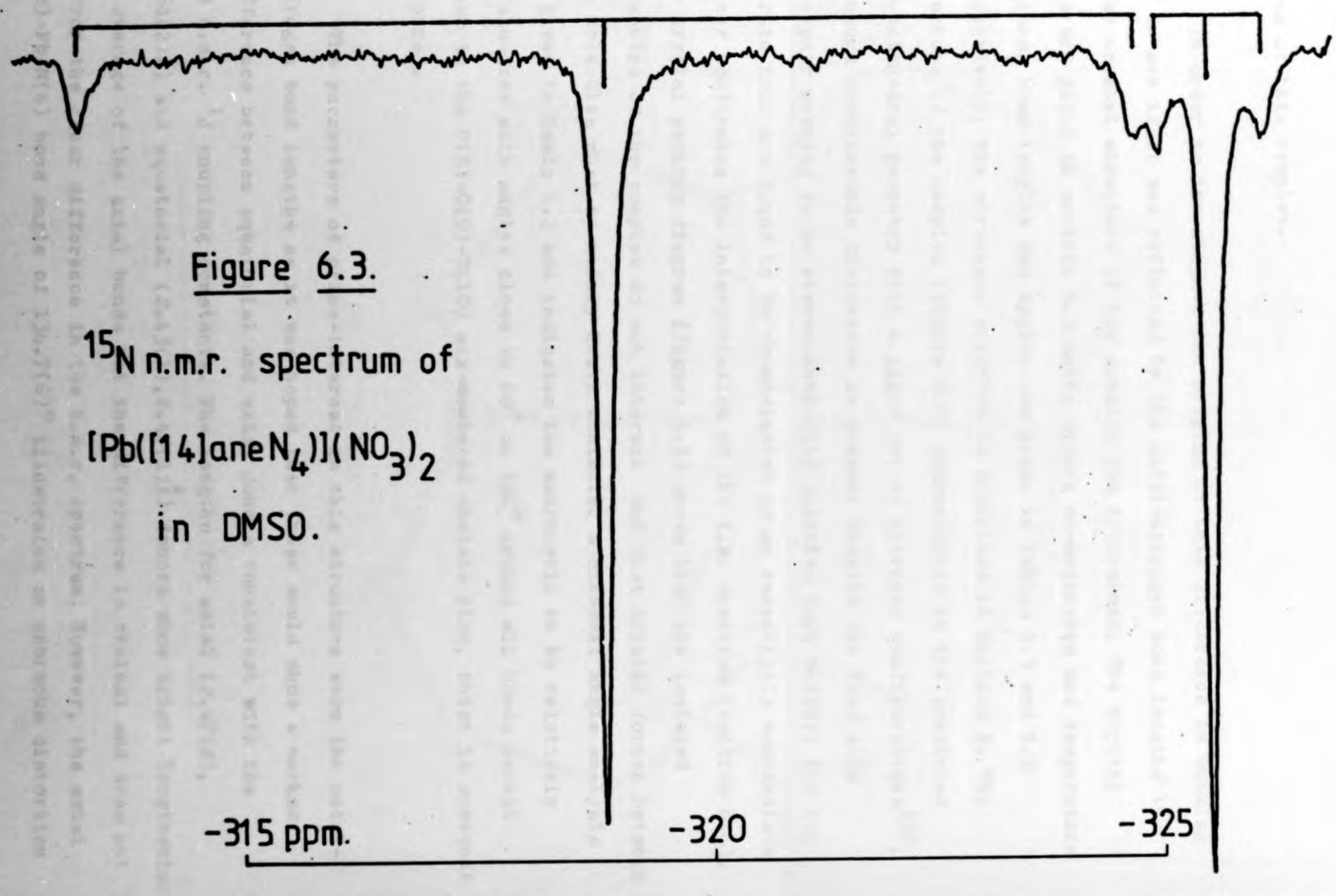

Figure 6.3.

^{15}N n.m.r. spectrum of

$[Pb([14]aneN_4)](NO_3)_2$

in DMSO.

sites of this complex.

In order to investigate the origins of this difference in bonding and to see if it was reflected in the metal-nitrogen bond lengths the X-ray crystal structure of the complex was determined. The crystal data are given in section 8.5 while atomic co-ordinates and temperature factors, bond lengths and angles are given in Tables 8.5 and 8.6 respectively; the structure solution is described in section 8. The structure of the complex (figure 6.4) approximates to the predicted cis-octahedral geometry with a cis-V set of nitrogen configurations[138], although considerable distortion is present despite the lead atom lone-pair seeming to be stereochemically inactive (see below); the two nitrate ions are found to be co-ordinated in an essentially monodentate manner confirming the interpretation of the I.R. spectrum (section 8.6). The crystal packing diagram (figure 6.5) shows that the isolated molecules of the complex do not interact and that crystal forces between the molecules must be mainly H...H contacts. A dihedral angle analysis is given in Table 6.2 and indicates the macrocycle to be relatively strain-free with angles close to 60^{o} or 180^{o} around all bonds except those in the C(8)-C(9)-C(10) six-membered chelate ring, which is somewhat strained.

The parameters of prime-interest in this structure were the metal-nitrogen bond lengths as it was hoped that these would show a marked difference between equatorial and axial donors consistent with the $^{15}_{N}$ n.m.r. $^{1}_{J}$ coupling constants. The lengths for axial (2.47(2), 2.58(2)Å) and equatorial (2.43(1),2.47(1)Å) donors show slight lengthening on average of the axial bonds but the difference is minimal and does not mirror the clear difference in the n.m.r. spectrum. However, the axial N(2)-Pb-N(4) bond angle of $134.7(6)^{o}$ illustrates an enormous distortion

Figure 6.4.

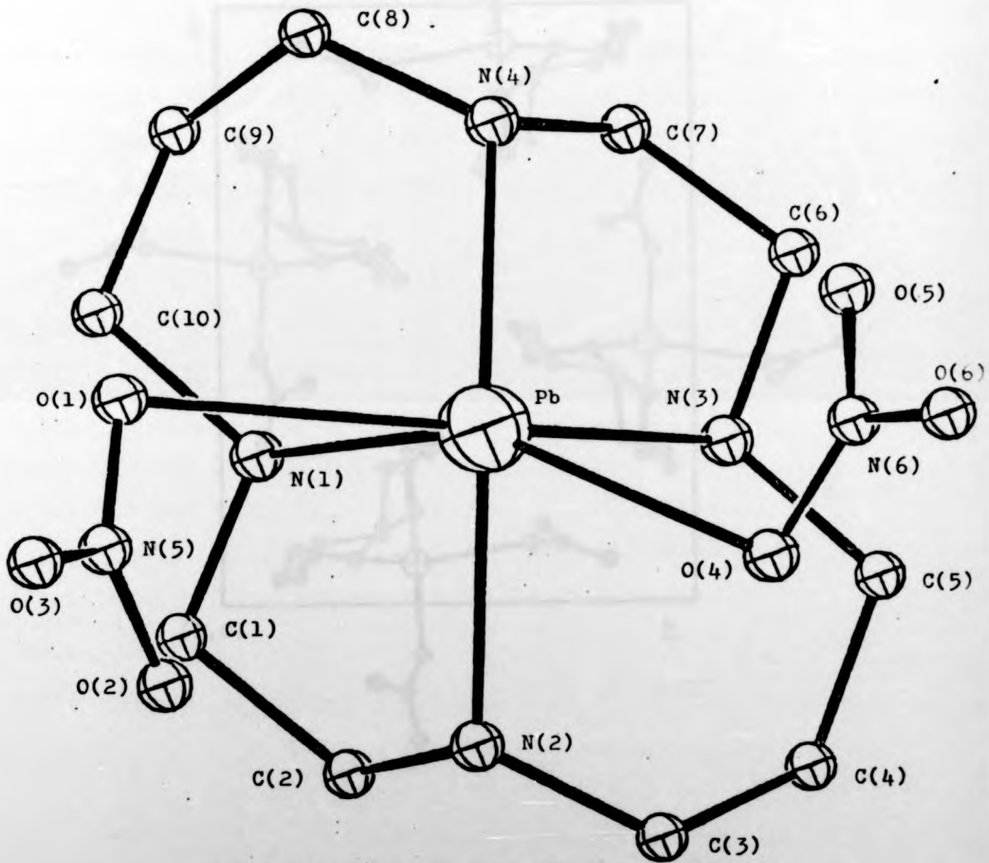

Molecular stucture of $[Pb([14]aneN_4)(NO_3)_2]$

Figure 6.5.

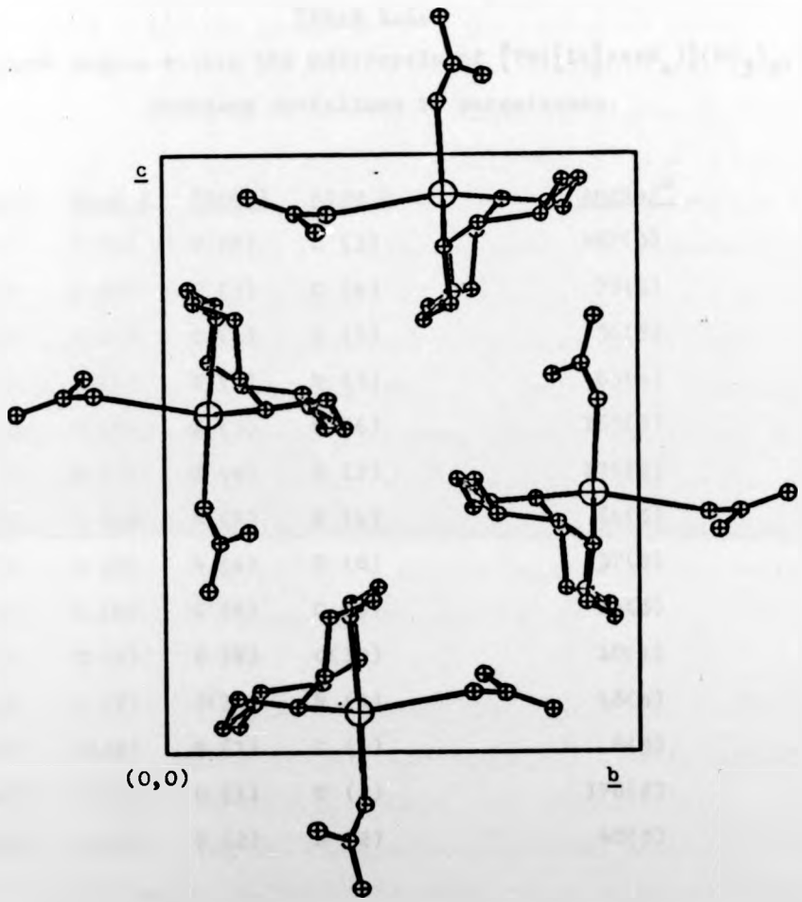

Crystal packing diagram for the complex $[Pb([14]aneN_4)](NO_3)_2$ viewed along the a axis.

Table 6.2.

Dihedral angles within the macrocycle of $[Pb([14]aneN_4)](NO_3)_2$, with standard deviations in parentheses.

Atom 1	Atom 2	Atom 3	Atom 4	Angle/°
C (1)	C (2)	N (2)	C (3)	167(3)
C (2)	N (2)	C (3)	C (4)	78(4)
N (2)	C (3)	C (4)	C (5)	56(5)
C (3)	C (4)	C (5)	N (3)	63(4)
C (4)	C (5)	N (3)	C (6)	165(2)
C (5)	N (3)	C (6)	C (7)	176(2)
N (3)	C (6)	C (7)	N (4)	64(3)
C (6)	C (7)	N (4)	C (8)	37(2)
C (7)	N (4)	C (8)	C (9)	86(3)
N (4)	C (8)	C (9)	C(10)	10(1)
C (8)	C (9)	C(10)	N (1)	48(4)
C (9)	C(10)	N (1)	C (1)	6(3)
C(10)	N (1)	C (1)	C (2)	178(2)
N (1)	C (1)	C (2)	N (2)	60(3)

from regular octahedral geometry while the equatorial N(1)-Pb-N(1) angle of 83.3(4)° is almost ideal. This distortion is undoubtedly a consequence of the large Pb(II) ionic radius which prevents the macrocycle from spanning the axial octahedral sites effectively. This then means that whereas the equatorial nitrogen atoms are in a favourable orientation for co-ordination and may be expected to form relatively normal bonds to lead (II), the axial donors are displaced from their most favourable positions for binding to the hybrid d^2sp^3 octahedral orbitals of the lead atom. This would imply that these latter Pb-N bonds must either be weaker, which is not evident from the bond lengths, or involve a substantial rehybridisation of the lead orbitals, which, if this meant considerably less s character or a smaller s overlap integral[204] in the new bonding hybrids, would be consistent with the ^{15}N coupling constant data.

It is therefore suggested that if the axial distortion is retained in solution (bearing in mind the conductivity data which indicates DMSO to be co-ordinated in place of nitrate ion), then the $^1J_{^{207}Pb-^{15}N}$ values can be assigned as 207.5Hz for equatorial nitrogen atoms (normal octahedral hybrid bonds) and 19.8Hz for axial nitrogen atoms (distorted octahedral rehybridisation involving less s character in the resulting bonds). This interpretation implicitly suggests that the 207.5Hz coupling constant can be regarded as 'normal' for lead-nitrogen bonds. Only one previous, indirectly obtained (double resonance) ^1J lead-nitrogen coupling constant has been reported (for an organoammine complex of the lead(IV) ion)[204]. The hybridisation of the lead(IV) ion is likely to be different to that of lead(II) (no inert-pair effect) but the value obtained of +261Hz does suggest that the 207.5Hz value obtained here is indeed normal. Furthermore the directly measured $^1J_{^{207}Pb-^{15}N}$

value in the complex $[Pb(C.D.T.A.)]^{2-}$ (a better comparison as this complex contains lead(II)) has been measured and found to be 188.3Hz again indicating that the value of 207.5Hz for the present complex may be regarded as normal. Also, comparing the reduced coupling constants[207] for axial $^{1}K_{PbN} = 7.8 \times 10^{20}$ N A m^{-3} and equatorial $^{1}K_{PbN} = 8.2 \times 10^{21}$ N A m^{-3} nitrogens with that for the Pb-C bond in Me_4Pb, $^{1}K_{PbC} = 4.0 \times 10^{21}$ N A m^{-3} shows the equatorial value to be more normal.

The rationalisation of why lead(II) should adopt a cis geometry in preference to the trans-I geometry proposed for the mercury complex is difficult but, as with this latter structure, ionic radius is probably a decisive factor. It may well be, for example, that in order for the very large lead(II) ion to have normal bond lengths to nitrogen the macrocycle must fold in the manner described - implying that a trans-I geometry is impossible because the lead(II) ion even with this macrocycle conformation is incapable of sitting at its optimum distance above the four nitrogen donors.

The identification of a cis geometry for this complex is the first reported instance of such a geometry with a labile metal ion (only previous cis geometries were with Cr(III), Co(III), Rh(III) see section 2). This, together with the demonstration of the existence of the complex and the obtaining of the first directly observed $^{1}J_{^{207}Pb-^{15}N}$ coupling constants for lead(II) complexes total the findings of this section. It may also be pointed out that this reported crystal structure is only the second containing more than one lead(II)-nitrogen bond (Previous Pb-N = 2.44Å [205]).

SECTION 7. CONCLUSIONS

The work reported in this chapter hopefully illustrates the

structural diversity, yet the high thermodynamic stability of complexes with the macrocycle [14]aneN$_4$. Apart from the previously reported complexes which all have either regular cis-V or trans-III geometries no other geometries had been characterised until this work. However, it has now been shown that as one moves to metal ions of ionic radius larger than the macrocycle cavity, stable complexes are still formed but with more unusual geometries. As one progresses in ionic radius, cadmium(II) (r = 0.97Å[6]) is intermediate in size for accommodation within the ring and hence produces folding to a trigonal-bipyramid; mercury(II) (r = 1.06Å[7]) is now too large to be spanned by the macrocycle and so adopts a square-pyramidal trans-I geometry; lead(II) (r = 1.20Å[6]) is now too large even to adopt a square-pyramidal structure and so folds to a cis-V geometry, the first instance of any labile metal ion forcing [14]aneN$_4$ to a cis geometry.

In addition to this structural characterisation the measurement of ^1J metal-nitrogen coupling constants has given an insight to the actual bonding of the macrocycles to the heavy metal ions. Many of the ^1J values and the shifts of the peaks are either unique or very rare and so all of the ^{15}N n.m.r. data is tabulated in Table 8.2. The rarity of the $^1J_{MN}$ coupling constants for these metals is a reflection of their high lability in complexes and so serves to illustrate how unusually inert the complexes of these metal ions with [14]aneN$_4$ are. Such inertness coupled with the high thermodynamic stability of these complexes indicates that the tetra-amine macrocycles of this type have precisely the complexing strength desired in a chemotherapeutic chelating agent for the toxic heavy metal ions.

Two apparently contradictory conclusions may be deduced from the

structural work. Firstly it is clear that the 14-membered ring is not really large enough to encompass the metal ion effectively and so any hopes of utilising the ring-size parameter for selective chelation purposes must rest with a bigger ring-size, say [16]aneN$_4$, which would then be expected to preferentially surround the large toxic ions whilst leaving the smaller ions weakly or non-complexed. On the other hand, the five-co-ordinated trans-I geometry which has been proposed for the mercury(II) complex of [14]aneN$_4$ is exactly the type of complex one is endeavouring to produce in any chelation therapy of the $MeHg^+$ ion for reasons discussed in Chapter 2 section 5, and this geometry may also be ideal for the simple metal ions.

Other workers in these laboratories have recently begun an extensive study of the metal complexes of [16]aneN$_4$ and so the remainder of the current work will focus on the ligand NMe$_4$-[14]aneN$_4$ which is well known to form five-co-ordinate trans-I type complexes. In addition to the structural studies which would be hoped to endorse or parallel the work of this chapter, the relatively neglected kinetic properties of macrocycle complexes will also be studied.

SECTION 8. EXPERIMENTAL

For a detailed discussion of individual techniques see Chapter 6.

INSTRUMENTATION

Routine ^1H n.m.r. spectra were recorded with a Perkin Elmer R12 spectrometer, while variable temperature ^1H and ^{13}C spectra were recorded with a Bruker WH90 pulse fourier transform spectrometer. Natural

abundance ^{15}N n.m.r. spectra were recorded with a wide-bore (25mm) Bruker WH180 p.f.t. spectrometer in conjunction with the P.C.M.U. Harwell. Both f.t. instruments were equipped with standard Bruker temperature control units capable of holding selected temperatures steady to $\pm 0.5^{\circ}C$. The probe temperature was accurately established, for kinetic data, by using a calibrated Comark thermocouple. All chemical shifts are quoted in ppm on the delta, δ, scale referenced to the standards quoted in text.

Exchange parameters for dynamic processes in n.m.r. spectra were established by complete lineshape analyses[143] of the spectra at several temperatures using either a Burroughs B6700 or Nicolet 1080 computer. Activation parameters were calculated using this data for a least-square fit to the Eyring equation (ln(k/T) plotted versus 1/T) with the former computer. (see Chapter 6 section 3)

Infra-red spectra were recorded with a Perkin Elmer 457 spectrometer as nujol mulls. UV/visible spectra were recorded in solution using either a Cary 14 or a Unicam SP800, and as powdered solids using the diffuse reflectance technique with the SP890 attachment to the latter spectrophotometer. Differential scanning calorimetry was performed using a Du Pont 900 Differential Thermal Analyser with the sample enclosed in a nitrogen atmosphere. (Courtaulds Ltd., Coventry). The pH of solutions during pH titrations was measured using a Radiometer PHM64 research pH meter calibrated with standard buffer solutions pH 4.00, 7.00 and 9.00. Conductivity measurements were performed with a Phillips PR9500 conductivity bridge.

Mass spectra were recorded with a V.G. Micromass 12 spectrometer, metal analyses were performed on a Varian AA6 atomic absorption

Table 8.1.

^{13}C n.m.r. data for complexes of [14]aneN$_4$, L.

Complex	Deuterated solvent	Temp. /K	δ/ppm (ref. dioxan 67.26ppm)	Intensities
L	DMSO	353	50.22, 49.31, 30.05	2:2:1
L	methanol	303	50.76, 48.91, 28.76	2:2:1
L	chloroform	303	50.92, 49.62, 29.67	2:2:1
cis-(Rh(L)Cl$_2$)Cl	water	323	55.10, 50.88, 48.93, 46.95, 23.68	equal
cis- Pb(L)(NO$_3$)$_2$	DMSO	303	50.93, 49.24, 48.01, 46.55, 26.11	equal
tbpy- Cd(L)(NO$_3$)$_2$	DMSO/D$_2$O	253	50.20, 49.66, 49.05, 44.53, 25.54	equal
trans-III Ni(L)(ClO$_4$)$_2$	nitromethane	303	50.88, 48.99, 26.63	2:2:1
trans-III Cd(L)(NO$_3$)$_2$	DMSO/D$_2$O	253	52.18, 49.51, 28.98	2:2:1
trans-I Hg(L)Cl$_2$	DMSO/methanol	303	52.67, 47.71, 29.31	2:2:1
trans-I Hg(L)(ClO$_4$)$_2$	DMSO/methanol	303	53.47, 46.76, 29.37	2:2:1

Table 8.2.

^{15}N n.m.r. data (Bruker WH180) for complexes of [14]aneN$_4$, L.

Complex	Geometry	Conc./mol dm^{-3} (Solvent)	Temp. /K	Probe /mm	δ/ppm ref $CD_3{}^{15}NO_2$ (δ=0ppm). [associated $^1J_{MN}$ coupling/Hz.]	Reduced Coupling constant. $^1K_{MN}$/N. A. m^{-3}
L		1.0 (methanol)	295	25	-344.9 [---] (571*)	
$Cd(L)(NO_3)_2$	square-planar trans-III	0.9 (methanol/ DMSO, 1:1)	233	25	-348.2 [110] (8616*)	4.2×10^{-21}
$Cd(L)(NO_3)_2$	trig-bipyramid trans-I	"	233	25	-344.1 [75] (8616*) -349.0 [125] "	2.8×10^{-21} 4.7×10^{-21}
$Hg(L)(ClO_4)_2$	square-pyramid trans-I	1.7 (methanol/ DMSO, 1:1)	303	10	-335.8 [318] (2100*)	14.6×10^{-21}
$Pb(L)(NO_3)_2$	cis-octahedral cis-V	0.9 (DMSO)	303	25	-318.8 [208] (20339*) -325.5 [20] " -11.8 [---] "	8.2×10^{-21} 0.8×10^{-21} ------

* number of scans required.

spectrometer and elemental analyses were carried out by C.H.N. Ltd.

CHEMICALS AND SOLVENTS

See Chapter 2 section 6.

SECTION 8.1. SYNTHESIS AND STUDY OF 1,4,8,11-tetraazacyclotetradecane, [14]aneN$_4$

The macrocycle [14]aneN$_4$ was prepared following published methods[89] and the synthesis is illustrated in the scheme shown overleaf.

The free macrocycle [14]aneN$_4$, B, may be recrystallised from chlorobenzene and sublimed to yield a crystalline white solid MPt. = 186° (reported[165] 185-186°C). Reported pK$_a$ values[89] for the protonated base are 10.76, 10.18, 3.54 and 2.67. The X-ray crystal structure of what was believed to be a lithium complex[206] but which turned out to be the dihydroperchlorate of [14]aneN$_4$ shows the macrocycle to be extensively intra as well as inter-molecularly hydrogen bonded with the four amine nitrogen atoms in a tetrahedral endo type conformation[207]. Infra-red spectral data for [14]aneN$_4$ tends to confirm this solid state structure and suggests that the intermolecular H-bonds become dissociated in dilute anhydrous aprotic media[208].

The ^{13}C n.m.r. spectra of the ligand in various solvents are reported in Table 8.1. whilst ^{15}N n.m.r. data is in Table 8.2. Mass spectrum showed no parent ion peak but peaks at m^+/e = 140, 111, and 83.

SECTION 8.2. cis-[Rh([14]aneN$_4$)Cl$_2$]Cl

The complex was prepared following published methods[165]. 0.5g of

Figure 8.1.

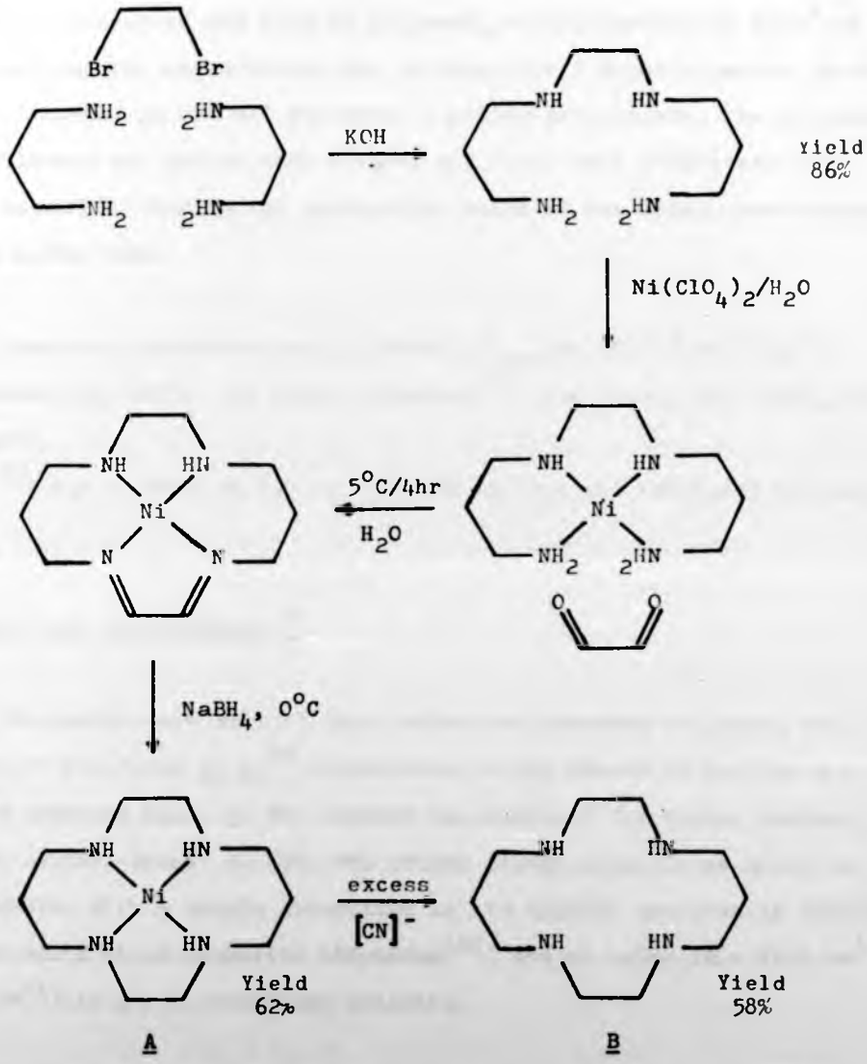

Schematic illustration of the synthesis of [14]aneN$_4$

overall yield = 31%.

rhodium trichloride and 0.5g of [14]aneN$_4$ were dissolved in 20cm^3 of methanol and the red solution was refluxed for 5 minutes during which time it turned yellow and deposited a yellow precipitate. The precipitate was filtered and washed with ethanol and ether then recrystallised from water/HCl. The yellow crystalline material was dried under vacuum. Yield 0.26g (26%)

Electronic spectrum in H_2O (SP800), λ_{max}/nm (ϵ/dm^3 mol^{-1}cm^{-1}), observed: 354 (226), 297 (310); reported[165]: 354 (223), 299 (308), 207 (33,900).

^{13}C n.m.r. data in D_2O is reported in text and tabulated in Table 8.1.

SECTION 8.3. Ni([14]aneN$_4$)$^{2+}$

The perchlorate salt of this cation was prepared following the method of Barefield et al[89] illustrated in the scheme of section 8.1. on the previous page, A. The complex was analysed for nickel content; calcd: 12.88%. found: 12.86%. The bright orange crystalline solid is diamagnetic with a single absorption in its visible spectrum at 453(5)nm in the solid state (reported 460-480nm[138]) and at 445nm (ϵ = 65.6 dm^3 mol^{-1}cm^{-1}) in dry nitromethane solution.

A saturated solution of the vacuum dried complex in dry [^{2}H]$_3$-nitromethane was dried over 3A molecular sieves in a nitrogen dry box for 2 months. The bright orange solution gave a ^{1}H n.m.r. spectrum qualitatively similar to, but quantitatively far better resolved than that reported previously[111]. The assignment of the spectrum is based on the assignments of the analogous complex (Zn(NMe$_4$-[14]aneN$_4$))$^{2+}$

discussed in Chapter 4 and on the results of homo-decoupling experiments Numbering scheme refers to protons as numbered in figure 3.1. δ ppm, (number in figure 3.1.): 1.27q (1+2), 1.71d (3), 2.29d (4), 2.78d (5), 3.15d (6), 3.60broad s (7).

The I.R. spectrum of the vacuum dried solid as a nujol mull in CsI windows shows observed (reported[89,138]): υ(NH) = 3208 (3220); $\upsilon(ClO_4)$ = 1080, 610 cm^{-1}. Also peaks at 532, 500 and 430 cm^{-1}.

The ^1H and ^{13}C n.m.r. data for the complex in water are reported in text and the ^{13}C spectral data in nitromethane is included in Table 8.1.

Solutions for the paramagnetic susceptibility measurements utilising the method of Evans[188] were 0.033 mol dm^{-3} in complex and the ionic strength of the solution was made up to I = 0.1 with oven dried (110°C) $NaClO_4$. The inert reference material chosen for this study was t-butanol, which was present at ca. 0.05 mol dm^{-3} in the bulk solution and was used ca. 0.5 mol dm^{-3} in the co-axial capillary. (For details of this technique see Chapter 6). Shift separations obtained were in the range 3 - 15Hz and were measured ± 0.05Hz, with temperatures held at±0.5°C by a Bruker temperature control unit and externally measured with a Comark thermocouple. Susceptibilities measured were corrected for diamagnetic effects using Pascal constants (see Chapter 6 section 2).

Solutions for the parallel thermodynamic study using visible spectroscopy were 0.0148 mol dm^{-3} in complex, again I = 0.1 with dry $NaClO_4$. Variable temperature spectra were run in the range 280 - 344K in the nitrogen flushed thermostated compartment of a Cary 14 spectrometer. Temperatures were held ± 0.05°C during the recording of spectra and were measured with an alcohol thermometer to ± 0.05°C.

The pH titration of the complex in aqueous solution was carried out on a 0.0346 mol dm^{-3} solution of ionic strength I = 1.11 (dry KNO_3). The pH was adjusted with 5 mol dm^{-3} KOH and measured before and after the recording of the spectrum, the value used in the subsequent calculation (and shown in figure 3.4.) was the average of these two values. The cell compartment of the SP800 spectrometer was thermostated at 298.0 ± 0.5°C. Spectral data are reported in text.

Solvento complexes of $[Ni([14]aneN_4)]^{2+}$ may be prepared by saturating very hot solutions (100°C) in acetonitrile, DMF and DMSO with the perchlorate salt. On cooling, well formed crystalline compounds precipitate and may be filtered under dry nitrogen. Attempts to wash all three compounds with any solvent other than diethyl-ether results in the loss of co-ordinated solvent, with the complex reverting to the orange square-planar species. With acetonitrile even diethyl-ether will cause decomposition and a slow decomposition in dry nujol was observed for this latter complex. It is,therefore, apparent that obtaining pure dry samples of these complexes for analysis is extremely difficult, even pumping under mild vacuum being sufficient to remove co-ordinated solvent. This difficulty is reflected in the poor Ni, C, H, and N analyses for these three complexes - Table 8.3. overleaf.

Diffuse reflectance spectra of all three compounds were run on fresh powdered samples and were consistent with tetragonal trans-octahedral co-ordination and are tabulated in text.(Table 3.2.)

Differential scanning calorimetry was performed on fresh, powdered samples of the acetonitrile and DMSO solvento complexes under a stream of dry nitrogen (2 ft^3 hr^{-1}). The sample was weighed before and after heating above the desolvation endotherm. For the acetonitrile complex

Table 8.3.

Elemental analyses for solvento complexes of $[Ni([14]aneN_4)](ClO_4)_2$, A.

Complex	%Ni req'd	%Ni found	%C req'd	%C found	%H req'd	%H found	%N req'd	%N found
$A(CH_3CN)_2$	10.88	10.57	31.1	30.3	5.56	5.62	15.6	15.0
$A(DMSO)_2$	9.57	8.32	27.4	27.5	5.87	6.00	9.1	6.6
$A(DMF)_2$	9.73	7.95	31.8	34.5	6.30	6.84	13.9	14.6

a 9.6mg sample lost 1.4mg corresponding to the dissociation of two solven molecules while a 9.6mg sample of the DMSO adduct lost 2.4mg again corresponding to the loss of two solvents from the complex. Heating differential was measured with respect to an empty sample pan and experimental conditions were: Heating rate = 20°C per minute and the thermal behaviour was plotted on a scale, T, of 20°C per inch and a sensitivity ΔT of 0.008mv per inch. The area in square inches under any given peak in the plot can be related to the enthalpy in calories required to bring about the particular process responsible, ΔH, by the empirical equation:

$$\Delta H_m = \frac{\text{Area under peak } (in^2) \times E \times T \times \Delta T \times K}{\text{Weight of solvent lost} \times \text{Heating rate}} \times 2.54^{-2}$$

where K = 1.4 (constant) and E = 40 (also constant of recording).

This mass enthalpy ΔH_m can be converted to molar enthalpy simply by multiplying by the molecular weght of the solvent molecule. In the present case the molar enthalpy is the energy required to break two metal-solvent bonds and so the energy per solvent is half this value.

The I.R. spectra of the acetonitrile and DMSO complexes were

recorded as nujol mulls, however, even in this medium the acetonitrile complex was found to partially decompose during the running of the spectrum. The spectra in CsI windows show:

Acetonitrile: υ(NH) = 3260 cm^{-1}, υ(C≡N) = 2264 cm^{-1} (compare with free acetonitrile at 2295 cm^{-1}) $\upsilon(ClO_4)$ = 1080, 618 cm^{-1}.

DMSO : υ(NH) = 3210 cm^{-1}, $\upsilon(ClO_4)$ = 1050, 615 cm^{-1}, υ(DMSO) = 303 (C-S-C deformations), 336, 385 (C-S-O antisymmetric and symmetric deformations), 668, 700 (C-S stretch), 955 cm^{-1} (S-O stretch of O bound DMSO[209]).

SECTION 8.4. $Cd([14]aneN_4)(NO_3)_2$

This complex may be prepared by mixing 0.617g of $Cd(NO_3)_2.4H_2O$ with 0.4g of $[14]aneN_4$ in methanol. Evaporation of the methanol solvent leaves a fine white powder which may be recrystallised from nitromethane, washed with chloroform and ether and vacuum dried. Yield 0.81g (92%). Found: Cd, 25.0; C, 27.3; H, 5.52; N, 19.1%. $C_{10}H_{24}N_6O_6Cd$ requires: Cd, 25.7; C, 27.5; H, 5.50; N, 19.2%.

Conductivity measurements of a 0.002 mol dm^{-3} solution of the complex in dry DMSO at 18.4 ± 0.2°C give a molar conductivity for the complex, shown in Table 8.4, which is consistent with a 2:1 electrolyte (cf. $NaClO_4$ reference).

The I.R. spectrum as a nujol mull in CsI windows shows, υ(NH) =3275. $\upsilon(NO_3)$ = 1480-1240 (υ_1,υ_4), 1020 (υ_2), 808 (υ_6), 742 (υ_3), 720 (υ_5) cm^{-1} consistent with monodentate nitrato co-ordination[157])

The ^{13}C spectral data is given in text and is tabulated in Table 8.1.

Natural abundance ^{15}N n.m.r. data is recorded in Table 8.2.

SECTION 8.5. $[Hg([14]aneN_4)]^{2+}$ ION.

The perchlorate salt of this complex may be prepared by mixing hydrated mercury(II) perchlorate, excess, with 0.5g $[14]aneN_4$ in methanol ($2cm^3$).A white precipitate crystallises from solution in 30s and may be filtered and washed with ice-cold methanol, chloroform and ether. Recrystallisation from methanol yields 0.9g (60%) of the complex.

An identical procedure may be employed for the preparation of the chloride complex. 0.28g of A.R. $HgCl_2$ are mixed with 0.2g $[14]aneN_4$ in methanol ($1cm^3$). Recrystallisation from methanol yields 0.32g (67%) of the complex.

Conductivity measurements of a 0.002 mol dm^{-3} solution of each complex in dry DMSO at 18.4 ± 0.2°C give molar conductivities as shown in Table 8.4. The perchlorate salt is a 2:1, whereas the chloride is a 1:1 electrolyte. The I.R. spectrum of the chloro complex shows $\nu(NH) = 3210$, $\upsilon(HgCl) = 260cm^{-1}$.

The ^{13}C and ^{15}N n.m.r. data for these complexes are discussed in text and summarised in Tables 8.1. and 8.2. respectively.

Table 8.4.

Conductivity data for complexes of [14]aneN$_4$, L.

Compound	10^3. Conc./ mol. dm.$^{-3}$	Solvent	Molar conductivity Λ_M/ohm^{-1}m.^{2}mol^{-1}.
$NaClO_4$	1.688	DMSO	0.573
$Cd(L)(NO_3)_2$	2.174	DMSO	0.219
$Hg(L)(ClO_4)_2$	2.091	DMSO	0.229
$Hg(L)Cl_2$	2.225	DMSO	0.536
$Pb(L)(NO_3)_2$	1.953	DMSO	0.238

SECTION 8.6. $[Pb([14]aneN_4)](NO_3)_2$

The complex may only be prepared using very dry reagents. 0.662g of powdered A.R. lead(II) nitrate were dissolved in dry DMSO, ($5cm^3$). 0.4g of $[14]aneN_4$ (which is insoluble in DMSO) was added to this solution and the slurry stirred for 1hr. After this time, all of the macrocycle is found to be in solution, solubilised as its lead complex. The complex is extremely soluble in DMSO and may only be obtained as a solid by pumping down the solution to very high concentration followed by the addition of dry A.R. methanol. This addition precipitate the complex as a fine white powder. Yield 0.94g (88.5%).
Found: Pb, 39.3; C, 21.8; H, 4.37; N, 15.5%. $C_{10}H_{24}N_6O_6Pb$ requires Pb, 39.0; C, 21.1; H, 4.52; N, 15.8%.

The molar conductivity of a 0.002 mol dm^{-3} solution in dry DMSO at 18.4 ± 0.2°C is given in Table 8.4. and is consistent with a 2:1 electrolyte. The I.R. spectrum (nujol mull) in CsI windows shows, $\upsilon(NH)$ = 3220, $\upsilon(NO_3)$ = 1360 (υ_4), 1299 (υ_1), 998 (υ_2), 795 (υ_6), 720 (υ_3,υ_5) cm^{-1}. (consistent with monodentate nitrato co-ordination[157]). ^{13}C and ^{15}N n.m.r. spectra are discussed in text and listed in Tables 8.1. and 8.2. respectively.

Crystals of the complex suitable for X-ray diffraction were prepared by slow cooling of a saturated DMSO/methanol solution (1:1) to give small, clear laths of crystalline material.

CRYSTAL DATA.- $PbC_{10}H_{24}N_6O_6$, M = 531.2, monoclinic, $\underline{a}$ = 10.326(2), $\underline{b}$ = 11.145(3), $\underline{c}$ = 14.832(4)Å, β = 96.19(2)°, $\underline{U}$ = 1697.0(7)$Å^3$, T = 18(2)°C, $\underline{Z}$ = 4, D_m = 2.12(5)g cm^{-3}, D_c = 2.08g cm^{-3}, F(0,0,0) = 1024. Space group $P2_1/c$, $\mu(MoK_\alpha)$ = 100.61 cm^{-1}.

DATA COLLECTION.- A crystal of approximate dimensions 0.06 x 0.10 x 0.25mm bounded by {011} {211} {120} was examined on a Syntex $P2_1$ four-circle automated diffractometer. The unit cell dimensions and their e.s.d.'s were obtained by a least squares fit to 15 strong reflections with MoK_α graphite monochromatised radiation (λ = 0.70926Å). Systematic absences, $h,0,l$ for $l = 2n+1$ and $0,k,0$ for $k = 2n+1$, indicate the space group $P2_1/c$. Intensity data in the range $3 \leqslant 2\theta \leqslant 55^\circ$ were collected by the θ-2θ scan technique and three check reflections were monitored every 100 measurements. 1909 reflections with $I \geqslant 3.0\sigma I$ were recorded and corrected for absorption (see Chapter 6) to give transmission factors in the range 0.397 - 0.604.

STRUCTURE SOLUTION AND REFINEMENT.- The structure was solved by the heavy atom method using a three-dimensional Patterson synthesis to locate the position of the lead atom. All remaining non-hydrogenic atoms were located in subsequent electron density maps and all atoms were refined by minimising the function $\Sigma(|F_o| - |F_c|)^2$. Refinement by the least-squares method with all atoms anisotropic gave an R value of 0.049. Weighting scheme 8 of the X-ray system was applied to the data following a weighting analysis. (see Chapter 6)

Scattering factors and anomalous dispersion factors from reference 158 were used, and all computing was performed with a Burroughs B6700 computer using the XRAY76 programs (Chapter 6) Final atomic co-ordinates and temperature factors are given in Table 8.5. while bond-lengths and angles for the complex are listed in Table 8.6a and b respectively. Structure factors may be consulted as supplementary data to the appropriate publication.

Table 8.5.

Atomic co-ordinates ($x10^4$) with standard deviations in parentheses for $[Pb([14]aneN_4)](NO_3)_2$.

Atom	X	Y	Z
Pb	2263(1)	4051(1)	669(1)
N(1)	2013(14)	3867(11)	2275(8)
N(2)	4452(16)	4048(17)	1532(13)
N(3)	2822(14)	1896(10)	809(9)
N(4)	163(15)	2822(18)	741(12)
C(1)	3114(42)	4482(30)	2759(24)
C(2)	4378(33)	3901(37)	2506(24)
C(3)	5432(41)	3316(43)	1151(38)
C(4)	5236(35)	2026(46)	1014(28)
C(5)	4048(22)	1578(17)	453(13)
C(6)	1655(25)	1207(14)	415(15)
C(7)	475(32)	1535(31)	901(23)
C(8)	9187(34)	3367(43)	1273(30)
C(9)	9601(33)	3470(42)	2258(29)
C(10)	704(35)	4370(24)	2529(20)
N(5)	7639(19)	2155(15)	4013(12)
O(1)	8649(27)	1512(21)	3998(17)
O(2)	6590(32)	1731(29)	3703(24)
O(3)	7690(35)	3173(18)	4293(21)
N(6)	2938(15)	1178(13)	3510(10)
O(4)	3707(21)	841(28)	4118(14)
O(5)	2016(24)	1805(21)	3687(17)
O(6)	3080(30)	931(26)	2708(12)

For Temperature Factors see appendix

Table 8.6a.

Bond lengths in Å with standard deviations in parentheses for $[Pb([14]aneN_4)](NO_3)_2$.

Bond	Length/Å	Bond	Length/Å
Pb-N(1)	2.432(13)	N(4)-C(8)	1.476(46)
Pb-N(2)	2.474(16)	N(5)-O(1)	1.268(33)
Pb-N(3)	2.474(11)	N(5)-O(2)	1.225(37)
Pb-N(4)	2.577(17)	N(5)-O(3)	1.207(28)
Pb-O(1)	2.958(24)	N(6)-O(4)	1.195(26)
Pb-O(4)	2.877(22)	N(6)-O(5)	1.232(29)
N(1)-C(1)	1.450(40)	N(6)-O(6)	1.254(25)
N(1)-C(10)	1.548(39)	C(1)-C(2)	1.539(55)
N(2)-C(2)	1.463(41)	C(3)-C(4)	1.463(69)
N(2)-C(3)	1.461(52)	C(4)-C(5)	1.493(43)
N(3)-C(5)	1.469(27)	C(6)-C(7)	1.526(43)
N(3)-C(6)	1.494(26)	C(8)-C(9)	1.482(60)
N(4)-C(7)	1.484(39)	C(9)-C(10)	1.538(51)

Table 8.6b.

Bond angles in degrees with standard deviations in parentheses.

Angle	°	Angle	°
N(1)-Pb-N(2)	71.4(6)	N(3)-Pb-O(1)	164.1(6)
N(1)-Pb-N(3)	83.3(4)	N(3)-Pb-O(4)	88.3(7)
N(1)-Pb-N(4)	74.7(5)	N(4)-Pb-O(1)	101.6(7)
N(1)-Pb-O(1)	81.2(6)	N(4)-Pb-O(4)	124.5(6)
N(1)-Pb-O(4)	154.9(5)	O(1)-Pb-O(4)	107.2(8)
N(2)-Pb-N(3)	76.3(5)	C(1)-N(1)-Pb	107(2)
N(2)-Pb-N(4)	134.7(6)	C(10)-N(1)-Pb	113(1)
N(2)-Pb-O(1)	101.8(7)	C(1)-N(1)-C(10)	112(2)
N(2)-Pb-O(4)	83.7(6)	C(2)-N(2)-Pb	112(2)
N(3)-Pb-N(4)	70.7(5)	C(3)-N(2)-Pb	116(2)

Table 8.6b. cont.

Angle	°	Angle	°
C(2)-N(2)-C(3)	116(3)	N(5)-O(1)-Pb	104(2)
C(5)-N(3)-Pb	114(1)	N(6)-O(4)-Pb	103(1)
C(6)-N(3)-Pb	107(1)	N(1)-C(1)-C(2)	109(3)
C(5)-N(3)-C(6)	115(1)	C(1)-C(2)-N(2)	109(3)
C(7)-N(4)-Pb	111(1)	N(2)-C(3)-C(4)	121(4)
C(8)-N(4)-Pb	115(2)	C(3)-C(4)-C(5)	120(3)
C(7)-N(4)-C(8)	117(3)	C(4)-C(5)-N(3)	114(2)
O(1)-N(5)-O(2)	118(2)	N(3)-C(6)-C(7)	110(2)
O(1)-N(5)-O(3)	122(3)	C(6)-C(7)-N(4)	109(2)
O(2)-N(5)-O(3)	120(3)	N(4)-C(8)-C(9)	115(3)
O(4)-N(6)-O(5)	119(2)	C(8)-C(9)-C(10)	116(3)
O(4)-N(6)-O(6)	121(2)	C(9)-C(10)-N(1)	110(2)
O(5)-N(6)-O(6)	120(2)		

CHAPTER 4

SOME CO-ORDINATION CHEMISTRY OF 1,4,8,11-TETRA METHYL 1,4,8,11 -TETRAAZACYCLOTETRADECANE, NMe_4-[14]ANE N_4.

SECTION 1. INTRODUCTION.

The work discussed so far has indicated that quadridentate saturated amine macrocycles form very inert complexes with the toxic heavy metal ions. In addition to this important feature, however, the heavy metal ion complexes of [14]aneN$_4$ are found to adopt rather unusual geometries because of the ionic size restrictions imposed by the macrocycle cavity. One of these geometries with a trans-I set of nitrogen configurations, has already been pointed out to be potentially useful from a chemotherapeutic viewpoint and an extended investigation of this stereochemistry would seem desirable, both in its own right and as an additional confirmation of the structural assignments in Chapter 3.

Such an investigation is made possible by the macrocycle NMe$_4$-[14]aneN$_4$, the N-tetramethylated analogue of [14]aneN$_4$, which was first prepared in 1973 by Barefield and Wagner[210] who methylated [14]aneN$_4$ by standard organic means (section 8.1.) The free ligand has been found to complex with several transition metals (Fe(II)[211], Co(II)[212], Ni(II)[210,212], Ag(II)[58], Zn(II)[210]) and in all cases forms either square-planar or (in the presence of other monodentate ligands) five-co-ordinate complexes. The formation of five-co-ordinate complexes was a strong indication that the macrocycle had adopted a trans-I conformation wherein the folding of the alkyl backbone effectively blocks the sixth co-ordination site. The first explicit description of this trans-I geometry was made by Barefield who prepared complexes of nickel(II), copper(II) and zinc(II), proving them to be five-co-ordinate with electronic spectral, magnetic and conductivity data[210]. The trans-I stereochemistry in a square-pyramidal complex was deduced for these compounds on the basis of the ^{1}H n.m.r. spectrum of the

zinc(II) chloro complex (section 2) Such a ligand conformation was apparently confirmed by a crystal structure analysis of the nickel(II) azido complex[213] wherein the macrocycle has a perfect trans-I geometry in the ideally square-pyramidal complex. Although the trans-I macrocycle configuration has never been questioned thereafter, Kaden has disputed the interpretation of the structure as square-pyramidal, favouring instead the assignment of a trigonal-bipyramidal geometry based on electronic spectroscopic evidence[212].(see section 2).

The production of the trans-I macrocycle conformation is assumed to be the result of kinetic control of the complex formation reaction mechanism. This implies that with all classes of quadridentate, 14-membered macrocycles the initially formed complex has a trans-I macrocycle conformation which then undergoes donor atom inversions to give the thermodynamically more stable trans-III geometry. In the case of the tertiary amine donors of NMe_4-[14]$aneN_4$ the second inversion step is impossible since the necessary intermediate amido nitrogen cannot be formed and so the complex is trapped with its trans-I five-co-ordinate structure[212,214].

Evidence that the penta-co-ordinated trans-I geometry is indeed the kinetically and not the thermodynamically determined product is provided by experiments devised to produce the most thermodynamically stable complex. Deprotonation of the co-ordinated amines of the complex $[Ni([14]aneN_4)](ClO_4)_2$ in DMSO followed by methylation with methyl iodide is expected to produce the thermodynamic product[215]. In this case a complex with a trans-III set of nitrogen configurations was produced proving this to be the thermodynamically favoured isomer.

The labilities of the two isomers of the nickel(II) complex are

markedly different, the trans-I complex being destroyed in dilute acid in minutes[212] whereas the trans-III complex is very inert to hot conc. acids and even to hot aqueous cyanide[215]. This difference is ascribed to the differing accessibilities of the nickel ion in each complex. In the trans-I geometry the metal ion sits above the macrocycle plane and so is easily stripped from it[210], the trans-III geometry on the other hand has the metal ion rigidly in the macrocycle plane and so much less available to competing ligands.

Apart fromthis essentially structural work with NMe_4-[14]aneN$_4$ complexes, Hertli and Kaden have studied the formation and dissociation kinetics of the trans-I five-co-ordinate complexes of Ni(II), Cu(II), Co(II) and Zn(II) and in all cases have found the stability constant of the complex formed to be less than that of the equivalent complex with a linear tetraamine, trien[216]. The kinetics of the fifth monodentate ligand for these complexes has been relatively ignored and only one solvent exchange study, of the cobalt(II) aquo complex, has been reported. The ^{17}O n.m.r. paramagnetic line-broadening data was found to indicate a relatively slow water exchange rate for cobalt(II) together with a negative entropy of activation[217]. This unusual result was not satisfactorily explained and so it is felt that the ligand exchange kinetics of such unusual five-co-ordinate complexes is of inherent interest as well as being of possible relevance to the present underlying theme of heavy metal ion co-ordination, since the kinetics may well be markedly influenced by the structural aspects of the complex itself.

This brief summary of the co-ordination chemistry of NMe_4-[14]aneN$_4$ indicates that its ability to, apparently always, form five-co-ordinate trans-I type geometries is exactly the behaviour required for the present

study. Together with the groundwork carried out on [14]aneN$_4$, the exploration of its structural co-ordination chemistry would be expected to yield information relevant to the current work. In addition, the ability of this macrocycle to stabilise unusual co-ordination geometries makes it of inherent interest in its own right, and worthy of more detailed investigation especially in relation to the trigonal-bipyramid/square-pyramid controversy discussed above. The solvent exchange kinetics of the penta-co-ordinate complexes have also proven unusual and so the exploration of such properties, apart from being of fundamental interest, is also potentially useful for the interpretation of structure.

These considerations have lead to the following investigation of the structure and kinetics of metal-NMe$_4$-[14]aneN$_4$ complexes.

SECTION 2. COMPLEXES WITH ZINC(II).

As was pointed out above (section 1) zinc(II) complexes of NMe$_4$-[14]aneN$_4$ were first prepared in 1973[210] and thought to be five-co-ordinate in both the solid phase and in nitromethane solution. ^{1}H n.m.r. data for the chloro complex in [^{2}H]$_3$-nitromethane indicated that all four N-methyl groups of the macrocycle were magnetically equivalent. This permitted the assignment of a structure with all four methyl groups on the same side of a plane defined by the four nitrogen atoms (trans-I, figure 2.1a) and effectively excluded the possibility of any non-planar arrangement of the four nitrogen atoms, as this would necessarily cause inequivalence of the N-methyl groups and hence splitting of their ^{1}H n.m.r. resonance. The structure was assigned as square-pyramidal.

Later, however, a trigonal-bipyramidal geometry was postulated[212]

for the analogous nickel(II) complexes, based on electronic spectra of these and related species. Weight was added to this view by the known trigonal-bipyramidal X-ray crystal structure of a similar copper(II complex with Me_6-[14]$aneN_4$ in the trans-I conformation[194]. In an attempt to assign unambiguously the stereochemistry of these complexes, an X-ray structural analysis of $[Ni(NMe_4\text{-}[14]aneN_4)N_3](ClO_4)$ was completed showing perfect square-pyramidal geometry[213].

Although this appeared to define the structure of these complexes completely there was still a lingering doubt over the electronic spectral data, so, in order to completely resolve this situation and to extend the present study, a detailed study of the zinc(II) system is now reported.

Solution Structure.- A variable temperature ^1H n.m.r. study in the temperature range 323-223K (freezing point of the $[^2H]_3$-nitromethane solutions) of the complexes $[Zn(NMe_4\text{-}[14]aneN_4)X](ClO_4)$ where X = Cl, Br, I, shows no splitting or broadening of the N-methyl resonance which remains a sharp singlet. This behaviour is identical to that observed previously for the chloro-complex[210], apparently indicating the absence of any dynamic process involving folding of the macrocycle away from planarity; this therefore implies square-pyramidal co-ordination of the zinc atom (figure 2.1a). The complex with X= NCS, however, does show slight broadening and eventually an ill-resolved splitting of the ^1H n.m.r. N-methyl resonance at 233K with a separation of ≈3Hz. (at 90MHz.)

A proton-decoupled ^{13}C n.m.r. study of the same solutions reveals the presence of a dynamic process much more clearly as illustrated in

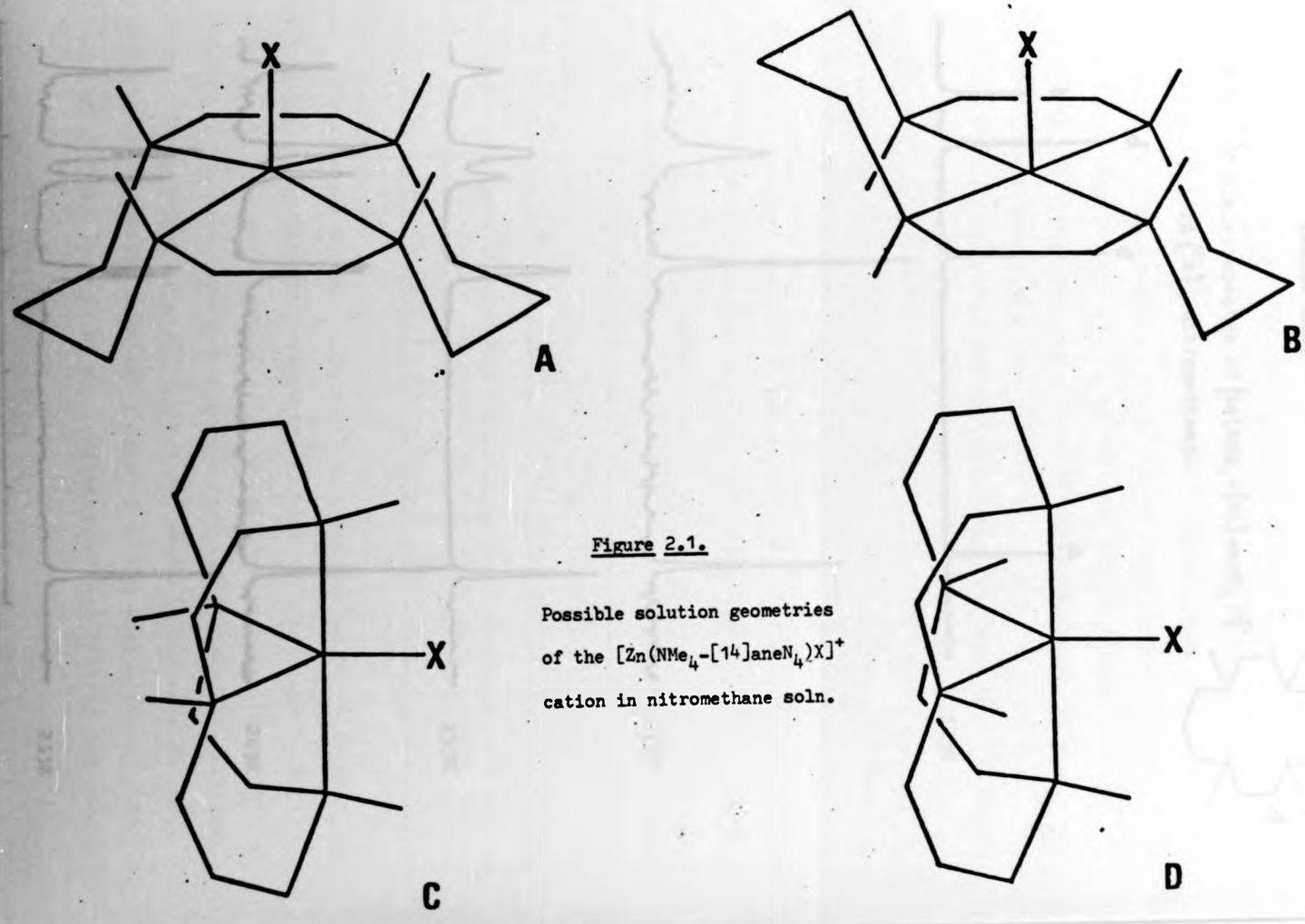

Figure 2.1.

Possible solution geometries of the $[Zn(NMe_4\text{-}[14]aneN_4)X]^+$ cation in nitromethane soln.

Figure 2.2.

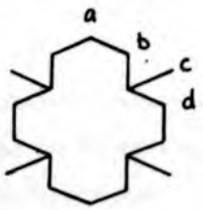

V.T. ^{13}C n.m.r. spectra of $[Zn(NMe_4\text{-}[14]aneN_4)I]^+$ in $[^2H]_3$-nitromethane.

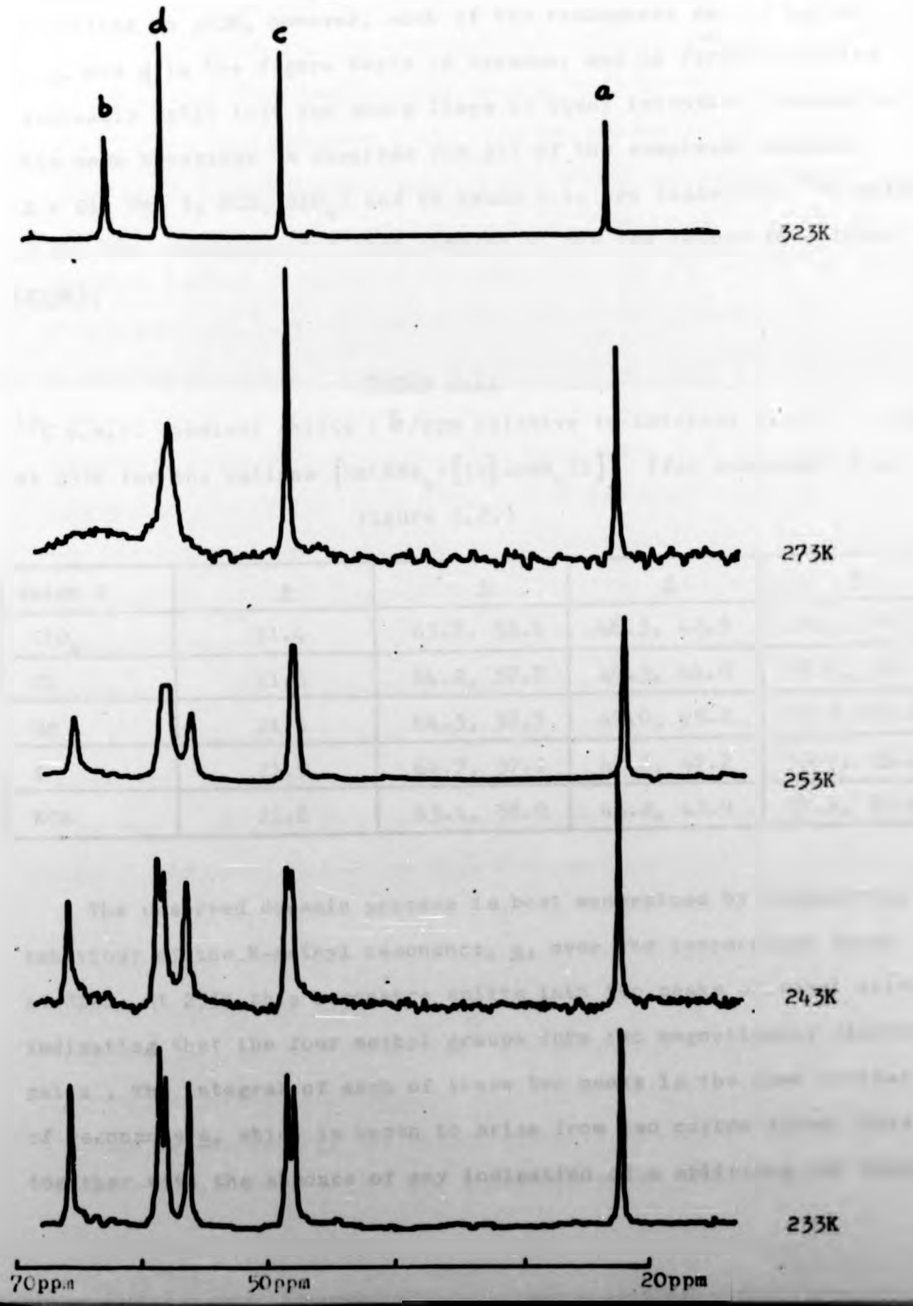

figure 2.2. At 323K the ^{13}C spectra of all of the complexes consist of the expected four sharp lines, with an assignment based on integrals and proton coupled spectra (see section 3) as shown in figure 2.2. On cooling to 303K, however, each of the resonances due to carbon atoms b, c, and d in the figure begin to broaden, and on further cooling eventually split into two sharp lines of equal intensity (population). This same behaviour is observed for all of the complexes studied (X = Cl, Br, I, NCS, ClO_4) and in Table 2.1. are listed the ^{13}C shifts of all the resonances for each complex at the low temperature limit (233K).

Table 2.1.

^{13}C n.m.r. chemical shifts (δ/ppm relative to internal dioxan 67.26ppm) at 233K for the cations $[Zn(NMe_4\text{-}[14]aneN_4)X]^+$ (for assignments see figure 2.2.)

Anion X	a	b	c	d
ClO_4	21.4	63.7, 58.8	46.3, 42.5	57.3, 56.5
Cl	21.6	64.2, 57.7	46.5, 44.0	57.7, 55.7
Br	21.6	64.5, 57.7	47.0, 45.2	57.5, 55.6
I	21.5	64.7, 57.2	47.8, 47.2	57.7, 55.4
NCS	21.6	63.4, 58.0	46.2, 42.9	57.7, 55.9

The observed dynamic process is best understood by considering the behaviour of the N-methyl resonance, c, over the temperature range studied. At 233K this resonance splits into two peaks of equal intensity indicating that the four methyl groups form two magnetically distinct pairs . The integral of each of these two peaks is the same as that of resonance a, which is known to arise from two carbon atoms. This, together with the absence of any indication of a splitting for resonance

a, strongly implies that the macrocycle dynamic behaviour arises from an intra- and not an inter-molecular process. There are four possible intramolecular structural processes which would cause equal splitting of the N-methyl resonance at the limit of slow exchange:

i) If the complex were square-pyramidal in solution with structure shown in figure 2.1b then the N-methyl groups would form two distinct pairs in the slow exchange limit, and on accelerating the rate of exchange of ligand X these pairs would become equivalent. This explanation is, however, readily discounted because such a slow exchange process is unlikely for zinc(II), and the structure observed in the limit of slow exchange would undoubtedly cause splitting of resonance a into two peaks of equal area. Also, one can see no reason why such a structure should be five-co-ordinate, since ligand X must necessarily co-ordinate with equal ease on both sides of the macrocycle plane. Finally structure 2.1b has never been observed for complexes of NMe_4-[14]aneN$_4$ prepared in this way, crystal structures of the nickel(II) azido[213] and zinc(II) chloro (vide infra) complexes showing structure 2.1a, and there are no low energy processes by which 2.1a and 2.1b can interconvert.

ii) Other explanations of the observed splitting are possible if the macrocycle is non-planar. Two such structures are shown in figure 2.1c and 2.1d; both have the complex effectively trigonal-bipyramidal with X equatorial. It is evident that structure 2.1c will give two pairs of non-equivalent N-methyl groups as required. However, to interconvert these pairs, and hence explain their observed equivalence in the 303K ^{13}C n.m.r. spectra, one must envisage a process such as that schematically illustrated in figure 2.3A. This macrocycle geometry is seen to be a distorted version of a cis-V octahedral structure, the set of nitrogen configurations being the same as that observed for the cis-complex [Co([14]aneN$_4$)en]Cl_3[177]

discussed in Chapter 3 section 2. As such this dynamic process is identical to that postulated for the lead(II) complex of [14]aneN$_4$ (Chapter 3 section 6) where the metal ion must pass through the macrocycle cavity in the exchange reaction.

However, no cis-type complexes of NMe$_4$-[14]aneN$_4$ have yet been prepared, probably because of the kinetic control of the complex stereochemistry discussed in section 1. This kinetically determined set of nitrogen configurations is inconsistent with a cis-macrocycle geometry, Also, since the crystals obtained from these solutions contain the macrocycle with the trans-I set of nitrogen configurations (vide infra), it is difficult to see why simple solution in a non-co-ordinating solvent should promote such drastic and complete conversion to a structure where alternate methyl groups are above and below the macrocycle plane (cis-V). Such a conversion would require a minimum of two nitrogen inversions for which there is no available low-energy process.

iii) A far more likely trigonal-bipyramidal geometry is illustrated in figure 2.1d; whereas structure 2.1c could be regarded as a distorted cis-complex, this structure is best thought of as a distorted square-pyramid. It is clear that structure 2.1d has a macrocycle conformation consistent with the slow-exchange (233K) ^{13}C n.m.r. spectrum (figure 2.2) the two axial N-methyl groups being magnetically distinct from the two equatorial groups. The exchange process required to inter-convert these N-methyl groups and so make them equivalent in the fast-exchanging n.m.r. limit is schematically illustrated in figure 2.3B. The plausibility of this scheme is immediately evident, it being able to explain the observed facile dynamic process in that

a) no bond cleavage is necessary,

b) relatively small bond rotations about the central metal are needed

Figure 2.3.

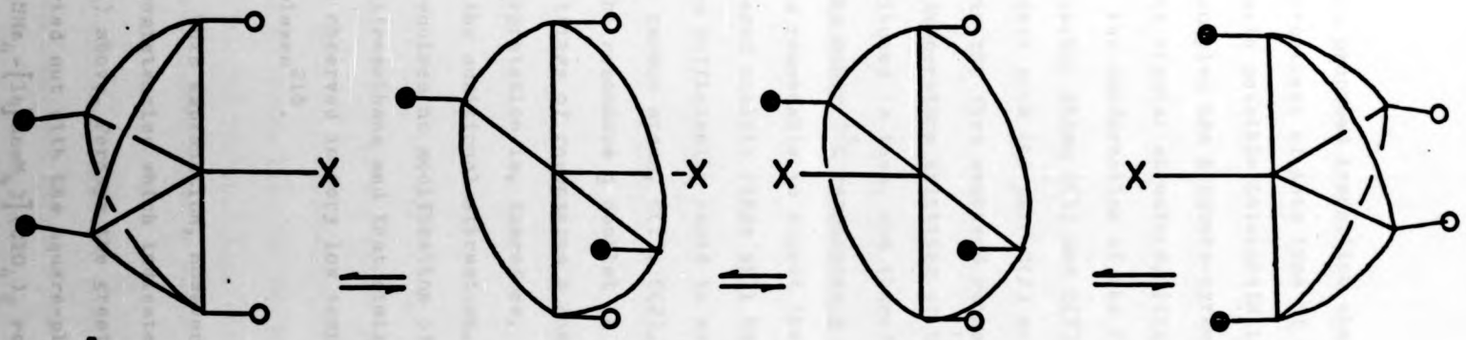

Possible solution dynamic processes for the $[Zn(NMe_4\text{-}[14]aneN_4)X]^+$ cation.

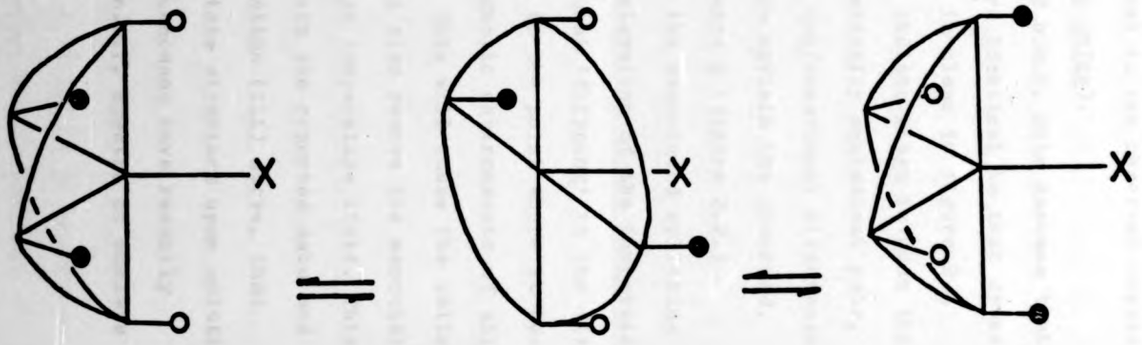

c) the proposed transition state is identical to the observed crystal structures of this type of complex (*vide infra*).

iv) A fourth possible interpretation of the ^{13}C n.m.r. data assumes that the complex has a square-pyramidal structure identical to that found in the crystal structure, (figure 2.4). It is clear in figure 2.4 that the conformation of the five-membered chelate rings is such that the carbon atoms C(1) and C(7) form a magnetically equivalent pair, distinct from the pair C(2) and C(6). This conformational difference within the five membered rings may therefore explain the observed, low temperature splitting of the ^{13}C resonance *d* (figure 2.2.) attributed to them, and therefore lead ,to the associated splitting of the other ^{13}C resonances *b* and *c*. upon elevation of the temperature it is reasonable to expect that conformational 'flipping' in the five membered chelate rings will be accelerated to the point where it becomes sufficiently rapid to average the magnetic environments of all four carbon atoms, C(1), C(2), C(6), C(7). This will cause the collapse of the resonance *d* doublet to a singlet and also remove the associated splittings of resonances *b* and *c* in the high temperature limit. This interpretation is, therefore, consistent with the reported data and has the additional attraction, over explanation (iii) above, that it requires no modification of the solid-state structure upon solution in nitromethane and that similar dynamic phenomena have recently been observed in very low temperature ^{13}C n.m.r. spectra of chelate complexes[218].

This explanation, however, though plausible has several inconsistencies which indicate it to be less likely than explanation (iii) above. Perhaps the greatest of these concerns other work carried out with the square-planar, diamagnetic complex $[Ni(NMe_4\text{-}[14]aneN_4)](ClO_4)_2$ reported in section 5. This four-co-

ordinate nickel(II) complex shows no dynamic behaviour in its ^{13}C n.m.r. spectra down to 233K but, when the analogous chloro complex $[Ni(NMe_4\text{-}[14]aneN_4)Cl](ClO_4)$ is examined, the ^{1}H n.m.r. spectrum shows the dynami c behaviour to be restored. This strongly indicates that the dynamic process depends directly on the presence of a fifth ligand in the metal co-ordination sphere. Closer consideration of the crystal structure of the complex in fig. 2.4 also indicates that carbon atoms C(9) and C(4) are inequivalent when the five-membered chelate rings have the frozen conformation shown and so the resonance a due to these atoms in the ^{13}C n.m.r. spectrum should be split in the slow-exchange limit. The absence of splitting or indeed of any detectable broadening (witness figure 2.2) of this resonance also implies that the dynamic process is not simply a function of the macrocyclic framework conformations which are therefore predicted to be interconverting in solution too rapidly to be detectable in the temperature range employed here.

It is therefore proposed that the solution structures of complexes of the type $[Zn(NMe_4\text{-}[14]aneN_4)X](ClO_4)$ are rapidly interconverting trigonal bipyramids (figure 2.3B). This Berry pseudo-rotation mechanism is essentially identical to that found for the trigonal-bipyramidal PF_5 molecule[219]. The activation parameters of the dynamic process were obtained by a full lineshape analysis[143] of the ^{13}C n.m.r. resonances b, c and d (figure 2.2) for the complex where X = [NCS] and of resonance c where X = Cl. The analysis, over the temperature range 233-293K, gives the results shown in Table 2.2. overleaf.

The two complexes have comparable activation parameters, the small differences may be explained in terms of the greater size of the chlorine

Table 2.2.

Activation parameters at 298K (standard deviations in parentheses) for the ^{13}C n.m.r. exchange process in solutions of $[Zn(NMe_4\text{-}[14]aneN_4)X]^+$.

X	Resonances fitted	$\Delta H^{\ddagger}$/kJ mol^{-1}	$\Delta S^{\ddagger}$/J K^{-1}mol^{-1}	$10^{-3}k_{ex}/s^{-1}$
NCS	b	45.7(2.5)	-15(10)	3.6
NCS	c	49.5(1.8)	-10(10)	4.1
NCS	d	46.2(2.6)	-14(10)	3.8
Cl	c	59.3(3.2)	15(12)	2.9

atom compared to the thiocyanate N atom (the I.R. spectrum shows the C-S stretching frequency at 804cm^{-1}, indicative of N-bound thiocyanate[220] as compared to S-bound thiocyanate which has a C-S stretch around 700cm^{-1}) which will therefore tend to disfavour the exchange transition state (figure 2.3b) because of greater steric interactions of the chlorine with the N-methyl groups (see below).

Crystal Structure.- In order to investigate the $[Zn(NMe_4\text{-}[14]aneN_4)X](ClO_4)$ system fully, a crystal structure of the complex where X = Cl was undertaken for comparison with the proposed solution structure (see section 8.2 for crystal data etc.). The complex has an almost perfect square-pyramidal geometry (figure 2.4) with the four nitrogen atoms, N(1)-N(4), of the macrocycle forming the basal plane (* 0.1Å) above which the zinc atom is centrally displaced by 0.57Å. A chlorine atom, Cl(1), is apically co-ordinated to complete the structure at a normal[221] Zn-Cl distance of 2.265(4)Å. In this structure the macrocycle has the trans-I set of nitrogen configurations previously observed in the nickel(II) azido complex[213]. A comparison of these two structures indicates further close similarities. In both, the macrocycle has an identical conformation, even to the twisting of the six- and five-

Figure 2.4.

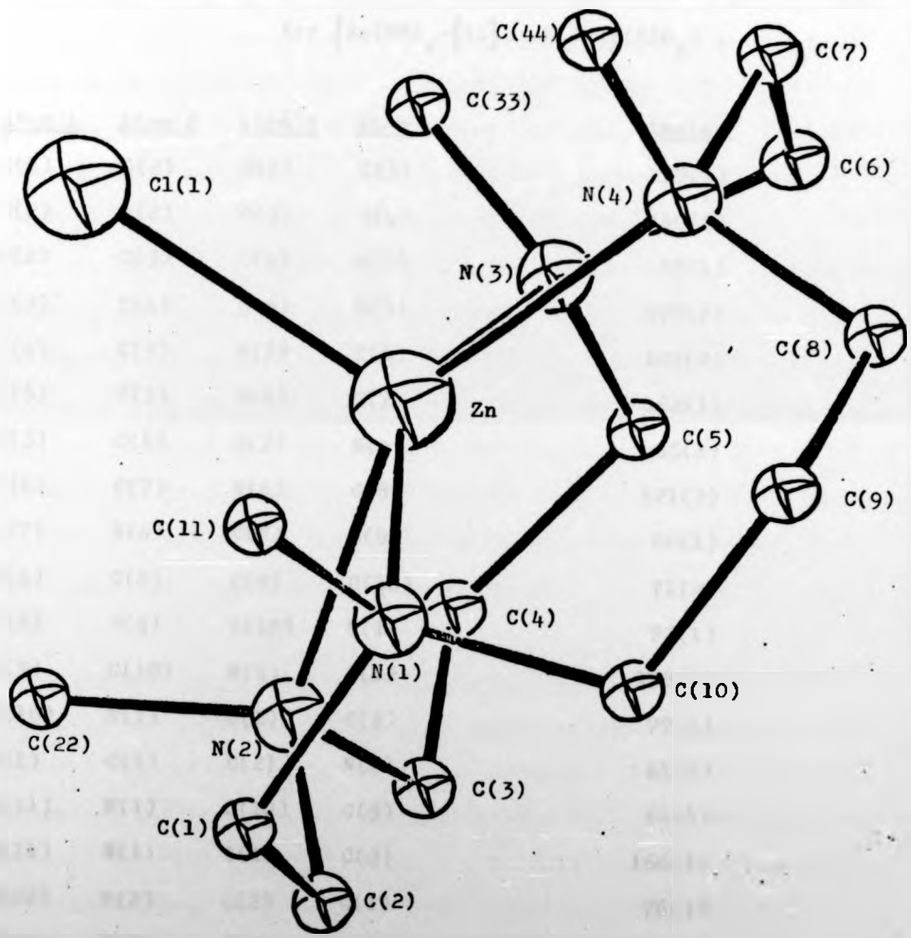

Molecular structure of the $[Zn(NMe_4\text{-}[14]aneN_4)Cl]^+$ cation.

Table 2.3.

Dihedral angles in degrees with standard deviations in parentheses for $[Zn(NMe_4\text{-}[14]aneN_4)Cl](ClO_4)$.

Atom 1	Atom 2	Atom 3	Atom 4	Angle/°
C(1)	C(2)	N(2)	C(3)	167(1)
C(2)	N(2)	C(3)	C(4)	140(2)
N(2)	C(3)	C(4)	C(5)	58(1)
C(3)	C(4)	C(5)	N(3)	177(2)
C(4)	C(5)	N(3)	C(6)	107(2)
C(5)	N(3)	C(6)	C(7)	162(1)
N(3)	C(6)	C(7)	N(4)	85(1)
C(6)	C(7)	N(4)	C(8)	121(2)
C(7)	N(4)	C(8)	C(9)	60(1)
N(4)	C(8)	C(9)	C(10)	71(2)
C(8)	C(9)	C(10)	N(1)	72(1)
C(9)	C(10)	N(1)	C(1)	178(1)
C(10)	N(1)	C(1)	C(2)	77(1)
N(1)	C(1)	C(2)	N(2)	61(1)
C(11)	N(1)	C(10)	C(9)	64(1)
C(11)	N(1)	C(1)	C(2)	166(1)
C(22)	N(2)	C(2)	C(1)	76(1)
C(22)	N(2)	C(3)	C(4)	102(1)
C(33)	N(3)	C(5)	C(4)	12(1)
C(33)	N(3)	C(6)	C(7)	83(1)
C(44)	N(4)	C(7)	C(6)	169(1)
C(44)	N(4)	C(8)	C(9)	64(1)

membered chelate rings. Also, in both, the metal ion is found to move out of the macrocyclic plane towards the apical ligand, by 0.57Å for zinc compared to 0.33Å for nickel. This increase with zinc is consistent with its larger ionic radius and is reflected in the metal-nitrogen distances Zn-N 2.20(1)Å, Ni-N 2.10(1)Å. Most of the bond angles and distances within the macrocycle of both complexes have normal values although small deviations, probably due to strain, are present in the five-membered chelate rings; for example, C(1)-C(2),1.45Å and C(6)-C(7), 1.36Å are both slightly shorter than expected, as are the corresponding distances in the nickel structure. The dihedral angles (Table 2.3.) are also indicative of this strain in the five-membered chelate rings, especially that containing C(6)-C(7). The crystal packing diagram (figure 2.5) shows that the isolated cations are flanked by non-co-ordinated perchlorate anions; the crystal forces between the ions must be mainly electrostatic. This solid-phase structure is seen to be inconsistent with that proposed in solution.

Comparison and Rationalisation of Structures.- The solution and solid phase structures (figures 2.1d and 2.1a respectively) of these complexes can be seen to be two modifications of the same basic macrocyclic conformation. In both structures the nitrogen atoms have the same configuration (trans-I) so that one could reasonably expect inter-conversion between them to be a relatively low-energy process.

Looking first at the solution structure (2.1d) it can be seen that co-ordination of the anion X has forced the macrocycle to fold, pushing back two of its nitrogen atoms to form a trigonal-bipyramidal complex. The structure has the advantage that it lessens any steric conflict between the anion X and the four N-methyl groups as these two are removed out of plane. Molecular models confirm that this arrangement does indeed

Figure 2.5.

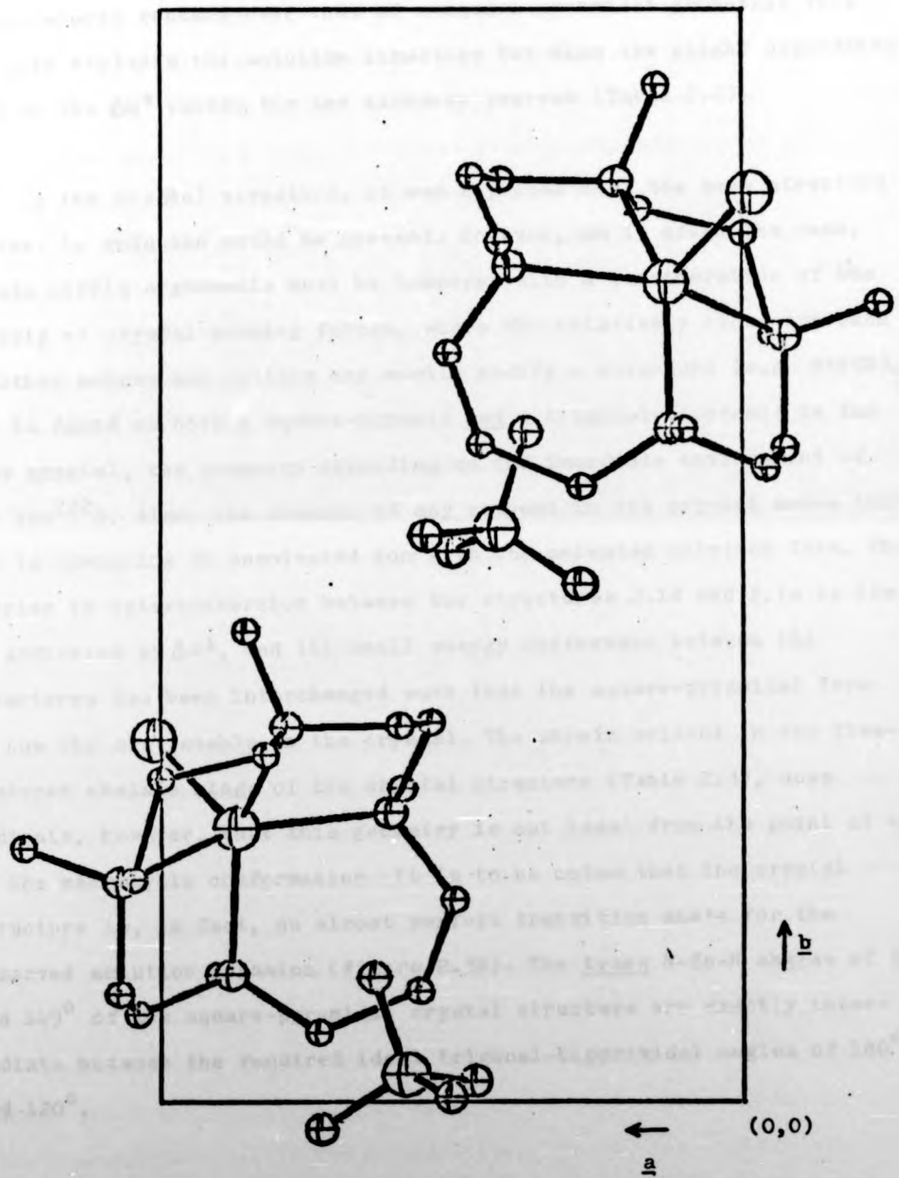

Crystal packing diagram for $[Zn(NMe_4\text{-}[14]aneN_4)Cl](ClO_4)$ viewed along the c axis.

reduce steric contact over that of a square-pyramidal geometry. This not only explains the solution structure but also the slight dependence on X of the $\Delta H^{\ddagger}$ values for the exchange process (Table 2.2).

In the crystal structure, it was expected that the same structure as that in solution would be present. However, as is often the case, simple steric arguements must be tempered with a consideration of the effects of crystal packing forces, where the relatively close approach of other anions and cations may easily modify a structure (e.g. $Ni(CN)_5^{3-}$ can be found as both a square-pyramid and a trigonal-bipyramid in the same crystal, the geometry depending on the immediate environment of the ion[222]). Also, the absence of any solvent in the crystal means that one is comparing an unsolvated ion with the solvated solution form. The barrier to interconversion between the structures 2.1d and 2.1a is low, as indicated by $\Delta H^{\ddagger}$, and the small energy difference between the structures has been interchanged such that the square-pyramidal form is now the most stable in the crystal. The strain evident in the five-membered chelate rings of the crystal structure (Table 2.3), does indicate, however, that this geometry is not ideal from the point of view of the macrocycle conformation. It is to be noted that the crystal structure is, in fact, an almost perfect transition state for the observed solution dynamics (figure 2.3B). The trans N-Zn-N angles of 154° and 149° of the square-pyramidal crystal structure are exactly intermediate between the required ideal trigonal-bipyramidal angles of 180° and 120°.

It is concluded therefore that the solution and crystallographic structures of the $[Zn(NMe_4\text{-}[14]aneN_4)X](ClO_4)$ system are trigonal-bipyramidal (figure 2.1d) and square-pyramidal (figure 2.1a) respectively but that conversion between them is a relatively low-energy process as

confirmed by the estimate of $\Delta H^{\ddagger}$ of the interconversion in solution. In a sense this vindicates the apparently diverse findings of previous workers[210,212,213]. The present results show the importance of ^{13}C n.m.r. data in studies of this type, the greater chemical shift scale available in ^{13}C compared to ^{1}H n.m.r. studies may, as in this case, reveal structural information which may easily be missed in any ^{1}H n.m.r. spectra.

It is reassuring to note that this present zinc study has revealed the plausibility of macrocyclic folding whilst in a trans-I configuration, exactly as was concluded for the cadmium(II)-[14]aneN$_4$ complex in Ch. 3. The generality of these results of this section were explored further with other metal ions and the results are now discussed below.

SECTION 3. COMPLEXES WITH CADMIUM(II) AND MERCURY(II).

No previous report of complexes of NMe$_4$-[14]aneN$_4$ with ions other than of first row transition metals and silver(II) has been published (section 1). As part of the present work two new complexes, with Cd(II) and Hg(II), have been prepared. The complexes with Cd(NO$_3$)$_2$ and HgCl$_2$ may be prepared as described in section 8 and are both white crystalline complexes soluble in nitromethane.

Both complexes give ^{1}H-decoupled variable temperature ^{13}C n.m.r. spectra which are qualitatively identical to those obtained for the five-co-ordinate zinc(II) complexes above. The cadmium complex spectra are shown in figure 3.1 and, as with the zinc complexes, the spectra show a dynamicsplitting of three of the room temperature resonances at low temperatures (233K). Identical behaviour is observed with the mercury(II) chloro complex and the shifts of all resonances at the slow-

Figure 3.1.

V.T. ^{13}C n.m.r. spectra of $Cd(NMe_4\text{-}[14]aneN_4)(NO_3)_2$ in $[^2H]_3$-nitromethane.

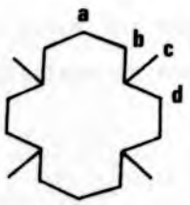

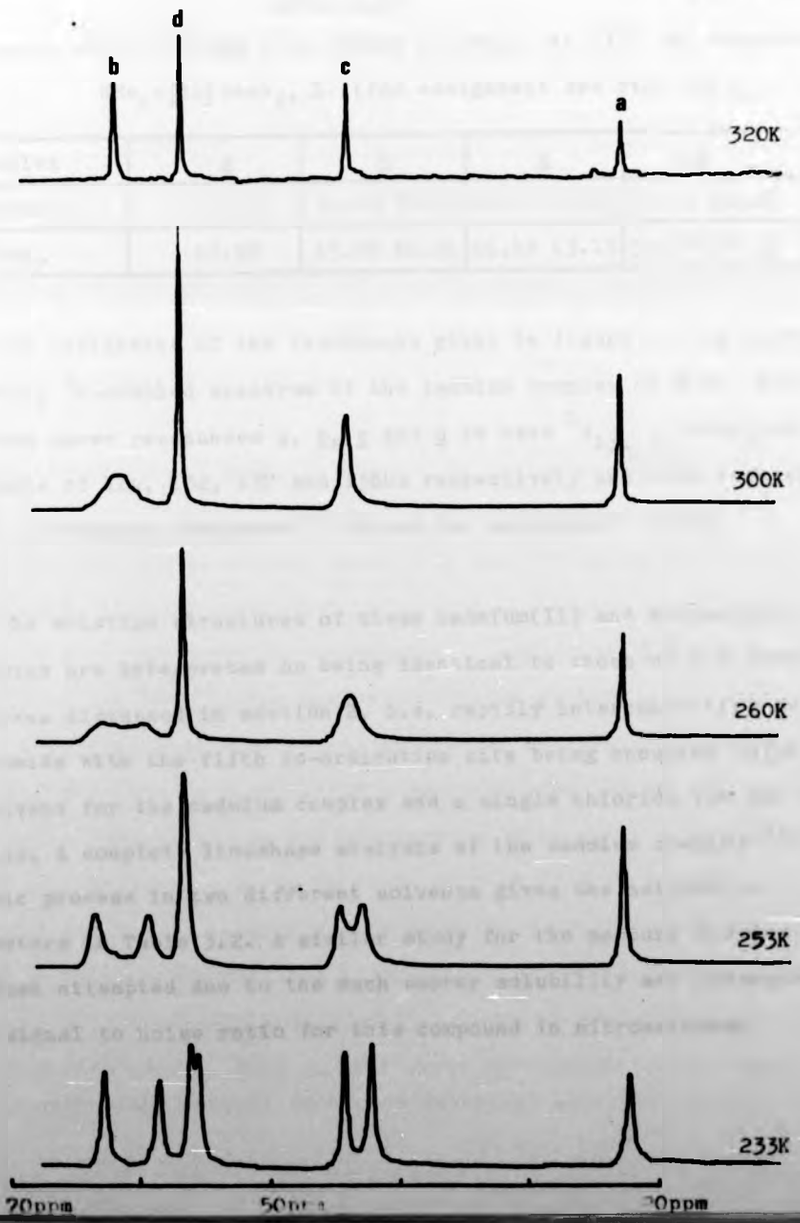

exchange limit in $[^2H]_3$-nitromethane for both complexes are listed in Table 3.1. These values may be compared with those given for the zinc complexes in Table 2.1. and the magnitudes of the splittings in each case are seen to be comparable.

Table 3.1.

^{13}C n.m.r. shifts (δ/ppm ref. dioxan 67.26ppm) at 233K for complexes of NMe_4-[14]aneN$_4$, L. (for assignment see fig. 3.1)

Complex	a	b	c	d
$Cd(L)(NO_3)_2$	22.30	63.08 59.53	45.34 43.26	57.04 56.83
$Hg(L)Cl_2$	22.98	65.85 60.26	46.18 43.15	57.57 56.52

The assignment of the resonances given in figure 3.1 is based on the fully ^1H-coupled spectrum of the cadmium complex at 303K. This spectrum shows resonances a, b, c and d to have $^1J_{^{13}C-^1H}$ coupling constants of 124, 132, 137 and 138Hz respectively and with reference to model cycloalkane compounds[149] allows the assignments shown.

The solution structures of these cadmium(II) and mercury(II) complexes are interpreted as being identical to those of the zinc(II) complexes discussed in section 2, i.e. rapidly interconverting trigonal-bipyramids with the fifth co-ordination site being occupied by $[NO_3]^-$ or solvent for the cadmium complex and a single chloride for the mercury complex. A complete lineshape analysis of the cadmium complex ^{13}C dynamic process in two different solvents gives the activation parameters in Table 3.2. A similar study for the mercury complex has not been attempted due to the much poorer solubility and consequently poor signal to noise ratio for this compound in nitromethane.

Table 3.2.

Activation Parameters* at 298K (standard deviations in parentheses) for the exchange process in solutions of $[Cd(NMe_4\text{-}[14]aneN_4)NO_3]NO_3$.

Solvent (Deuterated)	$\Delta H^{\ddagger}$/kJ mol^{-1}	$\Delta S^{\ddagger}$/J K^{-1}mol^{-1}	k_{ex}/S^{-1}
nitromethane	46.2(2.6)	-14(10)	9.1 x10^3
1:1, acetone/ chloroform	52.0(3.6)	3(13)	6.8 x10^3

*from rate data in the temperature range 243 - 283K.

The activation parameters are seen to be very similar to those obtained for the zinc(II) complexes in Table 2.2 and this adds support to the interpretation of similar structures.

The conclusion of trigonal-bipyramidal stereochemistry for the cadmium complex is especially significant since this geometry was deduced for one of the species present in the ^{13}C n.m.r. spectrum of $[Cd([14]aneN_4)](NO_3)_2$ in Chapter 3, section 4. In that case, however, the activation parameters for the dynamic process were $\Delta H^{\ddagger}$= 8.8(1.3)kJ mol^{-1}, $\Delta S^{\ddagger}$= -170(15)J K^{-1}mol^{-1}. The much higher value of $\Delta H^{\ddagger}$ for the present complex indicates that the folding process is energetically more difficult, and this is undoubtedly a manifestation of the steric requirements imposed by the N-methyl groups. These groups will disfavour the exchange transition state since in it they will be forced to approach each other and the fifth ligand more closely, so raising the enthalpic barrier to this motion relative to the unmethylated macrocycle complex with $[14]aneN_4$. Similarly the entropy differences are also a consequence of the N-methyl groups. When no such groups are present the large, negative activation entropy indicates increased solvation of the square-

pyramidal transition state (probably in the sixth octahedral site) whereas when the N-methyl groups are present their interaction with the fifth ligand in the transition state will tend to push the cadmium atom further out of plane in an attempt to reduce these steric contacts. If this happens then the macrocycle backbone continues to block the sixth octahedral site, preventing any increased solvation in the transition state and producing a very small entropy change as observed.

It is clear from this work that trigonal-bipyramidal solution stereochemistry would appear to be the norm for complexes of NMe_4-[14]aneN$_4$, however such a geometry is not found for the complexes of lead(II).

SECTION 4. COMPLEX WITH LEAD(II).

Just as the cadmium and mercury complexes, above, are new complexes of NMe_4-[14]aneN$_4$ with a second and third row transition element, the complex with lead(II) is the first with a non-transition metal to be reported. The white crystalline complex may only be prepared in dry DMSO, in exact analogy to the preparation of the complex with [14]aneN$_4$, by mixing $Pb(NO_3)_2$ with the macrocycle in equimolar proportions. The complex may only be obtained as a solid by pumping down a concentrated DMSO solution. The complex is very soluble in $[^2H]_6$-DMSO/$[^2H]_4$-methanol, 4:1, and ^1H-decoupled ^{13}C n.m.r. spectra were recorded in this medium.

Such a variable temperature n.m.r. study is shown in figure 4.1. At 330K the spectrum shows just four lines as expected for the trans-I geometry (δ = 56.99, 55.61, 42.79, 23.60ppm ref dioxan 67.26ppm; relative integrals 2:2:2:1.) However upon cooling the solution (the

Figure 4.1.

^{13}C n.m.r. of macrocycle exchange on $Pb(NMe_4\text{-}[14]aneN_4)(NO_3)_2$ in DMSO.

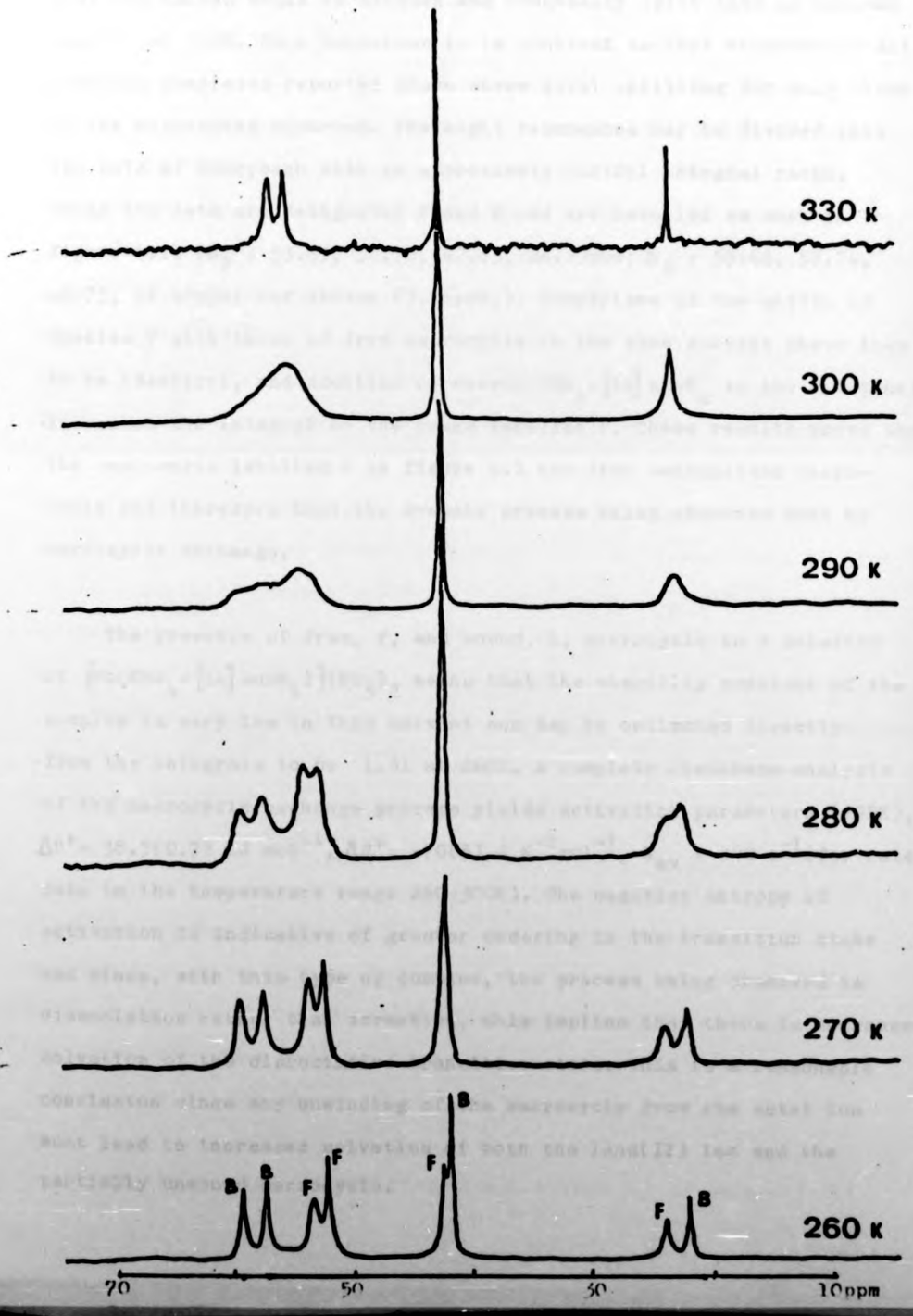

10% methanol being present to allow low temperature accumulations) all four resonances begin to broaden and eventually split into an unequal doublet at 260K. Such behaviour is in contrast to that observed in all previous complexes reported above where equal splitting for only three of the resonances occurred. The eight resonances may be divided into two sets of four, each with an approximate 2:2:2:1 integral ratio. These two sets are designated F and B and are labelled as such in figure 4.1. (δ_F = 53.89, 52.70, 42.83, 24.29ppm; δ_B = 59.68, 57.74, 42.75, 22.40ppm; ref dioxan 67.26ppm.). Comparison of the shifts of species F with those of free macrocycle in the same solvent shows them to be identical, and addition of excess NMe_4-[14]$aneN_4$ to the solutions increases the integral of the peaks labelled F. These results prove that the resonances labelled F in figure 4.1 are from uncomplexed macrocycle and therefore that the dynamic process being observed must be macrocycle exchange.

The presence of free, F, and bound, B, macrocycle in a solution of $[Pb(NMe_4$-[14]$aneN_4)](NO_3)_2$ means that the stability constant of the complex is very low in this solvent and may be estimated directly from the integrals to be 1.31 at 260K. A complete lineshape analysis of the macrocycle exchange process yields activation parameters (298K), $\Delta H^{\ddagger}$ = 38.5(0.7) kJ mol^{-1}, $\Delta S^{\ddagger}$ = -70(3) J $K^{-1}mol^{-1}$, k_{ex} = 240 s^{-1} (for rate data in the temperature range 260-300K). The negative entropy of activation is indicative of greater ordering in the transition state and since, with this type of complex, the process being observed is dissociation rather than formation, this implies that there is increased solvation of the dissociative transition state. This is a reasonable conclusion since any unwinding of the macrocycle from the metal ion must lead to increased solvation of both the lead(II) ion and the partially unwound macrocycle.

This complex is the only one studied in which the macrocycle exchange process is measurably fast, complexes of zinc(II), cadmium(II) and mercury(II) with NMe_4-[14]$aneN_4$, and all of the metal ions studied with [14]$aneN_4$ showing no macrocycle exchange on the n.m.r. timescale. It is clear that the present lead complex is unusual but its low stability and rapid macrocycle exchange may be explained by reference to the structure of the lead(II)-[14]$aneN_4$ complex (Chapter 3. section 6). The latter complex was found to be unique as the only instance of a cis-V macrocycle geometry for a labile metal ion, and this fact is neatly explained in terms of the very large ionic radius of lead(II) ($r = 1.21\text{Å}$[6]). This ion is too big to allow any kind of planar co-ordination of the four nitrogen donors so enforcing cis-stereochemistry upon the 14-membered ring. It is, therefore, understandable that in the case of the complex NMe_4-[14]$aneN_4$, the same ring size will again be forced to adopt a cis-V geometry. However, as has already been pointed out, the nitrogen configurations of co-ordinated NMe_4-[14]$aneN_4$ are inconsistent with a cis-V geometry and there is no available route for inverting these configurations. The macrocycle must therefore adopt a most unfavourable geometry for this very large ion and, as a consequence of this, the complex formed is comparatively very unstable towards dissociation.

It is also interesting to note that the resonances B of the complexed ligand, figure 4.1, do not split further down to 233K, indicating that the complex is not folding to a trigonal-bipyramid as is found for all of the other d^{10} metal ions above. This retention of the square-pyramidal geometry is again presumably due to the steric requirements of the large lead(II) ion.

This study completes the work with the heavy metal ions and the

remainder of the results in this chapter will concentrate on the study of the trans-I and trans-III isomers of the nickel(II)-NMe_4-[14]$aneN_4$ complex.

SECTION 5. STRUCTURAL STUDIES OF THE COMPLEXES WITH NICKEL(II).

The availability of two distinct, non-interconvertible isomers of the complex $[Ni(NMe_4\text{-}[14]aneN_4)](ClO_4)_2$ make this compound an ideal model for all of the previous work. The two isomers contain trans-I and trans-III forms of the macrocycle (figure 5.1.) and, as much of the work discussed in this thesis has been related to the structural relationships between these two isomers in a dynamic sense, it would seem logical to characterise them separately for the same metal ion. This will help to evaluate exactly how the macrocycle stereochemistry is capable of modifying both the structural and kinetic properties of a given metal ion. In this section the essentially structural aspects of the two isomers will be compared and in the following section their kinetic properties will be examined in greater detail. Firstly, however, the properties of both complexes are summarised below.

Nickel(II) complexes of NMe_4-[14]$aneN_4$ were first prepared by Barefield *et al.*[210,223] who established that the square-planar complexe could exist as two distinct non-interconvertible isomers. The complex prepared by adding hydrated nickel(II) perchlorate to the macrocycle has the same trans-I stereochemistry as all of the complexes discussed previously in this chapter. This has been pointed out to be a kinetically determined structure which has no available route whereby it can undergo inversion of two of its nitrogen atoms to produce the thermodynamically more favourable trans-III geometry. The trans-III complex may only be prepared by direct methylation of the nickel(II) complex

Figure 5.1.

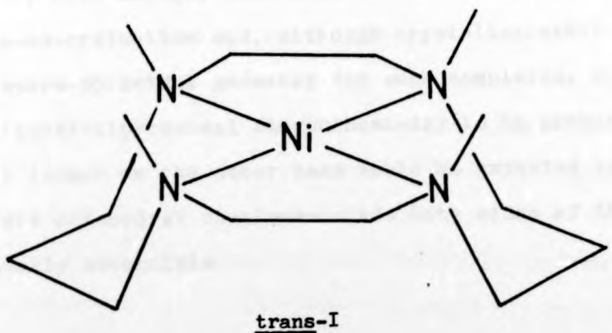

trans-I

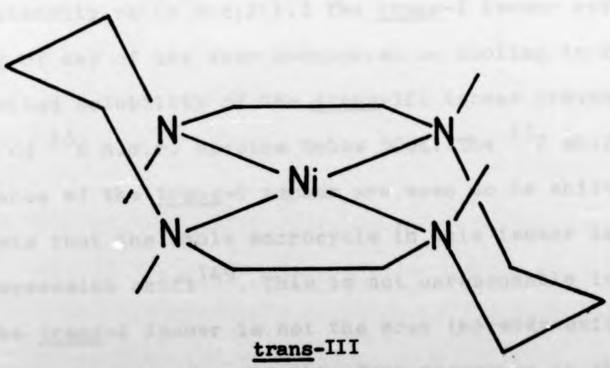

trans-III

The two possible isomers of $[Ni(NMe_4\text{-}[14]aneN_4)]^{2+}$ discussed in text.

Figure 5.1.

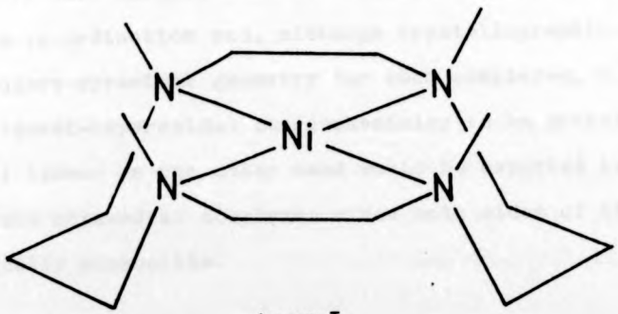

trans-I

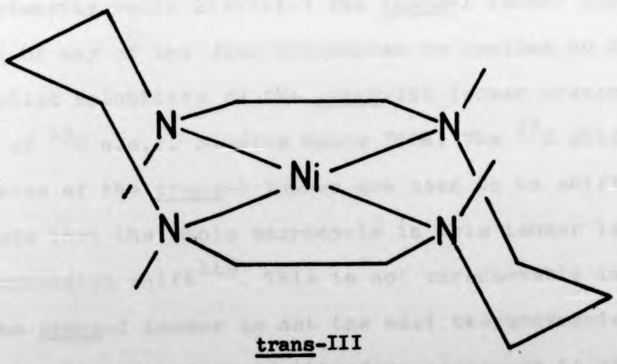

trans-III

The two possible isomers of $[Ni(NMe_4\text{-}[14]aneN_4)]^{2+}$ discussed in text.

of the parent macrocycle [14]aneN$_4$[223]. Complexes with the trans-I stereochemistry have already been seen to have a very marked propensity towards penta-co-ordination and, although crystallographic evidence suggests a square-pyramidal geometry for such complexes, n.m.r. data indicates trigonal-bipyramidal stereochemistry to be probable in solution. The trans-III isomer on the other hand would be expected to ligate on axis to produce octahedral complexes since both sides of the macrocycle plane are equally accessible.

As expected both isomers dissolve in D_2O to give solutions which are partially paramagnetic, and so the ^{13}C n.m.r. spectrum of each complex was recorded in dry $[^2H]_3$-nitromethane (trans-I, δ= 56.41, 53.61, 39.74, 20.54ppm; trans-III, δ= 59.82, 58.26, 45.91, 22.12ppm; ref dioxan 67.26ppm; intensity ratio 2:2:2:1.) The trans-I isomer appears to show no splitting of any of the four resonances on cooling to 240K, while the very limited solubility of the trans-III isomer prevents the acquisition of ^{13}C n.m.r. spectra below 300K. The ^{13}C shifts of all four resonances of the trans-I isomer are seen to be shifted upfield which suggests that the whole macrocycle in this isomer is subject to a steric compression shift[149]. This is not unreasonable in view of the fact that the trans-I isomer is not the most thermodynamically stable geometry of the ligand and would therefore rearrange to the trans-III form, if this were possible, in order to lessen these steric contacts.

Visible spectra of each isomer in dry nitromethane display only a single absorption maximum (λ_{max}nm, (ϵ dm^{3}mol^{-1}cm^{-1}) = 519(185) for trans-I and 492(83) for trans-III). In this non-co-ordinating solvent these maxima correspond to the $^3A_{2g} \leftarrow {}^1A_{1g}$ transition of simple square-planar nickel(II) species although the trans-I isomer has a comparatively large extinction coefficient. This may well be due to the removal of

strict square-planar symmetry by movement of the nickel atom out of the nitrogen donor plane. The greater in-plane ligand-field strength of the macrocycle in the trans-III isomer is evident from the greater energy of its $^3A_{2g} \leftarrow {}^1A_{1g}$ transition. Again this difference is probably the result of the movement of the nickel atom out of plane in the trans-I isomer where it will not experience the full constricting effect of the nitrogen donors. In water, both isomers have visible spectra which appear to be mixtures of square-planar and solvated species. Such behaviour exactly mirrors that observed for the nickel(II)-[14]aneN$_4$ complex discussed in Chapter 3, but in these instances the percentage of the solvated species is found to be much greater. The trans-I isomer displays three bands at λ_{max}nm(ϵ dm^{3}mol^{-1}cm^{-1}; Cary 14)= 654(32),510(70),391(112), in the visible region of the spectrum and these may be assigned to the square planar species, 510nm, and a five-co-ordinate species, 654,391nm. (High extinction coefficients for these latter bands are indicative of five-co-ordination[186]). The trans-III isomer has absorption bands at 494(27), and 367(10)nm and these may be assigned to a square-planar and an octahedral species respectively.

Adding increments of dry NaClO$_4$ to these solutions converted their spectra to those of the pure square-planar species (see Chapter 3, section 3 for details) and allowed the extraction of limiting extinction coefficients for these species in water (trans-I, ϵ_{510}= 143 dm^{3}mol^{-1}cm^{-1}; trans-III, ϵ_{494}= 72 dm^{3}mol^{-1}cm^{-1}). Variable temperature visible spectra (SP800) for both isomers are illustrated in figures 5.2 (trans-I) and 5.3 (trans-III) and, using the values of extinction coefficients for the pure square-planar species derived above, the percentages of square-planar diamagnetic and solvated paramagnetic species could be determined. From these values the equilibrium constant for the equilibrium:

$$[Ni(NMe_4\text{-}[14]aneN_4)]^{2+} + xH_2O \rightleftharpoons^{K_{eq}} [Ni(NMe_4\text{-}[14]aneN_4)(OH_2)_x]^{2+}$$

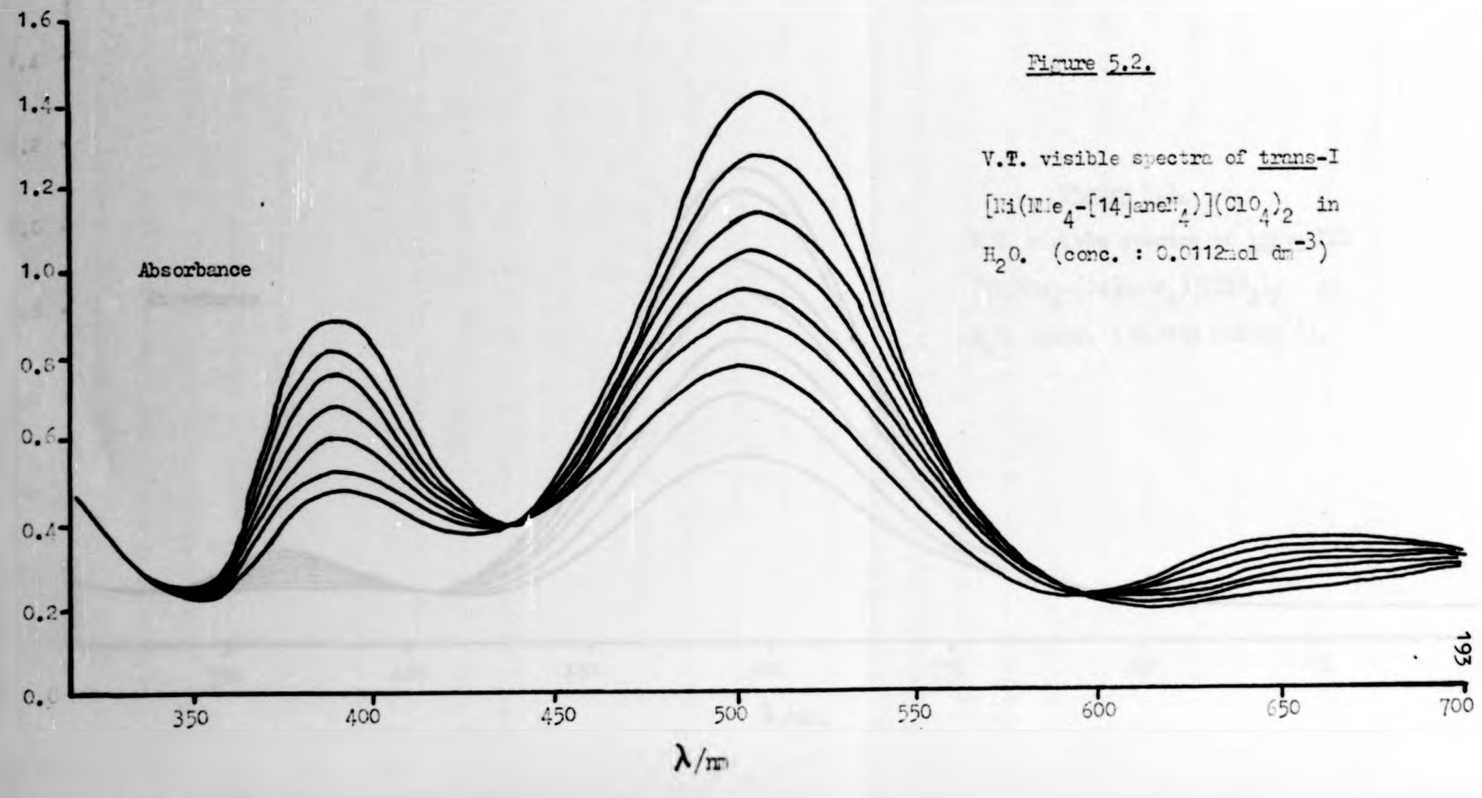

Figure 5.2.

V.T. visible spectra of trans-I $[Ni(MMe_4\text{-}[14]anecN_4)](ClO_4)_2$ in H_2O. (conc. : 0.0112mol dm^{-3})

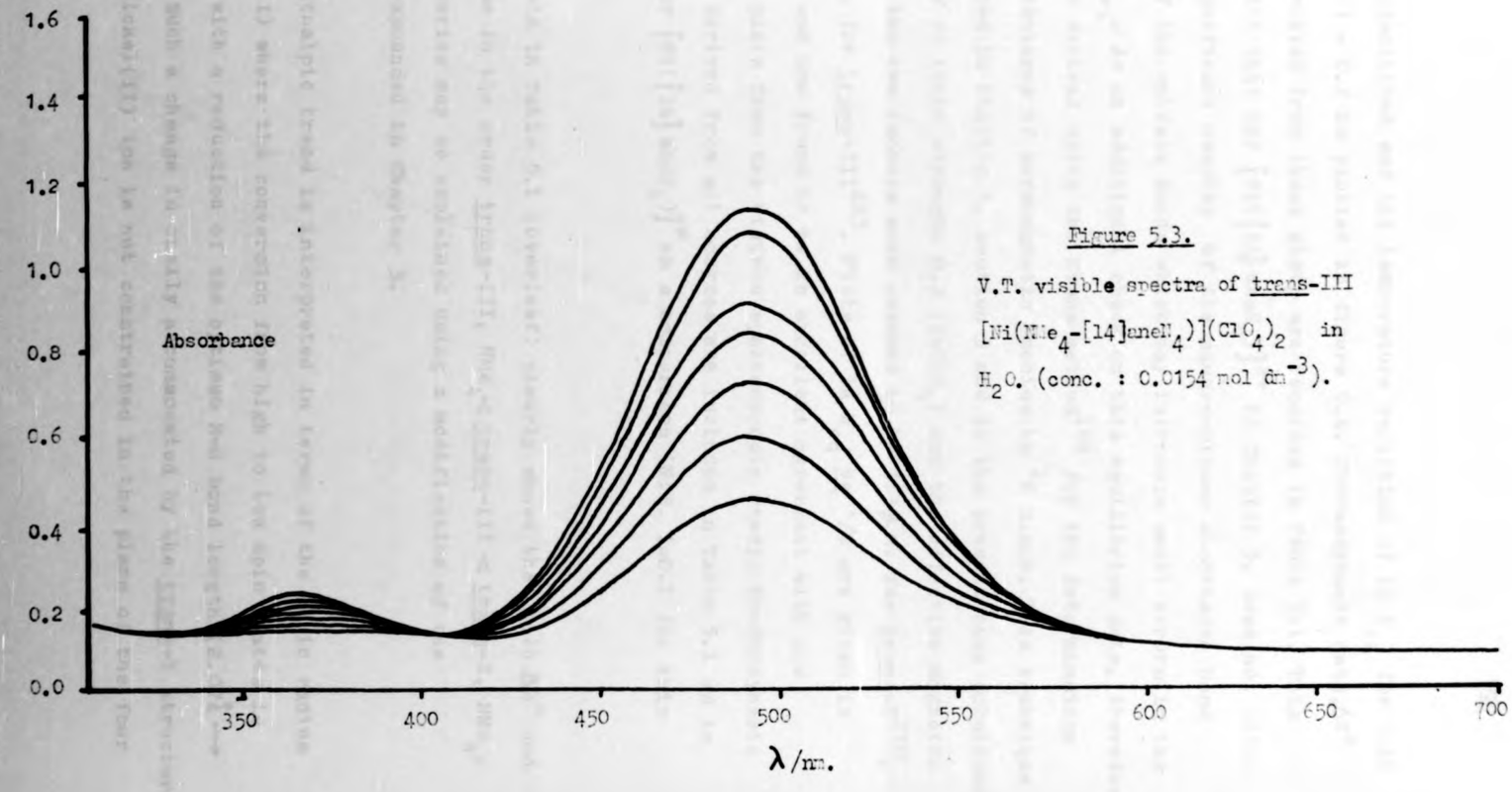

Figure 5.3.

V.T. visible spectra of trans-III $[Ni(NMe_4\text{-}[14]aneN_4)](ClO_4)_2$ in H_2O. (conc. : 0.0154 mol dm^{-3}).

could be established and the temperature variation of ln K_{eq} for both isomers at I = 0.2 is plotted in figure 5.4. Thermodynamic data, ΔH^{o} and ΔS^{o}, derived from these plots are recorded in Table 5.1. This data, as with that for $[Ni([14]aneN_4)]^{2+}$ in Chapter 3, does not allow for any significant overlap of the square-planar absorbance band with any of the solvate bands which may introduce small errors in the value of K_{eq}. As an additional check on this equilibrium data, therefore, it was also derived using the Evans method[188] for the determination of the percentages of paramagnetic species by ^{1}H n.m.r. This technique was described in Chapter 3, section 3 and in the present case solutions in D_2O were of ionic strength 0.2 ($NaClO_4$) and the effective magnetic moments of the two isomers were assumed to be 3.3β.M. for <u>trans</u>-I[210], and 3.3β.M. for <u>trans</u>-III[223]. Plots of ln K_{eq} <u>vs</u> $^{1}/T$ are given in figure 5.4 and are found to be in excellent agreement with the equivalent plots from the visible spectroscopic study. Thermodynamic parameters derived from all sources are included in Table 5.1 as is the data for $[Ni([14]aneN_4)]^{2+}$ as a comparison (N.B. I=0.1 for this complex).

The data in Table 5.1 (overleaf) clearly shows that both ΔH^{o} and ΔS^{o} increase in the order <u>trans</u>-III, NMe_4 < <u>trans</u>-III < <u>trans</u>-I, NMe_4, and these series may be explained using a modification of the arguments expounded in Chapter 3.

The enthalpic trend is interpreted in terms of the ionic radius of nickel(II) where the conversion from high to low spin states is associated with a reduction of the optimum M-N bond length (2.07Å $\longrightarrow$ 1.91Å[189]). Such a change is easily accommodated by the <u>trans</u>-I structure where the nickel(II) ion is not constrained in the plane of the four

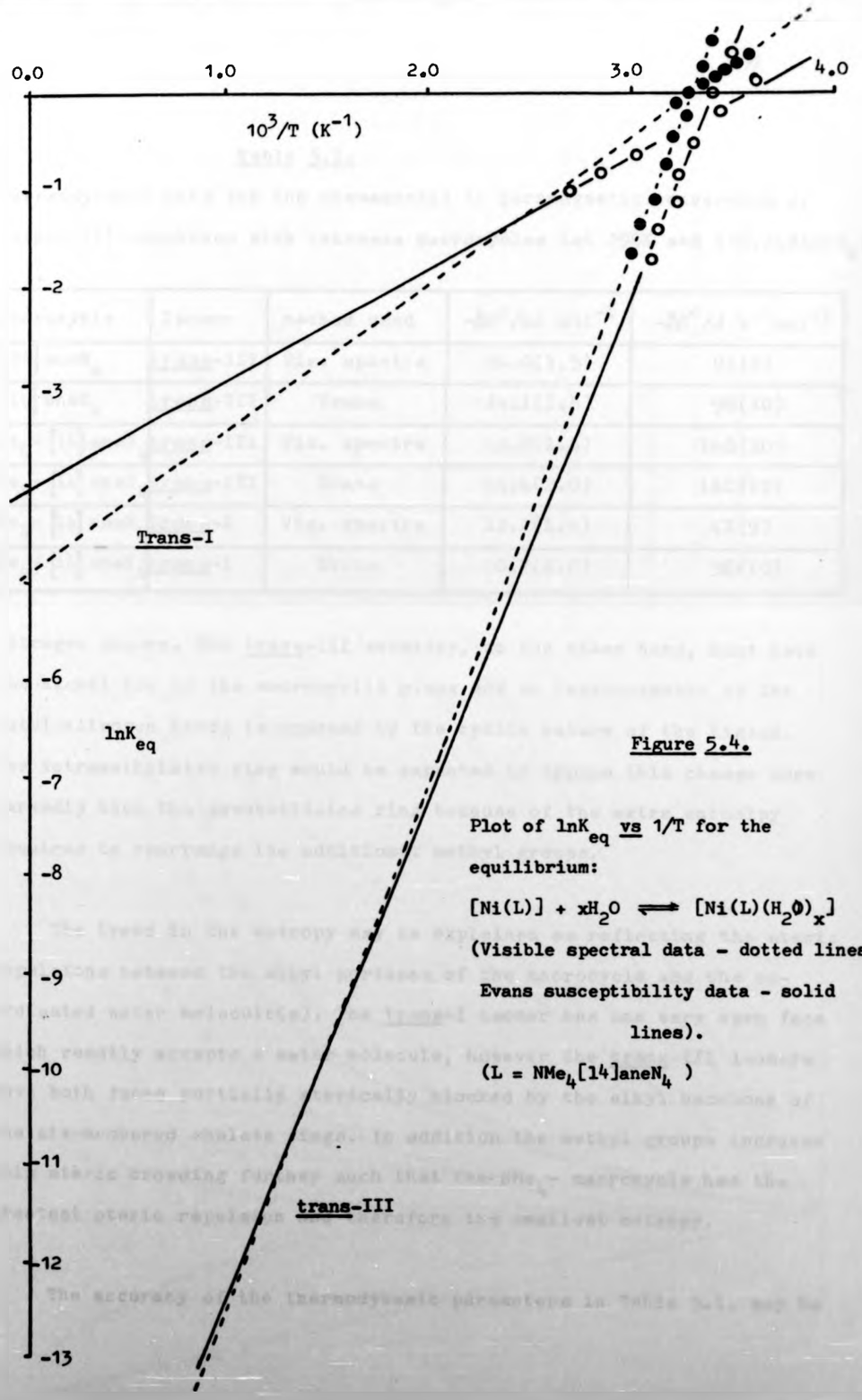

Figure 5.4.

Plot of $\ln K_{eq}$ vs 1/T for the equilibrium:

$[Ni(L)] + xH_2O \rightleftharpoons [Ni(L)(H_2O)_x]$

(Visible spectral data - dotted lines

Evans susceptibility data - solid lines).

($L = NMe_4[14]aneN_4$)

Table 5.1.

Thermodynamic data for the diamagnetic to paramagnetic conversion of nickel(II) complexes with tetraaza macrocycles (at 298K and I=0.2($NaClO_4$)

Macrocycle	Isomer	Method Used	$-\Delta H^o$/kJ mol^{-1}	$-\Delta S^o$/J $K^{-1}mol^{-1}$
[14]$aneN_4$	trans-III	Vis. spectra	24.0(1.5)	91(8)
[14]$aneN_4$	trans-III	Evans	24.1(1.8)	96(10)
NMe_4-[14]$aneN_4$	trans-III	Vis. spectra	43.8(1.6)	146(10)
NMe_4-[14]$aneN_4$	trans-III	Evans	44.4(2.0)	140(10)
NMe_4-[14]$aneN_4$	trans-I	Vis. spectra	12.2(1.6)	41(9)
NMe_4-[14]$aneN_4$	trans-I	Evans	10.7(2.0)	36(10)

nitrogen donors. The trans-III geometry, on the other hand, must have the nickel ion in the macrocyclic plane and so rearrangement of the metal-nitrogen bonds is opposed by the cyclic nature of the ligand. The tetramethylated ring would be expected to oppose this change more markedly then the unsubstituted ring because of the extra enthalpy required to rearrange the additional methyl groups.

The trend in the entropy may be explained as reflecting the steric repulsions between the alkyl portions of the macrocycle and the co-ordinated water molecule(s). The trans-I isomer has one very open face which readily accepts a water molecule, however the trans-III isomers have both faces partially sterically blocked by the alkyl backbone of the six-membered chelate rings. In addition the methyl groups increase this steric crowding further such that the NMe_4- macrocycle has the greatest steric repulsion and therefore the smallest entropy.

The accuracy of the thermodynamic parameters in Table 5.1. may be

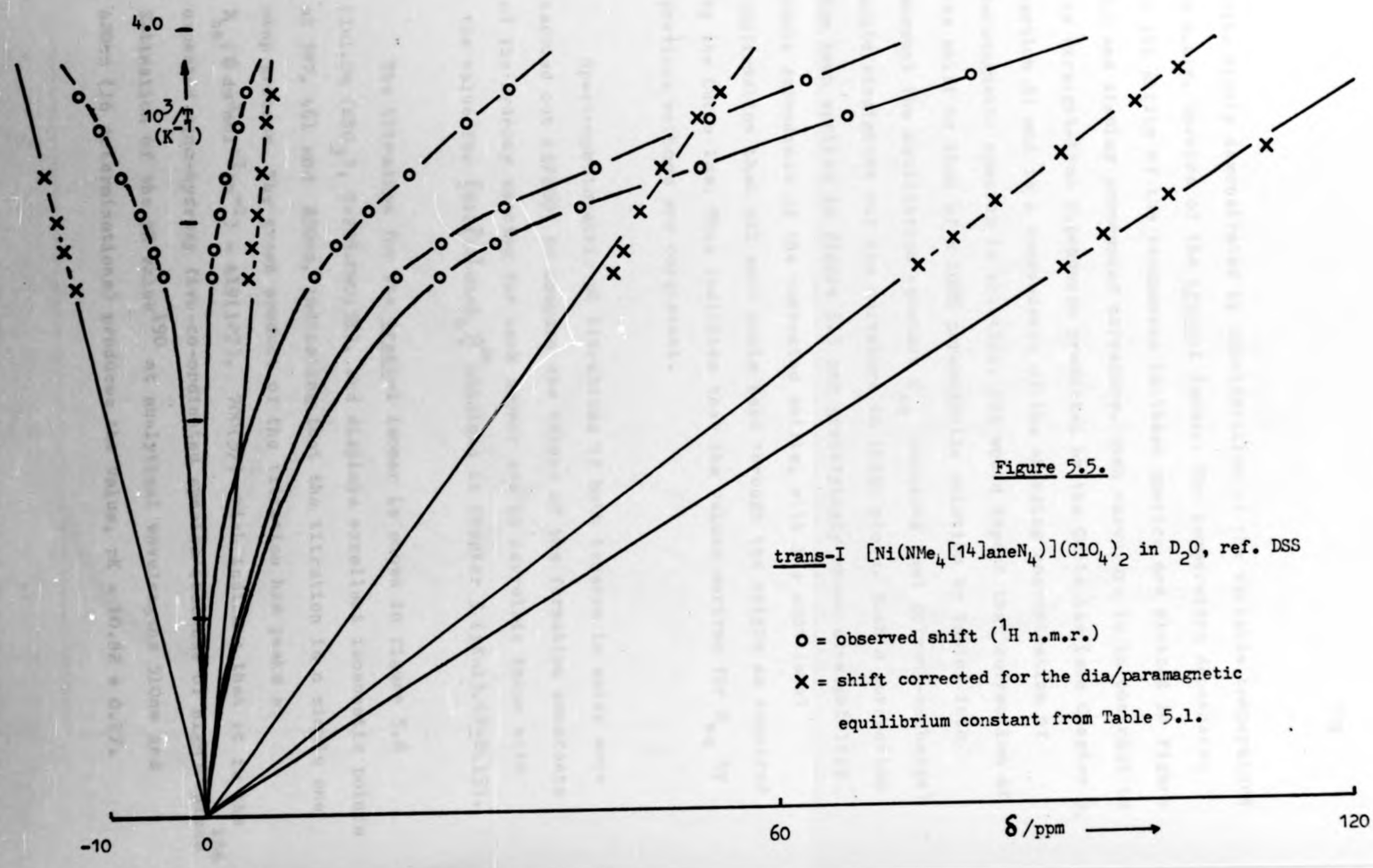

Figure 5.5.

trans-I $[Ni(NMe_4[14]aneN_4)](ClO_4)_2$ in D_2O, ref. DSS

o = observed shift (^1H n.m.r.)

× = shift corrected for the dia/paramagnetic equilibrium constant from Table 5.1.

quite nicely demonstrated by consideration of the variable temperature ^1H n.m.r. spectra of the trans-I isomer. The temperature dependence of the shifts of the resonances in these spectra are plotted in figure 5.5 and display pronounced curvature. Such curvature is in contrast to the straight-line dependence predicted by the Curie law (see Chapter 3, section 3) and is a consequence of the changing concentration of paramagnetic species in solution. One would expect that correction of the shift to that of a 100% paramagnetic solution by taking into account the equilibrium constant K_{eq} (assuming fast solvent-exchange) would straighten out the curvature in these plots. Such a correction has been applied in figure 5.5 and gratifyingly shows straight line Curie dependence of the corrected shifts, with the additional confirmation that all such plots pass through the origin as required by the Curie law. This indicates that the values derived for K_{eq} by previous methods are consistent.

Spectrophotometric pH titrations of both isomers in water were carried out (SP800) to compare the values of the formation constants of the hydroxy species for each isomer and to correlate these with the value for $[Ni([14]aneN_4)]^{2+}$ obtained in Chapter 3 (pK=13.67±0.15).

The titration for the trans-I isomer is shown in figure 5.6 (I=1.04 (KNO_3), T=298.0±0.5K), and displays excellent isosbestic points at 397, 461 and 630nm, indicating that the titration is a simple one step process. The green product of the titration has peaks at $\lambda_{nm}(\epsilon\ dm^3mol^{-1}cm^{-1})$ = 419(127), 700(57) which indicate that it is the expected mono-hydroxy five-co-ordinated species (because of high ϵ values[186]). Estimation of the pK value[190] at analytical wavelengths 510nm and 420nm (16 determinations) produces the value, pK = 10.82 ± 0.17.

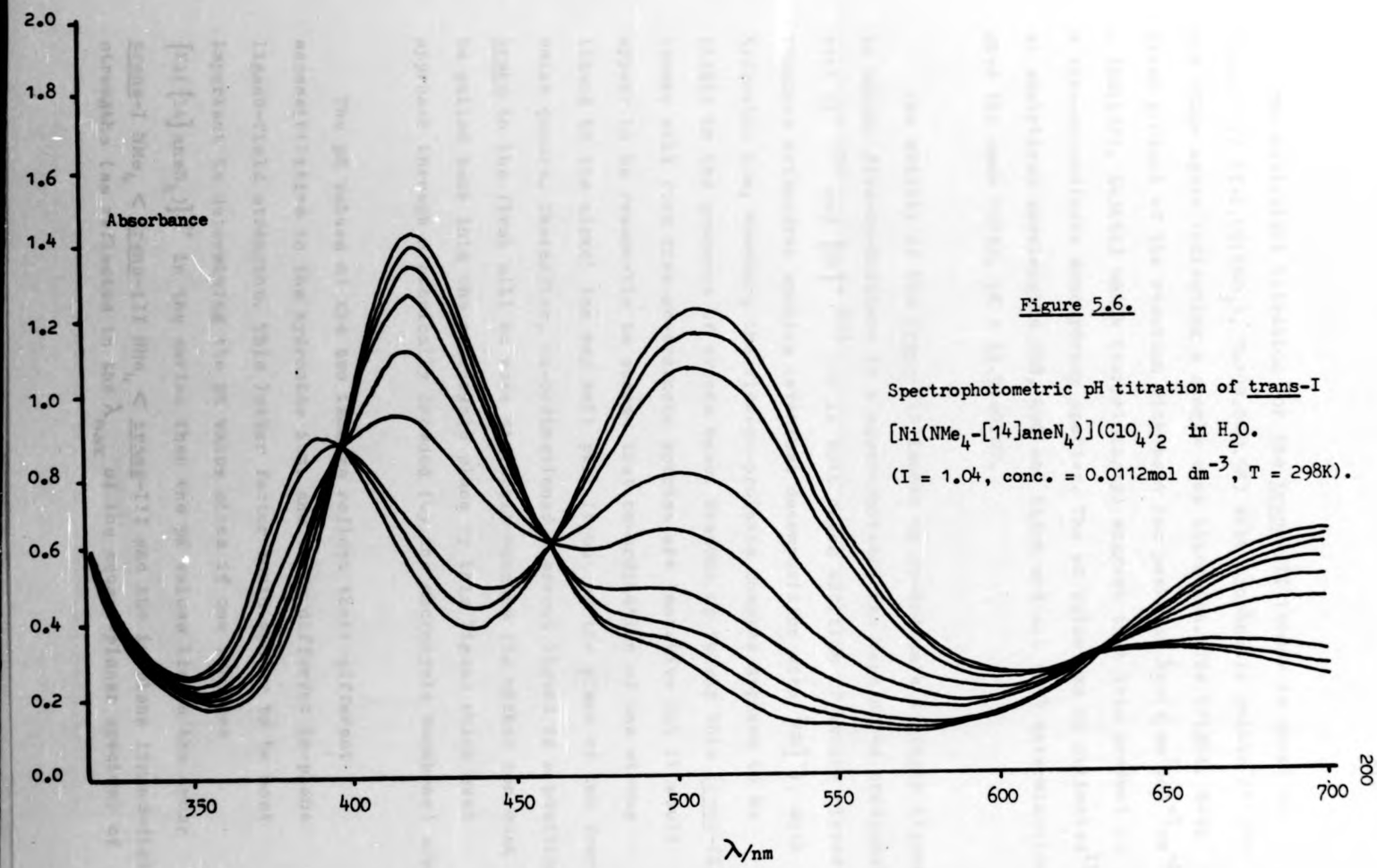

Figure 5.6.

Spectrophotometric pH titration of trans-I $[Ni(NMe_4\text{-}[14]aneN_4)](ClO_4)_2$ in H_2O.
(I = 1.04, conc. = 0.0112mol dm^{-3}, T = 298K).

The equivalent titration for the trans-III isomer is shown in figure 5.7 (I=1.06(KNO_3), T=298.0±0.5K) with isosbestic points at 452 and 551nm again indicating a single step titration. The bright, deep green product of the reaction with base has peaks at λnm(ϵ $dm^3mol^{-1}cm^{-1}$) = 398(132), 643(61) which (surprisingly) suggest that this product is a five-co-ordinate monohydroxy species. The pK value may be estimated[190] at analytical wavelengths 398, 490 and 643nm and all (15) determinations give the same value, pK = 11.94±0.07.

The ability of the trans-III isomer to co-ordinate a single ligand to become five-co-ordinate in a square-pyramid has been noted previously with Cl^- [101] and $[CN]^-$ [223] but in both cases addition of excess ligand produces octahedral species (eventual decomposition with $[CN]^-$). With hydroxide ion, however, the five-co-ordinate complex appears to be stable in the presence of excess base. Reasons as to why this trans-III isomer will form five-co-ordinate species are tentative but it would appear to be reasonable to assume that co-ordination of one strong ligand to the nickel ion may well pull it out of the plane of the four amine donors. Thereafter, co-ordinationof a second ligand in a position trans to the first will be more difficult because the nickel ion must be pulled back into the macrocycle plane by this ligand which must approach through a sterically crowded (by the macrocycle backbone) area.

The pK values of the two isomers reflect their different accessibilities to the hydroxide ion, and their different in-plane ligand-field strengths. This latter factor would appear to be most important in determining the pK value since if one includes $[Ni([14]aneN_4)]^{2+}$ in the series then the pK values lie in the order trans-I NMe_4 < trans-III NMe_4 < trans-III and the in-plane ligand-field strengths (as reflected in the $\tilde{\lambda}_{max}$ of the square-planar species) of

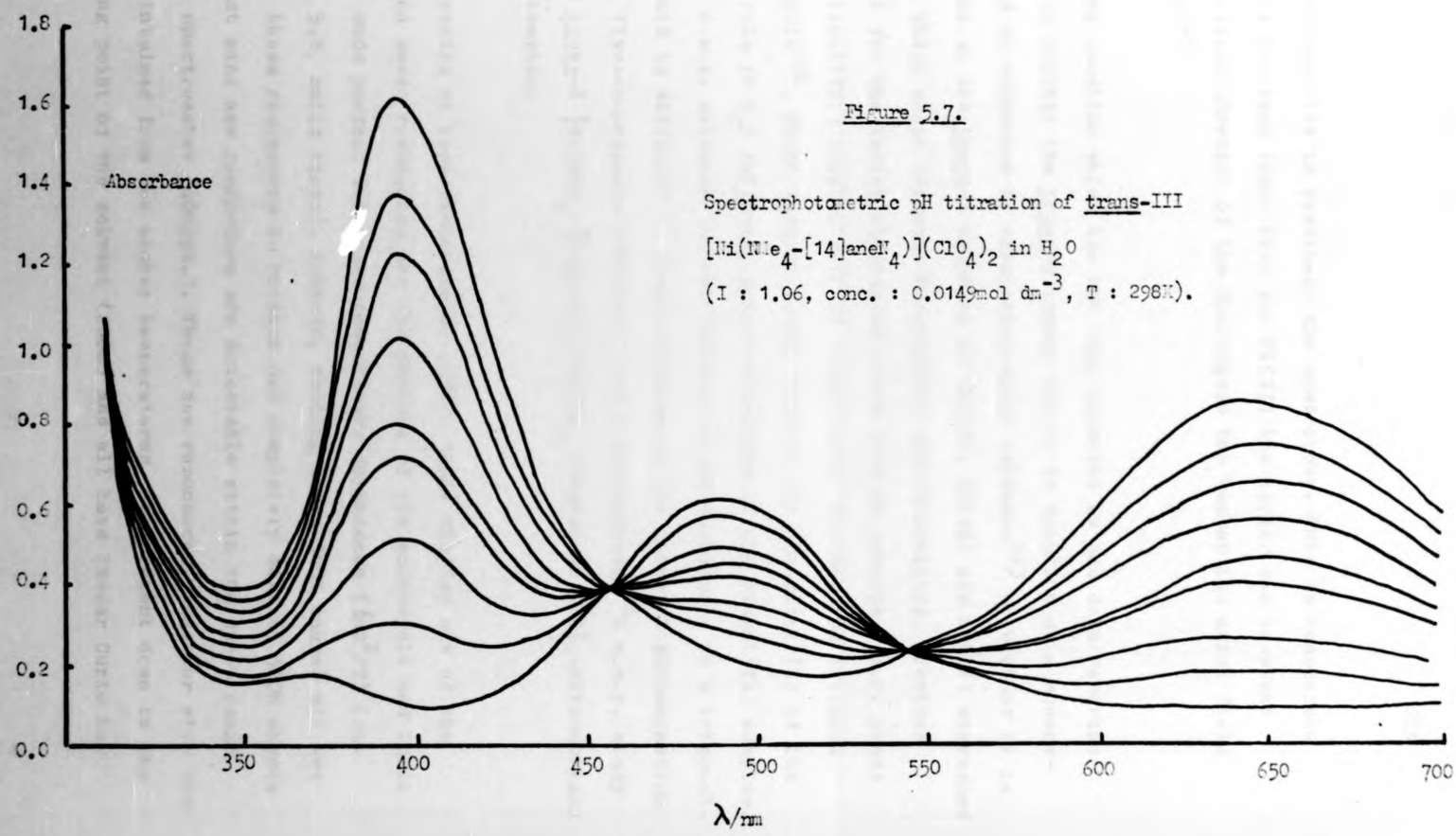

Figure 5.7.

Spectrophotometric pH titration of trans-III $[Ni(Me_4\text{-}[14]aneN_4)](ClO_4)_2$ in H_2O (I : 1.06, conc. : 0.0149mol dm^{-3}, T : 298K).

the complexes lie in precisely the same order. This is reasonable since it has been found that for Ni(II) the larger the in-plane ligand-field strength of the macrocycle the weaker the axial field strength[45].

One question which has not been answered by the data reported above is whether the trans-I isomer exists in solution as a square-pyramid as suggested by crystallographic evidence[213] or whether it is the same as the trans-I complexes of Zn(II), Cd(II) and Hg(II) discussed above, which adopt trigonal-bipyramidal stereochemistry. Previous support for the latter conclusion comes from an aqueous e.s.r. study of a nickel(III) complex with an unsaturated 14-membered tetraaza macrocycle[224]. These workers found evidence for non-planarity of the macrocycle in H_2O following pulse-radiolysis of the nickel(II) complex. Direct n.m.r. evidence for the folding of the macrocycle to a trigonal-bipyramid is difficult to obtain because of the inherent paramagnetism of the five-co-ordinate complexes, but a paramagnetic ^1H n.m.r. study of the trans-I $[Ni(NMe_4\text{-}[14]aneN_4)Cl]ClO_4$ complex in $[^2H]_3$-nitromethane was attempted.

Spectra at high temperatures (370 - 340K) display six of the expected seven resonances for the protons of the macrocycle and their shifts show perfect Curie law temperature dependence ($\delta \propto 1/T$) (see figure 5.8, solid lines). However, cooling below 340K causes all but two of these resonances to broaden out completely down to 300K whence at least nine new resonances are detectable within the sweep range of the spectrometer (400ppm.). These new resonances, together with the two maintained from the higher temperatures, are present down to the freezing point of the solvent (220K) and all have linear Curie law

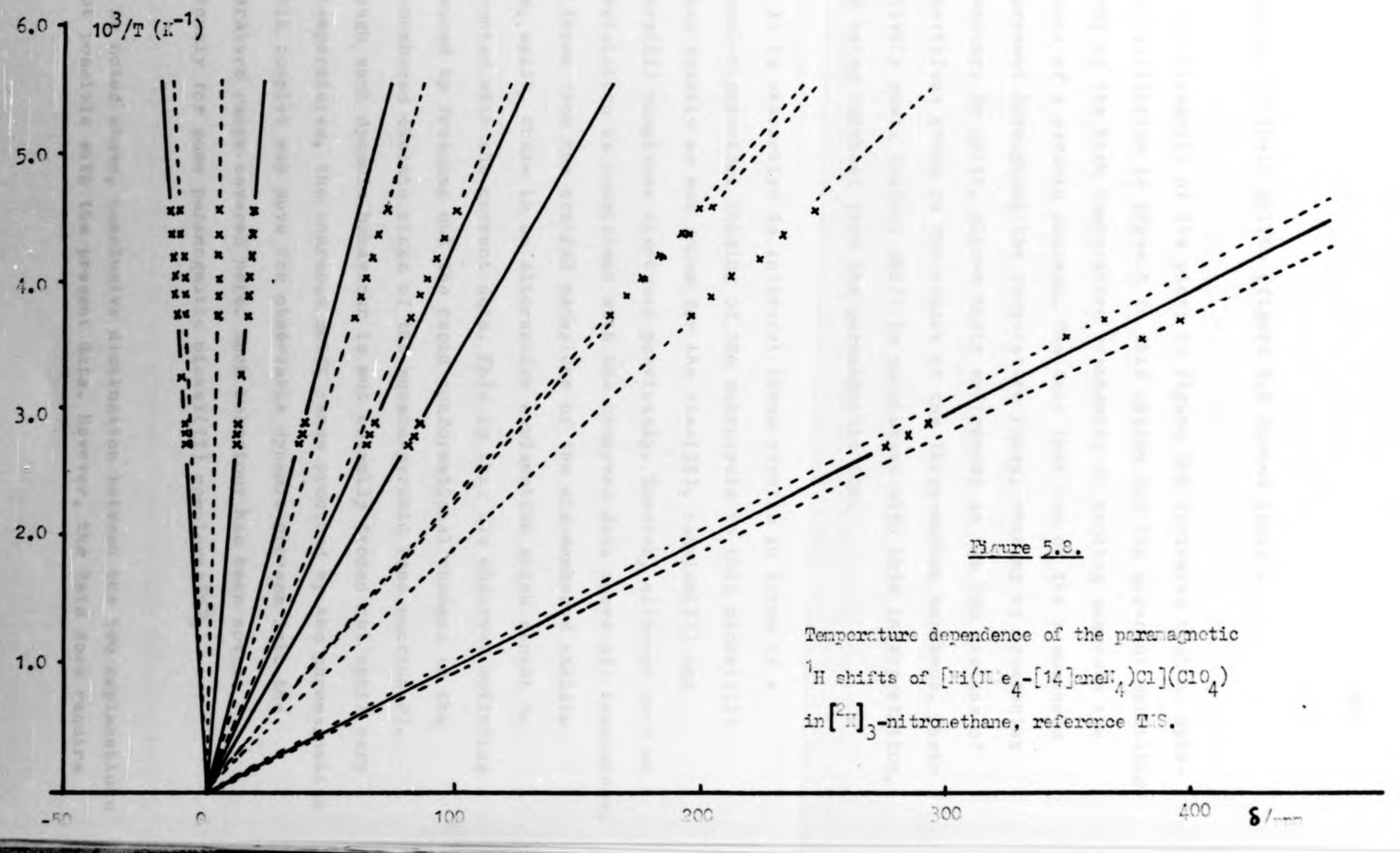

Figure 5.8.

Temperature dependence of the paramagnetic ^1H shifts of $[Ni(Me_4\text{-}[14]aneN_4)Cl](ClO_4)$ in $[^2H]_3$-nitromethane, reference TMS.

dependence of their shifts (figure 5.8 dashed lines).

The linearity of the plots in figure 5.8 indicates that no spin-state equilibrium is present in this system and the apparent splitting of four of the high temperature resonances on cooling suggests the presence of a dynamic process. The fact that two of the resonances are present throughout the temperature range, showing no broadening or tendency to split, allows their assignment as the two protons of the methylene group in the centre of the three-carbon backbone. Their relatively small contact shift is consistent with this interpretation, their being furthest from the paramagnetic ion.

It is attractive to interpret these results in terms of a trigonal-bipyramidal folding of the macrocycle in this nickel(II) complex exactly as was found for the zinc(II), cadmium(II) and mercury(II) complexes discussed previously. However, although such an interpretation is consistent with the observed data where all resonances, save those from the central methylene of the six-membered chelate rings, split, there is an alternative explanation which cannot be discounted with the current data. This is that the observed splitting is caused by freezing out the rapid conformational changes in the five-membered chelate rings of the square-pyramid (see section 2). Although such dynamic behaviour is not normally frozen out until very low temperatures, the enormous shift range produced by the paramagnetism in this complex may move the observable dynamic process into the temperature range covered here. Such behaviour has been noted previously for some paramagnetic nickel(II) complexes[225].

As noted above, conclusive distinction between the two explanations is not possible with the present data. However, the data does require

that any conformational process of the five-membered chelate rings may be synchronous between the rings, maintaining a two-fold symmetry relationship through the nickel atom in order that the resonances from the central methylene of the six-membered rings are not split. Such a requirement is inconsistent with the crystal structures of both nickel(II) azido[213] and zinc(II) chloro (above) square-pyramidal complexes which show the two five-membered chelate rings to be related by mirror symmetry which would cause splitting of these resonances. This conformational interpretation therefore requires complete conversion from the crystal structure upon dissolution in nitromethane with no possibility of the molecule adopting its crystalline structure in solution.

This latter point would tend to favour the trigonal-bipyramidal interpretation of the structure of the trans-I isomer in solution and further indirect evidence for this conclusion comes from the kinetic study reported below. An estimate of the activation parameters for the dynamic process in the ^{1}H spectra may crudely be made using the resonances to lowest field (250 - 400ppm.) which are assumed to be all the components of the exchanging system, i.e. high temperature resonance split to two at low temperature. Measurement of the line-widths of the two resonances in the low temperature region (250-270K) using the paramagnetic slow-exchange approximation for the rate data (see section 6 and Chapter 6) and taking into account the paramagnetic shifting with temperature, allows the calculation of approximate activation parameters (298K) $\Delta H^{\ddagger} = 40(10)kJmol^{-1}$ and $\Delta S^{\ddagger} = -20(20)JK^{-1}mol^{-1}$.

Even with such crude data the activation parameters are seen to be very similar to those derived for both zinc and cadmium complexes

(above), which would tend to support further the tentative conclusion that the trans-I five-co-ordinate nickel(II) complexes of this macrocycle may indeed fold to a trigonal-bipyramid in solution.

SECTION 6. SOLVENT EXCHANGE KINETICS OF NICKEL(II) COMPLEXES.

It is apparent that the two nickel(II) isomers, trans-I and trans-III, (figures 6.1c and 6.1d respectively) afford an opportunity to study the much-neglected area of solvent exchange kinetics of macrocyclic complexes. Such kinetic properties, as related to structural factors, would be expected to be relevant to the overall chemistry of these complexes and may add to the information available for the complexes with heavy metal ions discussed throughout this thesis.

In their own right, however, the two isomers provide the opportunity to compare the ligand substitution kinetics of five- and six-co-ordinate species, a topic which has been the subject of much interest in recent years[226,227], and to compare the enthalpies of activation with the changes in the metal ion co-ordination geometries. A recent ^{17}O n.m.r. study of the five-co-ordinate cobalt(II) complex ion $[Co(NMe_4\text{-}[14]aneN_4)(OH_2)]^{2+}$ with the trans-I ligand stereochemistry, has shown that the rate of water exchange is unusually slow, being some two orders of magnitude less than that observed for the $[Co(OH_2)_6]^{2+}$ ion[217]. This latter observation, and its possible structural implications, prompted an investigation into the rates of acetonitrile exchange with the two nickel(II) complexes (figures 6.1a and 6.1b) to examine the effect of changing the conformation of the macrocyclic ligand upon the rates of acetonitrile exchange.

Acetonitrile was chosen as the solvent for this study because it

Figure 6.1.

Possible species in the solvent (S= acetonitrile) exchange dynamics of $[Ni(NMe_4\text{-}[14]aneN_4)]^{2+}$ isomers.

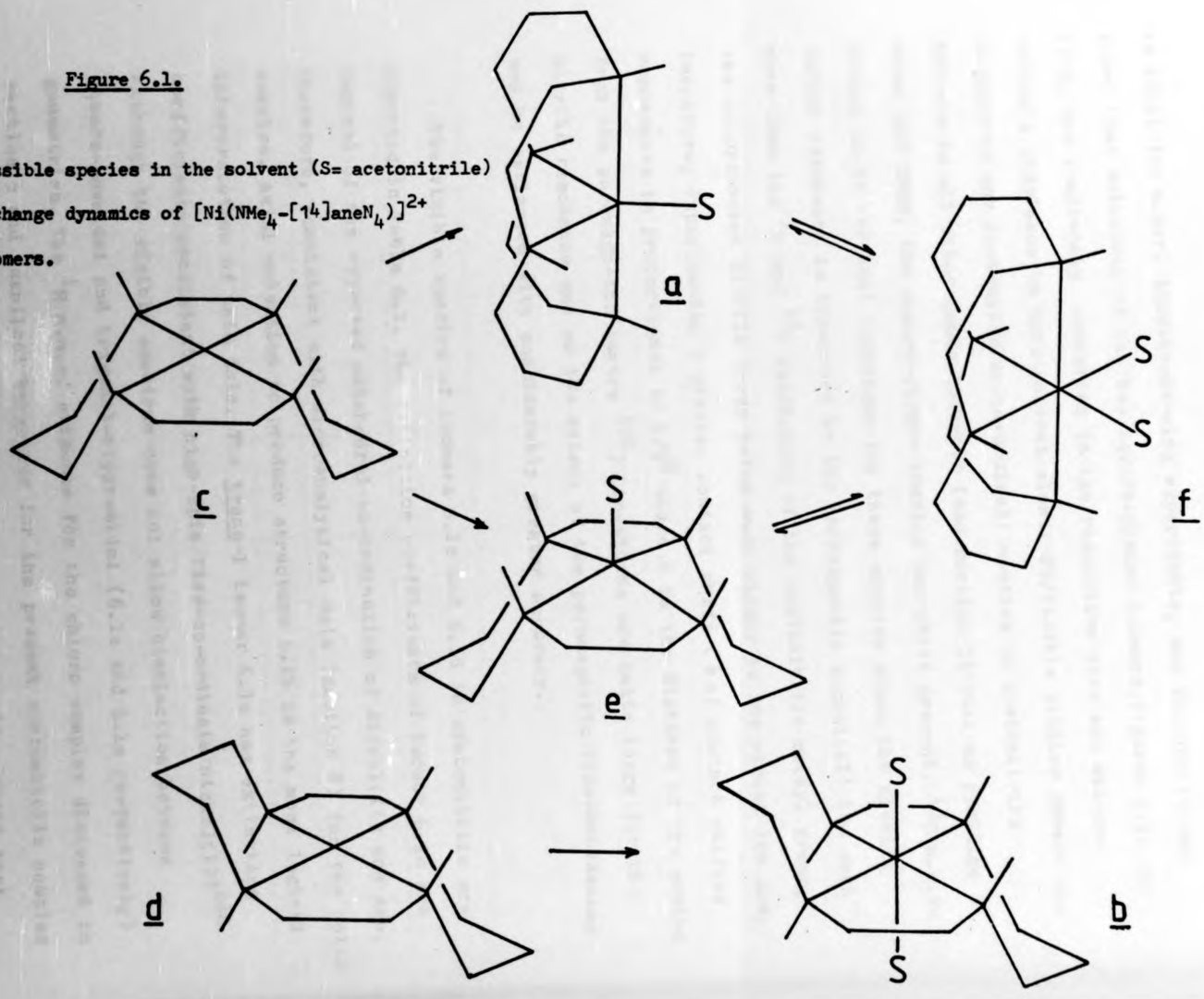

is ideal for n.m.r. line-broadening experiments, and because it was found that solutions of the two square-planar isomers, figures 6.1c and 6.1d, are completely converted to the respective five and six-co-ordinate complexes in this solvent alone; UV/visible studies showed the absence of any residual four-co-ordinate species in acetonitrile whereas in all other donor solvents (see section 5) such as pyridine water and DMSO, the square-planar complex was still present. ^{13}C n.m.r. proved to be the best technique for these studies since the nitrile carbon resonance is broadened by the paramagnetic nickel(II) ion much more than the ^{1}H and ^{13}C resonances of the acetonitrile methyl group, the co-ordinated nitrile group being much closer to the nickel ion and, therefore, experiencing a greater contact shift (δ of contact shifted resonances is proportional to $1/R^6$ where R is the distance of the proton from the paramagnetic centre [228]) Linewidths are quite large for the nitrile resonance and so the extent of the paramagnetic line-broadening may be estimated with considerably greater accuracy.

The visible spectra of isomers 6.1c and 6.1d in acetonitrile are reported in Table 6.1. The extinction coefficients of isomer 6.1d are typical of the expected octahedral co-ordination of nickel(II) and are, therefore, consistent with microanalytical data (section 8) for the solid complex. Axial solvation to produce structure 6.1b is the most logical interpretation of this data. The trans-I isomer 6.1c has extinction coefficients consistent with high-spin five-co-ordinate nickel(II)[186] although the visible spectrum does not allow distinction between square-pyramidal and trigonal-bipyramidal (6.1e and 6.1a respectively) geometries. The ^{1}H n.m.r. evidence for the chloro complex discussed in section 5 and identical behaviour for the present acetonitrile complex (splitting of ^{1}H resonances at low temperature) would suggest that

structure 6.1a, a trigonal bipyramid, is more likely.The spectra of both isomers indicate no residual square-planar species in acetonitrile, implying complete conversion to the high-spin species 6.1a and 6.1b in this solvent. This unique ability of acetonitrile to promote complete co-ordination is probably a result of its linear, 'rod-like' structure which allows it to penetrate to the sterically crowded co-ordination sites of the square-planar complex much more effectively than any other donor solvent.

Table 6.1.

Visible Spectra of $[Ni(NMe_4\text{-}[14]aneN_4)](ClO_4)_2$ complexes in nitromethane and acetonitrile solutions.

Complex Geometry	Solvent	Colour	λ/nm(ϵ/$dm^3mol^{-1}cm^{-1}$)
trans-I,6.1a or 6.1e	CH_3CN	Blue	obs. 1480(9),981(5),790sh(9), 610(40),386(128)
			ref.[210] 1480(9),981(3),790(7), 610(34),390(118)
trans-I,6.1c	CH_3NO_2	Purple	obs. 519(185)
			ref.[210] 519(184)
trans-III,6.1b	CH_3CN	Lilac	obs. 950sh(2.7),830(3.8), 540(5.9),340(14)
trans-III,6.1d	CH_3NO_2	Red	obs. 492(83)

N.m.r. Line-Broadening Studies. - The solvent n.m.r. line-broadening caused by a paramagnetic ion may be expressed as:

$$1/T_{2P}P_M = (\Delta\upsilon_{obs.} - \Delta\upsilon_{ref.})/P_M \qquad (1)$$

where $\Delta\upsilon_{obs.}$ and $\Delta\upsilon_{ref.}$ are the full line-widths at half maximum height

of the solvent and reference resonances in the presence of the paramagnetic ion, and P_M is the mole ratio of bound to free solvent (related to molality). The function $(T_{2P}P_M)^{-1}$ is dependent on the solvent-exchange lifetime (τ_M), the transverse relaxation time of the co-ordinated solvent nucleus (T_{2M}) and the difference in chemical shift between the free nucleus and that co-ordinated to the paramagnetic centre ($\Delta\omega_M$). These quantities are related by a set of well-established equations[229] which may be simplified in several limiting regions. Of these regions, that most useful for the determination of kinetic exchange data is where the rate of solvent exchange is not too great, (specifically either $\Delta\omega_M^2 \gg {}^1/T_{2M}^2, {}^1/\tau_M^2$ or ${}^1/T_{2M}^2 \gg \Delta\omega_M^2, {}^1/\tau_M^2$) so that relationship (2) holds:

$$ {}^1/T_{2P} = P_M/\tau_M \qquad (2) $$

Under these conditions, the temperature dependence of the linewidth related quantity $T_{2P}P_M^{-1}$ should be that of a reaction rate constant, since τ_M^{-1} is the solvent first-order exchange rate, ie:

$$ {}^1/\tau_M = \frac{kT}{h}\, e^{\Delta S^{\ddagger}/R}\, e^{-\Delta H^{\ddagger}/RT} \qquad (3) $$

This very brief introduction to the theory of paramagnetic solvent exchange is expanded upon in many excellent discussions in the literature (refs. 229, 230, 231) and only the results from the technique will be discussed in detail.

The results of the linewidth measurements for 6.1a and 6.1b are shown in figure 6.2. The quantity $\log(T_{2P}P_M)^{-1}$ is plotted versus 1/(absolute temperature) since this linearises all regions having an Arrhenius temperature dependence (equations 2 and 3). The various linear

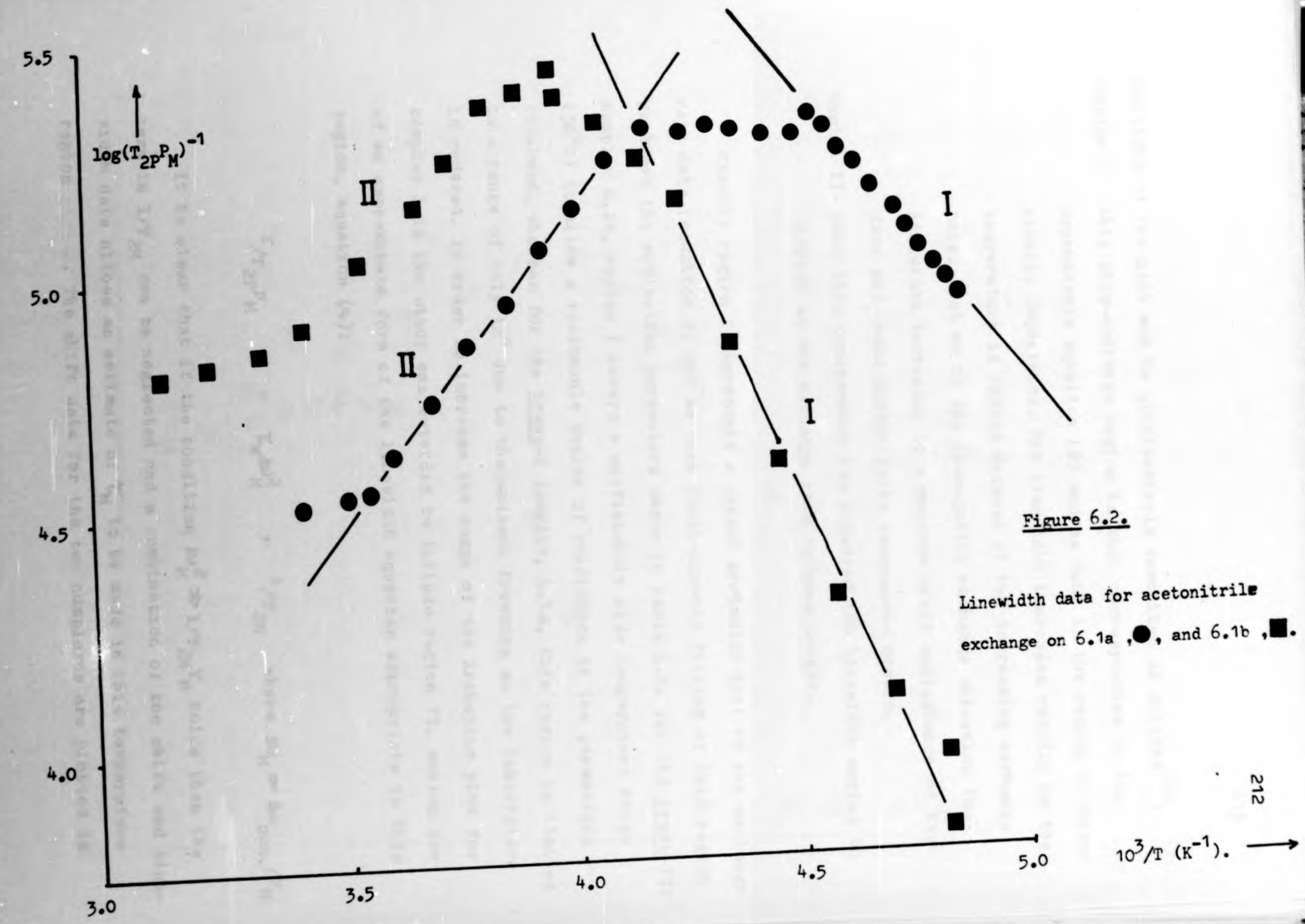

Figure 6.2.

Linewidth data for acetonitrile exchange on 6.1a ,●, and 6.1b ,■.

portions of the plot may be qualitatively described as follows[232]:

Region I - this slow-exchange region is that corresponding to the approximate equation (2) and as such is the region of major kinetic importance. The linewidth increases rapidly as the temperature is raised because of the increasing exchange rate. Just as in the diamagnetic exchange situation the linewidth increases to a maximum until coalescence of the free and bound acetonitrile resonances occurs.

Region II- once this coalescence has occurred the linewidth begins to sharpen as the exchange rate becomes larger.

Clearly region I represents a direct Arrhenius plot of the exchange rate data (equation 2) and as such least-squares fitting of this region produces the activation parameters shown in Table 6.2. For the trans-III complex 6.1b, region I covers a sufficiently wide temperature range ($30^{o}C$) to allow a reasonable degree of confidence in the parameters obtained, whereas for the trans-I complex, 6.1a, this region is limited to a range of only 12^{o} due to the solvent freezing as the temperature is reduced. In order to increase the range of the Arrhenius plot for complex 6.1a the study was extended to include region II, making use of an approximate form of the linewidth equation appropriate to this region, equation (4):

$$1/T_{2P}P_M = \tau_M \Delta\omega_M^2 + 1/T_{2M} \quad \text{where } \Delta\omega_M \propto \Delta\omega_{obs.}/P_M$$

It is clear that if the condition $\Delta\omega_M^2 \gg 1/T_{2M}\tau_M$ holds then the term in $1/T_{2M}$ can be neglected and a combination of the shift and linewidth data allows an estimate of τ_M to be made in this temperature region [illegible]. The shift data for the two complexes are plotted in

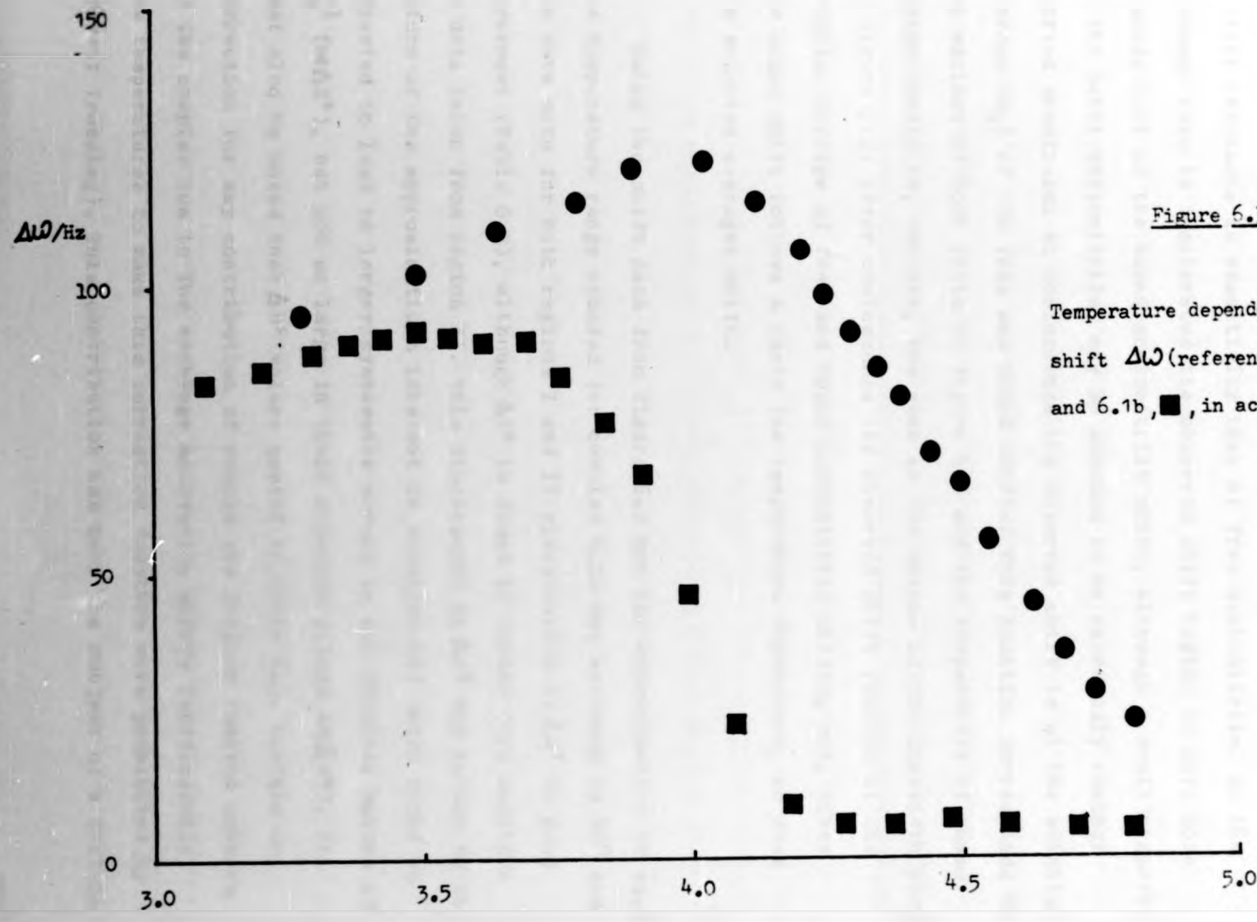

Figure 6.3.

Temperature dependence of the chemical shift $\Delta\omega$ (reference dioxan) for 6.1a, ●, and 6.1b, ■, in acetonitrile solution.

figure 6.3 and follow precisely the behaviour predicted by theory[229-232]. This behaviour may be verbally summarised thus:- at low temperatures where the solvent exchange rate is negligible the observed shift of the nitrile resonance is essentially that of free acetonitrile. As the exchange rate is accelerated the observed shift begins to move more towards that of the bound acetonitrile which, although a small proportion of the total acetonitrile, may be assumed to be enormously contact shifted downfield. At coalescence the observed shift is at the weighted average (P_M) of the free and bound shifts. This position corresponds to the maximum of both plots in figure 6.3 and the temperature of these maxima should be, and are, the same as the maxima in the linewidth plots of figure 6.2. After coalescence the observed shift remains at the weighted average of free and bound acetonitrile shifts, and, since the bound shift follows a Curie law temperature dependence, so does the weighted averaged shift.

Using the shift data from figure 6.3 and the approximation of eq.4 the temperature range studied for complex 6.1a was extended to 70° and the data sets for both regions I and II gives values of $\Delta H^{\ddagger}$ in good agreement (Table 6.2), although $\Delta S^{\ddagger}$ is found to become more negative in data taken from region II. This discrepancy in $\Delta S^{\ddagger}$ may be due to the nature of the approximations inherent in equation (4) which would be expected to lead to larger systematic errors in the absolute values of τ_M^{-1} ($\propto \Delta S^{\ddagger}$), but not so large in their relative values ($\propto \Delta H^{\ddagger}$). It must also be noted that $\Delta H^{\ddagger}$ values quoted in Table 6.2. contain no correction for any contribution of second and further removed spheres of the complex ion to the exchange activation energy (sufficiently low temperatures to make this correction feasible were prohibited by solvent freezing). This contribution has been the subject of a certain

degree of controversy, earlier workers[233] on $[Ni(CH_3CN)_6]^{2+}$ have suggested that the increasing linewidth at very low temperatures, after the inner-sphere solvent exchange rate has been frozen out, is due to the very rapid exchange of second, non-co-ordinated, solvents in the outer sphere of the complex ion with bulk solvent. This 'outer-sphere' contribution to the activation energy was found to be of the order of 6kJ mol^{-1} for nickel(II). However, when an internal reference is used for the natural linewidth there would seem to be no reason why the reference molecules should not enter the 'outer-sphere' as well as solvent, and so experience the same broadening. If this is true then this should internally compensate for any second co-ordination sphere effect, but leaves the problem of determining what is, in fact, causing the observed linewidth increase at very low temperatures. Richards et al[234] have attempted to explain this phenomenon by the extraordinary interpretation (from their detailed study of the $[Ni(CH_3CN)_6]^{2+}$ system) that the six co-ordinated acetonitrile molecules may be divided into two distinct groups. Four solvents in-plane and the remaining two trans solvents are postulated as exchanging with bulk solvents at very different rates, the four in-plane being slower and responsible for the previously observed linewidth profile whereas the two axial solvents exchange very much faster. It is the beginnings of this second kinetic process which was interpreted as being responsible for the previously labelled 'outer-sphere' effect. It is the author's feeling that in the present study 'outer-sphere' effects of whatever nature are not an important contribution to the activation energy.

It is worthy of mention that the nitrile carbon nucleus was chosen for two reasons. Firstly, of the possible choices of nuclei on the available spectrometer (^1H or ^{13}C), this nucleus, being closest to the

paramagnetic nickel centre, is most sensitive to the contact broadening produced by this ion. Secondly, it is the only nucleus which shows the complete linewidth profile expected in such cases (figures 6.2 and 6.3) for the temperature range accessible in this solvent system. This latter criterion is essential in order to establish the various regions to which approximate equations (3) and (4) apply[229]. Of course one would predict that the nitrogen nucleus of the acetonitrile (being even closer to the paramagnetic centre when co-ordinated) would show an even more pronounced linewidth profile, and several studies have used ^{14}N n.m.r. to good effect despite the quadrupolar nature of this nucleus[234]. Ideally, ^{15}N n.m.r. would be the perfect nucleus for such a study since it has nuclear spin = $\frac{1}{2}$ and therefore sharp n.m.r. resonances, but the very low sensitivity and natural abundance of this isotope have so far prevented its use.

As a feasibility study into future utilisation of ^{15}N n.m.r. for the extraction of kinetic data, the first ever ^{15}N n.m.r. line-broadening study was attempted for the trans-I isomer in acetonitrile (using a WH180 at P.C.M.U. Harwell). Although problems of (i) temperature control and homogeneity in a 25mm sample, (ii) natural linewidth references and (iii) actual linewidth measurements have all yet to be completely solved, the preliminary results obtained at six temperatures, plotted in figure 6.4, are extremely encouraging. These ^{15}N are seen to agree qualitatively with the ^{13}C data in region I, as would be predicted by theory, and this nucleus has the big advantage over ^{13}C that the usable temperature range of kinetic data is extended to nearly 45^{o}.

Returning, however, to the ^{13}C n.m.r. data, activation parameters

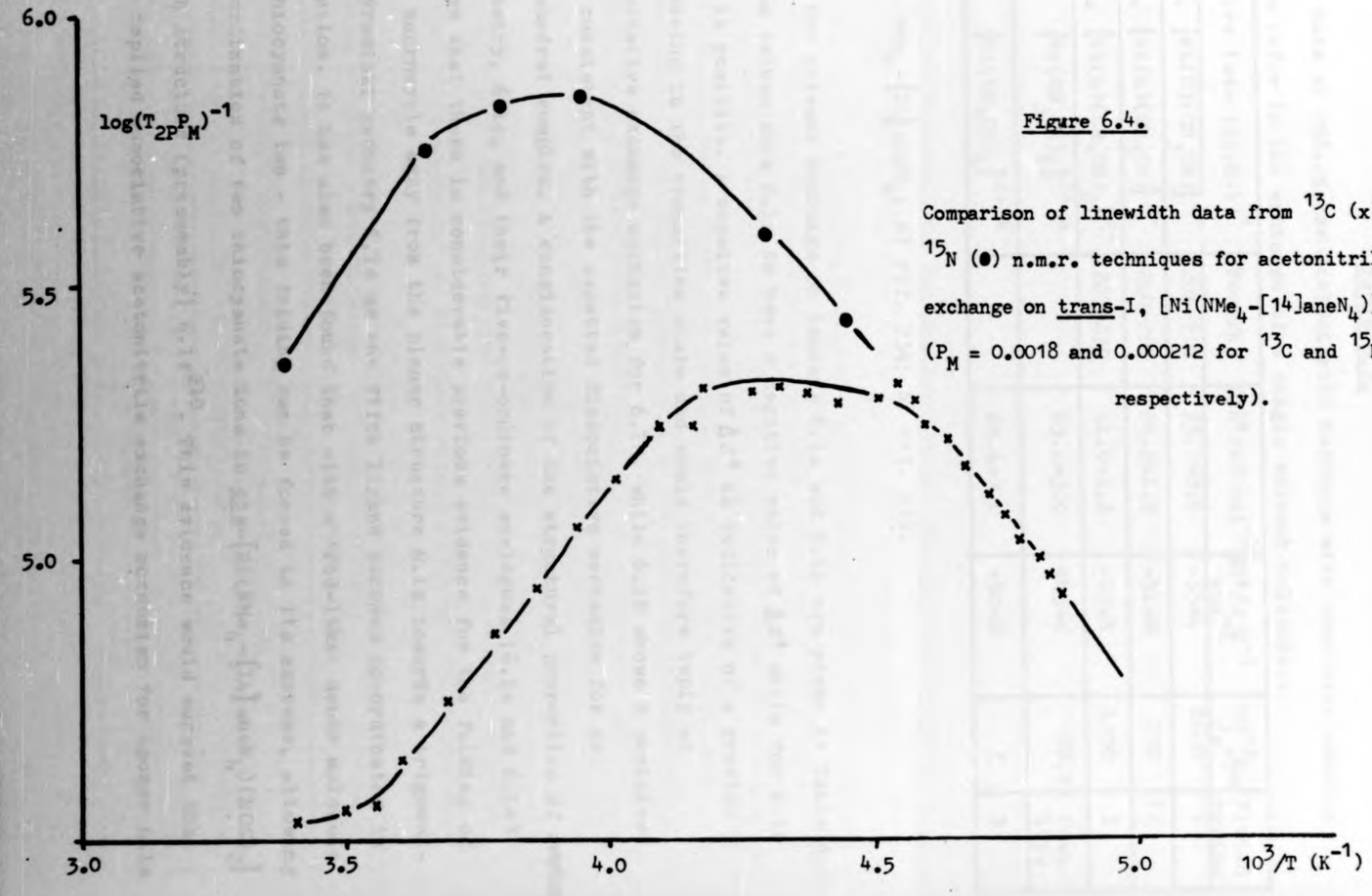

Figure 6.4.

Comparison of linewidth data from ^{13}C (x) and ^{15}N (●) n.m.r. techniques for acetonitrile exchange on trans-I, $[Ni(NMe_4\text{-}[14]aneN_4)](ClO_4)_2$ (P_M = 0.0018 and 0.000212 for ^{13}C and ^{15}N respectively).

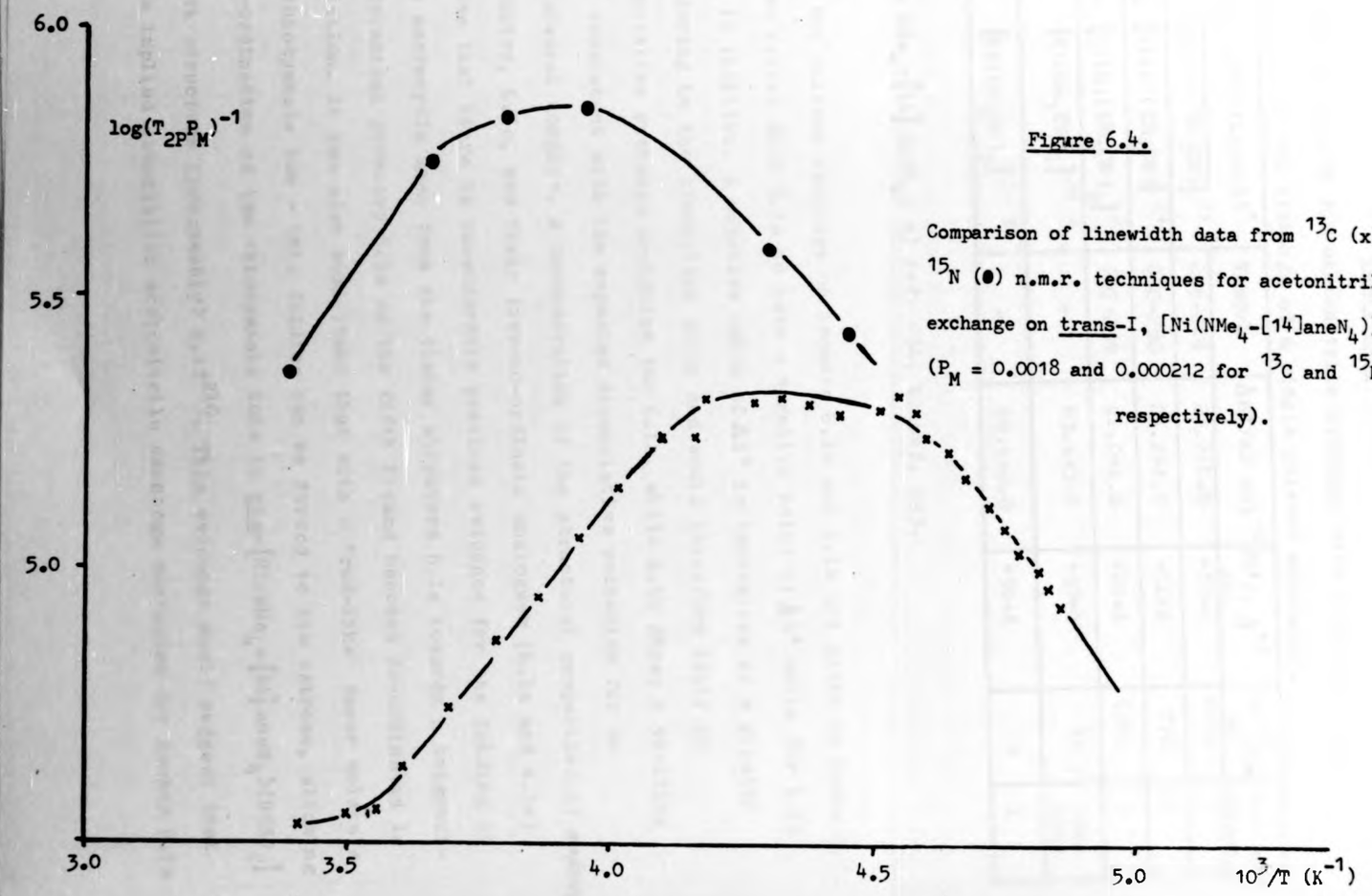

Figure 6.4.

Comparison of linewidth data from ^{13}C (x) and ^{15}N (●) n.m.r. techniques for acetonitrile exchange on trans-I, $[Ni(NMe_4\text{-}[14]aneN_4)](ClO_4)_2$ (P_M = 0.0018 and 0.000212 for ^{13}C and ^{15}N respectively).

Table 6.2.

Rate data at 298.2K for acetonitrile exchange with complexes studied (data refer to the exchange of a single solvent molecule).

Complex (see fig.6.1)*	Temp/K	$\Delta H^{\ddagger}$/kJ mol^{-1}	$\Delta S^{\ddagger}$/J K^{-1} mol^{-1}	$10^{-3} k_{ex}$ /s^{-1}	Fitted region
6.1a, $[Ni(L)(CH_3CN)]^{2+}$	206-218	23.2±0.8	-35±4	8400	I
6.1a, $[Ni(L)(CH_3CN)]^{2+}$	240-280	24.2±1.5	-51±8	770	II
6.1b, $[Ni(L)(CH_3CN)_2]^{2+}$	207-239	41.0±1.8	+22±8	6200	I
$[Ni(CH_3CN)_6]^{2+}$ a	-	63.4±3.0	+45±4	10.7	Complete
$[Ni(CH_3CN)_6]^{2+}$ b	-	68.4±2.0	+50±8	2	I

*L = NMe_4-[14]aneN$_4$; a) ref. 234; b) ref. 235.

for the solvent exchange on isomers 6.1a and 6.1b are given in Table 6.2. These values show 6.1a to have a negative value of $\Delta S^{\ddagger}$ while for 6.1b $\Delta S^{\ddagger}$ is positive. A negative value of $\Delta S^{\ddagger}$ is indicative of a greater ordering in the transition state and would therefore imply an associative exchange mechanism for 6.1a, while 6.1b shows a positive $\Delta S^{\ddagger}$ consistent with the expected dissociative mechanism for an octahedral complex. A consideration of the structural properties of complexes of geometry, 6.1c, and their five-co-ordinate analogues (6.1a and 6.1e) shows that there is considerable previous evidence for the folding of the macrocycle away from the planar structure 6.1e towards a trigonal-bipyramidal geometry 6.1a as the fifth ligand becomes co-ordinated in solution. It has also been found that with a 'rod-like' donor molecule - thiocyanate ion - this folding can be forced to its extreme, allowing co-ordination of two thiocyanate ions in cis-[Ni(NMe_4-[14]aneN$_4$)(NCS)$_2$] with structure (presumably) 6.1f[210]. This evidence would suggest that the implied associative acetonitrile exchange mechanism for isomer 6.1a

may well proceed through a transition state with two solvent molecules co-ordinated in a cis-geometry similar to structure 6.1f. It seems, therefore, that the values of ΔS^* are consistent with an associative mechanism for solvent exchange on 6.1a and a dissociative mechanism for 6.1b. This proposed associative pathway has been observed recently for another high-spin five-co-ordinate nickel(II) complex[227].

Turning now to the enthalpy data, this shows 6.1a to undergo solvent exchange with a markedly lower activation energy than for 6.1b. This may be explained, in part, in terms of the crystal field activation energies (CFAEs) of the two exchange mechanisms postulated above. Table 6.3 lists the crystal field stabilisation energies (CFSEs) of the starting and assumed transition state geometries for each isomer and the corresponing CFAE of the exchange mechanism[236,237]. These clearly indicate that the five-co-ordinate complex 6.1a has a negative CFAE for exchange whereas complex 6.1b has a positive value, and therefore these calculated values mirror the order of the observed activation enthalpies, 6.1a < 6.1b.

Table 6.3.

Crystal field stabilisation energies (CFSEs) and activation energies (CFAEs) in Dq units for d^8 high-spin nickel(II) complexes (data from refs. 236,237).

Complex	Ground State Geometry /CFSE	Transition State Geometry/CFSE	CFAE
6.1a	trigonal bipyramidal -6.67	octahedral -12	-5.33
6.1e	square pyramidal -9.96	octahedral -12	-2.04
6.1b	octahedral -12	square pyramidal -9.96	+2.04
6.1b	octahedral -12	trigonal bipyramidal -6.67	+5.33

The values of $\Delta H^{\ddagger}$ and $\Delta S^{\ddagger}$ for both complexes conspire to produce rate constants at 298K which are almost identical, and which are in the range expected for acetonitrile exchange on a nickel(II) complex with an N_4 set of donor atoms (ie. accelerated over the hexakis-acetonitrile cation exchange rate by at least two orders of magnitude (Table 6.2)[238,9]) This latter result for 6.1a is inconsistent with data derived for the analogous cobalt(II) aquo complex mentioned above where the solvent exchange rate was unusually found to be slower than for the corresponding hexa-aquo complex[217], although the result is in agreement with that found by Lincoln and West for a five-co-ordinate cobalt(II) complex. In this work[240] a comparison of the two penta-co-ordinate complexes, $[Co(tren)(CH_3CN)]^{2+}$, i, and $[Co(Me_6tren)(CH_3CN)]^{2+}$, ii, shows a very marked difference in the rate of acetonitrile exchange. For i with the relatively unhindered ligand tren, the rate is of the expected order[238], ($k_{ex} > 2 \times 10^6 s^{-1}$ at 233K), the acetonitrile being labilised with respect to the $[Co(CH_3CN)_6]^{2+}$ ion. For ii, however, the increase of steric hindrance in going to hexamethylated tren as the ligand markedly reduces the solvent exchange rate ($k_{ex} < 10^2 s^{-1}$ at 353K). The explanation given for these remarkable results is that the addition of the six methyl groups in ii so hinders the remaining co-ordination site that solvent-assisted exchange is severely limited. These findings would suggest, therefore, that the trans-I cobalt(II) and nickel(II) complexes with NMe_4-[14]aneN_4 might differ significantly in their ability to allow any bulk solvent involvement in the exchange mechanism, and more precisely that the cobalt(II) aquo ion may not as easily expand its co-ordination sphere in the exchange transition state whereas the nickel(II) acetonitrile complex may, as described above.

One elegant explanation of these results necessitates that the cobalt(II) complex contains a low-spin, d^7 cobalt ion. This assumption

has not been confirmed, but has precedent in that the cobalt(II) complex of the unmethylated macrocycle [14]aneN$_4$ is indeed low-spin d^7 [241] as are many other five-co-ordinate cobalt(II) tetraaza macrocycle complexes[242]. If one then considers the d-orbital energy-level diagrams for the two possible limiting five-co-ordinate geometries, trigonal-bipyramidal and square-pyramidal, in figure 6.5[200], for a low-spin d^7 metal ion, it is clear that the trigonal-bipyramidal geometry has an odd number of electrons (3) in the degenerate $d_{x^2-y^2}$, d_{xy} pair of orbitals. Such a situation is a classic case for a Jahn-Teller type distortion of the geometry (cf. octahedral copper(II), d^9). The Jahn-Teller effect will tend to remove the degeneracy of the orbitals containing the odd electron so that the overall energy of the system may be lowered. It is to be expected that the distortion removing the trigonal symmetry will be particularly large as the odd electron is in antibonding levels, where the splitting should be greater than that of non-bonding levels[243]. It is clear from figure 6.5 that the Jahn-Teller distortion required will produce an orbital energy-level diagram identical to that of the square-pyramid, and therefore this effect will tend to constrain any low-spin d^7 five-co-ordinate cobalt complexes to have square-pyramidal geometry. This effect has been well documented previously[200] and there are no known low-spin d^7 trigonal-bipyramidal structures; even complexes with tripod ligands distort towards a square-pyramid[244].

Applying these considerations to the complexes of cobalt(II) (d^7) and nickel(II) (d^8), although both are subject to Jahn-Teller distortions towards a square-pyramid, this distortion is far more rigorously applied to low-spin cobalt(II)[200] (spin-orbit coupling often overrides the Jahn-Teller effect for nickel(II)). In this case, the postulated

Figure 6.5.

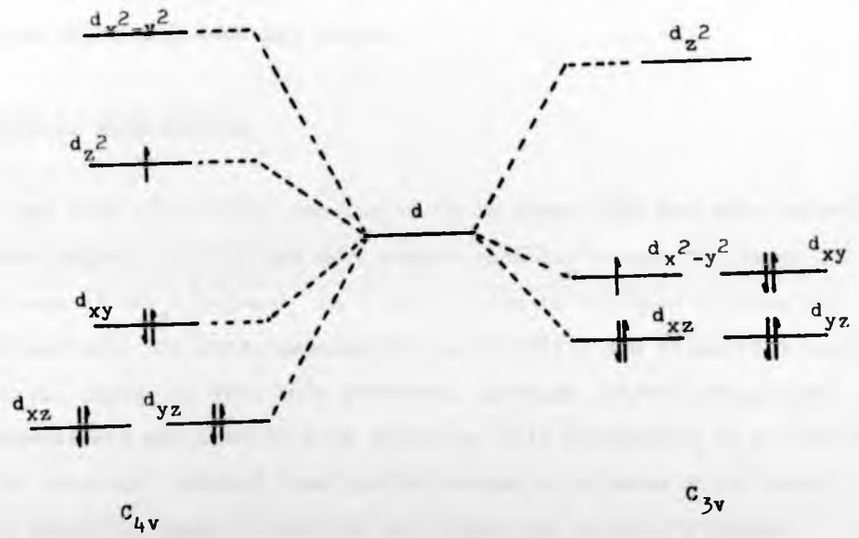

d orbital energy level splitting diagrams for a metal ion in a square-pyramidal (C_{4v}) or a trigonal-bipyramidal (C_{3v}) field. Electrons are placed in the levels for the low-spin cobalt(II), d^7 ion.

solvent exchange mechanism for such complexes, via a folded cis-complex (above), would be expected to proceed more readily for the nickel(II) complex, which may already be partially folded, than for the cobalt(II) complex which may well have a more rigid square-pyramidal geometry. Such an interpretation is seen to be in accord with the observed differences in solvent exchange rates.

SECTION 7. CONCLUSIONS.

The most significant conclusion to be drawn from the work described in this chapter is that the most common geometry adopted by metal complexes of NMe_4-[14]aneN_4 is five-co-ordinate trigonal-bipyramidal. Complexes with zinc(II), cadmium(II), mercury(II) and nickel(II) ions would all appear to have this geometry, although dynamic Berry-type rearrangements are occurring in solution. This conclusion is in contrast to the structure deduced from crystallographic evidence which invariably indicates square-pyramidal co-ordination. Square-pyramidal co-ordination is however postulated for the cobalt(II) aquo complex (which, if low-spin, is subject to Jahn-Teller distortion towards this geometry) and for the lead(II) complex because of the large metal ion radius.

The trans-I conformation, exclusively adopted by the complexes of this macrocycle made by simple combination of the free ligand with the metal ion, would be predicted to be ideal for the complexation of heavy metal ions such as methylmercury(II) and subsequent extraction of such ions from in vivo binding sites. However, the work reported with the lead(II) complex (section 4) also indicates that the trans-I geometry is not capable of forming the very strong complexes with

larger metal ions required in order to compete with *in vivo* binding sites. Conclusions from the work as a whole are included in Chapter 5.

SECTION 8. EXPERIMENTAL.

For a detailed discussion of individual techniques employed in this and previous chapters see Chapter 6.

INSTRUMENTATION.

See Chapter 3, section 8.

CHEMICALS AND SOLVENTS.

See Chapter 2, section 6.

SECTION 8.1. 1,4,8,11-tetramethyl-1,4,8,11-tetraazacyclotetradecane, NMe_4-[14]$aneN_4$.

The macrocycle was prepared following published procedures[210] using the parent, unmethylated macrocycle [14]$aneN_4$ as a starting reagent (see Chapter 3, section 8.1). A solution of 2.3g of [14]$aneN_4$ dissolved in 12cm^3 of formic acid (100%), 10cm^3 of formaldehyde (40%) and 1.3cm^3 of water was refluxed for 28 hours. The solution was transferred to a 250cm^3 beaker containing 15cm^3 of water and cooled to 5°C in a ice-bath. A concentrated solution of sodium hydroxide (7.5g in 25cm^3 of water) was stirred into the solution which was kept in the ice-bath throughout. The solution was extracted with 5 x 25cm^3 portions of chloroform which were combined and dried over anhydrous sodium sulphate. Removal of the chloroform on a rotary evaporator left

a pale yellow oil which was distilled (120°C, 0.1mm) without water-cooled condensing, to give a clear, thick liquid which solidified as white needles. Yield 1.8g (60%).

Reported pK_a values[214] for the protonated macrocycle are 10.10, 9.35, 3.45, and 2.7. ^1H n.m.r. ($CDCl_3$, 303K ref. TMS) shows observed (reported[210]) δ = 1.64quintet (1.62q), 2.20s (2.16s), singlet and overlapping triplet 2.30 (2.30)ppm. Intra-red (nujol mull) shows no NH stretch. The mass spectrum shows a parent molecular ion at 256 and major peaks at m^+/e = 180, 106.

^{13}C n.m.r. spectra of the macrocycle in a variety of solvents are reported in Table 8.1.

Table 8.1.

^{13}C n.m.r. data for NMe_4-[14]aneN_4 in various solvents.

Solvent	Temp./K	Shift* δ/ppm.	Intensity Ratio
$[^2H]_6$-DMSO	300	53.89,52.81,42.83,24.29	2:2:2:1
$[^2H]_3$-nitro-methane	320	54.85,54.00,42.55,23.48	2:2:2:1

*Reference dioxan 67.26ppm.

SECTION 8.2. COMPLEXES OF ZINC(II).

The complexes $[Zn(NMe_4$-[14]ane$N_4)X]ClO_4$ were prepared by published methods[210] which may be generally summarised as follows.

5g (excess) of $Zn(ClO_4)_2.6H_2O$, A.R., was dissolved in 10cm^3 of water, and mixed with 10cm^3 of ethanol containing 2g of NMe_4-[14]aneN_4. The solution was stirred for an hour, filtered and evaporated to

dryness. The product was washed with chloroform and ice-cold ethanol, and dried in vacuo to yield 2.38g (59%) of the complex X = ClO_4, (A). Other complexes with X = Cl, Br, NCS, I were prepared by adding excess A.R. sodium X to a saturated aqueous solution of A. The complexes readily precipitated from cold water and could be recrystallised from water, washed with ethanol and ether and air-dried. Micro-analysis for the complex X = I gave: C, 30.4; H, 5.77; N, 10.26%. $C_{14}H_{32}N_4IZn$ ClO_4 requires: C, 30.7; H, 5.85; N, 10.23%. The purity of all other complexes was checked by ^1H and ^{13}C n.m.r. spectroscopy. ^{13}C n.m.r. data for the complexes are reported in text (Table 2.1). The infra-red spectrum of the thiocyanato complex was recorded as a nujol mull and showed: $\upsilon(CS)$ = 804cm^{-1} indicative of N-bound thiocyanate[220], $\upsilon(C\equiv N)$, 2365cm^{-1}, $\upsilon(ClO_4)$ = 1085, 620cm^{-1}.

Crystals of the complex $[Zn(NMe_4\text{-}[14]aneN_4)Cl](ClO_4)$ suitable for X-ray diffraction were prepared by slow evaporation of an acetone solution to give clear hexagonal crystals.

Crystal Data.- $ZnC_{14}H_{32}N_4Cl_2O_4$, M = 456.4, monoclinic, a = 8.230(2), b = 15.156(3), c = 8.569(2)Å, β = 108.64(2)°, U = 1012.9(4)Å^3, T = 18(2)°C Z = 2, D_m = 1.50(5)g cm^{-3}, D_c = 1.496g cm^{-3}, F(0,0,0) =480. Space group $P2_1/m$ or $P2_1$, the latter confirmed by structural analysis, (MoK_α) μ = 15.32cm^{-1}.

Data Collection.- A crystal of approximate dimensions 0.13x0.15x0.25mm bounded by {010}{110}{011}{323} (see Table 8.2) was examined on a Syntex $P2_1$ four-circle diffractometer. The unit cell dimensions and their e.s.d.'s were obtained by a least-squares fit to 15 strong reflections with MoK_α graphite monochromatised radiation (λ = 0.70926Å). Systematic absence 0,k,0 for k = 2n+1 indicated space group $P2_1$ or $P2_1/m$, and crystal morphology indicated that the acentric group was more likely.

Intensity data in the range $3 < 2\theta < 55^{o}$ was recorded by the θ-2θ scan technique and three check reflections were monitored every 100 measurements. A decay of approximately 10% in the intensities of these standards during data collection was corrected during data processing. 1923 reflections with $I \geq 3.0\sigma I$ were recorded and corrected for absorption by the method of Alcock (see Chapter 6) to give transmission factors in the range 0.59-0.82.

Structure Solution and Refinement.- The structure was solved by the heavy atom method using a three dimensional Patterson synthesis to locate the position of the zinc atom. The remaining non-hydrogenic atoms were located in subsequent electron density maps and all atoms were refined by minimising the function $\Sigma(|F_o| - |F_c|)^2$. Refinement by the least-squares method with all non-hydrogenic atoms anisotropic gave an R value of 0.041. Weighting analysis indicated unit weights were satisfactory. Scattering factors and anomalous dispersion factors[158] were used, and all computing was done with the XRAY76 programs on a Burroughs B6700 computer. Final atomic co-ordinates are in Table 8.3. Structure factors and temperature factors may be obtained as supplementary information from the appropriate publication. Bond lengths and angles are included in Tables 8.4a and 8.4b respectively.

SECTION 8.3. $[Cd(NMe_4\text{-}[14]aneN_4)](NO_3)_2$.

This complex is readily prepared by mixing 0.617g of $Cd(NO_3)_2.4H_2O$ with 0.512g of NMe_4-[14]$aneN_4$ in $10cm^3$ of dry methanol. Stirring and heating for 30mins followed by evaporation to dryness gave a hard white crystalline solid which may be recrystallised from acetone/methanol. Yield 0.97g (90%).

Analysis. Calcd. for $[Cd(NMe_4\text{-}[14]aneN_4)](NO_3)_2$: Cd, 22.8; C, 34.1;

Table 8.2.

Miller indices and origin-plane distances for the facial planes of the crystal of $[Zn(NMe_4\text{-}[14]aneN_4)Cl](ClO_4)$ used in X-ray analysis.

h	k	l	d/cm	h	k	l	d/cm
0	1	0	0.0078	0	1	-1	0.0326
0	-1	0	0.0059	0	-1	-1	0.0325
1	-1	0	0.0174	0	1	1	0.0097
-1	1	0	0.0170	-3	2	3	0.0126
0	-1	1	0.0083	3	2	-3	0.0339

Table 8.3.

Atomic co-ordinates ($x10^4$) with standard deviations in parentheses.

Atom	X	Y	Z
Zn	1300 (1)	2500	3681 (1)
Cl(1)	-132 (4)	1685 (2)	5033 (4)
Cl(2)	4222 (4)	4753 (2)	707 (4)
N(1)	3873(11)	2352 (7)	5276(12)
N(2)	2175(12)	1576 (7)	2118(12)
N(3)	9283(13)	2991 (7)	1507(12)
N(4)	1227(14)	3836 (6)	4619(14)
O(1)	5425(16)	4815 (9)	2344(14)
O(2)	7219(16)	252(11)	9382(22)
O(3)	5018(26)	-41(15)	407(18)
O(4)	3694(19)	3864 (8)	486(19)
C(1)	4649(19)	1528(10)	4658(19)
C(2)	4134(17)	1559(10)	2873(17)
C(3)	1805(16)	1823 (9)	331(15)
C(4)	-9(18)	2047(10)	9452(17)
C(5)	9498(18)	2965(10)	-71(18)
C(6)	9279(20)	4014(11)	1834(20)
C(7)	9597(24)	4200(13)	3455(24)
C(8)	2752(17)	4368 (9)	4704(16)
C(9)	4475(16)	3985 (9)	5880(15)
C(10)	5051(16)	3148 (8)	5213(16)
C(11)	4166(18)	2134 (9)	7040(17)
C(22)	1473(17)	693(10)	2186(15)
C(33)	-2344(14)	2685 (7)	1427(13)
C(44)	1005(18)	3838(10)	6285(17)

Table 8.4a.

Bond lengths in Å with standard deviations in parentheses for

$[Zn(NMe_4\text{-}[14]aneN_4)Cl](ClO_4)$

Bond	Length/Å	Bond	Length/Å
Zn-Cl(1)	2.265 (4)	N(3)-C(5)	1.42(2)
Zn-N(1)	2.199 (8)	N(3)-C(6)	1.57(2)
Zn-N(2)	2.211(11)	N(3)-C(6)	1.40(2)
Zn-N(3)	2.192 (9)	N(4)-C(7)	1.50(2)
Zn-N(4)	2.186(10)	N(4)-C(8)	1.47(2)
N(1)-C(1)	1.53(2)	N(4)-C(44)	1.50(2)
N(1)-C(10)	1.51(2)	C(1)-C(2)	1.45(2)
N(1)-C(11)	1.50(2)	C(3)-C(4)	1.48(2)
N(2)-C(2)	1.53(2)	C(4)-C(5)	1.54(2)
N(2)-C(3)	1.51(2)	C(6)-C(7)	1.36(3)
N(2)-C(22)	1.47(2)	C(8)-C(9)	1.57(2)
		C(9)-C(10)	1.53(2)

Table 8.4b.

Bond angles in degrees with standard deviations in parentheses.

Angle	°	Angle	°
Cl(1)-Zn-N(1)	102.0(3)	Zn-N(1)-C(10)	112.3(7)
Cl(1)-Zn-N(2)	106.7(3)	Zn-N(1)-C(11)	114.2(8)
Cl(1)-Zn-N(3)	104.1(3)	C(1)-N(1)-C(10)	111(1)
Cl(1)-Zn-N(4)	103.7(4)	C(1)-N(1)-C(11)	104(1)
N(1)-Zn-N(2)	81.8(4)	C(10)-N(1)-C(11)	110(1)
N(1)-Zn-N(3)	153.9(4)	Zn-N(2)-C(2)	104.9(7)
N(1)-Zn-N(4)	90.3(4)	Zn-N(2)-C(3)	117.3(7)
N(2)-Zn-N(3)	90.3(4)	Zn-N(2)-C(22)	110.2(9)
N(2)-Zn-N(4)	150.0(4)	C(2)-N(2)-C(3)	106(1)
N(3)-Zn-N(4)	84.0(4)	C(2)-N(2)-C(22)	110(1)
Zn-N(1)-C(1)	105.7(7)	C(3)-N(2)-C(22)	108(1)

Table 8.4b. cont.

Angle	°	Angle	°
Zn-N(3)-C(5)	120.6(8)	C(8)-N(4)-C(44)	108(1)
Zn-N(3)-C(6)	103.1(7)	N(1)-C(1)-C(2)	109(1)
Zn-N(3)-C(33)	112.5(8)	N(2)-C(2)-C(1)	111(1)
C(5)-N(3)-C(6)	102(1)	N(2)-C(3)-C(4)	115(1)
C(5)-N(3)-C(33)	111(1)	C(3)-C(4)-C(5)	112(1)
C(6)-N(3)-C(33)	106(1)	C(4)-C(5)-N(3)	114(1)
Zn-N(4)-C(7)	102.7(9)	N(3)-C(6)-C(7)	112(1)
Zn-N(4)-C(8)	113.7(9)	C(6)-C(7)-N(4)	116(2)
Zn-N(4)-C(44)	112.3(8)	N(4)-C(8)-C(9)	114(1)
C(7)-N(4)-C(8)	113(1)	C(8)-C(9)-C(10)	113(1)
C(7)-N(4)-C(44)	106(1)	C(9)-C(10)-N(1)	113(1)

H, 6.50; N, 17.1%. Found: Cd, 22.7; C,33.4; H, 6.31; N, 16.6%.

Infra-red in CsI windows (nujol mull) shows: $\upsilon(NO_3)$ = 1480(υ_4), 1280(υ_1), 1020(υ_2), 747(υ_3), 819(υ_6) of monodentate nitrate ion[157], also free nitrate ion[220] 829(υ_2)cm^{-1}. ^{13}C n.m.r. data are reported in text.

SECTION 8.4. $[Hg(NMe_4\text{-}[14]aneN_4)Cl]Cl$.

This complex is prepared by mixing methanolic solutions of A.R. $HgCl_2$ (0.54g in $5cm^3$) and NMe_4-[14]$aneN_4$ (0.51g in $2cm^3$). After a brief induction period crystals of the complex begin to form and may be hastened by the addition of ether. The white powder may be recrystallised from nitromethane as clear crystals, yield 0.72g (70%).

Infra-red in CsI windows (nujol mull) shows: $\upsilon(HgCl)$ = 250cm^{-1}. ^{13}C n.m.r. data are reported in text.

SECTION 8.5. $[Pb(NMe_4\text{-}[14]aneN_4)](NO_3)_2$.

0.512g of solid NMe_4-[14]$aneN_4$ are added to a dried DMSO solution of A.R. $Pb(NO_3)_2$ (0.663g in $5cm^3$). The solution is stirred for 30mins and the DMSO is removed by vacuum distillation at room temperature. The white complex is unstable to solvents in which one or other of the components ($Pb(NO_3)_2$ and NMe_4-[14]$aneN_4$) are soluble, except DMSO into which the complex will dissolve with partial dissociation (see section 4). Metal analyses show; Calcd for $[Pb(NMe_4\text{-}[14]aneN_4)](NO_3)_2$: Pb, 35.3%. Found: Pb, 35.8%. ^{13}C n.m.r. data are reported in text.

SECTION 8.6. COMPLEXES WITH NICKEL(II).

The two isomers of $[Ni(NMe_4\text{-}[14]aneN_4)](ClO_4)_2$, trans-I and trans-III

figure 5.1, were prepared by standard procedures[210,223].

The purity of each isomer was checked by nickel elemental analysis Calcd: Ni, 11.42%. Found: trans-I, Ni, 11.43% and trans-III, Ni, 11.20%. The visible spectroscopic data for the isomers in nitromethane are reported in Table 6.1 and also indicate the complexes to be pure isomers. The ^{13}C n.m.r. data for both complexes saturated in $[^2H]_3$-nitromethane are reorted in text.

Solutions for the thermodynamic study, by variable temperature visible spectroscopy, of the diamagnetic/paramagnetic equilibrium in H_2Owere 0.0112 mol dm^{-3} (trans-I) and 0.0154 mol dm^{-3} (trans-III) both made up to ionic strength 0.2 with oven dried (110°C) A.R. $NaClO_4$. Variable temperature spectra were run in the range 294-348K in the thermostated compartment of a Unicam SP800 spectrophotometer. Temperatures were held ± 0.1°C during the recording of spectra and were measured with a mercury thermometer to ±0.1°C.

Solutions for the parallel paramagnetic susceptiblity study using the method of Evans[188] were 0.051 mol dm^{-3} (trans-I) and 0.057 mol dm^{-3} (trans-III), and the ionic strength was again adjusted with dry $NaClO_4$. The inert reference was t-butanol, which was present at ca. 0.05 mol dm^{-3} in the bulk solutions and was ca. 0.5 mol dm^{-3} in the coaxial capillary (for details of the technique see Chapter 6). Shift separations obtained were in the ranges 6 - 17Hz (trans-I) and 2 - 24Hz. (trans-III) and were measured ±0.01Hz, with temperatures held at ±0.5°C by a Bruker temperature control unit and measured externally with a Comark thermocouple. Susceptibilities derived were all treated to correction for the diamagnetic contribution with Pascal's constants (Chapter 6).

pH titrations in aqueous solution were performed on 0.0112 mol dm^{-3}

(trans-I) and 0.0154 mol dm^{-3} (trans-III) solutions of ionic strengths 1.04 and 1.06 respectively (dry KNO_3). The pH was adjusted with a 5 mol dm^{-3} solution of KOH the remaining procedure being identical to that described in Chapter 3 section 8.3.

The acetonitrile complexes of the two isomers were produced by simple dissolution of the square-planar complexes in acetonitrile. Spectral data for these solvento complexes are reported in Table 6.1. and indicate five-co-ordinate (trans-I) and octahedral (trans-III) geometries for the two complexes. The solvento complexes were characterised as crystalline solids (from evaporation of conc. acetonitrile solutions) by elemental analyses;

trans-I, Calcd. for $[Ni(NMe_4\text{-}[14]aneN_4)(CH_3CN)](ClO_4)_2$; Ni, 10.58; C, 34.6; H, 6.31; N, 12.6%. Found: Ni, 10.34; C, 33.8; H, 6.0; N, 12.2%.

trans-III, Calcd. for $[Ni(NMe_4\text{-}[14]aneN_4)(CH_3CN)_2](ClO_4)_2$: Ni, 9.85; C, 36.3; H, 6.38; N, 14.1%. Found: Ni, 9.22; C, 35.8; H, 6.0; N, 14.1%.

Again the analyses of the solvento complexes are very difficult to achieve accurately since the inherent instability of the co-ordinated solvents prevents any purification procedures such as vacuum drying of the solids .

The infra-red spectra of the two solvento adducts (nujol mull, CsI) show: $\upsilon(C\equiv N)$ = 2310cm^{-1}(trans-I), 2304cm^{-1}(trans-III). (cf. free acetonitrile $\upsilon(CN)$ = 2295cm^{-1})

For ^{13}C n.m.r. solvent exchange kinetics solutions of trans-I and trans-III isomers (trans-I, molality = 0.04390, 0.03171mol kg^{-1},

P_M = 0.0018, 0.0013; trans-III, molality = 0.0198 mol kg^{-1}, P_M = 0.0016) were made up in freshly distilled (from CaH_2) acetonitrile under an atmosphere of dry nitrogen. An n.m.r. lock signal of 10% $[^2H]_3$-nitromethane, and a shift and natural linewidth reference of 1,4-dioxan (ca. 5%) were added to the solutions. All ^{13}C n.m.r. spectra were recorded with a Bruker WH90 spectrometer at 22.63MHz. The sample temperature was measured internally with a calibrated Comark thermocouple and held constant ±0.5°C using a standard Bruker temperature control unit. Linewidth measurements (±0.5Hz) were carried out using an iterative line-fitting procedure[143] adapted for use with the on-line Nicolet 1080 computer, and fell in the range 5-140Hz. Good signal to noise ratios (≥100:1) for the broadened lines were obtained in 200-500 sweeps of 4000Hz.

A comparison of the measured dioxan reference linewidth in the presence and absence of the paramagnetic nickel(II) complexes showed no detectable broadening of this reference occurred in the paramagnetic samples. This allowed direct internal measurement of the natural linewidth in all samples. All shift data were recorded referenced to dioxan and normalised to the shift of acetonitrile in a solution containing all components save the paramagnetic ion.

The exploratory ^{15}N n.m.r. study was carried out on a solution of the trans-I isomer (P_M = 0.000212) made up as described above without dioxan, in 25cm^3 of solution. Spectra were recorded (undecoupled) with a Bruker WH180 spectrometer. The sample temperature was held constant ±1°C using a Bruker temperature control unit, but was measured internally. Linewidth measurements (±2Hz) were carried out by hand from plotted spectra and were in the range 25-50Hz for the temperature range observed

Good signal to noise ratios (>50:1) were obtained in 200-500 scans with a 25mm sample diameter. No internal reference, either linewidth or shift, was present and no correction for this width (estimated ~4Hz) was made to the data plotted in figure 6.4.

CHAPTER 5

CONCLUSIONS
AND
EXTENSIONS

The results of the work reported in this thesis have led to the following overall conclusions and suggestions for possible future extensions of this work:

1) Macrocyclic tetraaza ligands would appear to form very stable complexes with the toxic heavy metal ions, when the donors are secondary amines, since these allow the macrocycle to adopt its most thermodynamically stable structure (unlike tertiary amines). The 14-membered ring-size is found, however, to be too small to encompass these large metal ions, and therefore the hole-size parameter of this macrocycle is not being effectively employed in selection between metal ions. In order to improve this selection property the hole-size of the macrocycle should be increased to, say, a 16-membered ring, thereby allowing effective thermodynamically favourable planar co-ordination of the larger metal ions.

2) ^{15}N n.m.r. spectroscopy has been shown to be a valuable tool in the elucidation of both the structural (Chapter 3) and kinetic (Chapter 4) properties of the metal complexes of amine macrocycles. A detailed investigation of metal-nitrogen coupling constants in structurally well-established complexes would prove valuable for the interpretation of those obtained for the complexes studied here. In addition, ^{15}N n.m.r. spectroscopy has been shown to be a viable technique for the extraction of kinetic data for metal complexes by paramagnetic line-broadening, and this new aspect of its applications could be effectively explored in future work.

3) The paramagnetic exchange study in Chapter 4, section 6 has shown interesting differences not only between nickel(II) complexes of NMe_4-[14]aneN_4 with <u>trans</u>-I and <u>trans</u>-III geometries, but also between

The results of the work reported in this thesis have led to the following overall conclusions and suggestions for possible future extensions of this work:

1) Macrocyclic tetraaza ligands would appear to form very stable complexes with the toxic heavy metal ions, when the donors are secondary amines, since these allow the macrocycle to adopt its most thermodynamically stable structure (unlike tertiary amines). The 14-membered ring-size is found, however, to be too small to encompass these large metal ions, and therefore the hole-size parameter of this macrocycle is not being effectively employed in selection between metal ions. In order to improve this selection property the hole-size of the macrocycle should be increased to, say, a 16-membered ring, thereby allowing effective thermodynamically favourable planar co-ordination of the larger metal ions.

2) ^{15}N n.m.r. spectroscopy has been shown to be a valuable tool in the elucidation of both the structural (Chapter 3) and kinetic (Chapter 4) properties of the metal complexes of amine macrocycles. A detailed investigation of metal-nitrogen coupling constants in structurally well-established complexes would prove valuable for the interpretation of those obtained for the complexes studied here. In addition, ^{15}N n.m.r. spectroscopy has been shown to be a viable technique for the extraction of kinetic data for metal complexes by paramagnetic line-broadening, and this new aspect of its applications could be effectively explored in future work.

3) The paramagnetic exchange study in Chapter 4, section 6 has shown interesting differences not only between nickel(II) complexes of NMe_4-[14]aneN_4 with <u>trans</u>-I and <u>trans</u>-III geometries, but also between

the trans-I geometries of nickel(II) and cobalt(II). Further work to either confirm or modify the conclusions of that section regarding the occurrence of low-spin cobalt(II) is essential, and together with susceptibility measurements to establish spin-state, a study of the acetonitrile exchange rate for trans-I cobalt(II) would provide a very useful comparison. Such work is now under way by other workers in these laboratories.

4) It is very desirable to utilise all of the data obtained in paramagnetic exchange studies, such as that in Chapter 4, figure 6.2. This may be done by fitting all of the data points in such a figure to the complete theoretical equations of Swift and Connick [229,230] rather than to the approximate equations used in Chapter 4, section 6. Such a process requires a suitable computer program not yet available at Warwick University, but the data from Chapter 4, section 6 is in the process of being analysed by such a program in conjunction with Professor A.E. Merbach at the University of Lausanne. It is hoped that this program may be implemented at Warwick in the near future, but as yet no results for the data from Chapter 4, section 6 are available.

5) The solvent exchange work of Chapter 4, section 6 has prompted interest in the whole area of five-co-ordinate complexes formation and ligand exchange, and it would be interesting to study both solvent and anion exchange in such complexes by paramagnetic n.m.r. and their formation reactions from square-planar complexes by spectrophotometric techniques. Solvent exchange by n.m.r. has already been discussed, but extensions of the work may be to attempt paramagnetic ^{19}F n.m.r. fluoride anion exchange on the fluoro complex in order to compare the exchange mechanism with regard to the associative/dissociative question.

Spectrophotometric studies on the formation of the acetonitrile complexes and also the acido complexes require very rapid kinetic techniques not available at Warwick, but in conjunction with Doctor J.J. M^{c}Garvey, Queen's University, Belfast, such investigations are now under way using laser-photodissociation techniques.

6) Tetrathiaether macrocycles were shown in Chapter 2 to form relatively unstable complexes with labile metal ions such that their increased selectivity towards the soft metal ions is offset by these low stability constants. In devising a chemotherapeutic macrocycle it would therefore be desirable to combine the selectivity of a 16-membered tetrathiaether macrocycle with the high stability and rigid endo-stereochemistry conferred by amine macrocycles. Such a situation may possibly be achieved by a 'compromise' macrocycle containing a mixture of thiaether and amine donors.

7) The trans-I stereochemistry adopted by the tertiary amine macrocycle NMe_4-[14]aneN_4 discussed in the previous chapter is found to have a desirable complexing property in relation to heavy metal ions, such as methylmercury(II) (above). The ability of this geometry to enforce penta-co-ordination upon the metal ion should be explored further, especially with methylmercury(II), since such a geometry, which prevents residual (octahedral) binding of the ion to the in vivo binding site (thiol) may possibly be pharmaceutically important in the chelation therapy treatment of heavy metal poisoning.

8) In relation to the previous point, one interesting extension to the present work would involve the study of macrocycles with a 'dangling-arm' having a terminal functional group. Such macrocycles

were briefly discussed in Chapter 1[87] and Kaden has recently devised synthetic routes to 14-membered saturated tetraaza macrocycles of this type[84]. These macrocycles have the advantage over trans-I forms of quadridentate macrocycles that whereas both effectively occupy five co-ordination sites on the metal ion the 'capped' macrocycles would be expected to form much more stable complexes since the metal ion may sit in the macrocycle plane, which in turn may adopt a more thermodynamically stable trans-III geometry.

9) The availability, at Warwick, of facilities for the application of the rapid stopped-flow kinetic technique to ^{1}H n.m.r. spectroscopy may be used to study macrocycle complex formation with the aluminium ion. Previous studies by Moore et al in these laboratories on the formation reactions of amine chelates with the hexakis-(DMSO) aluminium(III) ionhave proven the value of the technique in elucidating the mechanistic course of the complexation reaction. If this work were to be extended to the macrocycle tetraamine field it would be expected to elucidate the somewhat hazy area of macrocycle complexation, a field which has been the subject of considerable effort and speculation[30,169,171,173,214,216,245]. Preliminary studies of the reaction with aluminium(III) during the course of this work indicate that the proposed study is feasible, and this whole aspect of the steric and geometric factors involved in complex formation is likely to be of relevance to the theme of this thesis.

In conclusion, the results of the work discussed in this thesis indicate that macrocycle amine ligands are a possible chemical answer to the problem of heavy metal ion toxicology, which deserve further investigation and refinement to produce a biologically viable chemo-

therapeutic chelate. Work in relation to their toxicology and chemical specificity is needed before any conclusions in the biological area may be reached. Chemically, the high stability constants of their complexes, their rigidly endo-conformations with the related possibility of tailoring hole-size to ion-size, and the kinetic inertness of their complexes, make such macrocycles attractive for further consideration in this respect.

CHAPTER 6

EXPERIMENTAL TECHNIQUES.

SECTION 1. FOURIER TRANSFORM N.M.R. SPECTROSCOPY - BASIC CONCEPTS.

In pulsed n.m.r. experiments, the resonance condition is achieved by a broadband excitation of the nuclear spin system with radio frequency pulses. Following switch off of the excitation pulse, one observes in the time domain, a nuclear induction signal representing all the frequencies present within the excited spectrum.(e.g. several narrow lines, a few broad lines or a single extremely broad line). A 90^{o} pulse rotates the net macroscopic magnetisation away from the Zeeman field direction (z axis) through 90^{o} into the observation plane (xy plane). A 180^{o} pulse inverts the direction of the magnetisation vector. The decaying spin system gives rise to an exponential signal (free induction decay, f.i.d.) which may be Fourier transformed to conver the time domain information to the conventional frequency domain of normal n.m.r. spectra.

This pulsed or free precession approach was pioneered theoretically by Torrey[246], and is inherently more efficient than field or frequency sweep experiments (with regard to information content) as all the nuclei are simultaneously and not sequentially observed. The efficiency and rapidity with which data may be accumulated make this technique ideal for signal averaging experiments which are essential for nuclei of low sensitivity or low natural abundance e.g. ^{13}C, ^{15}N.

Some properties of F.T. n.m.r. signals include:

1) Lineshape.- The shape of the f.i.d. in the time domain is just the fourier transform of the n.m.r. line in the frequency domain. It follows that an exponentially decaying f.i.d. will generate a Lorentzian n.m.r. line in the frequency domain.

2) Spin-lattice relaxation, T_1.- Following r.f. excitation, the nuclear spin system returns to thermal equilibrium with its surroundings, symbolically known as the'lattice', by means of a relaxation mechanism designated T_1. In general this relaxation process arises through an exchange of energy between the spin system and the lattice by means of fluctuating magnetic fields at a nuclear site. These relaxation interactions (e.g. magnetic dipolar, electric quadrupolar, spin rotation, scalar couplings etc.) are characterised by a molecular correlation time, which may be related to T_1, and as a practical consideration may limit the pulsing rate in order to prevent spin saturation effects due to incomplete relaxation between pulses.

3) Spin-spin relaxation, T_2.- Following partial or complete rotation of the magnetisation vector into a plane perpendicular to the field direction, the transverse component will decay in time to zero through a relaxation process arising from couplings between the nuclear spins. This process is known as spin-spin relaxation and is characterised by a relaxation time T_2 ($T_2 \leq T_1$). T_2 is proportional to the reciprocal value of the linewidth at half maximum intensity $\Delta\upsilon_{\frac{1}{2}}$. For a Lorentzian line, $T_2 = 1/\pi\Delta\upsilon_{\frac{1}{2}}$. In Chapter 4, section 6, it is T_2 which has been established in order to evaluate paramagnetic exchange rates and it is generally true that T_2 is directly related to the rate of any dynamic exchange process such as those discussed throughout this thesis. In section 3 below, line-fitting procedures for establishing T_2, and thence the exchange rate, are discussed.

4) Nuclear Overhauser Effect,- NOE.- The T_1 relaxation mechanism involves an exchange of energy between a nuclear spin system and the degrees of freedom of motion of the whole system (lattice) which gives rise to the relaxation field. Energy transfer is slow

and the relaxation times of the spin ½ nuclei are usually long. If, however, one group of nuclei is saturated, using a double irradiation transmitter, the nuclear populations are grossly perturbed. The relaxation field then attempts to return the populations to equilibriu and in so doing absorbs much more energy than is normal from the irradiated nuclei. If other nuclei lie close in space to these irradiated nuclei then there is a chance that they will individually absorb some of this energy and undergo nuclear transitions which will alter the populations of their spin states also. A change in their resonance intensity is observed and the phenomenon is known as the Overhauser effect. It occurs in all double resonance experiments and is especially important for spectra obtained under ^{1}H-decoupled conditions where the protons in the molecule are strongly irradiated to remove their coupling so as to simplify the spectra and intensify the resonances. For ^{13}C nuclei the Overhauser effect can lead to an additional increase in intensity of about 3, carbons not carrying hydrogen are not affected (to a first approximation) and give rise to weaker lines. The intensity data, useful for counting carbons, are then no longer reliable in such spectra.

Practical considerations in the accumulation of F.T. n.m.r. spectra may be summarised in terms of the nuclei studied in this work:

a) ^{1}H.- For routine diamagnetic samples, spectra were studied on $0.5cm^3$ of solution in 0.5cm diameter spinning sample tubes at 90MHz. Samples were generally at least 0.05 mol dm^{-3} in a deuterated field-lock solvent and spectra were generally observed (for a sweep width of 1200Hz.) in 10-100 scans. A 90° pulse was usually applied to give an 8k data point f.i.d. except where saturation effects were evident when the pulse angle was reduced. All accumulation control, fourier

transformations and subsequent data handling was performed with a dedicated Nicolet 1080 computer equipped with the DISKFT program written by D.A. Couch[247]. Peak positions were referenced to an internal standard and listed using a cursor peak-picking routine incorporated in the DISKFT program (accuracy dependent on scanned sweep width and therefore Hz/cursor point in transformed spectrum)

With paramagnetic nickel(II) samples the proton sweep width capability of the spectrometer in the direct recording mode is limited to ca. 15,000Hz.(170ppm) and so in order to record spectra having peaks in the range 100-400ppm (see Chapter 4 section 5) it was necessary to set a pulse offset frequency of OHz. and effectively record everything backwards, or rolled around, from there. With this technique, spectra, effectively reversed, could be obtained in the 0-400ppm range although the phasing routines could not produce a perfectly flat baseline in such cases.

b) ^{13}C.- Spectra were recorded at 22.63MHz. on ca. 1.5cm^3 of sample in a 10mm n.m.r. tube equipped with a teflon plug to prevent vortexing in the spinning solution. Samples were generally of concentration in the range 0.1 - 1.0 mol dm^{-3} in deuterated field-lock solvents, usually being as concentrated as possible in order to minimise accumulation time. Acceptable spectra (signal:noise >10:1) were obtained in 200-80,000 scans depending on concentration and decoupling mode. Spectra were almost always run with full ^1H-noise decoupling by saturating the frequency of the sample protons (3400Hz) so as to remove their couplings to the ^{13}C nuclei. The positive NOE ((4) above) for the ^{13}C nucleus leads to a maximum enhancement in the signal height of ca. 2.9 due to this ^1H-decoupling. Minimum sweep widths to include all resonances in the spectrum were generally

applied (typically 1500Hz. for the macrocycles employed here) so as to provide optimum resolution and accurate peak-shift information. A 90° pulse was applied wherever possible to the minimum number of data points which bounded the observable f.i.d. (typically 4k data points for 1500Hz. sweep width) DISKFT routines[247] were again applied to data accumulation and handling.

c) ^{15}N.- Spectra were recorded in conjunction with the P.C.M.U. Harwell at 18.24MHz, on approximately $15cm^3$ of sample in a 25mm (wide-bore) tube in the pole-gap of a superconducting magnet. The tube was fitted with a teflon or ceramic plug against vortexing and samples were at least 0.9 mol dm^{-3} in 10% of a deuterated field-lock solvent. ^{15}N, although a spin ½ nucleus with correspondingly sharp n.m.r. resonances, is 3 times less abundant than ^{13}C and is 10 times less sensitive for n.m.r. purposes. These properties make observation of this nucleus very difficult, hence the need for large, very concentrated samples and a supercon. magnet. In addition ^{15}N has a negative NOE (max.-4) which means that ^{1}H-decoupled spectra generally have negative peak intensities for nitrogen atoms which carry protons Unfortunately it may happen that if the NOE is ca. -1 then a 'null' peak may result ie. no signal due to its cancellation by the NOE. Typical values of T_1 are in the range $10-10^3$ seconds which mean that saturation of the ^{15}N resonances may occur unless a relaxing agent or long delays between pulses are used - this is especially true of nitrogen atoms which have no directly bound protons. Spectra in this thesis have only been obtained for secondary amines which carry a proton (complexes of [14]aneN$_4$) or for the nitrile resonance of acetonitrile in the presence of paramagnetic nickel(II) which acts as a relaxing agent (Chapter 4 section 6).

Acceptable spectra were obtained in 1000-20,000 scans (longer accumulation necessary to observe ^{1}J couplings) using a 90° pulse on 8k data points with a minimum sweep width (typically 1200Hz). Standard Bruker FTNMR data handling routines were applied on a Nicolet 1180 computer.

Many theoretical and practical discussions of the above phenomena and techniques have been produced and further details may be obtained from these sources[248].

SECTION 2. SUSCEPTIBILITY MEASUREMENTS BY THE EVANS N.M.R. METHOD.

Two n.m.r. related experimental techniques have been extensively employed during this work and will be discussed in this and the following section. The first is that due to Evans[188] who developed a technique for determining the paramagnetic susceptibility of substances in solution by n.m.r. spectroscopy. For an inert substance (reference) in solution, the shifts caused by paramagnetic ions are given by a theoretical expression[188]:

$$\Delta H/H = (2\pi/3)\Delta\chi$$

where $\Delta\chi$ is the change in volume susceptibility between the diamagnetic and paramagnetic solutions.

For the aqueous solutions of nickel complexes discussed in this thesis about 5% of t-butanol was used as the internal reference, and a coaxial capillary (Wilmad) containing 50% t-butanol was also placed in the 5mm n.m.r. tube. The tube was spun in the spectrometer and the sample was found to give rise to two resonances from the t-butanol methyl protons - one from the bulk paramagnetic solution and one from the capillary. The shift difference between these two resonances is

clearly related to the change in the volume susceptibility induced by the paramagnetic ion (above) and the corrected molar susceptibility of the dissolved substance, χ'_M, is given by the expression[188]:

$$\chi'_M = \frac{3.\Delta f.M}{2.\pi.f.m} + \chi_o.M + \frac{M.\chi_o.(d_o-d_s).10^3}{m} + DC. \quad (1)$$

Where $\frac{\Delta f}{f}$ = shift separation in ppm of the two resonances.

M = molecular weight of the complex.

m = mass of complex in $1cm^3$ of solution.

χ_o = mass susceptibility of the solvent (-0.72×10^{-6} for dil. t-butanol[188]).

d_o = density of the solvent.

d_s = density of the solution.

DC = diamagnetic correction for the complex using Pascal's constants[249] (DC = 274.7×10^{-6} for $[Ni(NMe_4\text{-}[14]aneN_4)](ClO_4)_2$ and 227.3×10^{-6} for $[Ni([14]aneN_4)](ClO_4)_2$ and were applied assuming no temperature independent paramagnetism.)

The density term (d_o-d_s) is often neglected without serious error[188] and values of χ'_M calculated from the equation may be related to the magnetic moment of the paramagnetic ion μ_{eff} by the equation:

$$\mu_{eff} = 2.84.(\chi'_M.T)^{\frac{1}{2}} \text{ Bohr Magnetons} \quad (2)$$

where T is the absolute temperature of the measurement. Clearly by assuming a value of μ_{eff} it is possible to work backwards through equations (2) and (1) to obtain a value of Δf_{calc}. From this value and that observed the percentage of paramagnetic ion in the solution may

be calculated ($= \Delta f_{obs}/\Delta f_{calc}$) which in turn may be used to evaluate the diamagnetic:paramagnetic equilibrium constant as in text.

SECTION 3. N.M.R. LINESHAPE FITTING AND EXCHANGE.

Considering the simple situation of two n.m.r. resonances undergoing site exchange, the lineshapes of the two resonances are described by the equations of Gutowsky and Holm[250]. These equations relate the lineshape to the exchange rate and by suitable fitting of these equations to an observed exchange process the exchange rate constant may be extracted. Previous methods of analysing data in this way are summarised in a recent review[251] and involve spectral simulation with the minimum least-squares criterion often being invoked as the test of the quality of the fit. However, the approach applied to such data analyses in this thesis is that due to Moore[143] where up to seven parameters may be adjusted simultaneously using the method of non-linear least-squares, the data being handled on either a Burroughs B6700 or a Nicolet 1080 computer.

A typical analysis is described in terms of the input requirements of the curve-fitting procedure:

1) A value of T_2 ($=1/\pi\Delta\upsilon_{\frac{1}{2}}$) is required by the equations and can be readily obtained by fitting n.m.r. data from a reference line in the spectrum which is not subject to exchange broadening. A resonance due to a species in a similar chemical environment to those undergoing exchange is usually chosen (e.g. 1,4-dioxan). This value of the natural linewidth is then fixed and applied to the exchange data.
2) Other requirements include:
   a- the frequency separation of the two exchanging resonances,
   b- the centre frequency of the exchange data,

c- the population of each of the two exchanging sites,

d- an initial estimate of τ (see below.)

The program will then iteratively match the observed data to that calculated from the equations of Gutowsky and Holm by varying up to seven parameters (a, b, c, d, normalisation constant, baseline correction, and natural linewidth) until convergence (as shown by a least-squares refinement parameter[143]) is achieved.

The calculated value of the relaxation time, τ, is then related to the rate constants k_A and k_B for exchange from site A to site B and site B to site A respectively by the equations:

$$\tau = 1/(k_A + k_B) \quad \text{where } k_A P_A = k_B P_B$$

P_A, P_B = populations of each site, $P_A = 1 - P_B$.

This procedure has been applied to all instances reported in this thesis for diamagnetic two site exchange. In the case of the paramagnetic solvent exchange discussed in Chapter 4 section 6, the program was simply used as an iterative means of accurately measuring the observed linewidth which was then used to plot figure 6.2. (Ch. 4).

Rate data derived from whatever n.m.r. source was fitted to the Eyring equation using the program ACTPAR due to Moore. The program calculates the Arrhenius factors, E_a (activation energy) and A (frequency factor) from the relation $k = A\exp(-E_a/RT)$ by a linear least-squares best fit to a plot of ln$k$ versus $1/T$. Values of $\Delta H^{\ddagger}$ and $\Delta S^{\ddagger}$ from the transition state theory Eyring equation:

$$k = (\kappa T/h).\exp(\Delta S^{\ddagger}/R).\ \exp(\Delta H^{\ddagger}/RT)$$

were derived at 298K by means of the relations:

$$\Delta H^{\ddagger} = E_a - RT.$$

$$\Delta S^{\ddagger} = R(\ln A - \ln(\kappa T/h) - 1)$$

These equations apply for both uni- and bimolecular reactions in solution[252].

SECTION 4. X-RAY CRYSTALLOGRAPHIC TECHNIQUES.

The general mathematical background to the theory of X-ray crystallography has been well documented[253] and so will not be covered in any detail.

A. Practical Considerations.

Crystals for analysis were mounted on fine quartz fibres using 'Araldite' epoxy resin and subsequently mounted and aligned with the X-ray beam on a goniometer head attached to a Syntex $P2_1$ four-circle automated diffractometer. Preliminary rotation photographs were used to identify the lattice and unit cell parameters (below) for subsequent refinement. Rotation photographs about each of the three cell axes were taken in order to verify their assignment, symmetry and length. Given these unit cell parameters the Syntex proceeds to calculate the position, and collect the intensity data of each reflection. This raw data was treated as described in text and below.

B. The Unit Cell and Lattice.

Each molecule in a crystal is associated with a regular three dimensional point array, the lattice. This may be generated by the

periodic repetition of three non-coplanar vectors, $\underline{a}$, $\underline{b}$, and $\underline{c}$ with interaxial angles α, β, and γ. These define the unit cell. An infinite number of sets of parallel planes, containing atoms, may be chosen from the lattice and specified by vectors ($\underline{h},\underline{k},\underline{l}$,) normal to them. An X-ray beam incident on a set of planes ($\underline{h},\underline{k},\underline{l}$) at the Bragg angle θ ($n\lambda = 2d.\sin\theta$, n = integer, λ = wavelength of the X-rays, d = spacing between like planes - Braggs law) will suffer diffraction and behave as if reflected - hence the common name 'reflections'.

C. The Structure Factor.

X-rays are scattered by the bound electrons, and the electron density $\rho(x,y,z)$ in the unit cell is a smooth periodic function over the whole lattice. Such functions may in general be expanded in terms of a Fourier series and the expansion of the electron density function is:

$$\rho(x,y,z) = 1/V.\sum_h \sum_k \sum_l F(hkl).\exp\left[-2\pi i(hx + ky + lz)\right] \quad -----(1)$$

where F(hkl) is the coefficient to be determined, and h,k and l are integers over which the series is summed. F(hkl) is known as the 'Structure Factor', and is a sum of the contributions of all atoms to reflection (hkl). It may be shown that:

$$F(hkl) = \sum_1^j f_j.\exp\left[2\pi i(hx + ky + lz)\right] \quad ----------(2)$$

where there are j atoms in the unit cell with phases ϕ given by:

$$\phi_j = 2\pi(hx + ky + lz) \quad ----------(3)$$

f is called the 'Atomic Scattering Factor' or 'Form Factor' and its value depends upon the type of atom and the Bragg angle θ. A scale is used such that f equals the number of electrons in the atom when $\theta = 0$.

D. The Temperature Factor.

Values of f must be corrected to allow for atomic vibration which

has the effect of 'smearing' the electron density out over a greater volume in the unit cell. For a simple spherical or isotropic vibration:

$$f' = f.\exp\left[-Bj(\sin\theta/\lambda)^2\right] \qquad \text{----------(4)}$$

more accurately a triaxial ellipsoidal anisotropic vibration may be assumed:

$$f' = f.\exp\left[-\tfrac{1}{4}(h^2B_{11}(a^*)^2 + k^2B_{22}(b^*)^2 + l^2B_{33}(c^*)^2 + 2hkB_{12}a^*b^* + 2hlB_{13}a^*c^* + 2klB_{23}b^*c^*)\right] \qquad \text{---------(5)}$$

the values of B in both cases define the extent of atomic motion allowed in the crystal. (* designates the reciprocal cell quantity).

E. Relation of F(hkl) to Observable Intensity.

The measured intensity of radiation reflected from plane (hkl) is proportional to $|F(hkl)|^2$. The magnitude of F(hkl), but not its phase, may therefore be determined experimentally. It is not possible however, to compute the electron density distribution using equation (1) and so solve the structure directly without the phase. There are various methods[254] of overcoming this so called 'phase problem'. Only the heavy atom method[255,256] will be considered due to its applicability to the compounds in the present study.

F. The Heavy Atom Method and Patterson Function.

A.L. Patterson[255,256] showed that a Fourier synthesis A(uvw) given by:

$$A(uvw) = 1/V.\sum_h \sum_k \sum_l \left[|F(hkl)|^2 \exp(2\pi i(hu + kv + lw)\right] \qquad \text{----(6)}$$

is a map of all interatomic vectors in the unit cell. Unlike $\rho(x,y,z)$ this may be synthesised directly from the observed $|F(hkl)|^2$ values since no phase information is required. The peak heights in the map are proportional to the atomic numbers of the atoms. If a unit cell contains N atoms there are N(N-1) non-origin vectors resulting in a very crowded and frequently intractable map. A molecule containing

only a few heavy atoms will, however, give a map dominated by heavy vectors[257]. In favourable cases these vectors may lead directly to the co-ordinates of the heavy atoms. The contribution of the fj phases for the heavy atoms may dominate F(hkl) and in this case an electron density synthesis using calculated values of F(hkl) based only on the heavy atoms should show the position of lighter atoms. The process may be iterated and if successful should converge rapidly to the final structure.

G. Least-Squares Refinement.

The refinement of a structure requires variation in the atomic parameters to be made such that a best fit is obtained between computed and observed structure factors. Legendre's method of minimising the sum of the squares of the errors is used to accomplish this. Both the theory and application of this method are well described in standard texts[258].

Progress in structure refinement is frequently measured by the value of 'The Residual, R', defined by:

$$R = \Sigma||F_o| - |F_c|| \,/\, \Sigma|F_o| \qquad \text{---------- (7)}$$

Wilson has shown[259] that an entirely wrong arrangement of atoms for a centric crystal has R- 0.828, correct structures have R 0.25 and well refined structures have R - 0.05.

H. Data Processing Corrections.

The raw diffractometer data must be corrected for effects which alter the observed value of F(hkl) from that calculated by first principles[253].

a) Background: (Syntex $P2_1$ manual)

The Syntex diffractometer measures a ninety-six step profile of

each reflection with background counts on either side of the peak maximum. The corrected intensity is calculated by the diffractometer using the relations:

$$I = \frac{\text{(total scan count - sum of background counts) x scan rate}}{\text{background to scan ratio}}$$

$$\text{e.s.d} = I(\text{total scan count - sum of background counts})^{-\frac{1}{2}}$$

b) Coincidence correction: (Syntex $\underline{P}2_1$ manual)

The detector and associatedcircuitry lose counts at high count rates due to an inability to respond to a second pulse before the first pulse is processed. The true intensity may be approximated to the observed intensity by the Schiff formula,

$$It = Io.\exp(It.\tau)$$

where τ is the dead time for an isolated event, and is an instrumental constant. The Syntex $\underline{P}2_1$ approximates this expression by a parabola,

$$It = Io + \tau It^2$$

which fits well up to 50,000 counts per second.

c) Polarisation:

The theory of polarisation effects is treated in standard texts[253]. The correction takes the form,

$$|F(hkl)| \propto (I(hkl)/p)^{\frac{1}{2}}$$

where p is the polarisation factor and is a simple function of 2θ.

$$p = \frac{1 + \cos^2 2\theta}{2}$$

d) The Lorentz Factor:

The time for a given reciprocal lattice point to travel through its diffraction position during data collection is not constant and is a function of data collection geometry. Since measured intensity is a function of scan rate a correction specific to the parallel geometry used inthis determination is applied[253]. The simple Lorentz factor, L, is given by $L = 1/\sin 2\theta$.

e) Absorption:

An X-ray beam travelling through a crystal is attenuated according to a normal exponential law,

$$I = I_o \exp(-\mu\tau) \qquad \text{----------(8)}$$

where I_o is the incident intensity, I the intensity after distance τ and μ is the linear absorption coefficient of the crystal. μ depends upon the number and type of atoms in the given unit cell and is very dependent upon the wavelength of the X-radiation[260]. Exact application of equation (8) requires a full knowledge of the crystal dimensions referenced to the same co-ordinate set used for data collection. A measuring procedure and an associated analytical absorption correction program, ABSCOR, due to Alcock[261-263] were used. The program functions by dividing the crystal into Howell's polyhedra so that rays are entering or leaving via one face only. For each of the polyhedra, the contribution to the total diffracted intensity is calculated (A_T). The transmission is then given by A_T/V (V = crystal volume)[262,263].

Raw diffractometer data was treated by the program SYNDAT[264] which applies Lorentz and Polarisation corrections (above) and reduces the observed intensities to unphased structne factors F(hkl). This data was reduced to binary data files acceptable to the XRAY76 system using the program DATRDN[265], which makes use of symmetry, unit cell constants and individual scattering factors. Subsequent data manipulations and structure solution as described above were accomplished using the XRAY76 programs[265] implemented on a Burroughs B6700 computer.

REFERENCES

1) A.J. Canty and R. Kishimoto, Nature, 1975, 253, 123. and refs therein.

2) A.M. Corrie, M.D. Walker and R.D. Williams, J.C.S. Dalton, 1976, 1012.

3) G.K.R. Makar, M.L.D. Touche and D.R. Williams, J.C.S. Dalton, 1976, 1016.

4) M.M. Jones, T.H. Pratt, W.G. Mitchell, R.D. Harbison and J.S. Macdonald, J.Inorg.Nucl.Chem., 1976, 38, 61

5) E.C. Faulkes, Am. J. Physiol., 1974, 227, 1356.

6) L.H. Ahrens, Gecchim.et Cosmochim. Acta, 1952, 2, 155.

7) D. Grdenic, Quart.Revs.Chem.Soc., 1965, 19, 303.

8) R.G. Pearson, J.Amer.Chem.Soc., 1963, 85, 3533; 1967, 89, 1827.

9) J.A. Nathanson, R. Freedman and B.J. Hoffer, Nature, 1975, 261, 330.

10) M. Eigen, Pure and Appl.Chem., 1963, 6, 105;
H.D. Bennet and B.F. Caldin, J.C.S. A, 1971, 2198

11) A.E. Martell,"Critical Stability Constants", Vol.2, Plenum,London,1975.

12) R.S. Reid, M.Sc. Thesis, University of Warwick, 1976.

13) A.E. Martell, Adv.Chem.Ser., 1967, 62, 272.

14) D.St.C. Black and E. Markham, Rev.Pure and Appl.Chem., 1965, 15, 109.

15) A.B.P. Lever, Adv. Inorg.Radiochem., 1965, 7, 27.

16) L.F. Lindoy and D.H. Busch, Prep.Inorg.Reactions, Vol.6, pl.

17) H.K. Frensdorff, J.Amer.Chem.Soc., 1971, 93, 600.

18) R.M. Izatt and J.J. Christensen, Structure & Bonding, 1973, 16, 161.

19) J.J. Christensen and R.M. Izatt, Science, 1971, 174, 459.

20) M.A. Bush and M.R. Truter, J.C.S. Perkin II, 1972, 345.

21) M.R. Truter, Structure and Bonding, 1973, 16, 1 and 71.

22) D.H. Busch, L.Y. Martin, L.J. Dehayes and L.J. Zompa, J.Amer.Chem.Soc., 1974, 96, 4046.

23) L.J. DeHayes and D.H. Busch, Inorg.Chem., 1973, 12, 1505 and 2010.

24) R.A.D. Wentworth and T.S. Piper, Inorg.Chem., 1965, 4, 709.

25) C.R. Sperati, Ph.D. Thesis, Ohio State University, 1974.

26) Y. Komiyama and E.C. Lingafelter, Acta Cryst., 1964, 17, 1145.

27) A. Anichini, L. Fabbrizzi, P. Paoletti and R.M. Clay, J.C.S. Dalton, 1978, 577.

28) M. Kodama and E. Kimura, J.C.S. Dalton, 1977, 2269.

29) M. Kodama and E. Kimura, J.C.S. Dalton, 1976, 2335.

30) M. Kodama and E. Kimura, Yuki.Gosei.Kagaku.Kyokai Shi., 1977, 35, 632.

31) P. Paoletti, L. Fabbrizzi and R. Barbucci, Inorg.Chim.Acta Rev., 1973, 7, 43.

32) D.K. Cabbiness and D.W. Margerum, J.Amer.Chem.Soc., 1969, 91, 6540.

33) G. Schwarzenbach, Helv.Chim.Acta, 1952, 35, 2344

34) D.K. Cabbiness and D.W. Margerum, J.Amer.Chem.Soc., 1970, 92, 2151.

35) P. Paoletti, L. Fabbrizzi and R. Barbucci, Inorg.Chem., 1973, 12, 1961

36) P. Paoletti, L. Fabbrizzi and A.B.P. Lever, Inorg.Chem., 1976, 15, 1502.

37) F. P. Hinz and D.W. Margerum, Inorg.Chem., 1974, 13, 2941.

38) R. Barbucci, L. Fabbrizzi, P. Paoletti and A. Vacca, J.C.S. Dalton, 1973, 1763.

39) M. Kodama and E. Kimura, J.C.S. Dalton, 1976, 116.

40) P. Monk and I. Wadso, Acta Chem.Scand., 1968, 22, 1842.

41) I. Wadso, Acta Chem.Scand., 1968, 22, 927.

42) M. Kodama and E. Kimura, J.C.S. Chem.Commun., 1975, 891.

43) G.F. Smith and D.W. Margerum, J.C.S. Chem.Commun., 1975, 807.

44) Y. Hung, L.Y. Martin, S.C. Jackels, A.M. Tait and D.H. Busch, J.Amer.Chem.Soc., 1977, 99, 4029.

45) L.Y. Martin, C.R. Sperati and D.H. Busch, J.Amer.Chem.Soc., 1977, 99, 2968.

46) L.Y. Martin, Ph.D. Thesis, Ohio State University, 1974.

47) A.B.P. Lever, "Inorganic Electronic Spectroscopy", Elsevier, Amsterdam, 1968.

48) C.G. Spike and R.W. Parry, J.Amer.Chem.Soc., 1953, 75, 2726.

49) N. Sadaswan, J.A. Kernohan and J.T. Endicott, Inorg.Chem., 1967,6,770.

50) D.A. Rowley and R.S. Drago, Inorg.Chem., 1968, 7, 795.

51) Y. Saito, "Spectroscopy and Structure of Metal Chelate Compounds", K. Nakamoto and P.J. M^{c}Carthy, Ed., Wiley, New York, N.Y., 1968.

52) L.N. Swink and M. Atoji, Acta Crystallogr., 1960, 13, 639.

53) D.C. Olson and J. Vasilevskis, Inorg. Chem., 1969, 8, 1611.

54) D.C. Olson and J. Vasilevskis, Inorg. Chem., 1971, 10, 463.

55) J.C. Dabrowiak, F.V. Lovecchio, V.L. Goedken and D.H. Busch, J.Amer.Chem.Soc., 1972, 94, 5502.

56) D.P. Rillema, J.F. Endicott and E. Papaconstantinou, Inorg.Chem., 1971, 10, 1739.

57) F.V. Lovecchio, E.S. Gore and D.H. Busch, J.Amer.Chem.Soc., 1974, 96, 3109.

58) E.K. Barefield and M.T. Mocella, Inorg.Chem., 1973, 12, 2829.

59) R.L. Denning, A.L. Allred, A.R. Dahl, A.W. Herlinger and M.O. Kestner, J.Amer.Chem.Soc., 1976, 98, 4132.

60) E.R. Dockal, J.E. Jones, W.F. Sokol, R.J. Engerer, D.B. Rorabacher and L.A. Ochrymowyez, J.Amer.Chem.Soc., 1976, 98, 4322.

61) P.K. Chan and C.K. Poon, J.C.S.Dalton, 1976, 858.

62) Yu.A. Ovchinnikov, V.T. Ivanov and A.M. Shkrob, "Membrane-Active Complexones", Elsevier, Amsterdam, 1974.

63) C.J. Pedersen, J.Amer.Chem.Soc., 1967, 89, 7017.

64) M. Dobler and R.P. Phizackerley, Helv.Chim.Acta, 1974, 57, 664.

65) J.M. Lehn, Structure and Bonding, 1973, 16, 1.

66) C.J. Pedersen and H.K. Frensdorff, Angew.Chem.Internat.Edn., 1972, 11, 16.

67) D.E. Fenton, Chem.Soc.Rev., 1977, 6, 325.

68) B. Dietrich, J.M. Lehn and J.P. Sauvage, Tet.Letts., 1969, 2885, 2889.

69) J.M. Lehn and J.P. Sauvage, Chem.Commun., 1971, 440.

70) J.M. Lehn, Accts.Chem.Res., 1978, 11, 49.

71) I.I. Creaser, J.M. Harrowfield, A.J. Herlt, A.M. Sargeson, J. Springborg, R.J. Gene and M.R. Snow, J.Amer.Chem.Soc., 1977, 99, 3181.

72) P. Baudot, M. Jacque and M. Robin, Toxicol.Appl.Pharmacol., 1977, 41, 113.

73) F. Arnaud-Neu, B. Spiess and M.J. Schwing-Weill, Helv.Chim.Acta, 1977, 60, 2633.

74) S.N. Rosenthal and J.H. Fendler, Adv.Phys.Org.Chem., 1976, 13, 279.

75) F. De Sarlo, A. Guarna and G.P. Speroni, J.C.S.Chem.Commun., 1977, 549.

76) D.E. Fenton, D.H. Cook, I.W. Nowell and P.E. Walker, J.C.S.Chem. Commun., 1977, 623.

77) R.D. Bereman and S.N. Choi, J.Inorg.Nucl.Chem., 1976, 38, 2304.

78) F. Mathieu and R. Weiss, J.C.S. Chem.Commun., 1973, 816.

79) J.F. Desreux, A. Renard and G. Duyckaerts, J.Inorg.Nucl.Chem., 1977, 39, 1587.

80) G. Bombieri, G.De Paoli and A. Immirizi, J.Inorg.Nucl.Chem., 1978, 40, 799.

81) G.W. Gokel and H.D. Durst, Synthesis, 1976, 168.

82) J. Dockx, Synthesis, 1973, 441.

83) J.E. Richman and T.J. Atkins, J.Amer.Chem.Soc., 1974, 96, 2268.

84) M. Hediger and T.A. Kaden, J.C.S. Chem.Commun., 1978, 14.

85) I. Tabushi, H. Okino and Y. Koruda, Tet.Letts., 1976, 4339.

86) I. Tabushi, Y. Taniguchi and H. Kato, Tet.Letts., 1977, 1049.

87) T.J. Lotz and T.A. Kaden, Helv.Chim.Acta, 1978, 61, 1376.

88) G.R. Newkome, J.D. Sauer, J.M. Roper and D.C. Hager, Chem.Rev., 1977, 77, 513.

89) E.K. Barefield, F. Wagner, A.W. Hrelinger and A.R. Dahl, Inorg.Synthesis, 1976, 16, 220.

90) N.F. Curtis, Coord.Chem.Rev., 1968, 3, 3.

91) J.D. Sauer, Diss.Abs.Int.B., 1976, 37, 2256.

92) D.H. Cook and D.E. Fenton, Inorg.Chim.Acta, 1977, 25, L95.

93) L.F. Lindoy, N.E. Tokel, L.B. Anderson and D.H. Busch, J.Co-ord.Chem., 1971, 1, 7.

94) D.H. Cook, D.E. Fenton, M.G.B. Drew, S.G. M^{c}Fall and S.M. Nelson, J.C.S. Dalton, 1977, 446.

95) D.E. Fenton, D.H. Cook and I.W. Nowell, J.C.S. Chem.Commun., 1977, 274

96) M.G. Drew, A.H. Othman, S.G. M^{c}Fall and S.M. Nelson, J.C.S. Chem.Commun, 1977, 370 & 558; J.C.S. Dalton, 1977, 1173.

97) Z.P. Haque, D.C. Liles, M. M^{c}Partlin and P.A. Tasker, Inorg.Chim.Acta, 1977, 23, L21.

C. Griggs, M. Hasan, K.F. Henrick, R.W. Matthews and P.A. Tasker, ibid., 1977, 25, L29.

98) D.P. Riley, J.A. Stone and D.H. Busch, J.Amer.Chem.Soc., 1977, 99, 767

99) K.B. Mertes, P.W.R. Corfield and D.H. Busch, Inorg.Chem., 1977, 16, 3226

100) J.D. Goddard, Inorg.Nucl.Chem.Letts., 1977, 13, 555.

101) M.J. D'Aniello and E.K. Barefield, J.Amer.Chem.Soc., 1976, 98, 1610.

102) C.Y. Mok and J.F. Endicott, J.Amer.Chem.Soc., 1978, 100, 123.

103) G.C. Gordon, P.W. Dehaven, M.C. Weiss and V.L. Goedken, J.Amer.Chem.Soc., 1978, 100, 1003

104) C.K. Poon and M.L. Tobe, Inorg.Chem., 1968, 7, 2398.

105) C.K. Poon and M.L. Tobe, J.C.S. A, 1968, 1549.

106) C.K. Poon and W.K. Lee, Inorg.Chem., 1973, 12, 2016.

107) C.K. Poon and C.L. Wong, J.C.S. Dalton, 1976, 966.

108) H. Stetter and W. Frank, Angew.Chem., 1976, 88, 760.

109) F.L. Weitl, K.N. Raymond, W.L. Smith and T.R. Howard, J.Amer.Chem.Soc., 1978, 100, 1170.

110) L. Field, Synthesis, 1972, 4, 101.

T.B. Rauchfuss, J. Shing Shu and D.M. Roundhill, Inorg.Chem., 1976, 15, 2096.

111) W. Rosen and D.H. Busch, J.Amer.Chem.Soc., 1969, 91, 4694.

112) L.A. Ochrymowycz, C.P. Mak, J.D. Michna, J.Org.Chem., 1974, 39, 2081.

113) W. Rosen and D.H. Busch, Inorg.Chem., 1970, 9, 262.

114) J.M. Bradshaw, J.Y. Hui, Y. Chan, B.L. Haymore, R.M. Izatt and J.J. Christensen, J.Hetero.Chem., 1974, 11,45.

115) D.C. Black and I.A. M^{c}Lean, Tet.Letts., 1969, 3961.

116) E. Weber and F. Voegtle, Just.Liebigs Annal.Chem., 1976, 5, 891& 916.

117) C.A. M^{c}Auliffe, Adv.Inorg.Radiochem., 1975, 17, 165.

118) M.A. Ali and S.E. Livingstone, Co-ord.Chem.Rev., 1974,13, 101.

119) S.E. Livingstone, Quart.Rev., 1965, 19, 386.

120) R.E. Desimone and M.D. Glick, J.Co-ord.Chem., 1976, 5, 181.

121) N.W. Alcock, N. Herron and P. Moore,J.C.S. Chem.Commun., 1976, 886.

122) E.R. Dockal, L.L. Diaddario, M.D. Glick and D.B. Rorabacher, J.Amer.Chem.Soc., 1977, 99, 4530.

123) P.H. Davis, L.K. White and R.L. Bedford, Inorg.Chem., 1975, 14, 1753.

124) D. Sevdic, L. Jovanovac and H. Meider-Gorican, Mikrochim.Acta, 1975, 235.

125) A.E. Martell and M.M. Taqui Khan, Inorg.Chem., 1975, 14, 676.

126) J.O. Cabral, M.F. Cabral, M.G.B. Drew,S.M. Nelson and A.M. Rodgers, Inorg.Chim.Acta, 1977, 25, L77.

127) T.A. Deldonno and W. Rosen, J.Amer.Chem.Soc., 1977, 99, 8051.

128) E.P. Kyba, C.W. Hudson, M.J. M^{c}Phaul and A.M. John, J.Amer.Chem.Soc., 1977, 99, 8053.

129) K.B. Yatsimirskii, E.I. Sinyavskaya and A.S. Shtepanek, Dokl.Akad.Nauk.SSSR., 1978, 238, 404.

130) R.W. Hardy, R.C. Burns and G.W. Parshall in "Inorganic Biochemistry", ed., G.L. Eichorn, Elsevier, New York, 1973.

131) T.N. Lockyer, Aust.J.Chem., 1974, 27, 259.

132) P.R.H. Alderman, P.G. Owston and J.M. Rowe, J.C.S., 1962, 668.

133) W. Levason, C.A. M^{c}Auliffe and S.G. Murray, Inorg.Chim.Acta, 1976, 17, 247.

134) J. Peisach, P. Aisen and W.E. Blumberg, Ed., "The Biochemistry of Copper.", Academic Press, New York, N.Y., 1966, p376.

135) T.E. Jones, D.B. Rorabacher and L.A. Ochrymowycz, J.Amer.Chem.Soc., 1975, 97, 7485.

136) T.E. Jones, L.L. Zimmer, L.L. Diaddario, D.B. Rorabacher and L.A. Ochrymowycz, J.Amer.Chem.Soc., 1975, 97, 7163.

137) O.W. Howarth, P. Moore and N.Winterton, J.C.S. Dalton, 1974, 2271; ibid., 1975, 360; Inorg.Nucl.Chem.Letts., 1974, 10, 553; J.C.S. Chem.Commun., 1974, 664.

138) B. Bosnich, C.K. Poon and M.L. Tobe, Inorg.Chem., 1965, 4, 1102.

139) W. Rosen and D.H. Busch, J.C.S. Chem.Commun., 1969, 148.

140) M.D. Glick, D.P. Gavel, L.L. Diaddario and D.B. Rorabacher, Inorg.Chem., 1976, 15, 1190.

141) C.J. Ballhausen, N. Bjerrum, R. Dingle, K. Eriiss and C.R. Hare, Inorg.Chem., 1965, 4, 514.

142) A. Hermann and R.M. Wing, Inorg.Chem., 1972, 11, 1415.

143) P. Moore, J.C.S. Faraday I, 1976, 72, 826.

144) P. Haake and P.C. Turley, J.Amer.Chem.Soc., 1967, 89, 4611 & 4617.

145) R.J. Cross, T.H. Green and R. Keat, J.C.S. Dalton, 1976, 1150.

146) K. Travis and D.H. Busch, Inorg.Chem., 1974, 13, 2591.

147) W.D. Lemke, K.E. Travis, N.E. Takvoryan and D.H. Busch, Adv.Chem.Ser., 1976, 150, 358.

148) R.A. Walton, J.C.S. A, 1967 1852.

149) J.B. Stothers, "^{13}C N.M.R. Spectroscopy", Academic Press, London and New York, 1972.

150) R.E. DeSimone and M.D. Glick, J.Amer.Chem.Soc., 1975, 97, 942.

151) S.L. Lawton, Inorg.Chem., 1971, 10, 328.

152) M.D. Glick, R.E. DeSimone, D.B. Rorabacher, D. Gavel and T. Jones, Abs. of A.C.S.Meeting, April, 1975, INOR 104.

153) B.V. Gorewit and W.K. Musker, J.Co-ord.Chem., 1976, 5, 67.

154) D. Sevdic and H. Meider, J.Inorg,Nucl.Chem., 1977, 39, 1403 & 1409.

155) R.E. DeSimone, M.J. Allbright, W.J. Kennedy and L.A. Ochrymowycz, Org.Mag.Res., 1974, 6, 583.

156) R.E. DeSimone and M.D. Glick, J.Amer.Chem.Soc., 1976, 98, 762.

157) J.R. Ferraro, "Low Frequency Vibrations of Inorganic and Co-ordinatio Compounds", Plenum Press, New York, 1971, p251.

158) "International Tables for X-Ray Crystallography", Kynoch Press, Birmingham, 1962, vol.3.

159) J. Ferguson and M.L. Tobe, Inorg.Chim.Acta, 1970, 4, 109.

160) R.C. Edwards, Ph.D. Thesis, Ohio State University, 1976.

161) D.D. Watkins, D.P. Riley, J.A. Stone and D.H. Busch, Inorg.Chem., 1976, 15, 387.

162) P.K. Chan, D.A. Isabirye and C.K. Poon, Inorg.Chem., 1975, 14, 2579.

163) J.F. Endicott, J. Lille, J.M. Kuszaj, B.S. Ramaswamy, W.G. Schmonsees, M.G. Simic, M.D. Glick and D.P. Rillema, J.Amer.Chem.Soc.,1977,99,429.

164) J. Cragel, Diss.Abs.Int.B., 1976, 36, 5023.

165) E.J. Bounsall and S.R. Koprich, Canad. J. Chem., 1970, 48, 1481.

166) B. Bosnich, M.L. Tobe and G.A. Webb, Inorg.Chem., 1965, 4, 1109.

167) P.A. Tasker and L. Sklar, J.Cryst.Mol.Struct., 1975, 5, 329.

168) F. Hinz, Diss.Abs.Int.B., 1974, 34, 239.

169) L.A. Funke, Diss.Abs.Int.B., 1977, 37, 4453.

170) M. Kodama and E. Kimura, J.C.S. Dalton, 1976, 2341.

171) M. Kodama and E. Kimura, J.C.S. Dalton, 1977, 1473.

172) T.A. Kaden, Helv.Chim.Acta, 1970, 53, 617.

173) C.T. Lin, D.B. Rorabacher, G.R. Cayley and D.W. Margerum, Inorg.Chem., 1975, 14, 919.

174) B.E. Douglas and J. Cragel, Inorg.Chim.Acta, 1974, 10, 33.

175) C.J. Cooksey and M.L. Tobe, Inorg.Chem., 1978, 17, 1558.

176) J. Sellan and R. Rumfeldt, Canad.J.Chem., 1976, 54, 1061.

177) T.F. Lai and C.K. Poon, Inorg.Chem., 1976,15, 1562.

178) K.B. Mertes, Inorg.Chem., 1978, 17, 49.

179) E.I. Ochiai, S.J. Rettig, J. Trotter, Canad.J.Chem., 1978, 56, 267.

180) C.K. Poon and D.A. Isabirye, J.C.S. Dalton, 1977, 2115.

181) C.K. Poon and D.A. Isabirye, J.C.S. Dalton, 1978, 740.

182) C.K. Poon and P. Mak, J.C.S. Dalton, 1978, 216.

183) C.K. Poon, Co-ord.Chem.Rev., 1973, 10, 1.

184) J.A. Happe and R.L. Ward, J.Chem.Phys., 1963, 39, 1211.

185) A. Anchini, L. Fabbrizzi, P. Paoletti and R.M. Clay, Inorg.Chim.Acta, 1977, 24, L21.

186) C. Furlani, Co-ord.Chem.Rev., 1968, 3, 141.

187) L. Fabbrizzi and P. Paoletti, Gazz.Chim.Ital., 1974, 104, 929.

188) D.F. Evans, J.C.S., 1959, 2003.

189) S.C. Nyburg and J.S. Wood, Inorg.Chem., 1964, 3, 468.

190) A. Albert and E.J. Serjeant, "Ionisation Constants of Acids and Bases", Methuen, London, 1962, Chapter 4.

191) O. Bostrup and C.K. Jorgensen, Acta Chem.Scand., 1957, 11, 1223.

192) C.K. Jorgensen, Acta Chem.Scand., 1956, 10, 887.

193) V. Gutmann, Co-ord.Chem.Rev., 1975, 15, 207.

194) R.A. Bauer, W.R. Robinson and D.W. Margerum, J.C.S.Chem.Commun., 1973, 289.

195) E.H. Curzon and P. Moore, private communication.

196) R. Hagen, J.P. Warren, D.H. Hunter and J.D. Roberts, J.Amer.Chem.Soc., 1973, 95, 5712.

197) J.A. Pople and D.P. Santry, Mol.Phys., 1964, 8, 1.

198) P.S. Pregosin, H. Omura and L.M. Venanzi, J.Amer.Chem.Soc., 1973, 95, 2047.

199) E.L. Muetterties and R.A. Schunn, Chem.Soc.Quart.Rev., 1966, 20, 245.

200) P.L. Orioli, Co-ord.Chem.Rev., 1971, 6, 285.

201) F.J. Weigert and J.D. Roberts, Inorg.Chem., 1973, 12, 313.

202) D. Shaw, "Fourier Transform N.M.R. Spectroscopy", Elsevier, New York, 1976, p220.

203) R.M. Lynden-Bell and R.K. Harris, "Nuclear Magnetic Resonance Spectroscopy", Appleton, New York, N.Y., 1969, Chapter 3.

204) J.D. Kennedy, W. M^{c}Farlane and B. Wrackenmeyer, Inorg.Chem., 1976, 15, 1299.

205) P.G. Harrison, Co-ord.Chem.Rev., 1976, 20, 27.

206) D.E. Fenton, C. Nave and M.R. Truter, J.C.S. Chem.Commun., 1973, 130.

207) D.E. Fenton, C. Nave and M.R. Truter, J.C.S. Chem.Commun., 1974, 116.

208) H. Dodzink, R.A. Kolinski and B. Korybut-Daszlewicz, Spectrochim.Acta, 1973, 29A, 511.

209) W.L. Reynolds, Prog.Inorg.Chem., 1970, 12, 76.

210) E.K. Barefield and F. Wagner, Inorg.Chem., 1973, 12, 2435.

211) K.D. Hodges, R.G. Wollmann, E.K. Barefield and D.N. Hendrickson, Inorg.Chem., 1977, 16, 2746.

212) R. Buxtorf, W. Steinmann and T.A. Kaden, Chimia, 1974, 28, 15.

213) M.J. D'Aniello, M.T. Mocella, F. Wagner, E.K. Barefield and I.C. Paul, J.Amer.Chem.Soc., 1975, 97, 192.

214) R. Buxtorf and T.A. Kaden, Helv.Chim.Acta, 1974, 57, 1035.

215) E.K. Barefield, F. Wagner, M.T. Mocella, M.J. D'Aniello and A.H.J. Wang, J.Amer.Chem.Soc., 1974, 96, 2625.

216) L. Hertli and T.A. Kaden, Helv.Chim.Acta, 1974, 57, 1328.

217) P. Meier, A. Merbach, S. Burki and T.A. Kaden, J.C.S.Chem.Commun., 1977, 56.

218) C.J. Hawkins, R.M. Peachey and C.L. Szoredi, Aust.J.Chem., 1978, 31, 973.

219) S. Berry, J.Chem.Phys., 1960, 32, 933.

220) K. Nakamoto, "Infra-red Spectra of Inorganic and Co-ordination Compounds", Willey Interscience, 2nd Edition, 1970, p187.

221) "Interatomic Distance Supplement", Chem.Soc., London, Special Publication No. 18, ed. L.E. Sutton, 1965, pS13s.

222) K.N. Raymond, P.W.R. Corfield and J.A. Ibers, Inorg.Chem.,1968,7,136.

223) E.K. Barefield and F. Wagner, Inorg.Chem., 1976, 15, 408.

224) G. Ferraudi and L. Patterson, J.C.S.Chem.Commun., 1977, 755.

225) R.F. Evilia, D.C. Young and C.N. Reilly, Inorg.Chem., 1971, 10, 433.

226) D.A. Sweigart and P. Heidtmann, J.C.S. Dalton, 1975, 1686.

227) M.J. Hynes and P.F. Brannick, J.C.S.Chem.Commun., 1977, 942.

228) J.P. Jesson in "N.M.R. of Paramagnetic Molecules", Academic Press, New York and London, 1973, Chapter 1.

229) T.J. Swift and R.E. Connick, J.Chem.Phys., 1962, 37, 307.

230) T.J. Swift in "N.M.R. of Paramagnetic Molecules", Academic Press, New York and London, 1973, Chapter 2.

231) S. Funahashi and R.B. Jordan, Inorg.Chem., 1977, 16, 1301.

232) T.R. Stengle and C.H. Langford, Co-ord.Chem.Rev., 1967, 2, 349.

233) D.K. Ravage, T.R. Stengle and C.H. Langford, Inorg.Chem.,1967,6,1252.

234) R.E. Richards et al., Mol.Phys., 1971, 20, 933.

235) S.F. Lincoln and R.J. West, Aust.J.Chem., 1973, 26, 255.

236) J.J. Zuckermann, J.Chem.Educ., 1965, 42, 315.

237) R. Krishnamurthy and W.B. Schaap, J.Chem.Educ., 1969, 46, 799.

238) J.P. Hunt, Co-ord.Chem.Rev., 1971, 7, 1.

239) S.F. Lincoln and R.J. West, J.Amer.Chem.Soc., 1974, 96, 400.

240) S.F. Lincoln and R.J. West, Inorg.Chem., 1973, 12, 494.

241) S.F. Lincoln and R.J. West, Aust.J.Chem., 1974, 27, 97.

242) V.L. Goedken, N.K. Kildahl and D.H. Busch, J.Co-ord.Chem.,1977,7, 89.

243) M.J. Norgett and L.M. Venanzi, Inorg.Chim.Acta, 1968, 2, 107.

244) P.L. Orioli and L. Sacconi, J.C.S.Chem.Commun., 1969, 1012.

245) M. Kodama and E. Kimura, J.C.S. Dalton, 1978, 247.

246) H.C. Torrey, Phys. Res., 1949, 76, 1059.

247) D.A. Couch, DISKFT, Nicolet Users Society.

248) O.W. Howarth, "Theory of Spectroscopy", Nelson, London, 1973.
J.W. Akitt, "N.M.R. and Chemistry", Chapman Hall, London, 1973.
D. Shaw, "F.T. N.M.R. Spectroscopy", Elsevier, Amsterdam, 1976.
E.W. Randall and G. Hawkes, "Advances in ^{15}N n.m.r." , presented in Sicilia 1976.

249) J. Lewis and R.G. Wilkins Ed., "Modern Co-ordination Chemistry", Interscience, New York, N.Y., 1960, p403.

250) H.S. Gutowsky and C.H. Holm, J.Chem.Phys., 1956, 25, 1228.

251) I.O. Sutherland, Ann.Rep.N.M.R.Spectroscopy, 1971, 4, 71.

252) A.A. Frost and R.G. Pearson, "Kinetics and Mechanism", 2nd Edn., Wiley, 1961, p98.

253) G.H. Stout and L.H. Jensen, "X-Ray Structure Determination", Macmillan, London, 1968.
M.J. Buerger, "X-Ray Crystallography", Wiley, N.Y., London, 1960.
M.J. Buerger, "Crystal Structure Analysis", Wiley, London, 1960.
M.M. Woolfson, "Direct Methods in Crystallography", Oxford Clarendon Press, 1961.

254) M.M. Woolfson, "X-Ray Crystallography", Cambridge Press, 1970.

255) A.L. Patterson, Phys.Rev., 1934, 46, 372.

256) A.L. Patterson, Z.Krist(A), 1935, 90, 517.

257) H. Lipson and W. Cochran, "The Determination of Crystal Structures", G. Bell and Sons, London, p207.

258) J.S. Rollett, "Computing Methods in Crystallography", Pergamon, 1965.

259) A.J.C. Wilson, Acta Cryst., 1950, 3, 397.

260) "International Tables for X-Ray Crystallography", Kynoch Press, Birmingham, 1974.

261) N.W. Alcock, Acta Cryst., 1970, A26, 437.

262) N.W. Alcock, G.S. Pawley, C.P. Rourke and M.R. Levine, Acta Cryst., 1972, A28, 440.

263) N.W. Alcock in "The Analytical Method for Absorption Correction", in 'Crystallographic Computing', ed. F. Ahmed, Munksgaard, Copenhagen, 1970, p271.

264) SYNDAT- data reduction program for a Syntex $P2_1$ diffractometer, N.W. Alcock, 1974.

265) J.M. Stewart, University of Maryland, TR-446, MARCH 1976.

APPENDIX

Final Temperature and Structure Factor Tables.

Final temperature and structure factor tables have been or will eventually be deposited when details of the individual crystal structures are published. Because of their length they have been omitted from this thesis but are available on request.